Designer Nonplanar Porphyrins with Tuned Properties for Application as Bifunctional Organocatalysts

Submitted by

Marie Roucan BSc

A thesis submitted to the University of Dublin, Trinity College for the degree of

Doctor of Philosophy

Under the supervision of Prof. Dr. Mathias O. Senge

Trinity College Dublin, the University of Dublin,

2020

DECLARATION

I declare that this thesis has not been submitted as an exercise for a degree at this or any other University and it is entirely my own work.

I agree to deposit this thesis in the University's open access institutional repository or allow the library to do so on my behalf, subject to Irish Copyright Legislation and Trinity College Library conditions of use and acknowledgement.

Furthermore, unpublished and/or published work of others, is duly acknowledged in the text wherever included

Signed: _____

February 2020, Trinity College Dublin

SUMMARY

The aim of this research was to investigate the use of different free base nonplanar porphyrins as bifunctional catalysts. This involved the tailored design of various porphyrin catalysts and the subsequent testing of said systems in catalytic screening reactions with small organic molecules. Porphyrins are a unique class of natural compounds that are omnipresent in nature. This results in them being involved in many important biological processes for example oxygen transport, electron transfer and oxidation reactions as well as photosynthesis. These versatile molecules can also be found in cofactors in nature and are crucial regulatory effectors in many biochemical processes. Nowadays the chemistry of porphyrins is well established and they can be found in a wide area of applications. However, porphyrins usually act as a simple ligands where the actual desired effect is subsequent to the formation of a tetrapyrrole metal complex. Most of the time the very interesting inner core N and NH units are deemed inaccessible, albeit they could offer an interesting entry point to a plethora of new applications and reactions.

This work focuses on taking advantage of these active inner units of the porphyrin by purposely fine-tuning and modulating the porphyrin periphery and hence making these formerly esoteric units available through the introduction of precise distortion to the porphyrin macrocycle. This is envisioned to lead to distorted free base tetrapyrroles that have tuneable properties and form complexes through weak interactions of the core with other molecules and therefore represent interesting candidates for organocatalysts. In order to achieve this goal the project was divided into two main parts:

a) The synthesis of a library of nonplanar porphyrins with various degrees of distortion.
b) The investigation into the activity of these molecules as effective catalysts in 1,4-addition reactions.

The first method employed to obtain the essential distortion of the porphyrin macrocycle and thus make the N and NH units of the porphyrin macrocycle available for catalytic activity was through crowding of the periphery of the porphyrin core. The synthesis of a large library of nonplanar highly substituted porphyrins was then achieved through condensation reactions. Therefore, a series of aldehydes with different electron donating substituents were chosen together with two types of substituted pyrrole units resulting in two families of highly substituted porphyrins. The electron donating effects of the respective aldehydes were quantified using Hammett's values to strategically design and fine-tune the electronic properties of the porphyrin macrocycles. The strong electron donating effects of the substituents on the aryl units decreases the electrophilicity of the

aldehyde group and thus its reactivity towards pyrrole molecules. More importantly the presence of strong electron donating groups induces a very high basicity to the inner core functional groups of the porphyrin, which could result in an enhanced reactivity toward binding of small molecules. Five new products were obtained which are promising candidates for the application as organocatalysts as they all possess the necessary requirements, namely a high degree of distortion and enhanced electron density of their macrocycle. Depending on the aldehyde used and the position of the substituents on the aldehyde (para, meta, ortho) yields of the porphyrin ranged from moderate to high. In some cases, no product formation was observed. One of these compounds was the *p*-dimethylamino-OETArX-porphyrin, which would be due to its electronic nature. As condensation reactions proved unsuccessful, other functionalization reactions, such as Buchwald-Hartwig reactions or reductions, were investigated. The spectral properties of the porphyrins were investigated by UV-vis and NMR spectroscopy. Furthermore, X-ray analysis showed some interesting results such as a cage formed by a dicationic porphyrin and acetic acid molecules, revealing possible binding abilities for various anions.

Another way of introducing distortion to a porphyrin macrocycle is *via* methylation of the inner nitrogen atoms of planar free base porphyrins. This results in a considerable distortion of the macrocycle. A library of *N*-methylated porphyrins with various aryl substituents was successfully synthesized. Optimizations of the methylation reaction were undertaken resulting in not only increased yields but also in the introduction of a precise and defined number of methyl groups to the porphyrin core. This allows for the tailored synthesis of *N*-methylated porphyrins bearing one to three methyl units in the porphyrin macrocycle. The efficiency and regioselectivity of the methylation are correlated to the peripheral substitution pattern. Additionally, the electron donating properties of the substituents tend to enhance the reactivity, while electron withdrawing groups lower the efficiency of the methylation reaction. Even so, yields of up to 95% were obtained. Furthermore, the very characteristic spectroscopic profiles of *N*-methylated porphyrins in both NMR and UV-vis spectroscopy were investigated, showcasing the correlation between the chemical and bathochromic shifts and the structural conformation of the porphyrins synthesized. Comparison of X-ray structures of porphyrins synthesized and literature known structures of the planar free base and nonplanar *N*-substituted porphyrins revealed that, from a structural point of view, *N*-methylation of planar porphyrins results in significant structural changes and a notable macrocycle distortion resulting in a similar distortion to that of a highly substituted porphyrin. NSD was successfully applied to all structures and used to determine the

distortion modes in porphyrin structures with an increasing number of *N*-substitutents.

Finally, the porphyrins synthesized in the previous chapters were tested for their catalytic activity. A sulfa-Michael addition reaction was selected as the catalytic test reaction of choice. Initial screening reactions were undertaken using the N^{21}-monomethylated tetraphenylporphyrin. As some conversion to desired target compound was observed during the initial reaction conditions (9%), optimizations of parameters such as; solvent, catalyst loading, concentration of the reaction, etc. were explored in order to achieve better yields and to establish standard reaction conditions to then reliably screen a panel of porphyrins. Screening of the porphyrin libraries revealed that in order for free base porphyrins to be catalytically active they require a) a high distortion of the macrocycle, b) an electron rich density of the porphyrin core and c) the availability of the amine and imine moieties. Considering these requirements, up to quantitative yields were achieved with some candidates of the prepared porphyrin library. Furthermore the mechanism of the porphyrin catalyst was explored. The initial results suggested a bifunctional catalytic activation of both the Michael acceptor and the nucleophile, with the monoprotonated porphyrin being the catalytically active species during the process. In order to confirm this mode of action, different spectroscopic studies were undertaken such as protonation studies of the porphyrin catalysts and activation studies of the electrophile. Further investigation of a range of different electrophiles were carried out in order to test the sensitivity of the catalysts. All electrophiles tested gave positive results with very high conversion up to quantitative yields. The most active catalyst in the Michael addition reactions was then trialled as a possible catalyst in Aldol and Diels-Alder reaction. Unfortunately, no activity was observed. In order to explore the role of basicity of the macrocycle further two families of catalysts with very high distortion and very strong electron donating groups were screened for their catalytic activity. It was revealed that these so-called “super bases” were not catalytically active anymore. At a certain point, the increased basicity of the porphyrin macrocycle resulted in inactivation of the porphyrin in the present conditions established, due to the instant protonation of the porphyrin by the acidity of the solvent. Thus, careful considerations and design of the porphyrin macrocycle are quintessential when using free base porphyrins as catalysts.

PUBLICATIONS

- **M. Roucan**, M. Kielmann, S. J. Connon, S. S. R. Berhnard, M. O. Senge, Conformational control of nonplanar free base porphyrins: Towards bifunctional catalysts of tunable basicity, *Chem. Comm.* **2018**, *54*, 26–29.
- **Cover Picture:** Conformational control of nonplanar free base porphyrins: Towards bifunctional catalysts of tunable basicity, *Chem. Comm.* **2018**, *54*, 1–1.

- **M. Roucan**, K. J. Flanagan, J. E. O'Brien, M. O. Senge, Nonplanar Porphyrins by *N*-Substitution: A Neglected Pathway, *Eur. J. Org. Chem.*, **2018**, *46*, 1518–1541.
- **Cover Picture** Nonplanar Porphyrins by *N*-Substitution: A Neglected Pathway, *Eur. J. Org. Chem.*, **2018**, *46*, 6388–6388.

Note on publications:

Chapter 4 contains details from paper 2

Chapter 5 contains details from paper 1

CONFERENCE ABSTRACTS

Poster:

- G. Locke, **M. Roucan**, S. Plunkett and M. O. Senge, “Functionalization of cubane scaffolds-Towards the use of cubane as a rigid linker in energy transfer compounds” in fourteenth Annual Symposium of the Centre for Synthesis and Chemical Biology (11.12.15), Royal College of Surgeons, Dublin, Ireland.

- **M. Roucan** and M. O. Senge, “Synthesis and functionalization methods for unsymmetrically meso-substituted porphyrins and their potential applications” in Tetrapyrrole Discussion Group Meeting (21.03.15 and 22.03.15), Liverpool, England, page 20.

- **M. Roucan**, K. J. Flanagan, T. Do Valle Moreira and M. O. Senge, “Synthesis of *N*-substituted porphyrins and their crystallographic studies”, ORCHEM 2016 congress (from 05.09.16-07.09.16), Weimar, Germany, Abstract T125.

- **M. Roucan**, K. J. Flanagan, T. Do Valle Moreira and M. O. Senge, “Synthesis of *N*-substituted porphyrins and their crystallographic studies” in fifteenth Annual Symposium of the Centre for Synthesis and Chemical Biology (09.12.16), Trinity College Dublin, Dublin, Ireland, Abstract P28.

- **M. Roucan**, M. Kielmann, S. S. R. Bernhard, S. J. Connon, M. O. Senge, “Bifunctional Organocatalysis Using Free Base and *N*-substituted Porphyrins”, GDCh-Wissenschaftsforum Chemie (10.09.17-14.09.17), Berlin, Germany, Poster ORG 058, abstract-ID: 7210_14224.

- **M. Roucan**, M. O. Senge, “*N*-Substituted Porphyrins”, GDCh-Wissenschaftsforum Chemie (10.09.17-14.09.17), Berlin, Germany, Poster ORG 059, Abstract-ID: 7210_14225.

- **M. Roucan**, M. Kielmann, S. S. R. Bernhard, S. J. Connon, M. O. Senge, “Bifunctional Organocatalysis Using Free Base and *N*-substituted Porphyrins”, Symposium of the Centre for Synthesis and Chemical Biology (12.12.2017), Dublin, Ireland, *Poster and abstract not yet available.*

- **M. Roucan**, M. Kielmann, S. S. R. Bernhard, S. J. Connon, M. O. Senge, “Bifunctional Organocatalysis Using Free Base and *N*-substituted Porphyrins”, ICPP-10 (01.07.18-06.07.2018), Munich, Germany, Poster S25-P-009.

- **M. Roucan**, K. J. Flanagan, J. O'Brien, M. O. Senge, "*N*-Substitution: the Neglected Path to Nonplanar Porphyrins", ICPP-10 (01.07.18-06.07.18), Munich, Germany, Poster S05-P-016.

- **M. Roucan**, K. J. Flanagan, J. O'Brien, M. O. Senge, "*N*-Substituted Porphyrins: crystal structure and application " in Symposium of the Centre for Synthesis and Chemical Biology (07.12.18), Royal College of Surgeons, Dublin, Ireland, Poster 054, abstract not available.

- **M. Roucan**, M. Kielmann, S. S. R. Bernhard, S. J. Connon, M. O. Senge, "Bifunctional Organocatalysis Using Free Base Nonplanar Porphyrins" in GDCh-Wissenschaftsforum Chemie (15.09.19-19.09.19), Aachen, Germany, Poster ORG 015, abstract-ID: 8454_21896.

Oral presentations:

- **M. Roucan** and M. O. Senge, "Synthesis of Highly Distorted Porphyrins Towards Their Use as Organocatalysts" in Third years talk, (23.06.18), Trinity College Dublin, Ireland.

- **M. Roucan** and M. O. Senge, "Bifunctional Organocatalysis Using Free Base Nonplanar Porphyrins" Poster-Flashtalk in the session "Young Chemist – The Collective" (16.09.2019) Aachen, Germany.

ACKNOWLEDGEMENTS

It is going to be difficult to acknowledge every people who made this whole experience possible but also as great as it was. This has been a wonderful adventure in term of learning, friendship and discovery.

First and foremost, I would like to thank my supervisor, Prof. Dr. Mathias O. Senge for giving me the opportunity to work in his research group and for having been given the chance to explore the vaste and interesting field of porphyrins, to discover their various facette and to improve my knowledge, competence and personal skills. But more importantly, I am truly grateful for his countless advices, his constant support and kindness during the all four years of my Ph.D.

On a second note I would like to thank all the Senge group members which over the four years have changed and evolved with members who left to give place to the new ones, but never lost its welcoming, friendly and funny spirit. This thanks goes to all my co-workers and friends, Alina Meindl, Jessica O'Brien, Keith Flanagan, Gemma Locke, Marc Kielmann, Susan Callaghan, Karolis Norvaiša, Elisabeth Sitte, Dáire Gibbons, Harry Sample, Piotr Gierlich, Zoi Melissari, Bhavya Khurana with whom I spend four exquisite years. I will cherish all memories, laugh and great moments we had together. A special thanks to the postdocs of the group Stefan Bernhard, Nitika Grover, Ganapathi Emandi and Mickail Filatov for their advice, their patience and their kindness. More special thanks you to Nitika, Alina and Keith for proof reading this thesis.

A special thanks to my collaborator Prof. Stephen Connon for his expertise on organocatalysis chemistry and his input and suggestions regarding this project. Working with him was a rewarding experience. I am also grateful to Dr. John O'Brien and Dr. Manuel Ruether for their help during the NMR characterization of my compounds. This has been some very nice conversation toward the understanding of the bizar spectrum obtain. Thank you for your many advices and also technical support.

To finish, I would also like to thanks Dr. Nathalie Solladie and Dr. Regis Rein, my master degree supervisors, for introducing me to Prof. Dr. M. O. Senge and to the fascinating field of which made this all adventure possible.

Finally, I would like to thank all the people who I had the chance to meet during my time as a postgraduate student in Trinity College Dublin. I had the opportunity to meet fascinating people and I will keep a very warm and positive filling about this all life experience that has been to do my Ph.D. in the Senge group in Dublin.

“There are no strangers here; Only friends who have not yet met.”

W. B. Yeats (1865–1939)

Je dédie cette thèse:

A mes parents Nicole et Jacques, qui m'ont toujours poussée à donner le meilleur de moi-même et à accomplir mes aspirations. Un grand merci à eux qui sont une source inépuisable de tendresse, de patience et de sacrifice.

A mon frère Julien, pour son aide, son soutien, ses encouragements et son sens de l'humour qui m'ont permise de tenir bon dans les moments les plus dures.

A Raphaël, qui m'a accompagnée dans cette expérience, qui a partagé mes peines et mes joies, qui m'a écoutée, conseillée et épaulée jusqu'à la fin.

Ce travail représente le fruit de vos sacrifices, de vos peines et de tous vos efforts. Vous serez toujours un exemple pour moi par votre persévérance et par vos qualités humaines.

A tous les autres membres de ma famille, avec qui j'ai la chance de partager des liens très forts; et pour finir à tous mes amis proches.

Je ne saurai exprimer ma grande affection et ma profonde reconnaissance pour votre soutien dans ce projet qui me tenait à cœur. Un immense merci à vous tous.

LIST OF ABBREVIATIONS

Å	Ångström
Ar.	Argon
Ar	Aryl
BINOL	1,1'-Bi-2-naphthol
BINAP	2,2'-Bis(diphenylphosphino)-1,1'-binaphthyl
Cat.	Catalyst
^{13}C NMR	Carbon NMR
Conv;	Conversion
δ	Chemical shift
Δ24	Average deviation from the 24-atom mean-plane (of the porphyrin)
ΔN	Simulated displacement of the four internal nitrogen atoms from the 24-atom mean-plane
Δoop	Simulated total out-of-plane distortion
d	Doublet
d.	Days
DBU	1,8-Diazabicyclo(5.4.0)undec-7-ene
dd	Doublet of doublet
DDQ	2,3-Dichloro-5,6-dicyano-1,4-benzoquinone
DMAP	4-Dimethylaminopyridine
DMF	Dimethylformamide
EDG	Electron donating group
ee.	Enantiomeric excess
eq.	Equivalents
Et	Ethyl
EtOAc	Ethyl acetate
EWG	Electron withdrawing group
h	Hours
^{1}H NMR	Proton NMR
HRMS	High resolution mass spectrometry
IR	Infrared
J	Coupling constant

λ	Wavelength
m	Multiplet
m-	Meta
M	Molar (mol/L)
MALDI	Matrix assisted laser desorption ionization
MeOH	Methanol
Me	Methyl
min	Minutes
mol%	Mole percent
m.p.	Melting point
MS	Mass spectrometry
NEt_3	Triethylamine
NMe_2	Dimethylamino
NMR	Nuclear magnetic resonance
NSD	Normal-coordinate structural decomposition
OMe	Methoxy
o-	*ortho*
p-	*para*
Ph	Phenyl
pK_a	Acidity constant
porph.	Porphyrin
ppm	Parts per million
q	Quartet
Quant.	Quantitative
R_f	Retention factor
r.t.	Room temperature
s	Singlet
S_NAr	Nucleophilic aromatic substitution
t	Triplet or time
*t*Bu	*tert*-Butyl
TEBA	Benzyltriethylammonium chloride
Temp.	Temperature
TFA	Trifluoroacetic acid

THF	Tetrahydrofuran
TLC	Thin layer chromatography
UV-vis	Ultraviolet-visible spectroscopy
% *v:v*	Volume percent
v:v	volume-to-volume ratio

TABLE OF CONTENTS

1 General Introduction

1.1 Porphyrins in nature

In nature, porphyrins and their derivatives, also known as the “pigments of life”, are systems which are essential for many life processes in animals, plants or even bacteria.[1] The term porphyrin comes from the Greek word “porphyria” meaning purple and relates to their specific coloration. When first isolated from blood in 1867 by Thudichun,[2] interest into porphyrin chemistry and their analogs drastically increased. They can be used as ligands for the complexation of various metal ions but are also encountered as “free base” porphyrins when they are not binding any metals.[3] The former are at the center of many important natural reactions. When chelating iron, they ensure the transport of oxygen in the body (heme in blood), complexing a magnesium ion, they form the chlorophyll complexes and are involved in the photosynthetic mechanism (chlorophyll in plants).[3d, 4] They also play an important role as cofactors for a plethora of biologically essential reactions, such as the decomposition of H_2O_2 (catalase and peroxidase) or metabolism of xenobiotics (cytochrome P450 enzymes).[4] As an example, the insertion of iron into protoporphyrin IX to form Heme b **1** (Fig. 1) requires the enzymatic attack of ferrochelatase, which results in distortion of the macrocycle through temporary binding of the enzyme to protoporphyrin IX, allowing the insertion of iron into the cavity.[5]

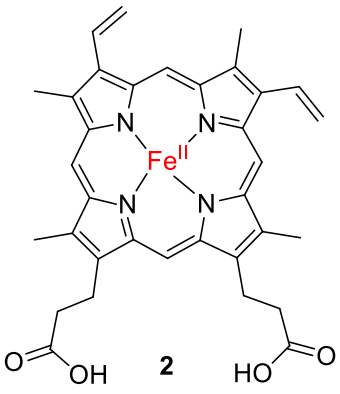

Heme *b*
Iron protoporphyrin IX

Figure 1: Structure of the heme b **1**.

1.2 Structure of porphyrins

From a structural point of view, porphyrins are tetrapyrrolic compounds containing four pyrrole units linked by methine bridges.[6,7] The macrocycle comprises 20 carbon atoms (positions 1–20) and four nitrogen atoms (positions 21–24). This porphyrinic skeleton, first proposed by Küster in 1912,[8] is presented in Fig. 2. Within the 22 π-electron system

of the macrocycle, 18 are part of the delocalized system, classifying it as an aromatic system (4n+2) in terms of Hückel's rule, with 22 π-electrons in total.

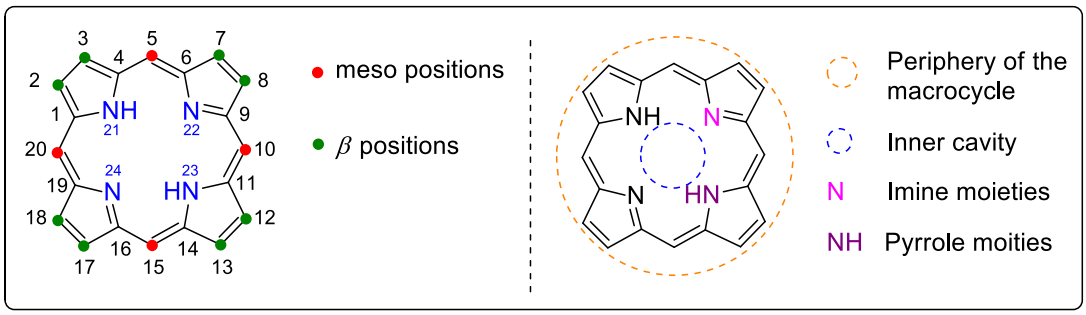

Figure 2: Nomenclature of porphyrins.

A panel of extensively studied derivatives such as chlorins, isobacteriochlorins, and bacteriochlorins (Fig. 3) can be formed by reductions of one or two double bonds within the macrocycle.[9] Porphyrins can also host a metal in their cavity, resulting in metalloporphyrins which represent the class of porphyrins used in all natural enzymatic reactions. Natural free base porphyrins are intermediates used in nature for the formation of these so called "metalloporphyrins".

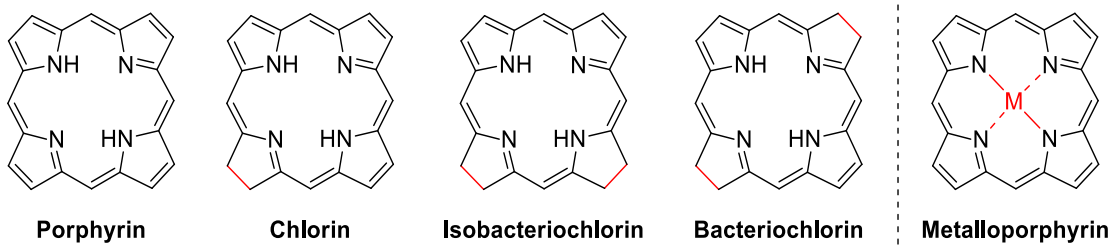

Figure 3: Various analogs of the porphyrin structure.

Furthermore, tuning of the porphyrin macrocycle can also be achieved by introducing various groups at the meso- and *β*-positions of the porphyrin. However, due to the important aromaticity, these positions are highly reactive and can undergo a wide range of reactions such as substitution, nitration, acylation, etc.[10] Consequently, a range of various designs and substitution patterns can be found in nature, as well as synthetically, depending on the number, type and position of the substituted units. Mainly, they are divided into two sub-categories, which are symmetrical and unsymmetrical porphyrins. In addition, due to the presence of two imine and two pyrrole moieties, the inner core can also be quite reactive allowing for acid/base properties leading to cationic species or complexation with diverse metals as seen in nature.

1.3 Synthesis of porphyrins

The methods utilized to synthesize porphyrins mostly involve condensation of pyrrole and aldehydes (or related building blocks) and all follow a common mechanistic pathway which first creates the tetrapyrrolic macrocycle. This is then followed by the oxidation of the methane bridges resulting in the π-conjugated system.

From a synthetic point of view, symmetrical meso-substituted porphyrins (A_4, **6**) are the most easily synthesized and the first synthetic symmetrical porphyrins were reported in 1935 by Rothemund.[11] His procedure employed the reaction of four pyrrole units with four corresponding aldehyde molecules in MeOH to give various meso-tetrasubstituted porphyrins in low yields (<5%). An optimized procedure for 5,10,15,20-tetraphenylporphyrin (H_2TPP) was developed later by Adler, Longo and co-workers in 1964.[12] The formation of H_2TPP was reported with a yield of about 35–40% in acidic benzene for 1–2 days at high temperature. The use of other acidic conditions leads to the formation of chlorins, hence decreasing the porphyrin yield. However, these conditions demand cumbersome purification processes to give the reported yields. An optimization of the previous condition resulted in a more convenient method for the synthesis of H_2TPP, in a rapid and reproducible manner, affording yields of 20–25 %.[13] Pyrrole and benzaldehyde were reacted in propionic acid for 30 min at 141 °C, leading to a mixture of the porphyrin and the chlorin contaminant (10–20 %). The purification, optimized by Dolphin *et al*. in 1974, resulted in solely the porphyrin as purple crystals through oxidation of the porphyrin/chlorin mixture with 2,3-dichloro-5,6-dicyano-1,4-benzoquinone (DDQ) in refluxing toluene.[14] The chlorin resulting from the reduction of the porphyrin macrocycle is reoxidized by DDQ and simple purification techniques using column chromatography and recrystallization can be used to purify H_2TPP. Today, this method stands out as the most commonly used to synthesize H_2TPP. However, this synthetic pathway can also be utilized to synthesize meso-tetrarylporphyrins. Moreover, it can also be utilized for the synthesis of unsymmetrical meso-tetrakisporphyrins through the use of mixed aldehydes.[15]

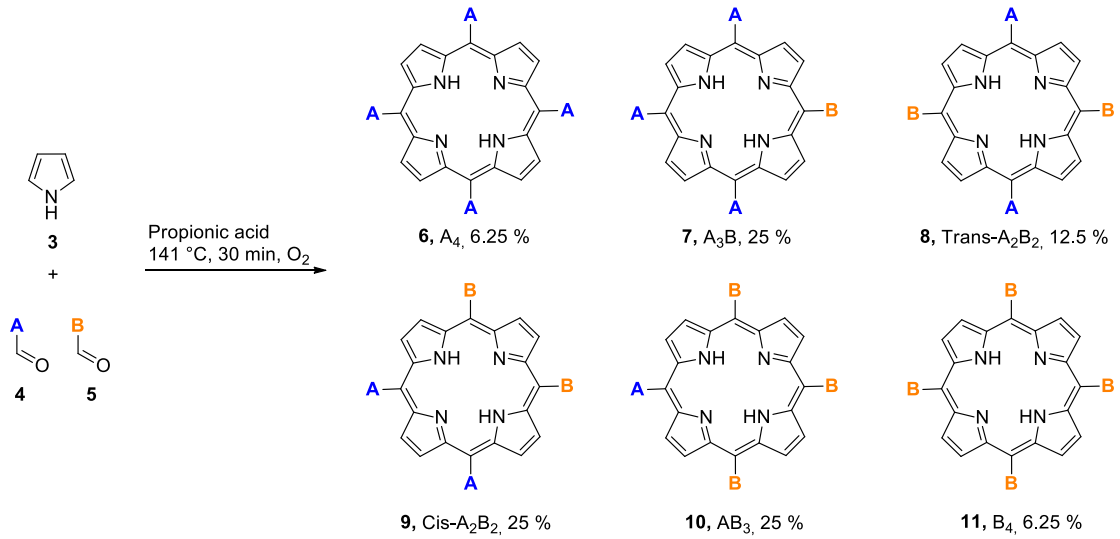

Scheme 1: Products resulting from mixed condensation reaction using conditions developed by Adler-Longo.

In principle, six different porphyrins (**6** to **11**) can be synthesized using condensation of pyrrole with two aldehydes (**4** and **5**, Scheme 1): the two parent porphyrins A_4 **6** and B_4 **11**, and the 4 hybrid porphyrins A_3B **7**, "*cis*"- and "*trans*"-A_2B_2 **8, 9 and** AB_3 **10**, each porphyrin being named depending on their meso substitution pattern. This type of condensation is challenging, mainly due to the tedious purification. However, the interest in these mixed condensations resides in the potential to control the product formation. The statistical expected distribution of each porphyrin is presented in Scheme 1.[16] This distribution can be modified to favor the A_3B pattern by changing the 1:1 ratio of aldehydes. For example, a 3:1 ratio of aldehydes would result in a relative yield of 42.2% for the A_3B porphyrin **7**. However, the formation of the parent porphyrins **6** and **8**–**11** is still observed lowering the experimental yield of porphyrin A_3B **7** to 10–16% yield.[16,17]

Even though the Adler-Longo method gives rapid and facile access to a range of meso-tetrasubstituted porphyrins, it only allows for the use of certain robust aldehydes. Consequently, a more general method was developed by Lindsey and co-workers for the synthesis of a wide variety of porphyrins in 35–55% yields (Scheme 2).[18] In this case, milder reaction conditions are employed, using Lewis acids as catalysts, to activate the reaction between the pyrrole and the aldehyde units. This reaction is performed in more dilute conditions (10^{-2} M) at room temperature in dichloromethane. Anhydrous conditions in the absence of any trace of oxygen are required to form the thermodynamic product, the porphyrinogen (as opposed to the Adler-Longo method were the porphyrinogen is oxidized by air directly after its formation). This allows for the use of acid labile aldehydes, which was previously impossible.

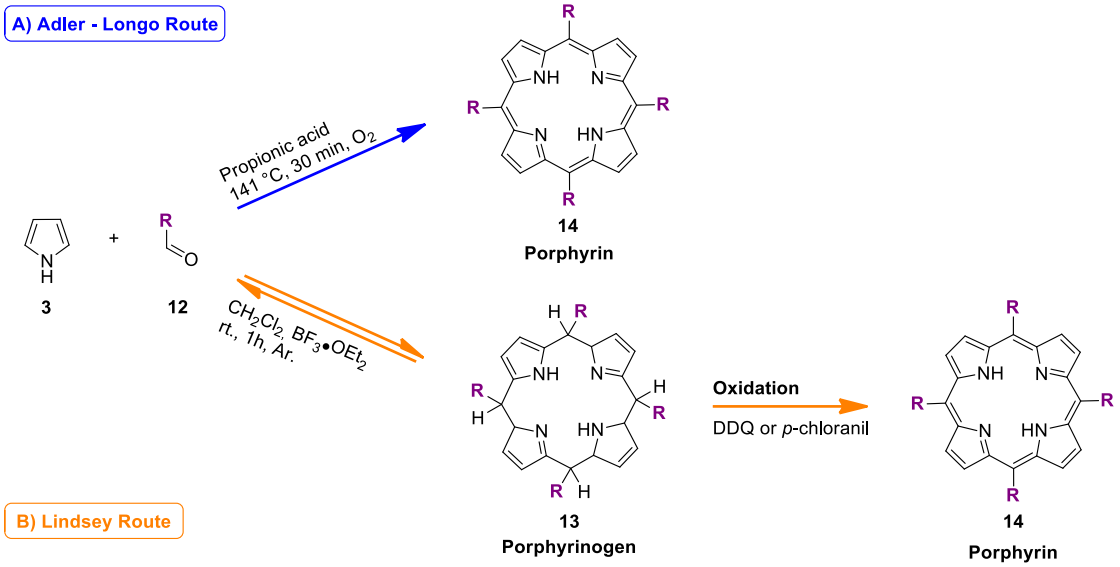

Scheme 2: Comparison of two common condensation reactions methods: A) Adler-Longo and B) Lindsey condensation reaction conditions.

The porphyrinogen is the intermediate formed by the electrophilic substitution of the pyrrole by the aldehyde after the ring closure. This is then followed by oxidation using DDQ or *p*-chloranil (Scheme 2), forming the typical π-conjugated system of porphyrins.

So far, the condensation pathways presented are based on the reaction between pyrrole units and an equimolar ratio of aldehydes. The use of mixed condensation reactions allows for the formation of unsymmetrical porphyrins. However, this results in many unwanted porphyrin side products (Scheme 1), lowering the overall yield of the desired porphyrin. Other routes were then developed allowing the generation of mixed meso-substituted porphyrins in higher yields. These methods are generally based on the coupling of di- or tripyrrolic intermediates such as dipyrromethane or tripyrrane moieties. These moieties are synthesized in a manner similar to porphyrins, using adaptations of the Lindsey condensation procedure between either two or three pyrrolic units with an aldehyde pattern under acidic conditions.[19] The dipyrromethane units allow for the formation of "*trans*"-A_2, "*trans*"-A_2B_2 or A_1 porphyrins, while "*cis*"-A_2 or "*cis*"-A_2B_2 porphyrins (Scheme 3) are accessible *via* reactions with tripyrrane. The reaction for each structure is then based on the same conditions developed by Lindsey.[18] However, the ratio of the different reactants plays a crucial role in the formation of the final product.

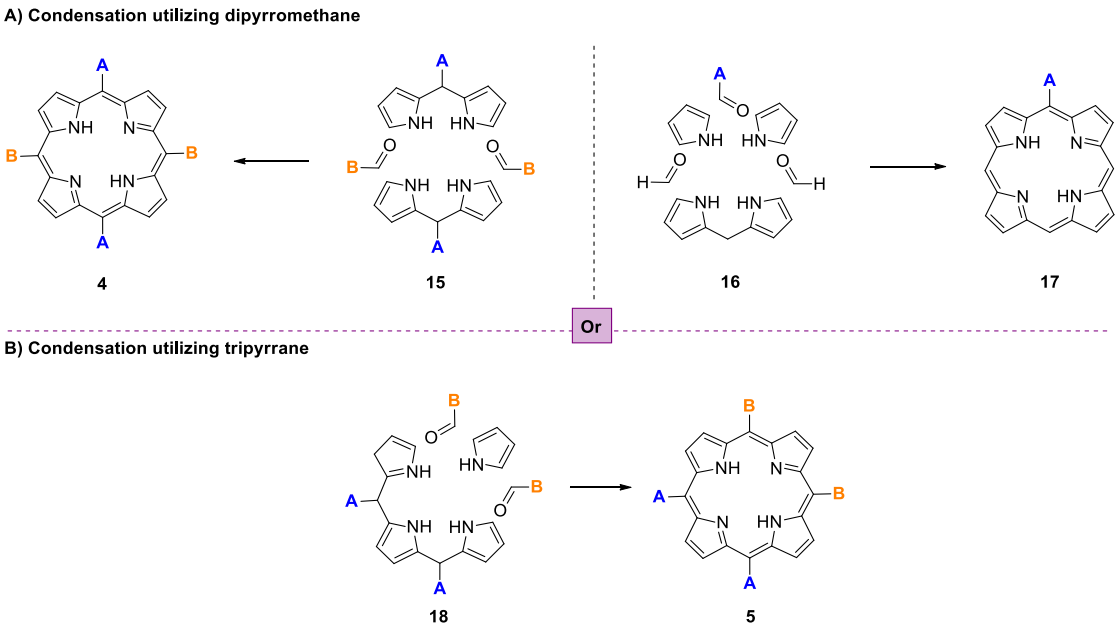

Scheme 3: Routes for unsymmetrical porphyrins. using A) dipyrromethane **15** or **16** and B) tripyrrane **18**.

A condensation reaction using a 2:2 ratio of dipyrromethane **15** units and various aldehydes leads to the formation of "*trans*"-A_2B_2 porphyrins **4**.[20] The reaction of one equivalent of dipyrromethane **16** and two equivalents of pyrrole and one equivalent of aldehyde results in the formation of the A-type porphyrin structure **17**.[21] Reports showed that yields from 30–40% could be obtained using Adler-Longo conditions.[22] The simple change in the oxidant from air[23] to quinone derivatives (p-chloranil or DDQ) led to an increase in yields to 72–93%.[23] Addition of an equivalent of tripyrrane **18** to a 2:1 ratio of aldehyde and pyrrole results in the formation of the "*cis*"-A_2B_2 porphyrins **5** (Scheme 2).[13,24] Consequently, a range of different structures can be obtained through the use of various aldehydes and deliberate design of the dipyrromethane **15** and tripyrrane **18** intermediates.

1.4 Biomimetic systems

Porphyrins, as mentioned previously, are at the center of a plethora of biological processes. These tetrapyrolic scaffolds are often tightly linked to proteins and the activity of these chromophore-protein systems resides in the tetrapyrrolic metal complex.[4] This metal complex is formed by chelation of a metal into the inner cavity of the chromophore. For example, in hemoglobin, iron(II) is inserted into the cavity of protoporphyrin IX resulting in an iron(II)protoporphyrin IX complex which is bound to a globin protein.[5] These hemoprotein type complexes are common examples of systems which show a wide range of indispensable functions such as oxygen storage and transport, gas

sensing, electron transfer, catalysis, or even gene regulation.[25] The multiple functions of the same cofactor resides in the effects of its various coordinations modes with the protein such as axial coordination: *e.g.*, heme a in cytochrome c oxidase, heme b in hemoglobin and myoglobin, or covalent linkage to proteins: *e.g.*, heme c in cytochrome c.[26] These factors influence the physicochemical properties resulting in various binding modes and thus, different natural functions of the same cofactor (*e.g.*, fine-tuning of reduction potentials over a wide range,[27] robustness,[28] interaction with proximal amino acids, metal-ligand interactions, metal spin state[29] and oxidation state.[30]) Consequently, nature gave the most thorough example of how molecular engineering of porphyrins and their binding modes drastically impacts their functions. Numerous tetrapyrroles were used to study the biological role of nonplanar macrocycle conformation[31] and their conformational control in enzymes.[32]

“Picket fence” porphyrins are a classical example of designer porphyrins capable of mimicking natural process.[33] More specifically, these sytems are well-known to be good analogs to understand the reversible oxygen binding process of hemoglobin. Hemoglobin is the most common carrier molecule for oxygen.[34] Its structure consists of a five-coordinated Fe(II) metal inserted in a protoporphyrin IX ligand and stabilized by proximal and distal histidine residues from the globin.[35] The proximal histidine stabilizes the system by acting as an axial ligand for the iron ion, while the distal histidine groups stabilize the oxygen binding by a hydrogen bonding interaction with the oxygen atoms. These two residues represent key units in the hemoglobin function (Fig. 4). These proteins have a very complex structure and their roles have been difficult to study,[36] although good advances have been made using synthetically designed Fe(II)porphyrins as biomimetic molecules.[37] However, the use of simple iron(II)porphyrins showed their incapacity to reversibly bind oxygen. The binding of the oxygen to the iron center, forming an oxy-iron(II) center, is immediately followed by the attack of a second iron(II) center. This subsequently results in the formation of a bridged oxo-bisiron(III) complex in which the oxygen is irreversibly bound to the iron(III) center.[38] The study of natural iron(II)porphyrins proved that the reactivity between the iron centers is not observed. Therefore, a major role of the protein consists in the protection of these reactive centers by encapsulating the chromophore.[36a],

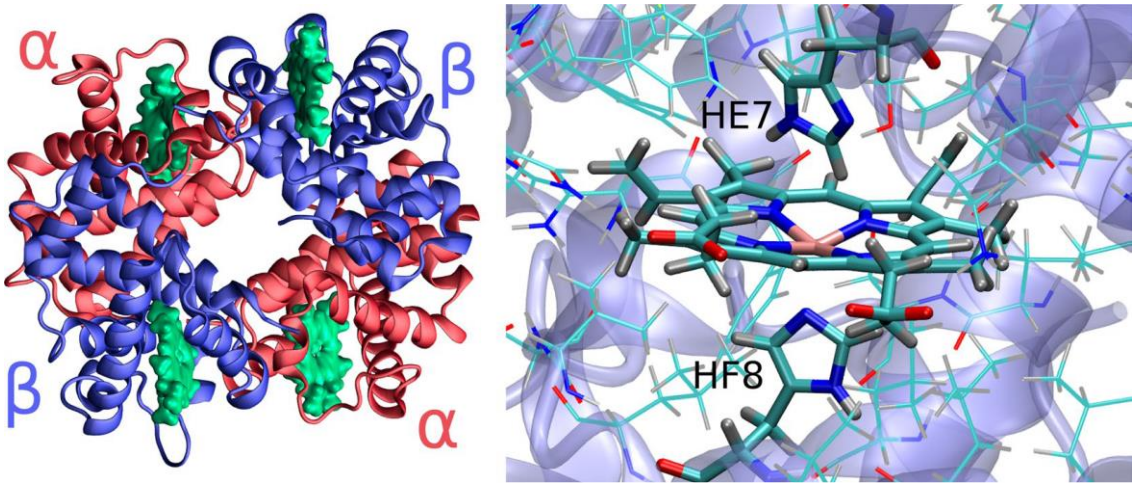

Figure 4: Hemoglobin structure on the left. Schematic representation of hemoglobin heme environment, highlighting both proximal and distal histidines, on the right.[34d]

Considering the problematic reactivity of a simple iron(II)porphyrin complex, the first "picket fence" porphyrin **19** was developed by Collmann (Fig. 5).[33a] This model represents one of the most successful systems and allowed an understanding and mimicking of the heme protein active site. His model prevents the reaction of the iron center by shielding the inner cavity of the porphyrin with four pivalamido groups located on the same side of the porphyrin (Fig. 5). The presence of these large units results in the formation of a pocket where the iron and oxygen species are buried. As in nature, the metal complex of the picket fence porphyrin was also stabilized by imidazole analogs on the unhindered side of the molecule.

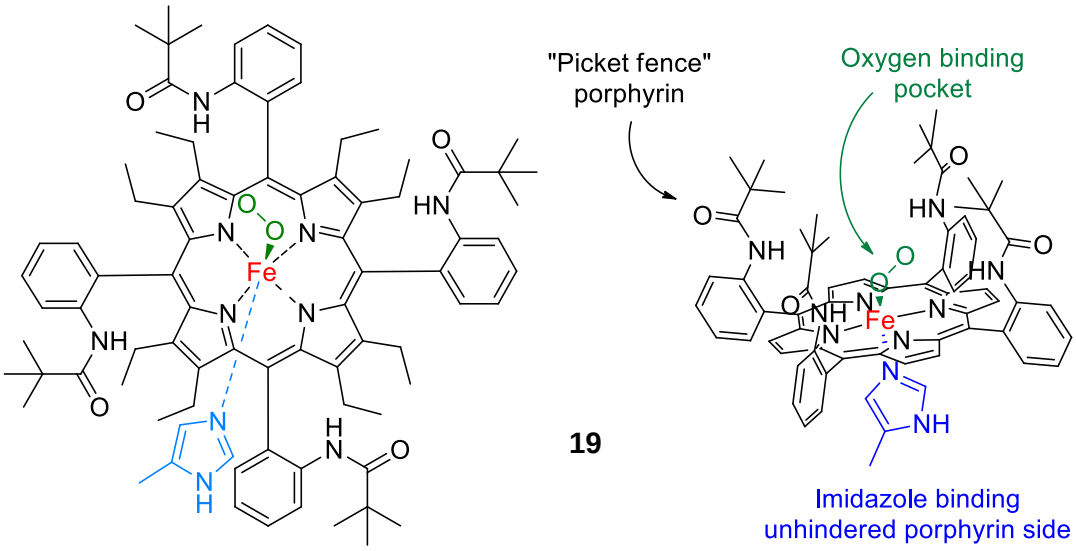

Figure 5: Schematic structure of the first picket fence porphyrin developed by J. Collman.[33a]

This approach of shielding one side of the chromophore has been investigated by many groups and has produced a wide variety of architecturally designed porphyrins other than “picket-fence”, *e.g.*, capped, crowned, strapped, or basket-handle.[39]

1.5 Nonplanar porphyrins as biomimetics

1.5.1 Concept

Natural and synthetical studies have shown that critical requirements of biological systems reside on the tight interaction between the bound chromophore and its protein as well as hydrogen bonding and electronic interactions. In addition, the nonplanarity of tetrapyrrole systems and the influence of the various conformations on their physicochemical properties is well established.[40]. Consequently, the various functions of an identical chromophore in nature have been linked to the diverse conformations the tetrapyrrolic pigment can adopt.[40a-c] In addition, a statistical study on the protein structural data of a bacteriochlorophyll, reported by Senge *et al*., support this principle.[41] The analysis gave convincing proof that the chemical role of various chromophores of the reaction center are influenced by the diverse conformation they display. A fine tuning of the cofactor properties can then be achieved *via* modulation of the tetrapyrrole conformation and thus, the same cofactor may present different functions.

The idea of nature using the flexibility of the macrocycle of porphyrins to facilitate interactions during natural reactions led to a significant development of conformationally designed systems.[42] Researchers have been focusing their attention on various synthetic methods to distort porphyrin structures.[43] An article in Chemical Communications, as well as a chapter in The Porphyrin Handbook, written by Prof. Dr. Mathias O. Senge, highlights every possible way of introducing conformational modifications to porphyrins (Fig. 6).[40a,44]

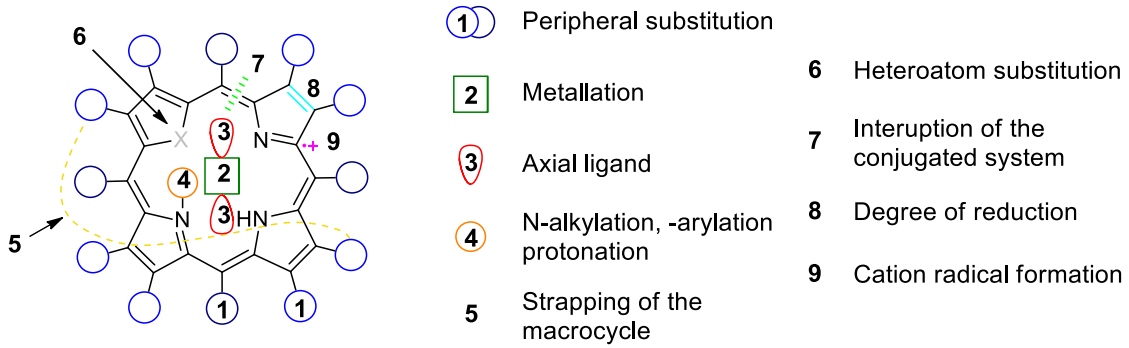

Figure 6: Possible modifications of the porphyrin macrocycle resulting in conformational changes.

At first, research investigations were directed toward metalloporphyrins to reproduce natural processes. The cavity, having a limited size, cannot accommodate large metals or, in an opposite manner, very small metals do not fit properly into the cavity. Thus, the macrocycle needs to reshape itself in order to bind to the metal.[45] The first experimental nonplanar porphyrin was introduced by E. B. Fleischer in 1963 using the reaction of H_2TPP **2** with various metal salts in order to prepare the metallated porphyrin.[46] Copper (Cu(II)TPP), palladium Pd(II)TPP, zinc Zn(II)TPP and iron Fe(II)TPP were used and illustrated the high macrocycle distortion obtained with copper and palladium compared to the planar structures seen with iron and zinc.

Alongside the insertion of small or large metal ions,[47] distorted tetrapyrrolic scaffolds can also be achieved by protonation of the macrocycle,[48] high peripheral substitution,[42b,c] or the insertion of bulky groups to the nitrogen atoms within the cavity.[49] The protonation and deprotonation relies on the acid-base properties of the macrocycle.[50] The reaction of the two imine moieties with an acid allows the formation of the mono- and dicationic forms. Conversely, the reaction of the porphyrin with strong bases can result in the loss of the two pyrrolic protons, forming the mono- and dianionic forms. The loss or gain of protons allows the formation of ionic bonds with the counter ions.[50] Peripheral substitution, on the other hand, will result in a crowded periphery of the macrocycle, which will force the macrocycle to reshape its structure in order to achieve a stable and lowest energy conformation. The core substitution is based on a similar concept; here, the substitution of groups causing the distortion is directed towards the inner cavity.[49] The size of the cavity does not allow for the incorporation of larger groups. Thus, the presence of groups, such as alkyl or aryl, will lead to a distortion of the macrocycle. In the two last cases, distortion is a result of the steric strain induced by the addition of a bulky substituent. The use of the methods introduced in Fig. 6 induces distortion and generates various conformational patterns with small to high distortion. Classical examples of the steric hindrance caused by peripheral or core substitution are shown in Fig. 7: 2,3,5,7,8,10,12,13,15,17,18,20-dodecaphenylporphyrins H_2DPP **20**,[51] 2,3,7,8,12,13,17,18-octaethyl-5,10,15,20-tetraphenylporphyrin H_2OETPP **21**,[43d] 5,10,15,20-tetra-(*tert*-butyl)porphyrin H_2T*t*BuP **22**,[48b,52] and N^{21},N^{22},N^{23}-trimethyl-5,10,15,20-tetraphenylporphyrin trifluoromethane sulfonate salt **23**.[53]

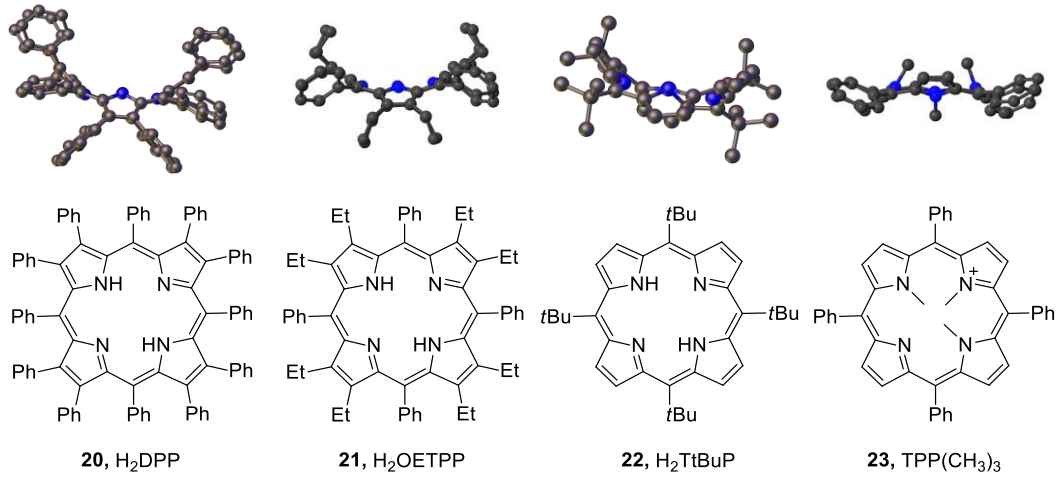

Figure 7: X-ray crystal structures of common nonplanar porphyrins.

The substitution of the macrocycle periphery (highly substituted porphyrins) is a simple means to achieve nonplanarity. Highly substituted porphyrins represent a family of porphyrins that bear substituents on both the meso- and *β*-positions. Their synthesis is based on a condensation reaction between a tailored pyrrole (substituent at positions 3 and 4) and an aldehyde using modified Lindsey conditions.[54] The asset of these compounds resides in the potential control over their nonplanarity introduced by the incorporation of groups at the *β*-positions. Depending on the number of peripheral substitutents, the degree of substitution can vary from slightly distorted to highly distorted porphyrins, with the highest degree of substitution being seen for the dodecasubstituted macrocycle. Medforth *et al*. also showed that conformational control can be achieved and fortified his argument using a series of porphyrins substituted with cycloalkenyl groups of various sizes at the *β*-positions.[55]

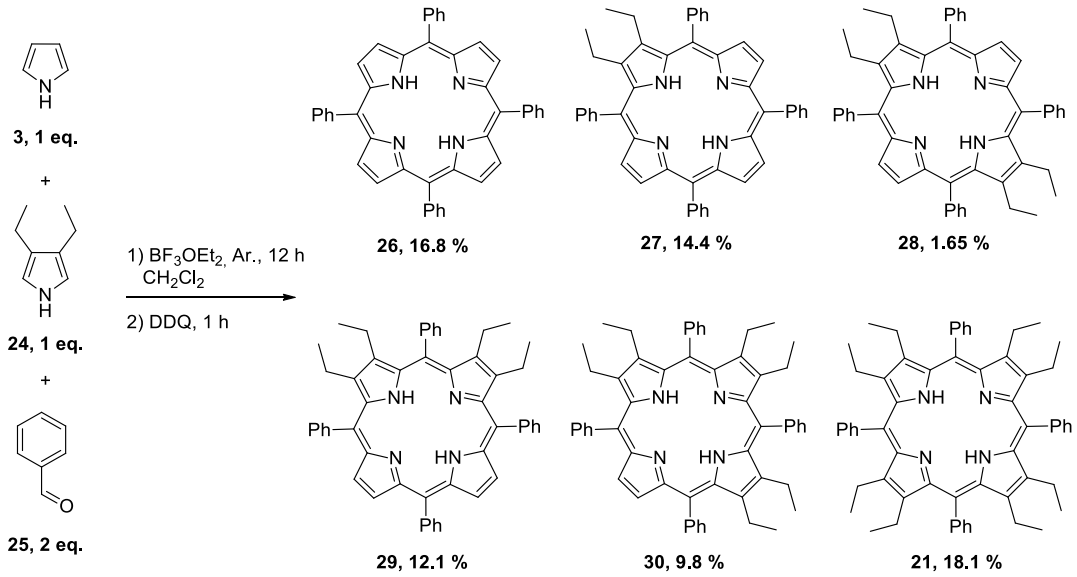

Scheme 4: Mixed condensation reaction conditions for the EtxTPP series.

In 1997, Senge *et al.* reported the synthesis of an EtxTPP series where x represents the number of ethyl groups present in the structure as shown in Scheme 4.[42b, 56] The study aimed to illustrate the various degrees of conformation obtained using porphyrins with graded numbers of ethyl groups at *β*-positions. This study also illustrates the change in spectroscopic properties (*i.e.*, bathochromic shift) with increasing distortion. Analysis of the UV-vis spectroscopy showed an increasing red-shift and broadening of the Soret bands upon increasing addition of ethyl groups. This, alongside the X-ray structural studies, shows that the increase in distortion of the compounds can be ordered as follows: H_2TPP **26** < H_2DETPP **27** < H_2tTETPP **28** < H_2cTETPP **29** < H_2HETPP **30** < H_2OETPP **21** (Fig. 8).

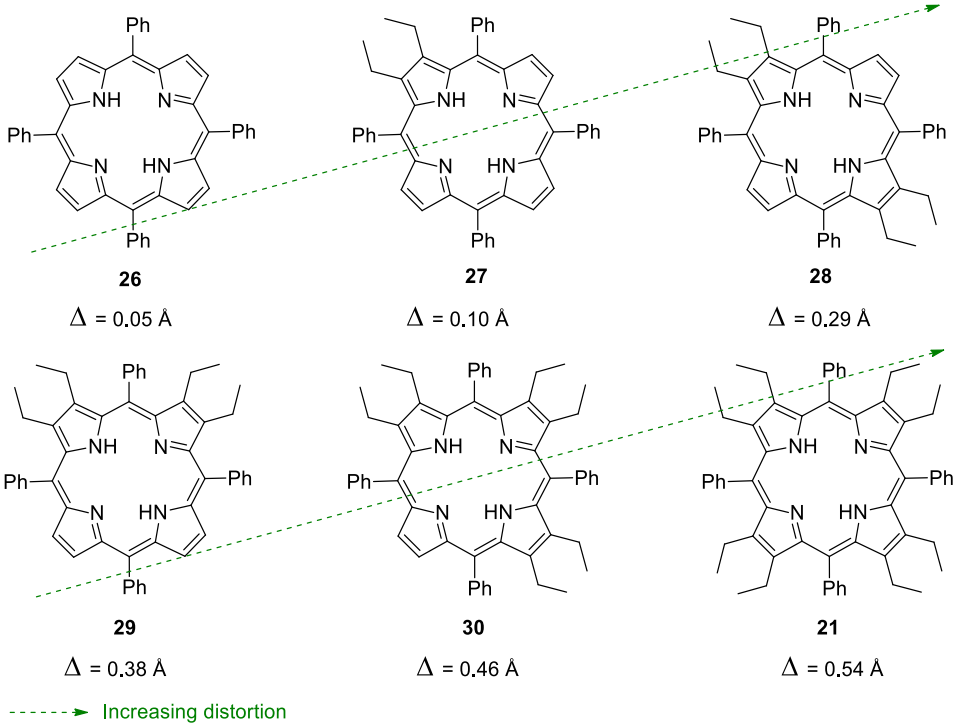

Figure 8: Various degrees of substitution on *β*-positions and their respective degree of distortion represented by the deviation from the 24-atom mean square plane (*Δ*24).

From compound **26** to **30** and then to compound **21** (Fig. 8), an increasing nonplanarity can be measured. The distortion starts with the introduction of the two first ethyl groups at the *β*-position and is further increased upon the introduction of additional *β*-ethyl units. This study gave a major boost to the synthesis and structural elucidation of many highly substituted systems, especially towards biomimetic studies.[1,44] A comparative study between H_2TPP **26** and H_2OETPP **21** (Fig. 9) showed that for the highest distortion, compound **21**, the central NHs are pushed out-of-plane, while repulsive *peri*-interactions are seen between neighboring meso- and *β*-units. An angle of 30° is measured between the plane and the pyrrole units as these units are alternatively pushed up and down,

resulting in a *sad*-distortion mode associated with the distortion obtained by a crowded periphery of the macrocycle.[57]

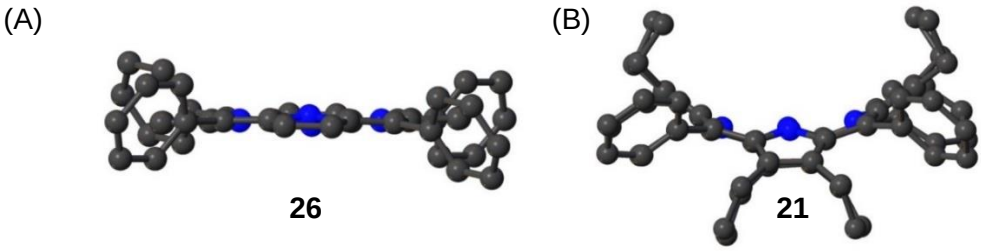

Figure 9: Comparison of the difference in distortion between the planar H_2TPP **26** (A) and the highly substituted H_2OETPP **21** (B), in the X-ray crystal structures. [57c,58] Hydrogen atoms have been omitted for clarity.

The nonplanarity observed in dodecasubstituted system **21** induces various changes to the properties of the macrocycle, such as an increase in positive charge on the nitrogen atoms, a better interaction with small molecules (stronger *N*-H bonding),[44,59] enhancement of their reactivity toward metals, a higher basicity,[50] an alteration of their photochemical properties and exited state dynamics,[44] oxidation potentials[60] or axial ligands affinities.[57a,61]

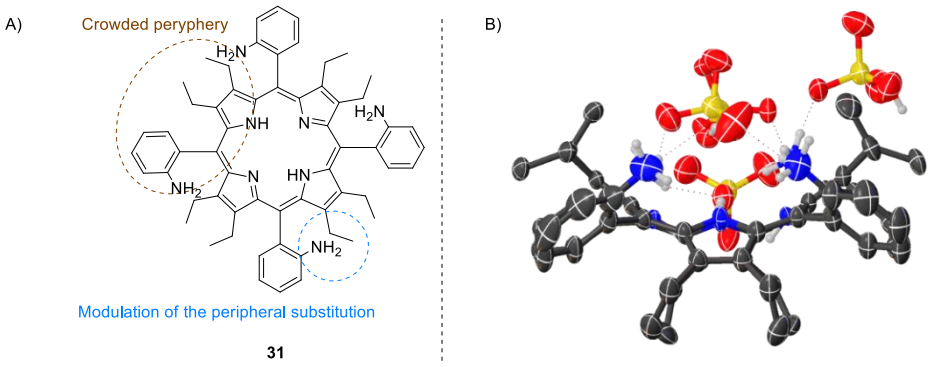

Figure 10: A) Possible modulation of the periphery of the macrocycle for improvement of the binding affinities. B) X-ray structure of 2,3,7,8,12,13,17,18-octaethyl-5,10,15,20-tetrakis(*o*-aminophenyl)porphyrin **31** showing its high binding capabilities.[59]

An alteration of their redox potential as well as their binding properties can also be noted, which can be modulated depending on the type of electronic substituents added to the periphery.[29,57] These nonplanar porphyrins are also more soluble due to the reduced π-stacking effect observed for their planar counterparts.[62] Overcrowding the porphyrin macrocycle will also affect the photophysical[63] and electrochemical properties[64] of the compounds in many ways. In terms of photophysical properties, conformational modulation can influence the (dynamic) photophysical and excited state properties[57c,65]

resulting in lower fluorescence yields, large Stokes shifts and shorter lifetimes of lowest excited states.[65e]

The binding abilities generated by the nonplanarity of the porphyrin results from the formation of cavities on each face of the macrocycle. These cavities allow the incorporation of small molecules, which bind to the inner core systems, such as solvent molecules, but also anions in the case of protonated porphyrins (Fig. 10, B). The development of such systems can be applied to sensing applications. Indeed, upon interaction with metals or small molecules, the change in the porphyrin properties results in a detectable response (color changes, fluorescence quenching, electrical signal). A recent publication from Norvaiša and co-workers illustrates the possibility to detect the switchable binding of analytes by the color change observed (Scheme 5).[60d] The design of porphyrin structures through modification of the nature and number of peripheral substituents results in a modulation of the selectivity and sensitivity towards small molecule binding abilities.

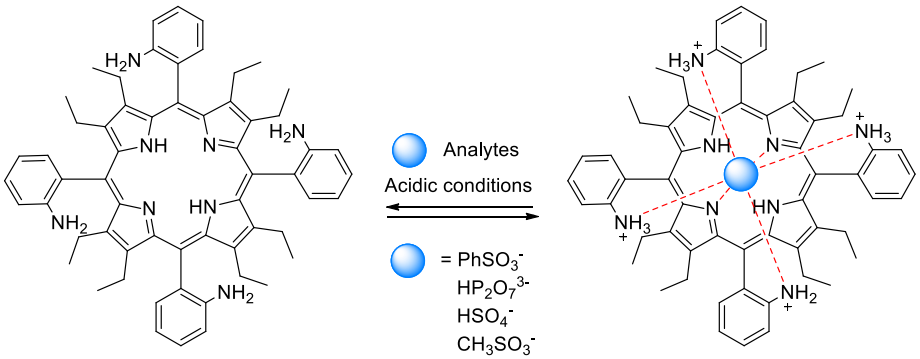

Scheme 5: Schematic representation of the binding of small molecules after *peri*-substitutents modification and conformational modulation of porphyrin **31**.[60d]

1.5.2 Analysis of nonplanar porphyrins

Scientists have always been fascinated by the ability to observe the structure of a molecule at its atomic level. Until 1914, when the first molecular structure (table salt) was determined by X-ray crystallography,[66] there was no specific equipment to show with complete certainty the structure of the compounds synthesized. However, scientists were still able to prove the structure of the products obtained with techniques such as UV-vis or NMR spectroscopy. In the present context, a fascinating concept resides on the fact that changes observed in their spectroscopic properties are closely related to the distortion induced by the fine tuning of the macrocycle. These properties have been widely studied to interpret how the various changes observed can be correlated to the

distortion. These variations in properties imply the possibility to recognize and quantify the resulting distortion. This distortion can be easily quantified using structural characterization techniques such as normal-coordinate structural decomposition (NSD)[27b, 40d, 67] and X-ray diffraction crystallography (XRD).

1.5.2.1 Structural analysis: X-ray and NSD structural analysis

X-ray crystallography is a specific technique based on the diffraction of X-rays by crystalline material. Many organic and inorganic materials can form crystals, thus, XRD drastically helps in advancing various scientific fields. Porphyrins can also form crystalline materials and these techniques have been fundamental to study many biological processes involving porphyrins. XRD analysis of materials is a very useful method to visualize the distortion present in porphyrins, but also to observe the arrangements they can adopt within their environment. This is important as this information can help to interpret their behaviors in solution. Porphyrins are known to form various types of bonding with metals, solvents, ions or small molecules and X-ray diffraction analysis is a good method to further prove their reactivity and behavior in fields such as, for example, hydrogen-bonding catalysis (Fig. 11).

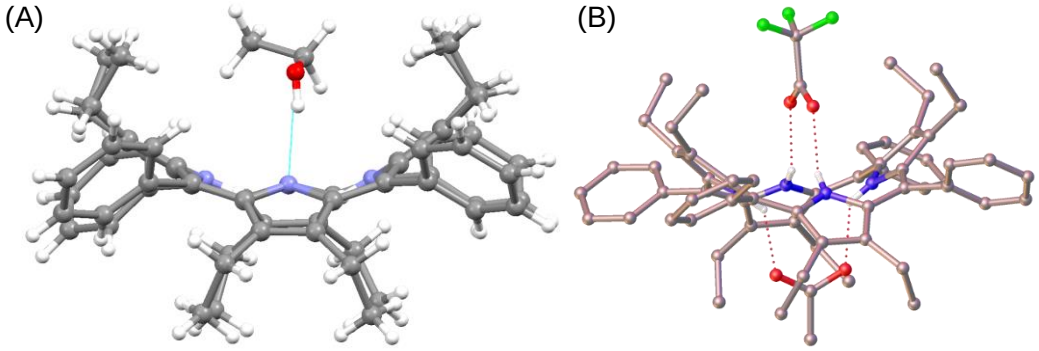

Figure 11: Example of hydrogen bonding formation between the inner function of the porphyrin and an acetic acid molecule shown by XRD analysis. **A)** Hydrogen-bonding with free base H_2OETPP **21** and (B) Hydrogen-bonding with the dicationic H_4OETPP^{2+}.[57c,68]

In addition, the NSD method can be used to quantify the degree of distortion. NSD is a conceptually simple technique to quantify out-of-plane or in plane distortion of molecules using vibrational normal coordinates. The conformation of the macrocycle (porphyrin skeleton) and the vibration normal modes are projected on a plane in a quantitative manner. This results in various distortion modes, described by Scheidt and Lee,[57a,68a] from which only the out-of-plane distortion will be discussed in the context of this Ph.D. thesis. The most common modes reported for porphyrins are saddled (*sad* (B_{2u})), ruffled (*ruf* (B_{1u})), domed (*dom* (A_{2u})), and waved (*wav* ($E_g(x)$ and $E_g(y)$)) (Fig. 12).

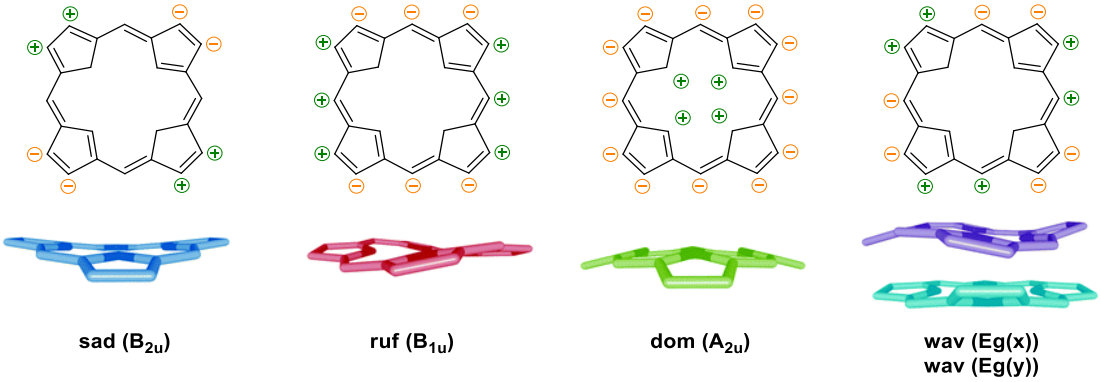

Figure 12: Representation of the four most widely found distortion modes for porphyrins. Only the most significant displacements are shown. Displacements above the plane and below the plane are indicated by (+) and (-), respectively.

Ruffled and domed distorted macrocycles are often observed in metalloporphyrins,[57a,69] where domed distortion is associated with the axial ligand found in five-coordinated metalloporphyrin complexes or with metalloporphyrins chelating large metal ions.[70] However, a unique case of a free base ruffled porphyrin has been reported in the literature (Fig. 13).[52b] The H_2T*t*BuP **22** bears four *tert*-butyl groups at the meso-positions, which due to their size cannot be accommodated without twisting the macrocycle, resulting in a *ruf*-distortion mode. Protonation of porphyrins as well as steric strain due to peripheral or inner core substitution results in a saddled distortion of the macrocycle. This distinction is required in order to compare the degree of nonplanarity of porphyrins.

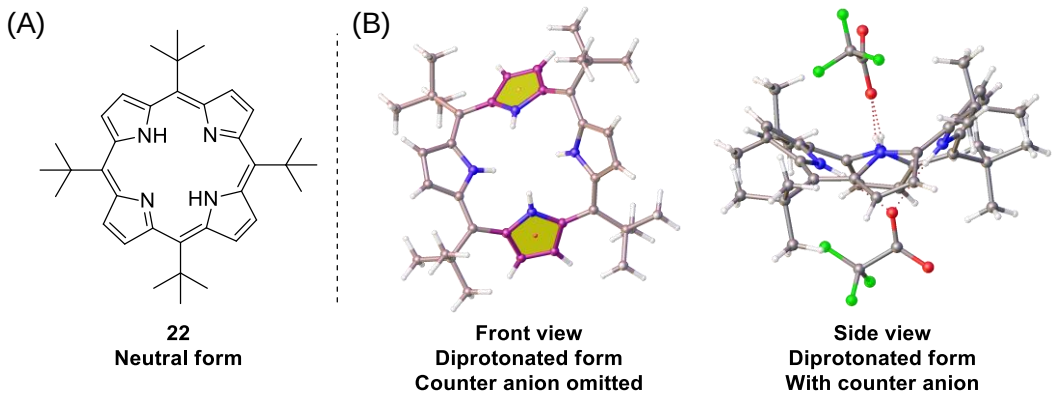

Figure 13: A) Structure of the tetra-*tert*-butylporphyrin; B) X-ray structure of the dicationic form of tetra-*tert*-butylporphyrin **22**.[48b] Counter anions have been omitted for clarity. Twisting of the pyrrole (in purple) is highlighted by the yellow plane drawn in the figure.

In addition to the visual effect and the various distortion modes obtained, NSD and X-ray methods yield several parameters which can be used to quantify and compare macrocycle distortion between different molecules. Among them, the overall out-of-plane

distortion (Δ_{oop}) and the deviation from the 24-atoms least square plane (Δ24) are the most representative parameter for the distortion in a molecule. The Δ_{oop} represents the overall contribution of every distortion mode (B_{2u}, B_{1u}, A_{2u}, $E_g(x)$ and $E_g(y)$) observed in the molecule. The Δ24 is the average deviation of the 24 macrocycle atoms from their least square plane. Consequently, high Δ24 indicates highly distorted macrocycles.

1.5.2.2 Spectroscopic analysis

Changes in the spectroscopic pattern are closely related to the various modifications of the macrocycle such as change in the peripheral substitutents (push-pull porphyrins, porphyrin dimers, porphyrin based molecular tectons, pH dependent units, etc.),[59,71] modification of the inner cavity (*N*-substitution, counter ions *via* protonations, metallation),[42b,c,48b,49] reduction of the π-conjugated systems (chlorins, porpho(di)methenes),[72] or distortion of the macrocycle.[73] In the panel of spectroscopic methods, UV-vis and NMR spectroscopic techniques are the most commonly used to characterize porphyrins. These modifications induce chemical shifts of the NH protons or modulation of the light absorbing ability of the porphyrin.[1,44,74] These changes are often good indicators to determine the structure and conformation of tetrapyrrolic compounds.

To visualize the effects that different modifications of the macrocycle can have on the UV-vis and NMR spectra of porphyrins, a selection of illustrative porphyrins has been chosen which range from planar to very nonplanar molecules in Fig. 14.

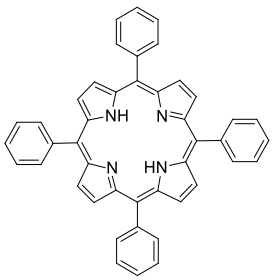

26, H_2TPP

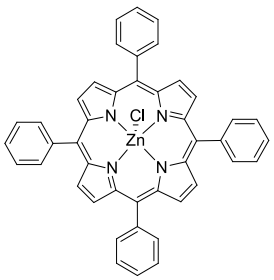

33, ZnClTPP

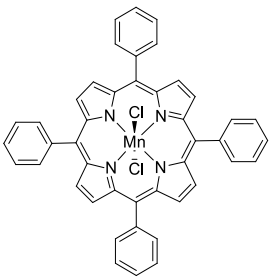

34, $MnCl_2TPP$

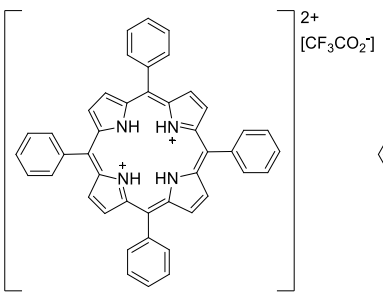

35, H_4TPP^{2+}

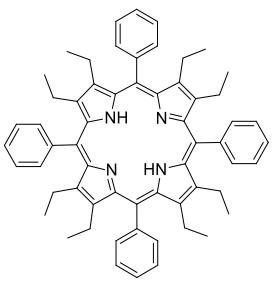

21, OETPP

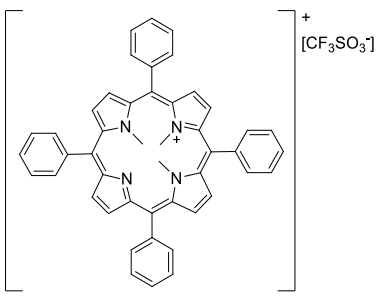

23, N_{21},N_{22},N_{23}-trimethyl TPP ($TPP(CH_3)_3^+$)

Figure 14: Various examples of possible modification of the macrocycle. Porphyrin **26** is shown as a planar and comparative reference.

1.5.2.3 UV-vis spectroscopy

Porphyrins have very specific UV-vis spectra due to their highly conjugated systems. UV-vis spectra of free base porphyrins can be divided into two main parts; a Soret band and four weaker Q bands. The four orbital model which describes the particular UV-vis spectra of porphyrins has been developed by Gouterman.[75] This model looks at the two highest occupied molecular orbitals (HOMOs) and the two lowest unoccupied molecular orbitals (LUMOs) localized in the porphyrin (Fig. 15). The UV-vis spectrum is a result of the π–π* transitions observed between the HOMOs and LUMOs. The Soret band arises from the degenerated pairs of higher energy state (transition from ground state S_0 to excited state S_2) and the Q bands from the degenerate pairs of lower energy state (transition from S_0 to excited state S_1).[76]

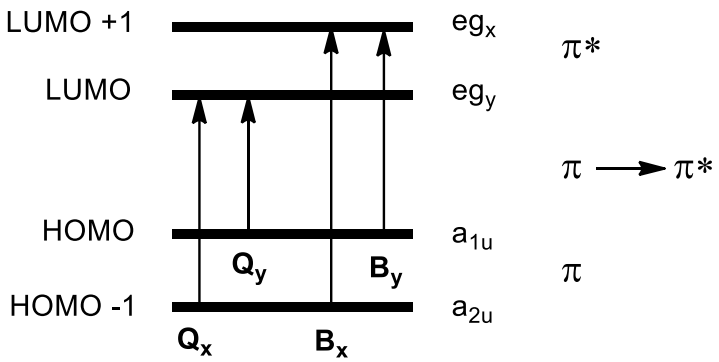

Figure 15: Energy diagram of HOMO/ LUMO transition states.

However, the Soret or B band is represented by an intense and usually sharp absorption band between 380 and 500 nm. This unique intense band results from the overlapping of the two expected B bands. The Q bands are four broader bands between 480 and 800 nm with much lower intensity. In theory, the Q bands of free base porphyrins are split in two, due to vibrational excitation. A transition is observed from ground state (HOMOs) to two vibrational states of the excited state (LUMOs) resulting in the two Q bands Q(0,0) and Q(1,0). Therefore, the rise of the two additional Q bands (four in total) is caused by the presence of the NH protons, breaking the symmetry of the porphyrin. As a result, the two Q bands from the vibrational excitation are further split into two more Q bands, resulting in the four Q bands observed (Qx(0,0), Qy(0,0), Qx(1,0) and Qy(1,0)).

The UV-vis spectrum of a porphyrin is highly dependent on the porphyrin structure: changes can be induced by nonplanarity, chelation of a metal, and functionalization on the periphery or in the inner core (Fig. 16).[77] For example, insertion of a metal into the

cavity of the macrocycle will restore the symmetry and thus results in only two Q-bands.[78] A shift can be observed for the B bands influenced by the type of metal complex formed. Divalent metal ions such as Ni(II), Cu(II), Zn(II) or Mn(II) form tetracoordinated complexes.[79] Low affinity for additional ligands is observed in the case of Cu(II) and Ni(II) complexes; however, this is not the case for Zn(II) and Mn(II). While Zn(II) metal complexes can easily combine with an extra ligand forming a pentacoordinated complex with a square pyramidal structure, two additional ligands can be added to the Mn(II) complex forming a distorted octahedral complex.[80] The resulting distortion induced by the addition of the two ligands leads to the distortion of the macrocycle, resulting in the bathochromic shift observed for $MnCl_2TPP$ (Fig. 16, (A)).

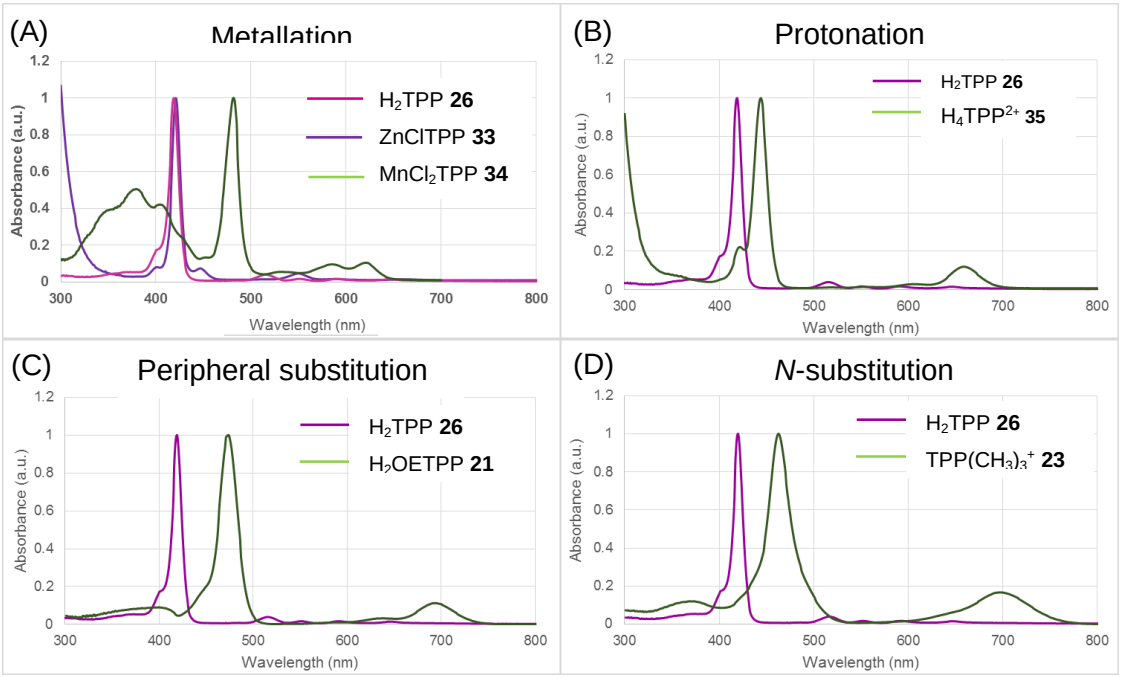

Figure 16: Influence of the macrocycle modification on the UV-vis spectrum. Porphyrins utilized to plot the various UV-vis spectra correspond to the porphyrins presented in Fig 14.

Changes in the absorption spectrum can also be seen after diprotonation of the porphyrin with acid, which results in a shift of the Soret band of 10 to 20 nm due to the distortion induced by the two added protons (Fig. 16, (B)).[78b,81] In a similar manner, nonplanarity obtained by high peripheral substitution or inner core substitution also results in a red-shift of up to ~40 nm (depending on the degree of distortion) compared to the planar analogs (Fig. 16, (C) and (D)).[42c] Q bands are also affected by the different distortion modes, as shown in spectrum (D) (Fig. 16), where the insertion of three methyl units leads to a higher distortion of the macrocycle and thus, only one broad Q band is observed.

1.5.2.4 ^{1}H NMR spectra of porphyrins

The first report of a NMR spectrum of a porphyrin was published by Becker & Bradley[82] and Ellis *et al*.[83] A large magnetic anisotropy (ring current) is observed in porphyrin structures due to the aromaticity of the macrocycle.[84] The ring current, seen in aromatic systems, is induced by the electrons circulating over the aromatic ring of the π-system and makes an important contribution to the chemical shift variations observed in NMR spectra.[85] The main consequence of this anisotropy is seen by the deshielding of the protons in the plane and the peripheral protons.[86] Protons in the region above and below the plane are shielded. Porphyrins are aromatic structures, which can be approximately seen as the sum of five aromatic rings: four from the pyrrole units and one from the sixteen central membered ring (Fig.17, A).[87] The ^{1}H NMR spectrum of a porphyrin is then spread over 15–16 ppm. Peripheral protons are shifted by about 4–5 ppm to the lower field in comparison to common chemical shifts observed for protons of the pyrrole molecule itself,[88] and inner protons are shifted by 11–12 ppm to higher fields. Any modification of the porphyrin structure will result in an alteration of the overall ring current and hence induces a change in the chemical signals observed. However, other additional factors need to be considered to explain changes observed in the NMR spectra. For example, conformational changes can be induced by local modifications of the macrocycle resulting in variations of the environment of the proton. Considering the possibility that the macrocycle can be substituted in three different ways: a) by *β*-functionalization, b) by meso-substitution and c) inner core substitution (metal, protonation or alkyl or aryl groups), the change in the environment can often be important and results in small to large chemical shifts. In addition, the nonplanarity which can be induced by these modifications can affect the ring current effect, *i.e.*, aromaticity.

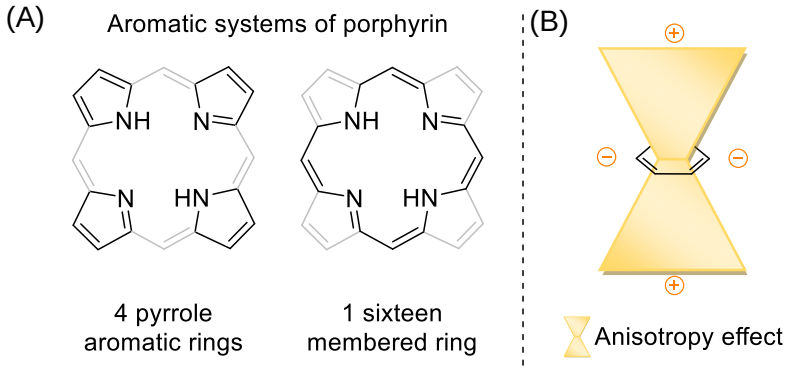

Figure 17: a) Aromatic rings present in the macrocycle of porphyrins, b) Ring current and anisotropic effect on the macrocycle.

The π–π orbitals are destabilized by the new shape of the porphyrin and their overlap is reduced by the steric hindrance of the macrocycle. A lower electron density of the π-

system is observed, reducing the ring current and resulting in an upfield shift of the peripheral protons. In parallel, a shift in the opposite direction (high field) is observed for the signals of the inner protons which is caused by the inner protons suddenly being exposed to the outside of the magnetic anisotropy due to the distortion.[57c]

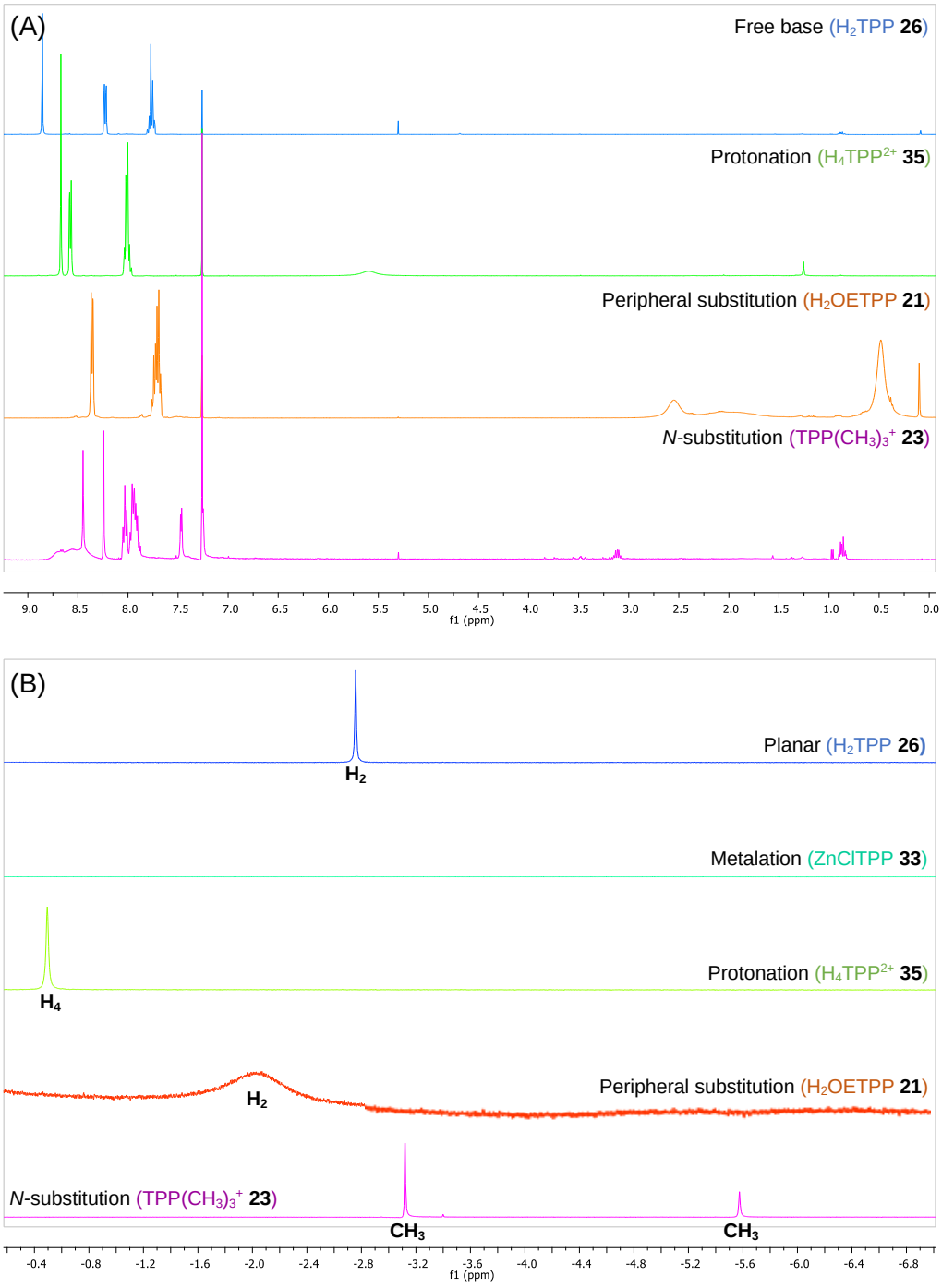

Figure 18: Influence of the modification of the porphyrin macrocycle on the peripheral protons (A) and inner protons (B). Porphyrins utilized to obtain the various ^{1}H NMR spectra correspond to the porphyrins presented in Fig 14. Spectra were recorded in $CDCl_3$.

Chemical signals for the peripheral and inner protons for each modification are shown in Fig. 18, respectively. When comparing the planar H_2TPP **26** to the nonplanar H_2OETPP **21**, it can be seen that the addition of alkyl groups to the *β*-positions induced a shift of the ethyl and NH inner protons (Fig. 18).[89] An upfield shift is observed for the ethyl proton signals while the inner proton signals are deshielded.[90] Literature has shown that an even stronger effect can be noted when larger substitutents are used for the *β*-positions.[91,92] The insertion of a metal into the cavity or the protonation of the inner core of the porphyrin restores the symmetry (Fig. 18, (B), ZnTPP **33** and H_4TPP^{2+} **35**). A larger ring current can then be observed due to better stabilization of the resonance form.[93] In metalloporphyrins the presence of the metal leads to the disappearance of the NH peaks (loss of the protons) (Fig. 18, (B), ZnTPP **33**). For the dicationic species, the downfield shift of the peripheral protons is more dominant than the upfield shift of the NH protons compared to their free base analogs. While the C-H protons are shifted upfield due to the ring current effect, that same effect is compensated around the NH protons by the charge formed.[62]

The changes in NMR spectra of *N*-substituted porphyrins are mainly due to the steric hindrance caused by the central substituents replacing the inner core hydrogen atoms (Fig. 18, $TPP(CH_3)_3^+$ **23**). The size of these substituents results in a steric clash as they cannot be accommodated in the cavity. The changes in the NMR spectrum are attributed to the distortion induced by the *N*-substitution, including a decrease in the aromatic ring current. This decrease changes the local environment due to the distortion (proton outside the ring current) and increases the sp^3 hybridization at the *N*-substituted atoms.[94] A shift to the higher field is observed for the *β*-protons of pyrrole opposite to the *N*-substituted pyrrole due to the conservation of its planarity. In contrast, the *β*-protons from the *N*-substituted pyrrole are more shifted due to the out-of-plane distortion of the pyrrole ring caused by the *N*-substituents. However, this is only observed for the N^{21}-monosubstituted porphyrins. Upon insertion of more *N*-substituents, a higher distortion is observed, resulting in a more significant shift of the proton signals of the *N*-substitutents but also, in some cases, from the loss of symmetry. The shift is then observed for every proton of every inner substituent, which are all tilted out of the ring current by the nonplanarity.[95]

2 Objectives

The overall concept of this project consisted of synthesizing nonplanar porphyrins with modulated conformations and tuned properties in order to be tested as potential organocatalysts for reactions using small organic molecules. Consequently, this project is divided into three main objectives: first the synthesis of highly distorted porphyrins with tuned electronic properties, second the elaboration of a library of *N*-methylated porphyrins and to finish, the use of the whole panel of synthesized porphyrins to examine their potential as organocatalysts.

Substitution of the periphery of porphyrin macrocycles is a simple way to induce macrocycle distortion. This method leaves the NH intact and the distortion pushes these units out-of-plane. Their ability to interact with surrounding small molecules is consequently improved. Moreover, using this method enables the fine-tuning of the basicity and electronic properties *via* modulation of the peripheral groups. Thus, the objective of the first chapter was to synthesize a catalog of highly nonplanar porphyrins with various electronic properties using peripherally crowded macrocycles (Fig. 19).

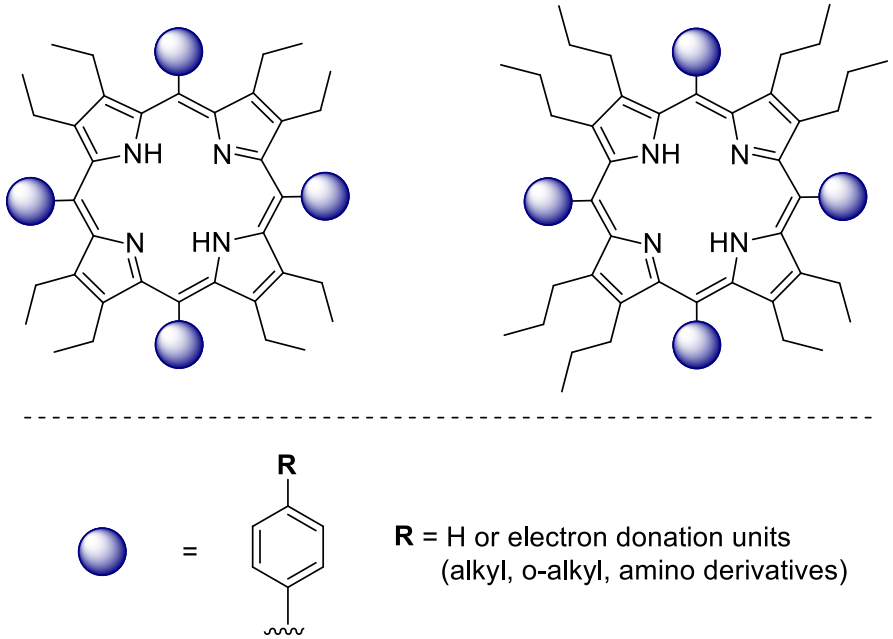

Figure 19: Targeted highly substituted porphyrins.

Modulation of basicity could be achieved using aldehydes bearing aryl substituents with various electron-donating groups. The electron-rich macrocycle has increased the binding capabilities of the inner moieties and thus enhanced their reactivity toward their environment.

The second project discusses the modification of porphyrin macrocycles through molecular engineering of the inner cavity. Here, *N*-methylations of the porphyrin core were exploited to induce conformational changes. A variety of porphyrins were synthesized presenting low to high meso-substitution with different electronic substituent effects to allow comparative conformational and structural analyses (Fig. 20). Symmetric porphyrins were used to allow for a facile distinction between precursors and compounds formed upon *N*-methylation.

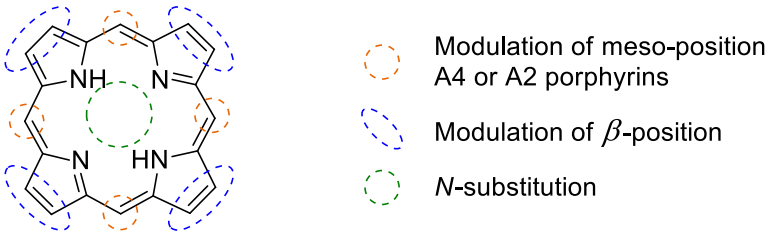

Figure 20: Various positions used during the second objective, in order to functionalize and distort the porphyrin macrocycle.

Further investigations on the influence of meso-peripheral units on the methylation process were also anticipated. *N*-alkylated porphyrinoids are of interest as they allow an investigation of the correlation between increasing distortion and *N*-substitution pattern. Such conformational modification induces distinct changes in their spectral and electrochemical properties, notably, an increase in basicity and an improvement in the binding properties (small molecules or anions). Further advances in this area require access to a broader range of core-alkylated porphyrins and, herein, a comparative investigation of the synthesis and structures of *N*-substituted 5,10,15,20- and 5,15-substituted porphyrins containing groups with various electron-dependent properties was targeted.

With this broad catalog of porphyrins in hand, an examination of their potential as organocatalysts was anticipated.[96] The exploration of free base nonplanar and *N*-substituted porphyrins as potential catalysts is a novel challenge as such systems have never been employed in this field, even though they possess common catalytic functionalities. The overall concept of the last chapter of this project would then consist in using these compounds for sulfa-Michael addition reactions. The efficiency of the distorted *N*-methyl-5,10,15,20-tetrasubstituted porphyrins were compared to one of the highly distorted porphyrins systems (*e.g.*, H_2OETPP). The hypothesis is that distorted porphyrins can activate Michael acceptors as their pyrollic protons are tilted outward by the saddle distortion (activation *via* hydrogen-bonding to the acceptor, Lewis acid).

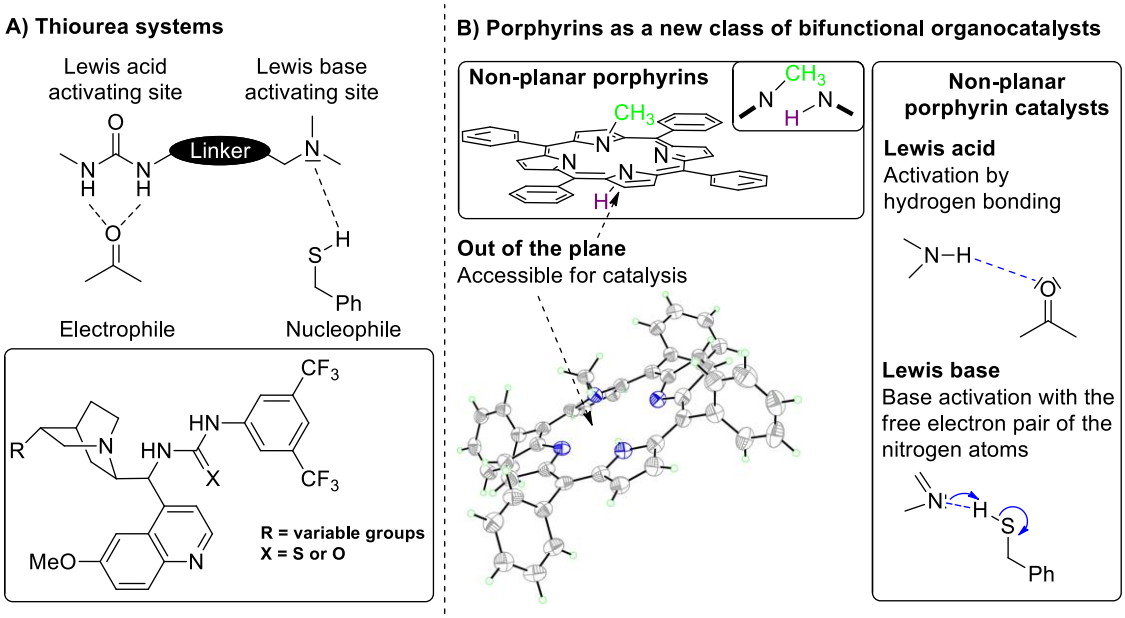

Figure 21: Hypothetical behavior of *N*-substituted porphyrins compared to the well-known thio(urea) systems.

Moreover, due to the macrocyclic distortion, the basicity of the porphyrin imine groups is highly increased.[97] This effect could lead to an additional activation of the nucleophile (Lewis base). Both effects together will generate a new class of bifunctional organocatalysts (Fig. 21). This concept of catalysis by such distorted porphyrins can be compared to the well-established (thio)urea-substituted cinchona alkaloid systems (**A**, Fig. 21).[98]

3 Highly substituted porphyrins

3.1 Introduction

Natural tetrapyrrole-containing proteins stand among the most fundamental class of enzymes and are able to catalyze a multitude of biological processes. The chemical structure of the protein cofactors determines the biological function it may play and many processes are seen to be activated by chemically identical cofactors (*e.g.*, hemoglobins, myoglobins and cytochromes P450).[99] To understand how nature induces various roles to the same chromophore, the development of synthetic biomimetic compounds have been an ongoing challenge.[42] Variations in the sequence of protein cannot be considered as the sole reason for the various functions observed for the same cofactor. A critical factor common to all protein systems resides in the close structural interplay between the protein and its chromophore, which induces conformational changes in the tetrapyrrole.[1]

Synthetically, the variation of conformation for the same tetrapyrrole molecule can be achieved by modification of the macrocycle structure.[42b,42c,45,48b,49] The various ways of modifying the macrocycle have been detailed in the general introduction in Fig. 6. Even though they all result in conformational changes, peripheral substitution stands among one of the best techniques to control the conformation (*e.g.*, H_2TtBuP **22**,[52] EtXTPP series[56]). Techniques such as NSD, XRD, UV-vis and NRM spectroscopy have proven to be very useful in examining the various conformations obtained and to observe the effects of these conformational changes on the photophysical and electrochemical properties.[64,65]

The example of the EtXTPP series is a very interesting case. The incorporation of graded degrees of ethyl groups at the *β*-position of the planar H_2TPP skeleton (Δ24 = 0.05) results in an increase in distortion until the complete substitution of the *β*-positions (Δ24 = 0.54).[43d,53,58] This former compound displays a very high distortion relative to the important hindrance caused by the dodecasubstitution. In terms of spectroscopic properties, the H_2OETPP compound **21** shows a notable bathochromic shift of its Soret band (as opposed to the H_2TPP **26**) resulting from the new conformation.[42c,78] Changes in the ^{1}H NMR can also be observed due to the distortion and affects chemical signals of both peripheral and inner protons.[90] More importantly, higher basicity can be achieved *via* distortion of the tetrapyrrole as it pushes the pyrrolic and imine units out-of-plane.[31,50] Consequently, these units are now available for a wide range of various applications (*e.g.*, catalysis, anion and gas sensing, molecule binding).[25,59]

3.2 Results and discussion

A series of aldehydes **25**, **38**–**46** bearing different electron donating units in either the *o*-, *p*- or *m*-position of the meso-aryl residue were reacted with 3,4-diethylpyrrole **24** or 3,4-dipropylpyrrole **35,** to form a series of octaethyl- (OETArX-porphyrin) and octapropylporphyrins (OPTArX-porphyrin) with various residues at the meso-position (Fig. 22). The electron donating effects were quantified using Hammett's values (σ) of the various substituents depending on their position (*meta* (σ_m) or *para* (σ_p)) on the aryl groups.[100] Hammett's values are quantified using the carboxylic acid of the corresponding aldehyde shown in Fig. 22. No reports of Hammett's values for the *o*-position have been published to-date due to the steric hindrance resulting between the *o*-substituents and the carbonyl functionality. This resulted in a strategically designed series of porphyrins with increasingly electron-rich macrocycles.

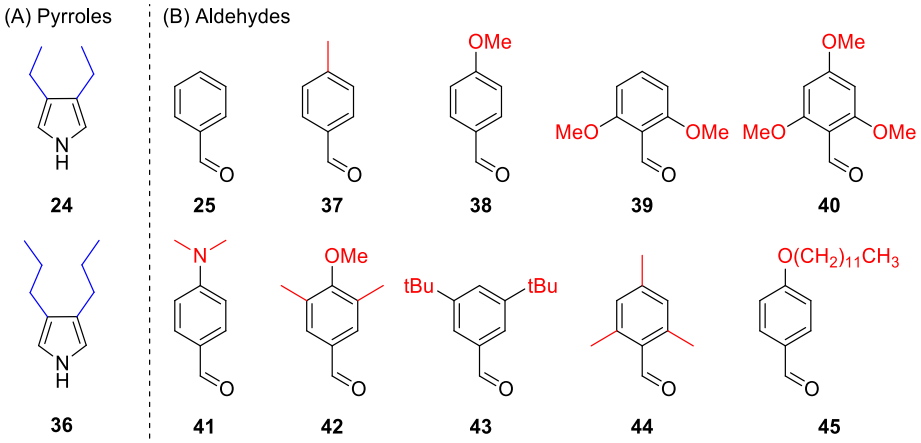

Figure 22: Library of pyrroles and aldeydes used to form the target porphyrins.

The investigation started with the synthesis of the 4-methylphenyl-OETArX-porphyrin **46** and the 3,5-di-*tert*butyl-phenyl-OETArX-porphyrin **52** in order to examine the effect of the mild electron donating effect of the *p*-substitutents (σ_p = -0.17). Following this, aldehydes bearing aryl units with stronger electron donating groups were chosen to synthesize porphyrins with an increased electron density of the macrocycle, 4-methoxyphenyl-OETArX-porphyrin **47** (σ_p = -0.17), 3,5-dimethyl-6-methoxyphenyl-OETArXporphyrin **50** (σ_p = -0.17 and σ_m = -0.07), 4-dodecacyloxyphenyl-OETArX-porphyrin **54** (σ_p > -0.45) and 4-dimethylaminophenyl-OETArX-porphyrin **50** (σ_p = -0.83). The presence of strong electron donating groups increases the electron density of the macrocycle, thus inducing a higher basicity to the inner core functional groups of the porphyrin. Three more porphyrins, 2,4,6-trimethylphenyl-OETArX-porphyrin **53**, 2,6-dimethoxyphenyl-OETArX-porphyrin **48**, and 2,4,6-trimethoxyphenyl-OETArX-porphyrin **49** were synthesized in order to study the effect of meso-hindered porphyrins.

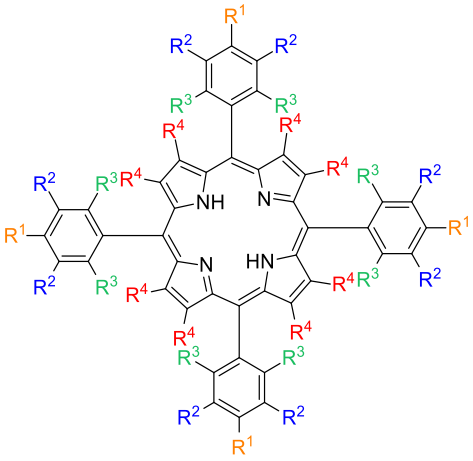

46, R^1 = Me, R^2 = R^3 = H, R^4 = Et
47, R^1 = OMe, R^2 = R^3 = H, R^4 = Et
48, R^1 = R^2 = H, R^3 = OMe, R^4 = Et
49, R^1 = R^3 = OMe, R^2 = H, R^4 = Et
50, R^1 = NMe_2, R^2 = R^3 = H, R^4 = Et
51, R^1 = OMe, R^2 = Me, R^3 = H, R^4 = Et
52, R^1 = H, R^2 = tBu, R^3 = H, R^4 = Et
53, R^1 = R^3 = Me, R^2 = H, R^4 = Et
54, R^1 = $O(CH_2)_{11}CH_3$, R^2 = R^3 = H, R^4 = Et
55, R^1 = R^2 = R^3 = H, R^4 = Pr
56, R^1 = OMe, R^2 = R^3 = H, R^4 = Pr

Figure 23: Target porphyrin library.

The hindrance caused by a steric clash of the alkyl groups in the *β*-positions and the groups in the *ortho*-position of the meso-aryl groups forces a high distortion onto the macrocycle and thus results in a better availability of the NH and imine moieties. By increasing the steric demand and the donating effect of the *β*-alkyl units, this would result in free base porphyrins with better reactive centers. Consequently, two other porphyrins **55** and **56** were examined following a condensation reaction between the 3,4-dipropylpyrrole **36** and the corresponding aldehyde.

3.2.1 Pyrrole Synthesis

Two different pyrroles were synthesized in order to achieve the various porphyrin structures. Even though they have a close resemblance in structure, the synthetic pathways used for their preparation are very different.

3.2.1.1 Preparation of the 3,4-diethylpyrrole

The preparation of 3,4-diethylpyrrole (**24**) requires two different components (**60** and **64**) which each have to be synthesized over several steps. The different reactions are outlined in Scheme 6.[101] The route towards compound **60** starts with reacting the commercial propionaldehyde **57** in isopropanol with 1-nitropropane **58** in the presence of potassium fluoride for 18 h. This step leads to the formation of 4-nitrohexan-3-ol **59** which is further treated with sulfuric acid and acetic anhydride for 1 h to give 4-acetoxy-3-nitrohexane **60**. The formation of compound **64** begins with the synthesis of the *N*-formylglycine ethyl ester **61**. This compound is obtained upon reaction of the commercially available glycine ethyl ether hydrochloride **61** and methyl formate **62** with NEt_3 for 20 h at 35 °C. The compound formed (**62**) is then treated with phosphorous oxochloride, NEt_3 and anhydrous sodium carbonate to afford product **64**, the ethyl isocyanoacetate. This compound is very unstable and needs to be used within the

following 24 h of its synthesis. In the next step compound **60** and **64** are reacted to afford the protected pyrrole, 3,4-diethylpyrrole-2-carboxylate **65**. The literature procedure for this reaction using 1,8-diazabicyclo[5.4.0]undec-7-ene (DBU) results in the formation of compound **65** in a very good yield after only 4 h.[102] However, another method, using potassium carbonate K_2CO_3 over 3 days, also leads to high yields of the same compound.[103] While the latter reaction conditions are more time consuming, they allow for large scale synthesis using cheap reagents and result in better yields.

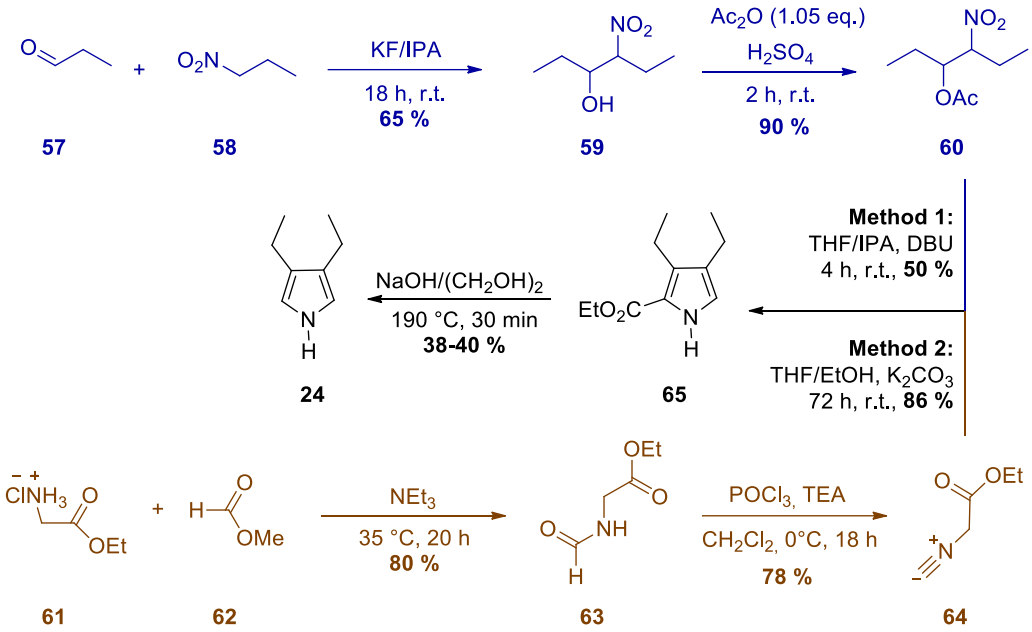

Scheme 6: Synthesis of 3,4-diethylpyrrole **22**.

The last step consists of the deprotection of the pyrrole using sodium hydroxide in ethylene glycol over 30 min at 190 °C.[101] For this reaction, it was noticed that time and temperature influenced the yield obtained. The last step of the synthesis of the 3,4-diethylpyrrole **24** was repeated several times in order to find the optimum conditions of time and temperature for the reaction. The results are compiled in Table 1.

Table 1: Variations of conditions used for the synthesis of compound **24**.

Entry	Temp. (°C)	Time (h)	Yield (%)
1	160	3	27
2	170	2	40
3	165	2	40
4	165	2	40
5	160	2	46
6	160	2	50

Entry 1 and **2** clearly show that the reaction is time and temperature dependent. For **entry 1**, a 3 h reaction leads to a noticeable decrease of the yield compared to the literature reports (27% instead of 40%, respectively). Comparing **entry 1** and **2**, the reduction of reaction time allowed for comparable yields to the literature with a lower temperature. Lowering the temperature by 10 °C is necessary to increase the yield to 50% (**entry 3-6**). This can be rationalized by the rapid and easy polymerization of the pyrrole. The decrease in temperature improves the rate of deprotection; however, it also enhances the polymerization of the pyrrole. The temperature, even though it is already lower than the initial 190 °C, still enhances the polymerization reaction. The difference in yields between **entry 5** and **6** can be explained by the work-up process. The product is extracted from the reaction mixture using hexane. This step is time consuming as it requires an excessive amount of hexane. Unfortunately, the use of potential other solvents in order to speed up the process resulted in the extraction of impurities along with the pyrrole. Careful monitoring of the various fractions extracted is necessary to obtain the optimum yield. At this stage further optimization was deemed unnecessary; however, it could be interesting to further decrease the temperature to examine the effect it would have on the yields obtained.

3.2.1.2 Synthesis of the 3,4-dipropylpyrrole 36

The 3,4-dipropyl pyrrole **36** was synthesized according to a literature procedure[104] and begins with the reaction of the *trans*-2-hexenal **66** with ethyl magnesium bromide as a Grignard reagent in ether at room temperature over 1 h. The compound **36** obtained (4-octen-3-ol) is then oxidized with DDQ for 16 h at room temperature in anhydrous benzene to form 4-octen-3-one **67**. Following this, compound **68** was reacted with *p*-toluenesulfonylmethyl isocyanate and sodium hydride for 2.5 h at room temperature to obtain the 4-propyl-3-propanoyl pyrrole **69**. Upon treatment with $LiAlH_4$, this leads to the desired 3,4-dipropylpyrrole **36**.

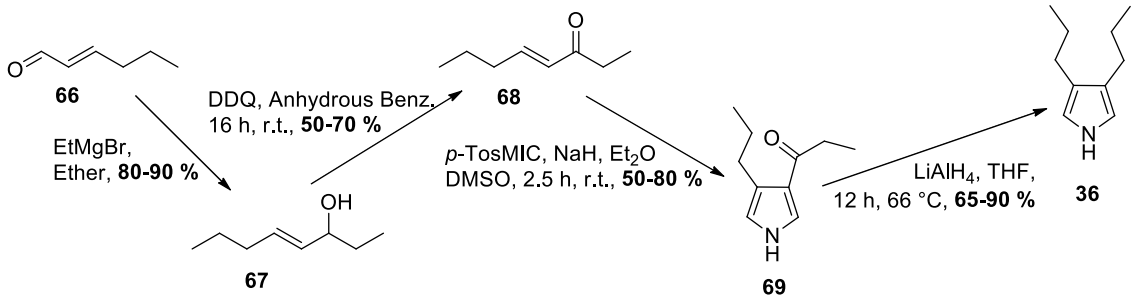

Scheme 7: Synthesis of 3,4-dipropylpyrrole **36**.

Moderate to high yields can be obtained for each step. The first step allows one to obtain compound **66** in 80–90% yield as a pale yellow liquid. The next step also gave a yellow liquid in 50–70% yield. Step 3 represents a more tedious procedure, especially concerning the purification process. The compound is obtained in yields of 50–80%. The difference in yield is mainly due to the issues during purification. *p*-tosMIC is used in order to perform the cyclization leading to the pyrrole. This reagent is very cumbersome to remove and is still present in a 50:50 mixture resulting in a brown oil with some colorless crystals. A crystal structure of the product was obtained and is presented in Fig. 24. Several purification attempts (column chromatography, recrystallization) proved unsuccessful and only resulted in a slight decrease of the *p*-tosMIC along with a decreased yield of the desired compound. The yields reported in Scheme 7 only represent indicative yields for the product. These yields were estimated by comparison of the ratio between the integrated NMR signals for both the pyrrole and *p*-tosMIC. The next step is then achieved using the crude mixture obtained from step 3. This mixture was treated with $LiAlH_4$ and the product was obtained in 70–90% yields as a brown oil.

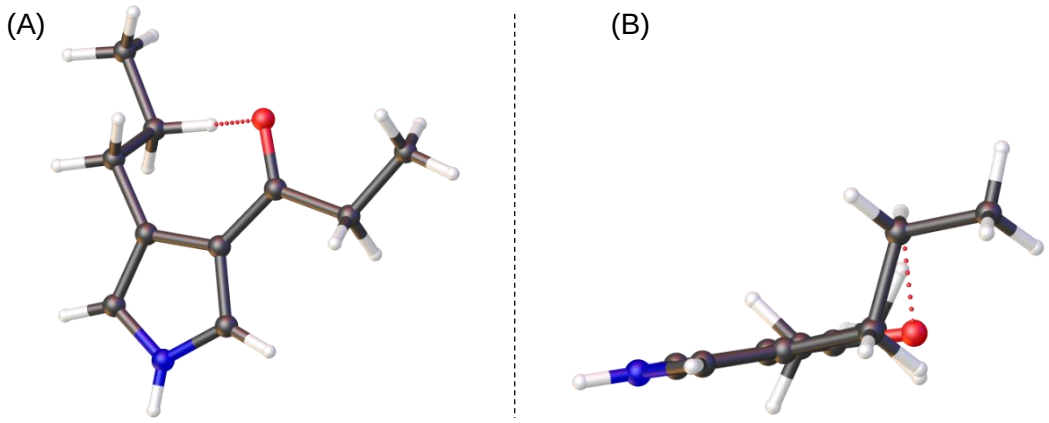

Figure 24: View of the molecular structure of compound **69** in the crystal. Dashed lines indicate the intramolecular interaction between the carbonyl group and the ethyl chain.

The crystal structure of the pyrrole is mostly planar with the exception of the propyl units located at position 4 of the pyrrole which tilts above the plane (Fig. 24, (B)). Looking closer at the picture, internal bonding can be observed between the oxygen atoms of the carbonyl groups and the hydrogen atoms from the second carbon of the propyl substituent.

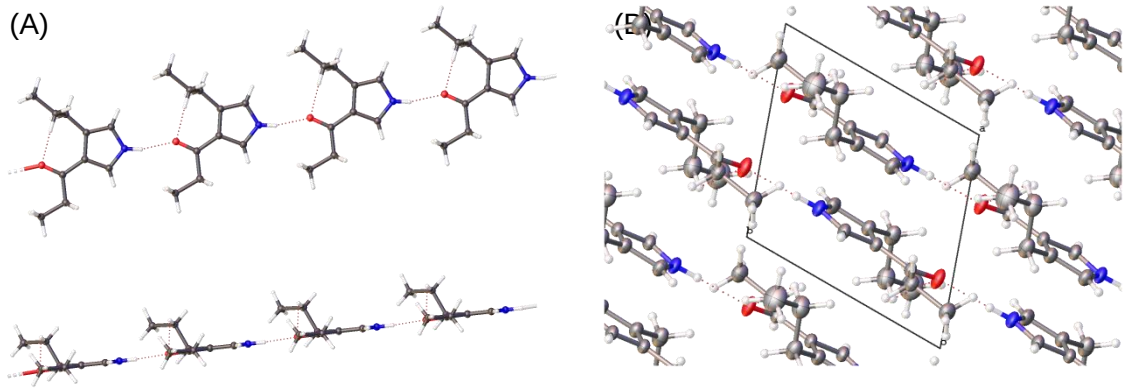

Figure 25: Arrangement of the molecule in the crystal (A) and crystal packing (B) of compound **35**.

With regards to the packing systems, intermolecular bonding is present in a head-to-tail type bonding from the oxygen atoms of the carbonyl groups of one pyrrole unit to the hydrogen atoms of the amine groups of a second pyrrole molecule. This intermolecular bonding type then repeats itself, forming a 2D linear network.

3.2.2 Synthesis of Free Base Porphyrins

3.2.2.1 Synthesis of the OETArXP series

The condensation reaction based on the Lindsey conditions[54] between the pyrrole and the aldehyde, catalyzed by BF_3•OEt_2, results in the formation of the porphyrinogen, which is subsequently oxidized by DDQ (Scheme 8). The work-up of the reaction mixture requires concentration of the solvent used and consequent filtration through a small silica column using ethyl acetate as eluent. Generally, this step results in the removal of most of the impurities; however, the unreacted aldehyde is still present in a mixture with the porphyrin after filtration. A second purification step utilizing column chromatography with hexane:CH_2Cl_2 to eluate the aldehyde is then required.

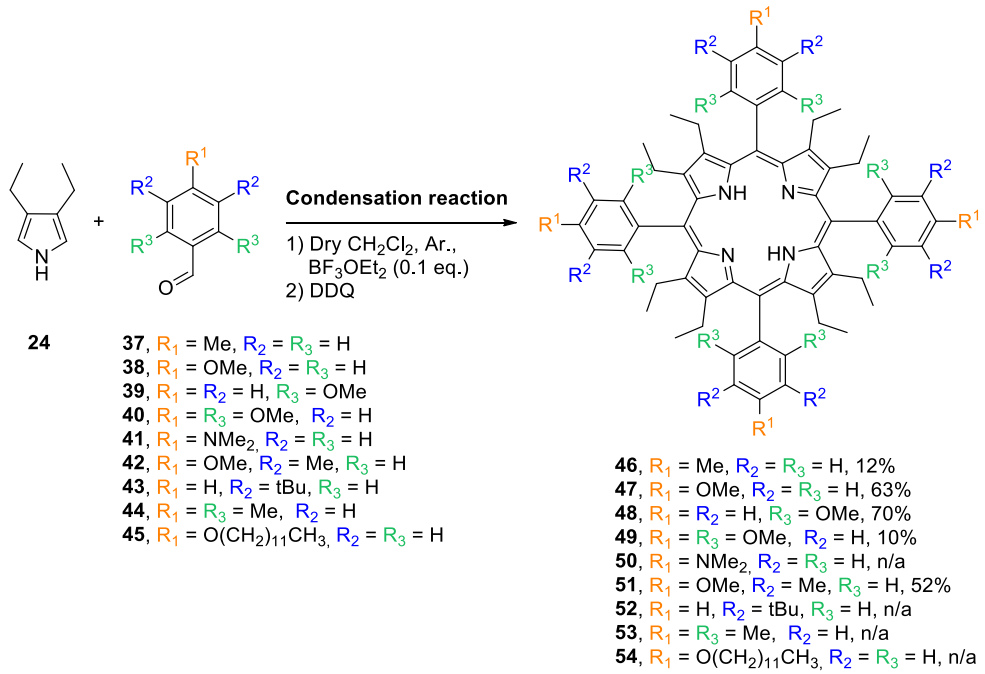

Scheme 8: Synthesis of free base OETArXPs.

In comparison to planar systems, where the formation of the porphyrinogen requires only 1 h, the condensation using 3,4-diethylpyrrole **24** requires at least 12 h to proceed to completion. The reaction was monitored throughout by TLC before adding the DDQ to the reaction.

Table 2: Correlation between Hammett's values of the aldehyde and yields obtained.

Entry	Porphyrin	Hammett values σ	Yield (%)
1	**46**	-0.17	12
2	**53**	-0.20	-
3	**47**	-0.27	63
4	**51**	-0.41	52
5	**52**	-0.51[a]	-
6	**48**	-0.53[b]	70
7	**43**	-0.81[a]	10
8	**50**	-0.83	-
9	**54**	n/a[b]	-

[a] The Hammett values presented here are indicative. There is no report of Hammett values calculated for the *ortho*-position due to the proximity of these positions with the aldehyde functional groups. However, due to the aromaticity of the six-membered ring, a similar effect to the one observed in the *p*-position can be rationalized for the *ortho*-positions. [b] The Hammett value for this substituent is not available, however the Hammett values from the OMe to the $O(CH_2)4CH_3$ substituents are increasing from -0.27 to -0.45, respectively. Thus, it can be assumed that the substituent of porphyrin **44** is highly electron donating.

Table 2 contains the yields obtained for each porphyrin. Porphyrins **47** and **48** were obtained in yields of 63 and 70%. These yields are considered very high for condensation reactions to obtain porphyrins. Usually, several competitive reactions are

observed during the condensation reaction: a) the condensation between the pyrrole and the aldehyde, b) the polymerization of the pyrrole resulting in polypyrromethene **72**, and c) the formation of dipyrrylmethene **73** (Scheme 9). The polymerization of the pyrrole is the main competitive reaction responsible for the usual low yields of reaction for the porphyrin formation. Nevertheless, the polymerization can be reduced using diluted conditions (*e.g.*, 10^{-2} M).

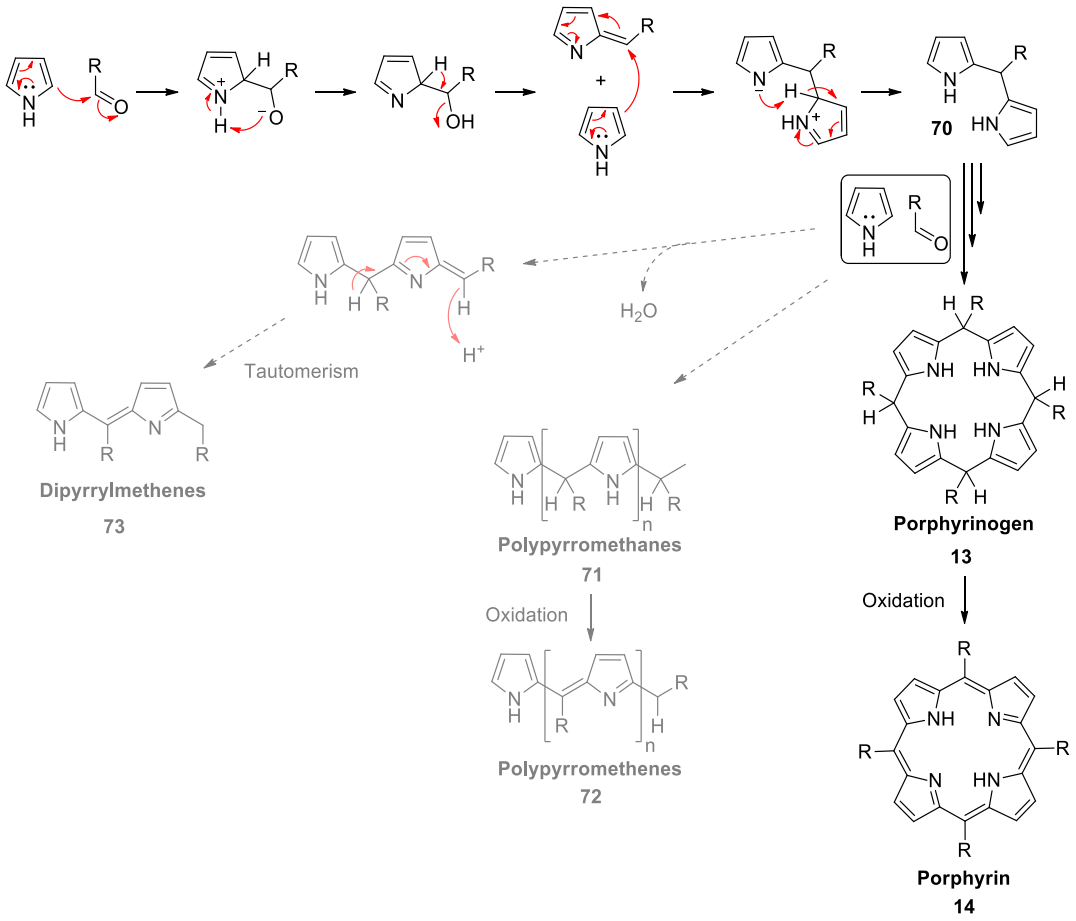

Scheme 9: Mechanism toward the formation of porphyrin and by-products.

In the case of the porphyrins studied herein, porphyrin **47** is the only example where the porphyrin was formed after only 12 h. For all other porphyrins, this step required 36 h before the addition of the oxidant. The variation in rates observed for porphyrinogen formation can be rationalized by the electronic properties of the aryl substituents of the aldehyde used for the reaction. The substitution of multiple positions on the meso-aryl groups with electron donating units lowers the reactivity of the electrophile used for the condensation by increasing its electron density. Thus, the reactivity of the aldehyde towards the pyrrole is decreased, lowering the reaction process. In the condensation pathway of the porphyrin, the first step consists of the attack of the pyrrole on the electrophilic carbonyl center of the aldehyde, which has previously been activated by the

acid to increase its electrophilicity. The addition of too many electron donating groups can affect that first step by decreasing this needed electrophilicity.

Another parameter that also influences the reaction outcome is the steric hindrance seen in the highly substituted porphyrins. These porphyrins, as mentioned before, have bulky groups on the *β*-positions of the macrocycle. The incorporation of substituents at the meso-aryl groups usually does not present a problem. However, in the cases of some compounds examined in this project, the aryl groups are substituted at various positions, which can generate additional hindrance. This can explain the disparity observed in the yields obtained. Table 2 shows the Hammett values of each individual aldehyde, the positions of the aryl substituents, and the yields obtained. Looking into compounds **47**, **49**, **50**, and **51**, the increase in electron density of the aldehydes correlates directly to the decrease in the yields from 63% to no product formation, respectively. This strongly supports the hypothesis that electron-rich aldehydes are less reactive towards the pyrrole. Comparing compounds **46** and **53**, a yield of 12% and no product was obtained, respectively. A high yield was obtained for compound **48** (70%) which possesses two methoxy groups at the *ortho*-positions in contrast to compound **53** for which no yield was obtained. This can be rationalized by the flexibility of the methoxy units due to the presence of the oxygen, while methyl substituents are more rigid and cannot twist or bend to accommodate the space. The two last compounds **52** and **54** were also not formed due to a similar reason; the *tert*-butyl groups of compound **52** induce a steric clash with the *β*-ethyl groups, while the failure to prepare compound **54** is due to its strong electron donating effect.

Compound **50** resembles a promising candidate to form a porphyrin with a highly reactive inner cavity. The dimethylamino substituents result in a high electron density on the macrocycle. In addition, the presence of the substituents in the *para*-positions rather than the *ortho*-positions prevents the excessive hindrance caused by the substitutents. Further condensation condition reactions were investigated in order to form porphyrin **50**. An increase in reaction time of the previous attempt from 12 h to 36 h and finally 72 h was also unsuccessful. TFA was then used instead of BF_3•OEt_2, however did not improve the reaction outcome. Finally, the Adler-Longo conditions using propionic acid were attempted, but again this endeavor was unfruitful.

Consequently, other means to functionalize porphyrin macrocycles were explored; namely, a) amination *via* Buchwald-Hartwig reaction, and b) methylation of amino groups. The Buchwald-Hartwig amination reaction was attempted first. It is a well-established method,[105] though it has been only recently utilized for porphyrins.[106] This

pathway allows for the insertion of amino groups at either *β*-or meso-positions starting from the bromo-aryl porphyrin species. In case of the dimethyl amino-OETArX-porphyrin, the bromine groups of the starting material are present at the *p*-position of each meso-aryl group **74** (Table 3), which was provided by K. J. Flanagan. Conditions were chosen and modified according to literature procedures and are presented in Table 3.[71a,107]

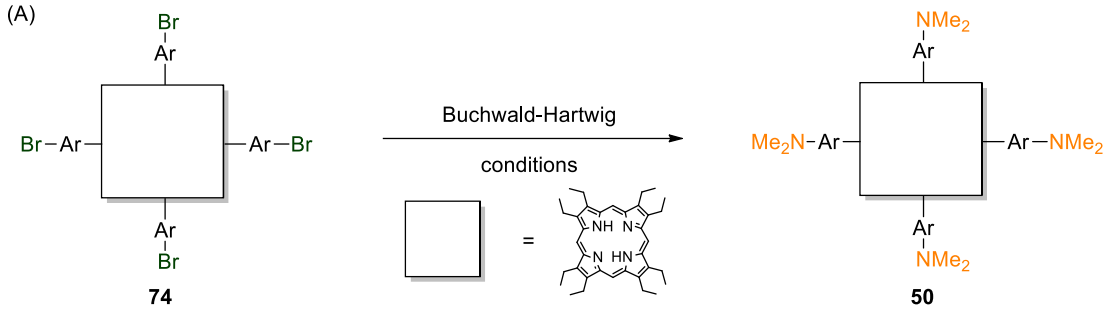

Table 3 Conditions investigated for the Buchwald-Hartwig amination reaction.

Entry	Reagents and catalyst	Solvent	Conditions	Results
1	$NHMe_2$ (8 eq.), Cs_2CO_3 (10 eq.) $Pd(OAc)_2$ (0.2 eq.), BINAP (0.3 eq.)	DMF	Microwave 6 min, 60 °C	-
2	$NHMe_2$ (8 eq.), Cs_2CO_3 (10 eq.) $Pd(OAc)_2$ (0.2 eq.), BINAP (0.3 eq.)	DMF	Microwave 1 h, 60 °C	-
3	$NHMe_2$ (16 eq.), Cs_2CO_3 (10 eq.) $Pd(OAc)_2$ (0.2 eq.), BINAP (0.3 eq.)	THF	Bench reaction, Ar., 16 h, 60 °C	MS hit. Traces.

Compound **74** was reacted with dimethyl amine in 1:8 ratios. The reaction was catalyzed using $Pd(OAc)_2$ in the presence of BINAP ligand and $CsCO_3$ as buffer agent. The reaction conditions proved to be unsuccessful even after several modifications, including change in solvent, ratio between porphyrin and amine, and reaction time.

The synthesis of compound **50** can also be achieved through the second route mentioned consisting in the functionalization of the amino group of *p*-amino-OETArXP **75** with methyl units. The formation of porphyrin **75** *via* condensation reaction cannot be performed due to the reactivity of the *p*-amino groups of the aldehyde with the carbonyl group of another aldehyde molecule.[108] Thus, porphyrin **75** can be obtained v*ia* reaction of *p*-nitro-OETArXP **77** (provided by K. J. Flanagan). The reduction of the *p*-nitro groups thus results in the formation of the *p*-amino groups. The *p*-dimethylamino functional groups can then be generated using either a methylation reaction or a reductive amination.

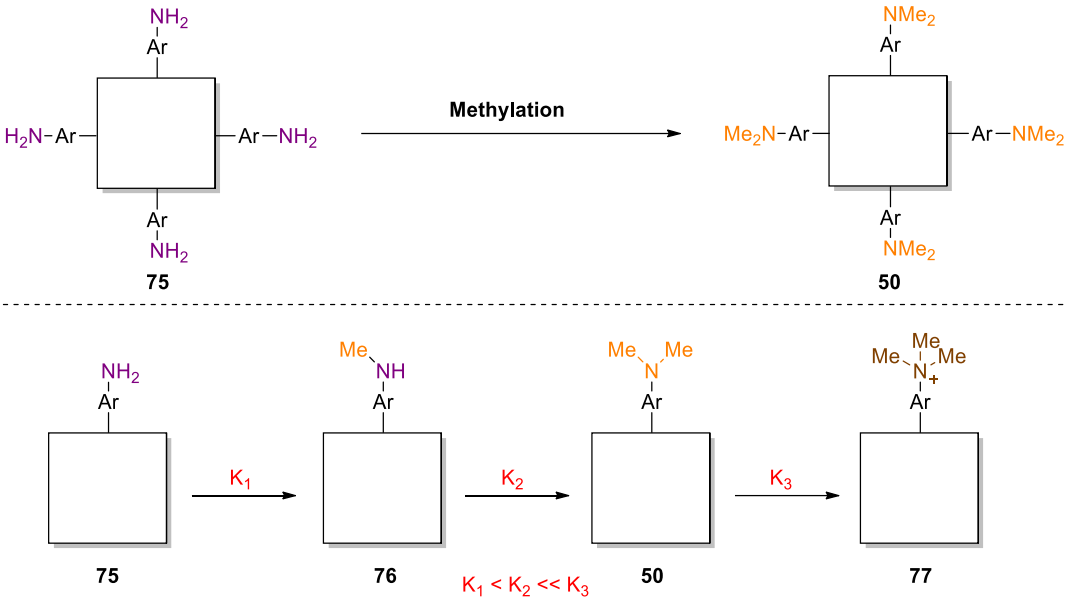

Scheme 10: Issues encountered using direct methylation reaction pathway.

The direct *N*-alkylation is based on a nucleophilic substitution which may result in the formation of the undesired *p*-trimethylamonium OETArXP **77** due to the high reactivity of the amino intermediates formed toward the methylating reagent (Scheme 10). The latter units are strongly electron withdrawing (σ_p = 0.77) and are therefore not suitable for our means.[109] In consequence, a reductive animation would be a more suitable method to form porphyrin **50** rather than using a direct alkylation (Scheme 11).

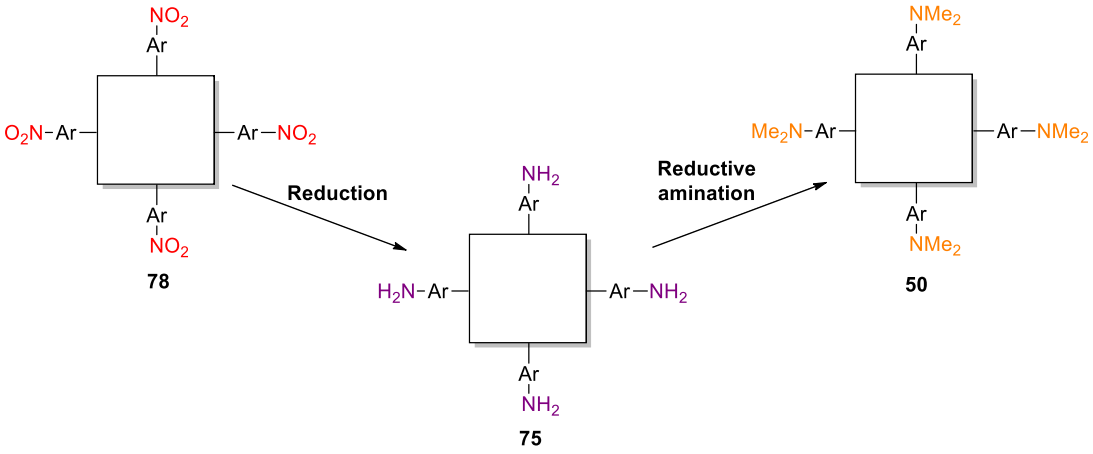

Scheme 11: Strategy for the formation of the *p*-dimethylamino-OEtArX-porphyrin **50**.

Usually, reductions of nitro groups are performed using catalytic hydrogenation with palladium/charcoal catalysts, though this catalyst also has a strong affinity toward other functionalities.[110] Other methods using metal or metal salts have been developed, employing for *e.g.*, Raney nickel, iron, zinc, or $SnCl_2$.[111] In this project $SnCl_2$ was chosen as a method to reduce nitro groups as it involves milder reaction conditions.

The reduction of the nitro groups was investigated and results are presented in Table 4. The porphyrin was used on a scale of 25 to 50 mg and several parameters were varied such as time, temperature, solvent and reagents in an attempt to optimize the reaction conditions.

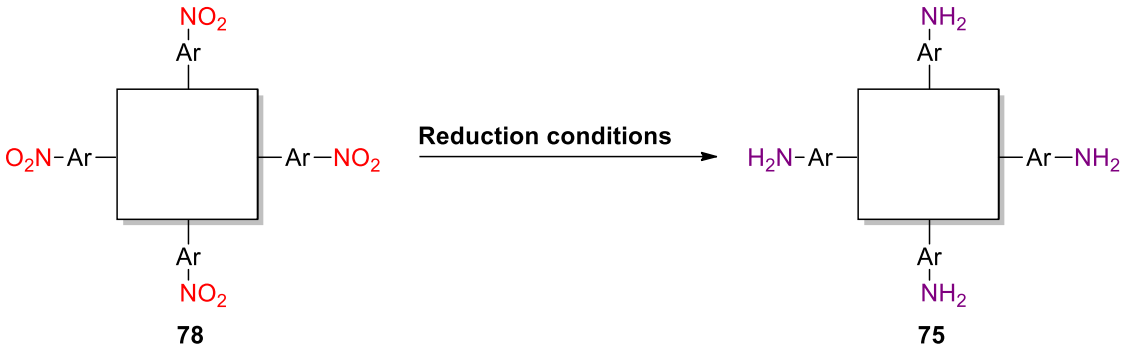

78 75

Table 4: Various conditions utilized for the reduction of nitro functional groups.

Entry	Reagents and catalysts	Solvents	Conditions	Results
1	$SnCl_2$, H_2O	HCl/EtOH	1 h, 60 °C, Ar.	Non soluble-
2	$SnCl_2$, H_2O	HCl/$CHCl_3$	1) 2 h, 80 °C, Ar. 2) 16 h, 80 °C, Ar.	Starting material Decomposition product
3	$SnCl_2$, H_2O	HCl/$CHCl_3$	16 h, 80 °C, Ar.	Starting material
4	$SnCl_2$	$CHCl_3$/EtOH Then HCl	3 d., 80 °C, Ar.	Starting material Decomposition product

Change in solvents from ethanol to chloroform, in temperature and reaction time (*e.g.*, 1 h up to 3 d.) were examined, however no reduction of the *p*-nitro groups of the meso-aryl units of porphyrin **78** could be observed.

3.2.2.2 Synthesis of the OPTArXP series

The two last porphyrins synthesized were the OPTArX-porphyrin series compounds **55** and **56**. Propyl units are more electron donating than ethyl groups resulting in a higher nucleophilicity of the pyrrole. In addition, propyl substituents are also more sterically demanding. Consequently, from the previous investigation using 3,4-diethylpyrrole to form the OETArXP series, the 3,4-dipropylpyrrole was only reacted with benzaldehyde **25** and *p*-methoxybenzaldehyde **38** (Fig. 26).[54]

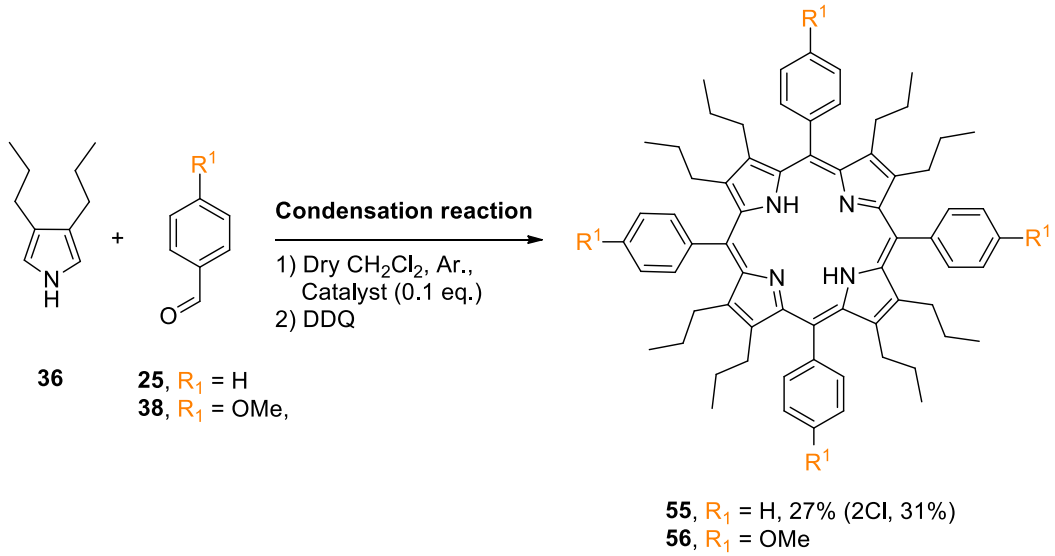

Scheme 12: Synthesis of free base OETArX-porphyrins.

Porphyrins **55** and **56** were synthesized using similar conditions as for the OETArX-porphyrin analogs. Therefore, the condensation was carried out for 72 h instead of 36 h using BF_3•OEt_2, before the addition of the oxidant. These conditions led to the formation of two species: the neutral porphyrin **55** in 27% and its diatonic form, 2,3,7,8,12,13,17,18-octapropyl-5,10,15,20-tetraphenylporphyrin chloride **55**·2Cl in 31% yield. Compounds **55**·2Cl proved difficult to neutralize, as porphyrin **55** represents a very strong base due to its high degree of distortion and its electron-rich macrocycle (Fig. 27) and reacts readily with any slight acidity present in solvents.

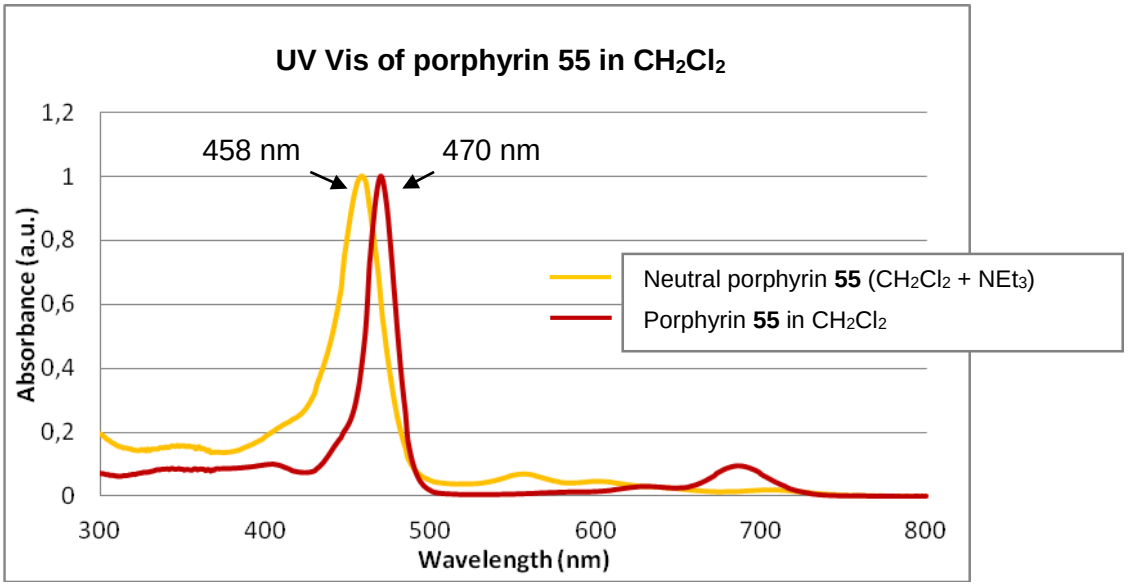

Figure 26: Fast protonation of compound **55** in CH_2Cl_2 (no acid added). The protonation is induced by the acidity of the CH_2Cl_2.

The use of aldehyde **38** did not lead to any product formation. This can be rationalized by low electrophilicity of both the aldehyde (due to the methoxy groups) and pyrrole (due to the propyl units) which results in a decrease of the reactivity between the two molecules. The use of BF_3•OEt_2 as well as TFA (stronger catalyst) for up to five days did not result in any yield. Another explanation could be the hindrance introduced by the propyl groups and will be discussed later in this chapter (see 3.4).

3.2.3 Examination of their spectroscopic and structural properties

Alongside the fact that these structures possess interesting properties in terms of electron density, they are also very interesting in respect of their spectroscopic properties. Due to the nonplanarity induced by the severe substitution of their macrocycle, various changes can be observed in either their UV-vis or NMR spectra.

3.2.3.1 ^{1}H NMR spectroscopy

Highly substituted free base porphyrins all display similar chemical shifts of the protons at the *β*-positions, so called *β*-protons. The ^{1}H NMR proton signals of the planar systems show NMR signals of the *β*-protons between 7 and 9 ppm. In the case of the systems presented herein, the *β*-protons are shielded due to the macrocycle distortion and are now observed between 0 and 3 ppm. Moreover, in comparison to symmetrical planar A_4 systems where the *β*-signals are seen as a well-defined doublet, symmetrical nonplanar A_4 porphyrins such as the porphyrin series synthesized herein, show broad singlets for their *β*-protons signals. Usually, one signal is observed for the CH_3 protons, while two signals are noted for the CH_2 protons and is characteristic of these systems. The splitting results from the different ethyl conformations being formed at low temperature. Medforth *et al*. showed that an increase in temperature from 25 °C (two signals) to 90 °C, results in the merging of the two signals to only one sharp and well defined signal. High temperatures induce more flexibility to the system, resulting in a loss of distinction between the two isomers. A second specificity of highly substituted porphyrin systems is the absence of signals for the inner NH protons in contrast to their planar analogs.[112] This is due to the fast exchange of the NH protons between the imine and amine moieties of the porphyrin macrocycle (*e.g.*, NH tautomerism).[113]

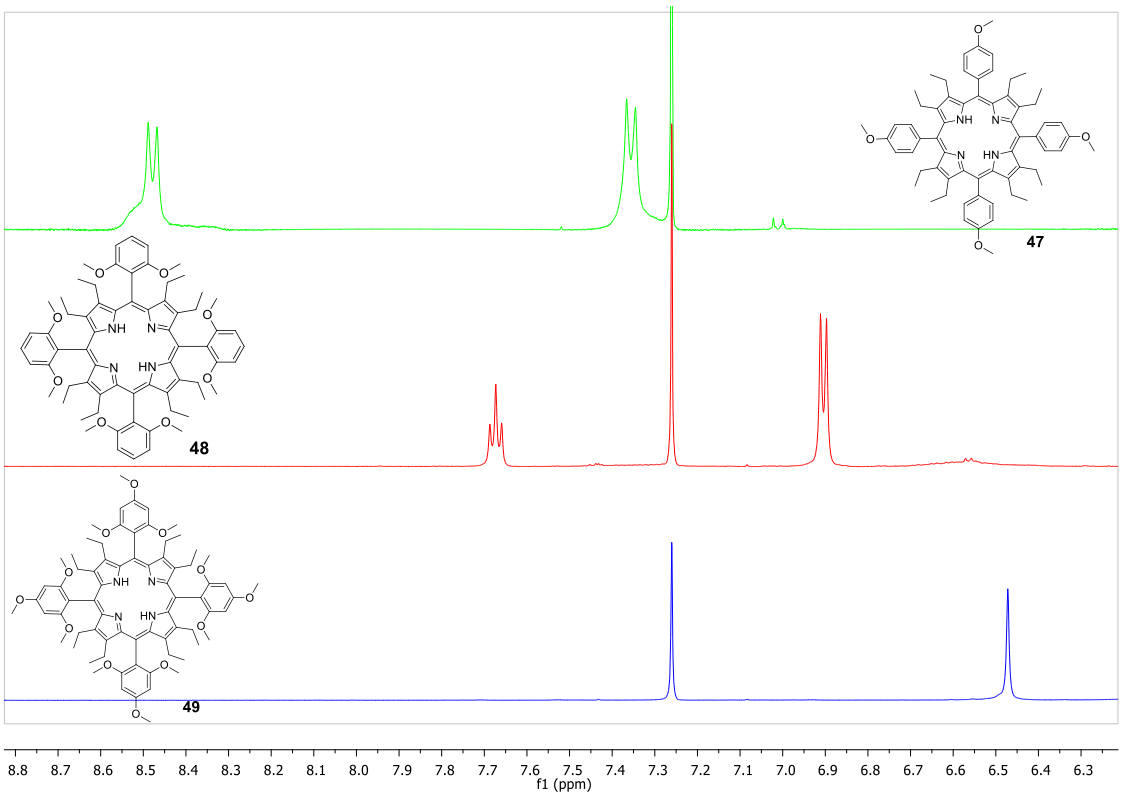

Figure 27: ^{1}H NMR chemical shifts of the aryl protons of compounds **47**, **48** and **49** in $CDCl_3$ depending on the aryl substitution pattern. The picture only shows the relevant area of the spectrum from 6 to 9 ppm.

Looking closer at compounds **47**, **48**, and **49**, it can be seen that upon addition of methoxy groups, the proton signals for the meso-aryl substituents are strongly shielded (Fig. 28).

Table 5: ^{1}H NMR values for chemical shifts of compounds **47**, **48** and **49** in $CHCl_3$ and 1% NEt_3 observed in Fig. 28.

Entry	Porphyrin	δ_o (ppm)	δ_m (ppm)	δ_p (ppm)
1	**21**	8.36-8.46	7.88	7.71
2	**47**	8.46	7.36	-
3	**48**	-	6.90	7.36
4	**49**	-	6.47	-

Compound **47** has methoxy groups at the *p*-positions of the meso-aryl substituents with free *o*- and *m*-positions. The *o*- and *m*-protons display chemical signals at 8.46 and 7.36 ppm, respectively. No change in the chemical signal for the *o*-protons is observed compared to H_2OETPP **21** where the *o*-, *m*- and *p*- position of the aryl groups are unsubstituted. This is due to the *p*-methoxy groups and the *o*-proton being too far from each other to induce variations in the proton environment. With regards to the *m*-protons,

a variation of the chemical signal is observed from 7.88 to 7.36 ppm. This variation is even higher, from 7.88 to 6.90 ppm, for compound **48**, where the methoxy groups are present at each *o*-position. The presence of a second methoxy group also affects the chemical signal of the *p*-proton which is shifted from 7.71 to 7.36 ppm. However, the effect is weaker due to the distance between the methoxy group and the *p*-protons as compared to the *m*-protons. Compound **49** combines the substitution pattern of porphyrins **47** and **48**, which results in a stronger shift of the chemical signals of the *m*-proton environment and a stronger shielding of the chemical signal and hence a shift to 6.47 ppm. It is clear that the methoxy groups have an important impact on the chemical signal of the aryl protons as the chemical signals of the *m*-protons are experiencing an upfield shift of more than 2 ppm going from porphyrin **21** to porphyrin **49**.

3.2.3.2 UV-vis spectroscopy

The UV-vis spectra of nonplanar highly substituted porphyrins are all very similar and are composed of broad bands (shoulders) preceding the Soret band followed by 2–3 weaker Q bands. The usual effect of the substituents added can also be seen.

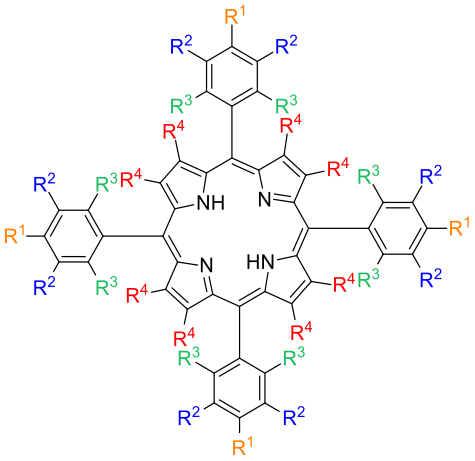

21, R^1 = R^2 = R^3 = H, R^4 = Et
46, R^1 = Me, R^2 = R^3 = H, R^4 = Et
47, R^1 = OMe, R^2 = R^3 = H, R^4 = Et
48, R^1 = R^2 = H, R^3 = OMe, R^4 = Et
49, R^1 = R^3 = OMe, R^2 = H, R^4 = Et
51, R^1 = OMe, R^2 = Me, R^3 = H, R^4 = Et
55, R^1 = R^2 = R^3 = H, R^4 = Pr

Figure 28: Target porphyrins for UV-vis studies.

Table 6: UV-vis main absorption bands observed for the Soret and the last Q band for the library of porphyrins synthesized recorded in $CHCl_3$ + 1% NEt_3.

Entry	Porphyrin	$\lambda_{Soret\ band}$ (nm)	$\lambda_{Qy(1,0)}$ (nm)
1	**21**	456	555
2	**46**	457	710
3	**47**	454	703
4	**48**	464	689
5	**49**	472	697
6	**51**	458	706
7	**55**	458	707

Table 6 compiles the Soret bands and last Q bands of the panel of porphyrins synthesized in this chapter and H_2OETPP **21**. H_2OETPP will be used in the discussion as a reference due to the unsubstitution of its meso-aryl groups. For example, the Soret bands of porphyrins **47**, **48** and **49** present an increasing bathochromic shift from 454, to 464, and then to 472 nm, respectively. The absorption peak observed for the former porphyrin is comparable to the one observed for H_2OETPP **21** which has no substitutents on the phenyl residues. However, the Soret bands of the two other porphyrins **48** and **49** are red-shifted by about 10 and 20 nm. In contrast, the Q bands display a hypsochromic shift upon addition of the methoxy groups. Usually, the bathochromic shift observed for nonplanar porphyrins can be correlated to the increased distortion of their macrocycle.[42c] In the case of these three structures, the red-shift compared to their planar analogs can be correlated to the distortion induced. However, the 10 and 20 nm bathochromic shift seen for the Soret band in porphyrins **48** and **49**, respectively, compared to H_2OETPP **21** is influenced by the presence of the methoxy groups. Compound **55** shows similar absorption values for its Soret band than compound **21** which can be interpreted by a similar distortion induced by *β*-propyl groups than the one induced by the presence of *β*-ethyl groups. This interpretation is supported by the study of the X-ray structure of compound **55**·2Cl (see section 3.2.3.3).

3.2.3.3 X-ray crystal structure

A crystal structure of the protonated form of porphyrin **55**·$2CH_3CO_2H$ was obtained after crystallization from $CHCl_3$ and hexane containing acetic acid. The side and top views of the porphyrin are presented in Fig. 29.

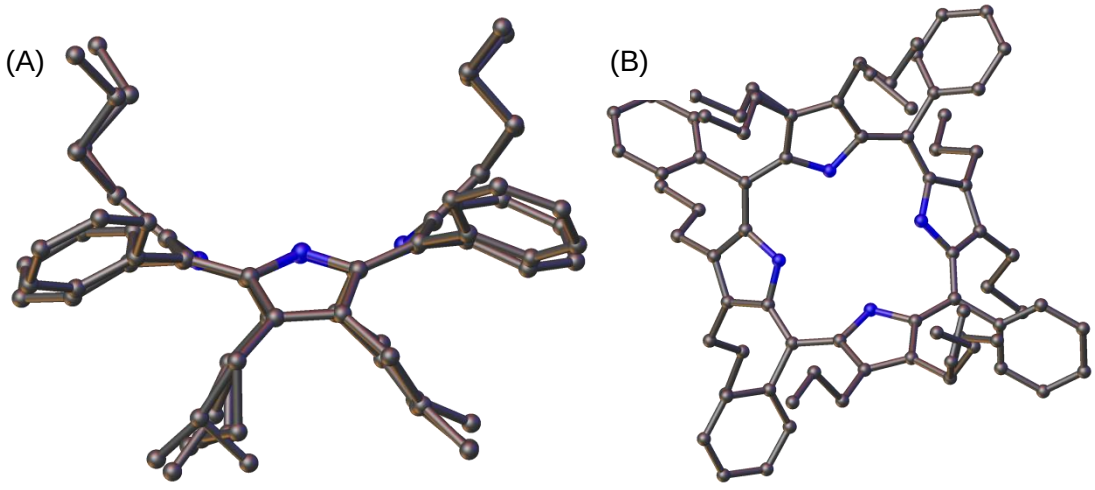

Figure 29: View of the molecular crystal structure of side view (A) and (B) top view of porphyrin **55**·$2CH_3CO_2H$. Hydrogen atoms and counter anions have been omitted for clarity. The crystal structure was determined by Dr. Brendan Twamley.

From this representative X-ray crystal structure (Fig. 29), a severe saddle distortion of the macrocycle, similar to other highly substituted porphyrins is evident.[73] This distortion is induced by the propyl groups which are pushed “up and down” from the mean plane.[57] The structure of porphyrin **55**·2CH_3CO_2H (Δ24 = 0.88 Å) was compared to the well-known example of porphyrin **21** for which the cationic from **21**·2TFA shows a Δ24 of 0.84 Å. Consequently, the distortion achieved using propyl groups is comparable to the one achieved using ethyl groups. Thus, the study of this porphyrin will allow researchers to specifically investigate the effect of more donating groups at the β-positions.

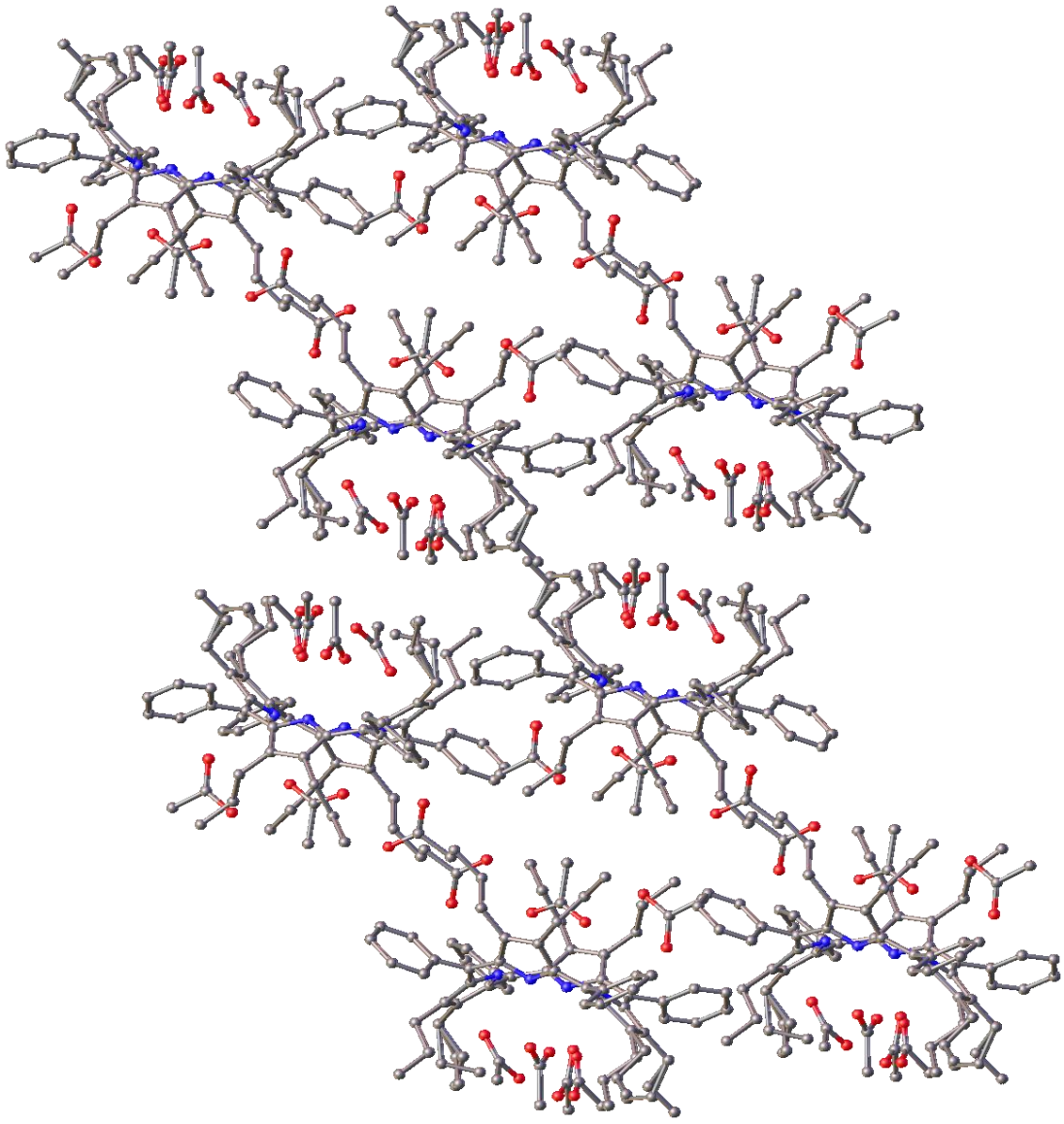

Figure 30: Excerpt of the crystal structure lattice diagram of porphyrin **55**·2CH_3CO_2H. Hydrogen atoms not involved in the hydrogen bonding network were omitted for clarity.

In addition, the crystal structure lattice diagram of **55**·2CH_3CO_2H also showed the formation of cavities where the counter anions are located (Fig. 30). It can also be

noticed that the same side of two independent molecules are facing each other creating a complete cage.

These type of structures are similar to the ones observed in Fig. 31 where a Cu(II)OETPP·2CH_2Cl_2 entrapped CH_2Cl_2 molecules in their cavities.[43d] It then became possible to use these cage-type structures for potential receptor applications due to the possibility to form small molecule binding pockets.

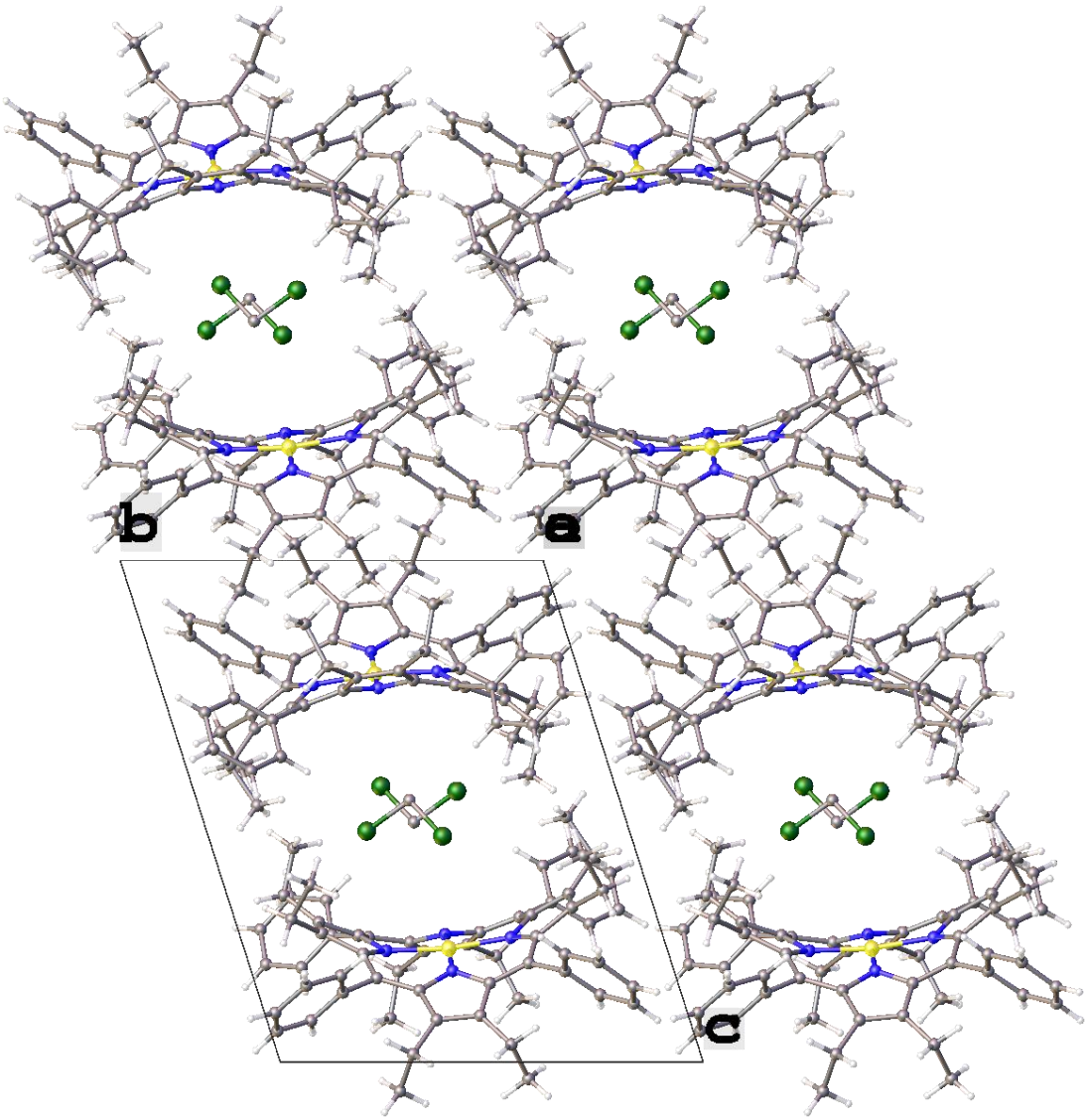

Figure 31: Molecular view of an excerpt of the crystal structure lattice diagram of Cu(II)OETPP·2CH_2Cl_2.[43b]

3.3 Conclusion and Outlook

The synthesis of highly substituted porphyrins can be achieved *via* the use of condensation reactions. While the pyrrole used for planar structures is commercially

available, pyrrole units used for the synthesis of highly substituted systems need to be synthesized. Two different routes were then used to form the 3,4-diethyl- and 3,4-dipropylpyrrole, **24** and **36**, respectively. Moreover, a panel of aldehydes bearing various electron donating substituents where chosen to be reacted with the pyrrole molecule. This examination showed that the increase of the electron donating effect is accompanied with a decrease in the reactivity between pyrrole and aldehyde. The positions of the substituents on the meso-aryl residues also contribute to diminishment in the reactivity between the two reagents of the condensation reaction. This is mainly explained by the steric hindrance between the *β*-substituents and some *m*- or *o*-groups of the meso aryl groups (*e.g.*, *tert*-butyl, methoxy). Five new porphyrins were synthesized in moderate to good yields. However, attempts to synthesize porphyrin **50** were unfruitful - using condensation reactions as well as various other pathways such as the Buchwald-Hartwig amination, or the synthesis of the *p*-amino intermediate. Further trials are still ongoing as this porphyrin would represent a good candidate towards the synthesis of a porphyrin “superbase”. The distortion observed for its macrocycle would be similar to the one observed in H_2OETPP **21**. In addition, the presence of the dimethylamino substituents which are strong electron donating groups (σ = 0.83) would result in an electron-rich macrocycle while circumventing any potential steric hindrance caused using *m*- or *o*-substitutents. No formation of the *p*-methoxy-OPTArX-porphyrin **47** was observed due to high electron density of the aldehyde. However, further investigation of aldehydes bearing electron withdrawing groups could be a very interesting alternative, especially those with halogen residues. These specific substituents would add further functionalities to the porphyrin concerning bonding possibilities as they can undergo halogen bonding.

4 *N*-Methylated porphyrins

4.1 Introduction

Historically, *N*-methylated porphyrins represent the oldest example of nonplanar porphyrins.[114] The nonplanarity of the porphyrin is a parameter that can be utilized for tailoring their binding abilities. In contrast to highly substituted porphyrins, *N*-substituted porphyrins enable the possibility of blocking some of the inner functionalities while maintaining the high levels of distortion within the macrocycle. This could be advantageous in examining the changes in the binding abilities of the NH and N moieties present in the porphyrin, and their availabilities as bases or nucleophiles.

N-Methylated porphyrins are a subcategory of *N*-substituted porphyrins. These so-called "green pigments" are porphyrin analogs wherein various groups (excluding hydrogen atoms or metal ions) are attached to the inner nitrogen atoms. A variety of *N*-substitution patterns have been reported in the literature so far and can be sorted into the three following categories: free base, metallated, and bridged porphyrins, including *N*-R-*N* or *N*-R-M types of bridges in the case of the latter (Fig. 32).[115]

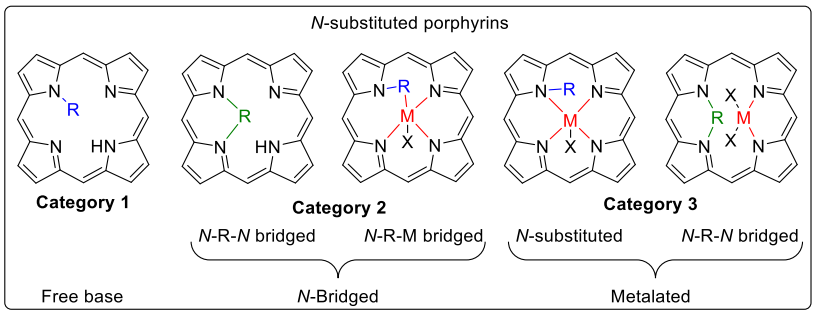

Figure 32: Various *N*-substitution patterns.

The free base *N*-substituted porphyrins possess one or more groups, on one or more of the inner nitrogen atoms (**category 1**). Groups utilized thus far include alkyl, phenyl, vinyl, benzyl, and allyl moieties. The *N*-methylated porphyrins studied in this project belong to this class. The second category consists of bridged porphyrins, which can be obtained through the insertion of various groups between two of the nitrogen atoms (*N*-R-*N* bridges) or between a pyrrolic nitrogen atom and the metal coordinated in the tetrapyrrole cavity (*N*-R-M bridges). Substituents introduced include amine groups, saturated or unsaturated carbon groups, and oxygen atoms (**category 2**). The insertion of a metal into the center of any **category 1** or **category 2** porphyrin results in the formation of metallated *N*-substituted porphyrins (**category 3**).

In nature, the function of *N*-methylated porphyrins has not yet been fully understood; however, these so called “green pigments” have been shown to be strong inhibitors of the enzyme protoporphyin IX ferrochelatase.[116] Ferrochelatase is an enzyme which catalyzes the insertion of iron into protoporphyrin IX to give protoheme b.[60] *N*-Alkyl porphyrins competitively inhibit ferrochelatase. Their distorted macrocycle mimics the transition state of the enzyme and is tightly bound to the ferrochelatase binding site.[47,117] The species responsible for the inhibition of human ferrochelatase has been isolated from the liver and appears to be *N*-methylprotoporphyrin IX (Fig. 33).[118] Their ability to bind proteins in such a strong manner that it results in an inhibition of other proteins potentially binding is a valid proof for the strong binding abilities of these systems. These *N*-methylated porphyrins could then be regarded as very good candidates for organocatalysis applications.

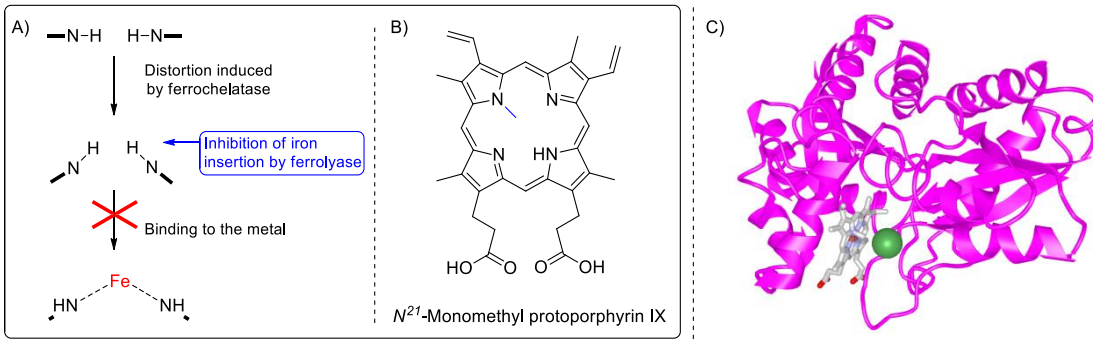

Figure 33: A**)** Inhibition of the ferrochelatase enzyme, B) Structure of the *N*-monomethyl protoporphyrin IX, C) Structure of ferrochelatase with Cu(II) *N*-methylmesoporphyrin IX complex bound at the active site.[119]

N-Methylated porphyrins are also produced in the body when xenobiotics react with cytochromes P-450 in the liver,[4b, 120] or upon interaction with some prescription drugs and anesthetics. They are also by-products, so-called “Heinz body” aggregates, which are formed during the reaction between hydrazine and hemoglobin. Furthermore, they are of biological and medicinal importance as they mimic capillary blocking aggregates, seen in malaria.[121] Initial research on *N*-substituted porphyrins and the work published on that topic until 1987 has been covered extensively in a book by Lavallee.[49]

4.2 Historical synthesis of *N*-methylated porphyrin

The first *N*-methylated tetrapyrrolic system was reported by McEwen in 1936. The discovery of these *N*-substituted tetrapyrrolic compounds did not only lead to a deeper understanding of biological mechanisms, but has also helped to deduce important features of biological compounds. They are considered as relevant molecules in the

synthesis of radiolabelled metalloporphyrins for medical diagnostic imaging.[122] Countless methodologies have been developed for accessing peripherally substituted nonplanar tetrapyrroles; however, synthetic pathways towards *N*-substitution are limited and have been somewhat neglected. The first direct alkylation of a porphyrin was reported in 1946, again by McEwen,[123] and since then only a few methods have been developed and optimized to target various *N*-substitution patterns.

These compounds are interesting due to the resulting distortion of the molecule induced by substitution of the pyrrolic hydrogens within the porphyrin core.[49] This results from the steric clash due to the inability of the hydrogen atoms and substituent groups to occupy the cavity at the same time. Moreover, this distortion allows small molecules to access the pyrrolic nitrogen, thereby enhancing the reactivity of these inner units compared to the corresponding planar free base.

Different strategies are employed to synthesize *N*-substituted porphyrins, depending on the kind of substitution required; however, the direct methylation represents the most convenient route towards *N*-alkylation. This method relies on a nucleophilic substitution, using either alkyl halides, dimethylsulfate (safer) or alkyl trifluoromethanesulfonate (safer and stronger) as alkylating agents.[124]

4.2.1 Synthesis using alkyl halides reagent

The first successful *N*-methylation was achieved with etioporphyrin I (EP I). Its synthesis was achieved using direct alkylation with methyl iodide, as both the alkylating reagent and solvent, in a sealed tube at 100 °C, leading to the N^{21}-monomethyl etioporphyrin I (Fig. 34).[123]

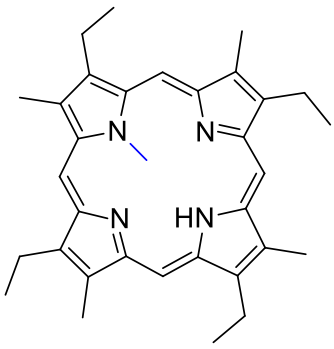

N^{21}-Monomethyl etioporphyrin I

Figure 34: Structure of the first *N*-substituted porphyrin reported.

Jackson and co-workers used the direct methylation method with methyl iodide as solvent for octaethylporphyrin (OEP) and achieved the N^{21}-mono- and *cis*-N^{21},N^{22}-

dimethyl OEP in 40% and 25% yields, respectively.[125] A study on the basicity of *N*-substituted porphyrins, performed by Neuberger *et al*., showed that they are stronger bases than their non-*N*-alkylated counterparts.[50a] Acidity/basicity studies represented, at that time, a very useful tool for researchers as they allowed them to better understand the reactivity of this type of porphyrin, and hence allowed the optimization of the respective reaction conditions. As a result of this study, an excess of methyl iodide and high temperatures were used with tetraphenylporphyrin (TPP), in order to obtain the N^{21}-monoalkylated form.[58a] However, *N*-monoalkylation, was only achieved in 5% yield and the main fraction contained higher alkylated porphyrins, such as N^{21},N^{22}-dimethyl and N^{21},N^{22},N^{23}-trimethyl TPP in an overall yield of 20%. Further basicity studies of free base and *N*-substituted porphyrins revealed that upon *N*-alkylation of porphyrins, the *N*-substituted species became a much more effective base compared to their corresponding free base precursors. This results in a higher reactivity of the N^{21}-monoalkylated porphyrin towards alkylation, compared to its former free base, hence giving rise to the rapid formation of higher degrees of *N*-methylation.[50a] Due to the higher pK_a of the free base TPP, the addition of a base (*e.g.*, potassium carbonate) resulted in optimized reaction conditions for the formation of higher degrees of alkylation; for example, the *cis*-N^{21},N^{22}-dimethylTPP iodide **26(b)[I]** was obtained in 41% yield and additionally the N^{21},N^{22},N^{23}-trimethylTPP **26(c)[I]** iodide was isolated in 6% yield (Scheme 13).[58a] Later, the N^{21},N^{22},N^{23}-trimethyl TPP **26(c)** was synthesized by Senge and co-workers in 92% yield using a methylating reagent and potassium carbonate in dichloromethane.[95] An improved method from Abeysekera *et al.* for EP I systems allowed the formation of the N^{21}-mono- **79(a)**, the cis-N^{21},N^{22}-di- **79(b)** and the N^{21},N^{22},N^{23}-methyl EP I **79(c)** (Scheme 13) in quantitative, 71 and 92% yields, respectively. The use of different bases, such as K_2CO_3, was employed for monoethylation or trisubstitution.[126]

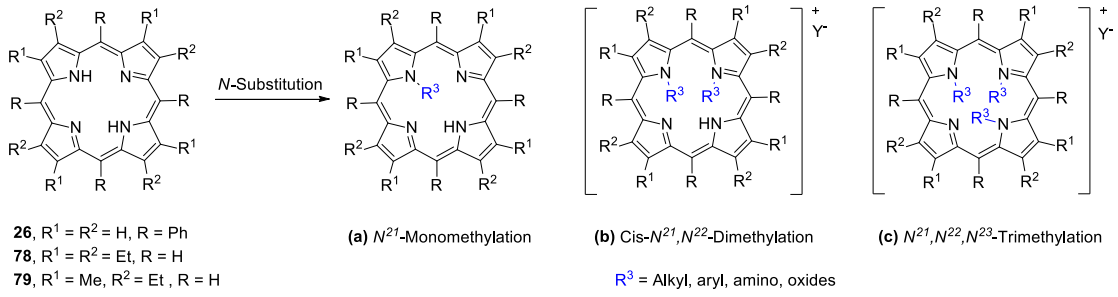

Scheme 13: *N*-Substitution reported for OEP, TPP and EP I systems.

Senge and co-workers investigated the combination of both peripheral and core substitution to study the structural and spectroscopic changes of so-called “highly

distorted" structures.[95] Attention was consequently focused on distorted porphyrins such as H_2OETPP **21**. They showed that the direct addition of methyl iodide to the porphyrin is possible under mild conditions upon addition of potassium carbonate, resulting in the N^{21},N^{22},N^{23}-trimethylated OETPP[I] salt in 75% yield.

The direct alkylation is highly dependent on the reactivity of the porphyrin, which itself is linked to the distortion of the macrocycle and accessibility of the inner core nitrogen atoms.[42b,73,127] For planar porphyrins, the core N/NH units are shielded by the macrocycle; in contrast, the generation of *sad*-distorted nonplanar porphyrins leads to greater accessibility of these units.[48a,97a,128] It has been observed that the substitution of at least one of the inner hydrogen atoms on the pyrrole moieties increases the potential of the cavity to bind molecules.[51a,64c,129] This is explained by the slight distortion induced by the *N*-substitution, increasing the reactivity of the newly formed product. However, only *N*-methyl or *N*-ethyl addition results in good yields of the N^{21}-monosubstituted products, due to the small size of the molecule inserted. Callot *et al.* developed a new route towards *N*-substitution of planar porphyrins by introducing more hindered groups such as phenyl, benzyl or vinyl units. His work focused on the *N*-addition of aryl and alkyl (other than methyl) moieties to H_2TPP using an N^{21},N^{22}-bridged porphyrin as an intermediate (Scheme 14).

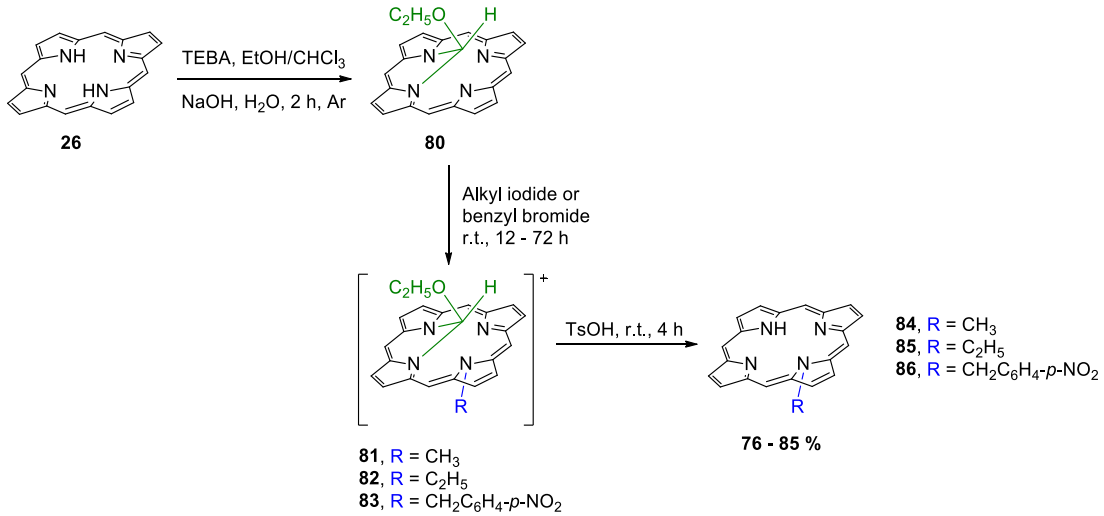

Scheme 14: *N*-Substitution *via N*-bridge intermediate (meso-substituents are not shown).

Their idea was to overcome the problem of the weak reactivity of the N/NH inner groups inherent to the planarity of the macrocycle. The formation of N^{21},N^{22}-bridged TPP was based on the implementation of distortion of the macrocycle through phase transfer conditions. The resulting N^{21},N^{22}-bridged TPP **80** then was more inclined to react with the following alkylating agent forming the trimethylated salts **81**–**83** depending on the

methylating agent used. Upon treatment with acid, a loss of the bridge was noticed and porphyrins **84**–**86** were obtained in 75 to 85% yields.[130]

4.2.2 Synthesis utilizing alkyl triflate/sulfate reagent

Another method investigated by several groups for meso-tetraarylporphyrins involves the use of alkyl triflates, which are stronger alkylating reagents compared to the alkyl iodides. The results are comparable to those with methyl iodide; an excess of the triflate reagent also leads to a mixture of various degrees of *N*-alkylation. However, a stoichiometric amount of methyl triflate in chloroform gave the N^{21}-monomethylated TPP as the major product in much higher yield of 30–35%. Only 3% of higher degree *N*-substituted products and starting material were formed.[131] Cavaleiro and co-workers, based on the increased basicity of the N^{21}-monoalkylated species compared to their starting material, showed that the addition of a weak acid to the solution of alkylating reagent can prevent further *N*-alkylation of the N^{21}-monomethylated form. Due to its basicity, the *N*-alkylated product became protonated upon addition of the acid and therefore further reaction of the remaining alkylating agent was inhibited. This was applied to the methylation of meso-free and meso-arylsubstituted porphyrins. In both cases, an increase in yield could be observed for the formation of the N^{21}-monomethylated product of up to 90% and 60% yields, respectively.[28,132]

In 1997 our group investigated the effect of direct *N*-alkylation on planar systems (*e. g.*, meso-tetraarylporphyrin (mTArP), meso-tetraalkylporphyrin (mTAlP)) and nonplanar macrocycles (*e. g.*, H_2OETPP **21**).[95] N^{21},N^{22},N^{23}-Trimethylated TPP **23** could be achieved in quantitative yield, using potassium carbonate and methyl triflate at room temperature, compared to the highest previously recorded yield of 60%.[132] Furthermore, a library of N^{21}-monomethylated mTAlP was generated, using methyl triflate under increased reaction temperatures. Yields of 30 to 40% were reported, while much lower yields were obtained utilizing methyl iodide. While polymethylation could be achieved readily for mTArP, it was not possible for mTAlP under any conditions employed.[95] Higher degrees of substitution were obtained *in situ*, however, these decomposed during chromatographic purification. Moreover, adding methyl trifluoromethanesulfonate dropwise to H_2OETPP **21**, under inert atmosphere and at elevated temperatures, gave the N^{21}-mono- and cis-N^{21},N^{22}-dimethyl substituted OETPP in 18 and 28% yields, respectively. The use of methyl triflate under mild conditions led to quantitative $N^{21},N^{22},N^{23},N^{24}$-tetramethylation of OETPP.

In 1979, Henrick *et al.* reported the use of dimethyl sulfate for the synthesis of various *N*-methylated porphyrins.[126] Upon insertion of the first methyl group into the cavity of the

porphyrin, an increase in the basicity of the porphyrin is observed. The porphyrin could then react with an acidic residue from the respective methylating agent, thus preventing insertion of further methyl units into the macrocycle. In this work, [18] buffer solutions were employed, and this showed to be particularly effective in preventing the monomethyl porphyrin reacting with the acidic residue, therefore resulting in the *trans*-N^{21},N^{23}-dimethylporphyrins which were synthesized in 70% yield.

4.2.3 Total synthesis using *N*-substituted pyrroles

Most of the past studies investigating direct *N*-alkylation methods have focused on symmetrical porphyrins (*e.g.*, mTArP, mTAlP, H_2OEP, H_2EP I), due to the formation of only one constitutional isomer, hence simplifying the already tedious purification procedures associated with porphyrins. In contrast, *N*-alkylation of unsymmetrical porphyrins would lead to several positional isomers. However, the chirality inherent to their asymmetry is of utter interest from a chemical and biological viewpoint. Consequently, even though it represents a vast challenge, a few reports discussed the preparation of *N*-substituted unsymmetrical porphyrins using a total synthetic pathway.

This route requires a MacDonald type approach[133] for either the [2+2]-type condensation of *N*-substituted dipyrromethanes or the condensation of tripyrranes with *N*-alkylated pyrroles.[134] The goal was to induce *N*-alkylation prior to the macrocycle formation in the condensation step, in order to avoid the steric hindrance normally experienced during *N*-methylation due to the cavity size. The strategic positioning of the *N*-substituents on the dipyrromethanes or pyrroles also reduced the time-consuming process of purification.[4b] Normally, typical conditions for the cyclization process involve the use of copper(II) to catalyze the ring closure. However, this results in the loss of the *N*-methyl groups.[135]

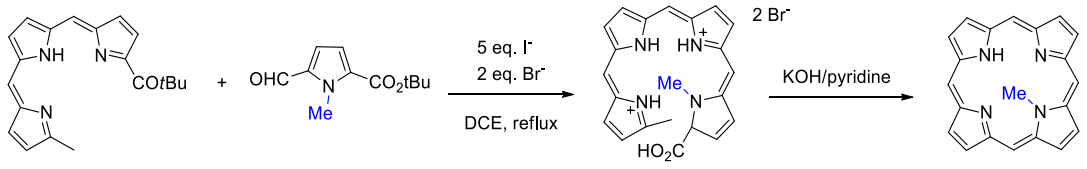

87 **88** **89** **90**

20 % **45 %**

Scheme 15: Total synthesis of an *N*-substituted porphyrin *via* improved MacDonald condensation (*β*-substituents are not shown).

To circumvent this setback Smith and co-workers reported the use of iodine or bromine in *o*-dichlorobenzene to prevent the cleavage of the *N*-methyl groups. With this method,

they were able to synthesize *N*-methyl protoporphyrin IX dimethyl esters (PP-IX DME) **90** through cyclization of tripyrrane **87** with *N*-methyl pyrrole **88** (Scheme 15).[134a]

4.2.4 *N*-Substitution of porphyrins *via* metalloporphyrin intermediates

Direct alkylation is very efficient for the *N*-methylation of various types of porphyrins (*e.g.*, meso-substituted or *β*-substituted porphyrins). However, *N*-alkylation of porphyrins with larger groups, such as ethyl moieties, using a direct *N*-alkylation approach resulted in much lower yields due to the steric hindrance. Any attempts to introduce bulkier substituents, such as aryl groups, failed.[131,132,136] The deformation of the macrocycle, induced by the addition of an inner substituent, implements drastic changes to the properties of the porphyrin, namely: spectroscopic characteristics,[137] redox potentials,[138] metal coordination,[139] dealkylation,[94a, 125a] and solvolysis.[140]

Such alternative methods were developed by Callot, employing metalloporphyrins which initially carry the designated *N*-substituent as an axial ligand coordinated to the metal.[141] He showed that an effective addition of diazoacetate to the zinc(II) porphyrin generates the corresponding diazoacetoxy zinc(II) complexes. After migration of the acetoxy group from the central zinc metal to the nitrogen and consecutive removal of the metal utilizing acid, the free base N^{21}-monoester tetraphenylporphyrin was obtained in 66% yield. Subsequent saponification of the ester and decarboxylation induced by irradiation with light gave an overall yield of 53% for the *N*-methyl TPP.[141]

They also investigated the formation of cobalt(III) complexes of H_2TPP and H_2OEP. *N*-Substituted systems were formed by treatment of a cobalt(II) porphyrin **91** with either alkyl iodide, to created σ-alkyl groups attached to the cobalt, or Grignard and aryllithium reagents to introduce σ-aryl groups as axial ligands to the cobalt atom (compound **92**).[142] The final product was achieved through an intramolecular migration of the σ-substituent to the nearest nitrogen atom forming **95** or **96** and the consecutive removal of the metal center under acidic conditions resulting in the *N*-substituted porphyrin **97**.

The intramolecular migration can be induced by two different methods. The first method requires oxidizing conditions and addition of an acid to form a cationic radical intermediate of the porphyrin complex **93** and is mainly used for σ-alkyl groups (Scheme 16, A).[143] The second route involves the use of oxidizing reagents such as cation radical salts which form the same porphyrin intermediate **93** as mentioned before and are mostly used for σ-aryl groups.[130,144] Subsequent elimination of the metal results in a

quantitative yield of the *N*-methyl TPP and a yield of more than 85% for the *N*-ethyl TPP (Scheme 16, B).

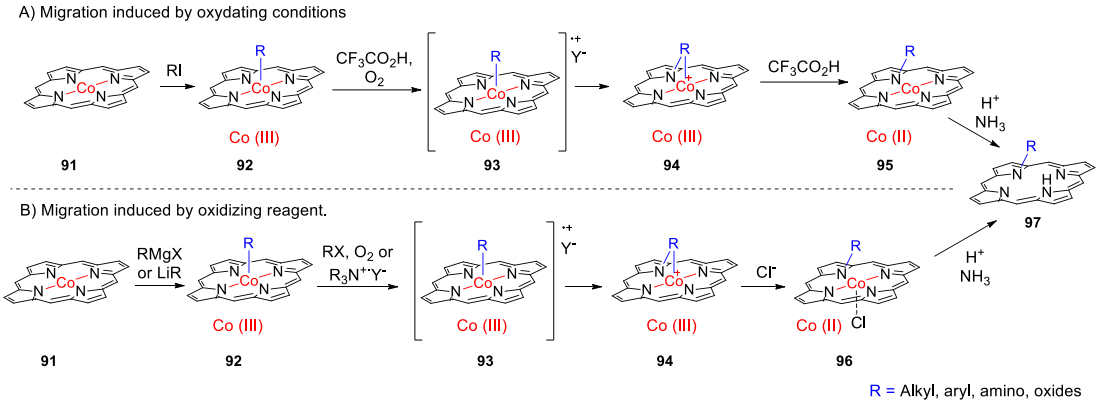

Scheme 16: Formation of *N*-substituted porphyrin *via* A) an intramolecular migration in oxidizing conditions, B) the use of an oxidizing agent (meso- and *β*-substituents are not shown).

The intramolecular migration involves the incorporation of the σ-substituent between the pyrrolic nitrogen and the cobalt atom, forming *N*-R-Co bridged porphyrins. Reduction of the cobalt(II) atom to cobalt(I) is necessary before the addition of acid and can be achieved either through treatment with $NaBH_4$ for mTArP or through utilization of a stronger reducing agent, such as sodium amalgam, for *β*-substituted porphyrins.[145] Cobalt(I), being a very unstable species, rapidly undergoes another intramolecular rearrangement from the cobalt(I) complex to the initial cobalt(III) complex.[143a] *N*-Methylation of meso-free systems resulted in much lower yields due to the difficulty in reducing the metal systems. This method represents an interesting alternative, allowing the selective generation of only N^{21}-monomethylated products in good yields. It also exhibits a facile and rapid approach towards systems containing *N*-vinyl or *N*-aryl groups. In 1993, Aizawa *et al.* synthesized *N*-*p*- and *N*-*o*-tolyl, and *N*-phenyl substituted TPP in 65, 68 and 87% yields, respectively, using intramolecular migration of cobalt(III) complexes under acidic conditions.[146] However, this methodology strongly depends on the strength of the σ-bonds the cobalt(III) porphyrin can form and can be limited due to instability of certain intermediates (*e.g.*, σ-benzyl).

4.2.5 *N*-Substitution utilizing sulfonium salts

The two aforementioned methods were also applied to σ-benzyl and σ-allyl groups. However, these groups showed insufficient stability under these reaction conditions.[49] This problem can be circumvented using carbocations. This led to the development of a new methodology utilizing diphenylsulfonium salts **98** as alkylating agents (Scheme 17).[49] These salts represent a highly reactive species[147] and provide *N*-benzyl porphyrins **99** in up to 90% yield for both meso-substituted and meso-free porphyrins.

The use of alkyl diphenylsulfonium salts, utilized in order to introduce *N*-alkyl groups, results in yields of up to 65%. However, rapid decomposition is observed in the solid state, especially when compared to other *N*-*p*-benzyl derivatives which can be formed using aryl diphenyl sulfonium salts.[49]

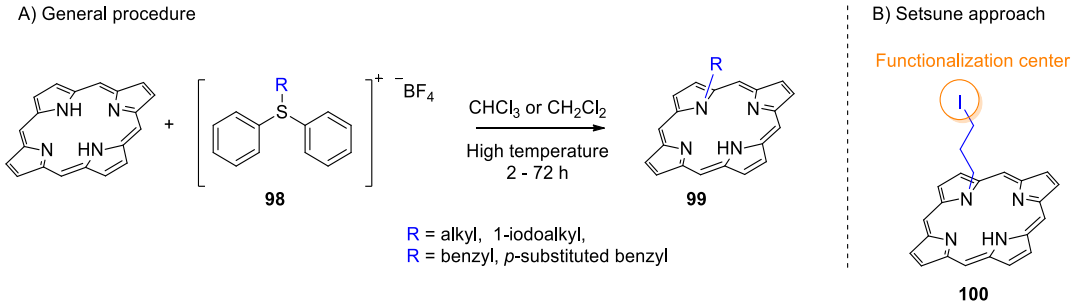

Scheme 17: Synthesis of *N*-monosubstituted porphyrins *via* the use of sulfonium salts (meso- and *β*-substituents are not shown).

Later, Setsune and coworkers prepared N^{21}-mono-iodoalkyl substituted OEP **100** with various alkyl groups *via* the *N*-substitution of 3-iodopropyl moieties (Scheme 17, B). The *N*-(3-iodopropyl)OEP•BF_4 was synthesized in 82% yield, which after additional functionalization of the terminal position of the propyl groups led to the further addition of either (*S*)-1-phenylethylamine, diethylamine or two different macrocyclic polyamines in 93, 71, 84 and 48% yields, respectively.[148]

4.3 Application

N-Substituted porphyrins have mostly been used to understand biological processes involving cytochromes P-450[115] or to study the metabolic process of heme formation.[115–118] However, their distorted macrocycle and specific structures can be very useful for applications involving core hydrogen bonding properties. As mentioned in previous chapters, the incorporation of units into their cavity results in the distortion of the macrocycle due to steric clash in the cavity of the porphyrin. This, however, results in the accessibility of the imine and amine moieties which can then form various bonds with small molecules.

Inoue and co-workers showed that the zinc *N*-substituted porphyrin **101** can be used as an initiator for visible light mediated polymerization of epoxides.[149] The reaction is carried out under mild conditions using benzene at room temperature for the polymerization of ethylene oxide (EO) and propylene sulphide (PS) (Scheme 18). The active site of the initiator resides on the axial ligand of the metal coordinated to the

porphyrin. The reaction proceeds *via* the attack of the propylthio axial ligand of the zinc porphyrin to the monomer generating a zinc thiolate species growing from the porphyrin.

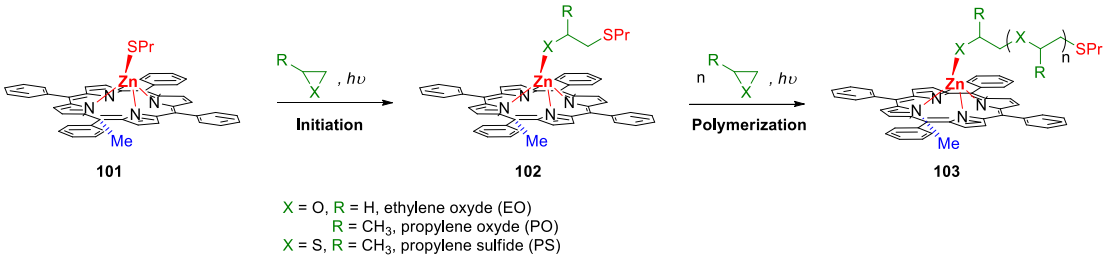

Scheme 18: Initiation and polymerization steps of various epoxides.

The initiation and polymerization process can be performed in the dark; however, light irradiation allows for a better and faster initiation of the reaction,[150] and is not required during the polymerization phase. Using zinc propylthio N^{21}-methyltetraphenyl porphyrin (NMTPP)ZnSPr **101**, complete polymerization is achieved in approximately 80 min with light irradiation or in 80% yield in the dark after 9 h. Copolymerization using both EO and PS was also investigated and proved to give very satisfying results.[151] When similar conditions were applied (benzene at room temperature under xenon light irradiation), it led to complete formation of a copolymer with uniform block lengths after 2.5 h (Scheme 19).

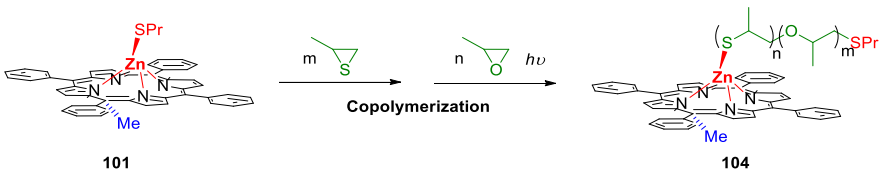

Scheme 19: Copolymerization of epoxides.

A final report carried by the same group focused on the enhancement of the copolymerization using the most efficient porphyrin, (NMTPP)ZnSPr **101**.[152] This study revealed that in the absence of light, the copolymerization of EO and PS exhibited very different conversions of each monomer. However, upon light irradiation, a very good ratio is obtained after only 5.3 h.

Another application was published by Kojima *et al.* and utilized the H-bonding and electron transfer properties of *N*-substituted porphyrins to demonstrate their potential as oxidants for H_2O_2/O_2 interconversion.[153] In the presence of hydrogen peroxide, an N^{21},N^{23}-dimethylated dodecaphenylporphyrin (N^{21},N^{23}-DPP) **105** can be reversibly reduced to its corresponding N^{21},N^{23}-dimethylated dodecaphenylisophlorin (N^{21},N^{23}-DPIPhl) **106** to generate O_2. The porphyrin acts as an electron and proton acceptor to oxidize the H_2O_2, generating its phlorin analog and O_2 (Scheme 20).

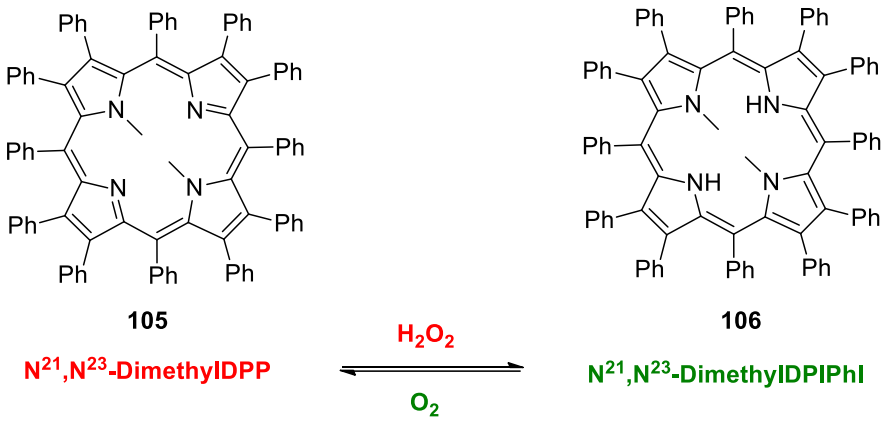

Scheme 20: Interconversion of hydrogen peroxide by the *N*[21],*N*[23]-dimethylated DPP.

The saddle shape of the porphyrins allows for good H-bonding properties of the imine units. This property is fortified by the high electronic density caused by the two *N*-methyl groups and the *syn*-conformation of these two *N*-methyl moieties. The inner units are also required for the stability of the phlorin analog which would otherwise be too reactive towards the oxygen species formed simultaneously. The electron-rich macrocycle of the porphyrin also results in a reversibility of the process from the phlorin, which upon reduction of the oxygen species reformed the 18π macrocycle, producing H_2O_2.

4.4 Results and discussion

This chapter is aimed at the synthesis of a library of *N*-methylated porphyrins with differing electronic (EDG and EWG) and structural properties (A4- and A2-mesosubstituted porphyrins, *β*-substituted porphyrins). In order to achieve this library, it was necessary to first generate the corresponding library of free base porphyrins. These free base porphyrins were chosen due to their planar conformations (as opposed to the highly substituted porphyrins) which allowed us to investigate the impact of various *N*-methylation patterns on the distortion of the macrocycle. This may also allow an investigation, if it is possible, into how to control the degree of distortion *via* different *N*-methylation patterns through the incorporation of one to four *N*-methyl substitutents.

4.4.1 Overall panel of synthesized *N*-methylated porphyrins

The 5,10,15,20-tetraarylporphyrin precursors (A_4) H_2**26**, H_2**107** to H_2**114** (Fig. 35) were synthesized *via* Adler-Longo or Lindsey condensation reactions[13,154] from the corresponding pyrroles and aldehydes in stoichiometric amounts. The 5,15-diarylporphyrin precursors (A_2) H_2**115**–H_2**119** (Fig. 35) were produced through condensation reactions using dipyrromethane and the corresponding aldehyde.[155]

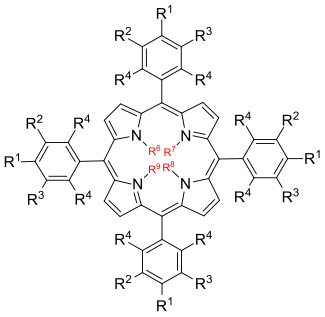

X	R^1	R^2	R^3	R^4
26	H	H	H	H
107	F	F	F	F
108	Cl	H	H	H
109	I	H	H	H
110	Br	H	H	H
111	H	OMe	H	H
112	OMe	H	H	H
113	Me	H	H	H
114	H	tBu	tBu	H

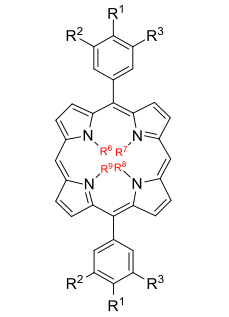

X	R^1	R^2	R^3
115	OMe	OMe	OMe
116	OMe	OMe	H
117	Me	H	H
118	H	H	H
119	H	OMe	H

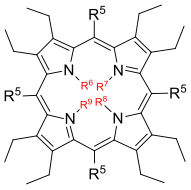

X	R^5
120	H
21	Ph

Methylation pattern:
H_2X, $R^6 = R^7 = R^8 = R^9 = H$
Xm, $R^6 = CH_3$, $R^8 = H$, no R^7/R^9
Xd, $R^6 = R^8 = CH_3$, no R^7/R^9
[Xd]$^+$, $R^6 = H$, $R^8 = R^9 = CH_3$, no R^7
[Xt]$^+$, $R^6 = R^7 = R^8 = CH_3$, $R^9 = H$
[Xtt]$^{2+}$, $R^6 = R^7 = R^8 = R^9 = CH_3$

Figure 35: Library of porphyrins synthesized.[1]

[1] For this chapter, it seems clearer to use the following numeration system: Number **X** represents the porphyrin, H_2**X** indicates the free base form of the porphyrin, **Xm** represents the N^{21}-monomethylated species, **Xd** the N^{21},N^{23}-dimethylated species, **[Xd]$^+$** the H^{21},N^{23},N^{24}-dimethylated species, **[Xt]$^+$** the N^{21},N^{22},N^{23}-trimethylated species (salt) and **[Xtt]$^{2+}$** the N^{21},N^{22},N^{23},N^{24}-tetramethylated species (salt). The numeration will be then conserved in part 5 which refers to the porphyrin synthesis carried out within part 4.

In order to generate the library of *N*-methylated porphyrins presented in Fig. 35 and explore their spectroscopic properties, the respective free base porphyrins were converted into various *N*-substituted porphyrins *via* direct methylation using respective equivalents of methyl triflate. Each porphyrin has different properties induced by their structure: steric effects such meso-substitution (**26**, **115**–**119**) or *β*-substitutions (**119**) pattern on the macrocycle, and withdrawing- (**107**–**111**) or electron-donating effects (**112**–**114**). These properties can affect the pattern of *N*-methylation. For example, it was noticed that in H_2**26**, methylation occurs on both pyrrole units (nitrogen 21 and 23) but in highly distorted porphyrins (*e.g.*, 2,3,7,8,12,13,17,18-octaethyl-5,10,15,20-tetraphenylporphyrin OETPP), methyl groups are substituted on adjacent nitrogens (21 and 22) leaving one pyrrole unchanged.[149]

4.4.2 Synthesis of precursors

As mentioned above, the *N*-methylation was carried out on A_4 and A_2 precursors. A_2 precursors were already available in the group, as were most of the A_4 precursors. However, some of them were synthesized for this project. The porphyrin precursors synthesized were compounds H_2**26,** H_2**107,** H_2**108**, and H_2**109**. The general synthetic methods are presented in Scheme 21 and they were all synthesized using either the Adler-Longo method or Lindsey conditions.[13,16,154]

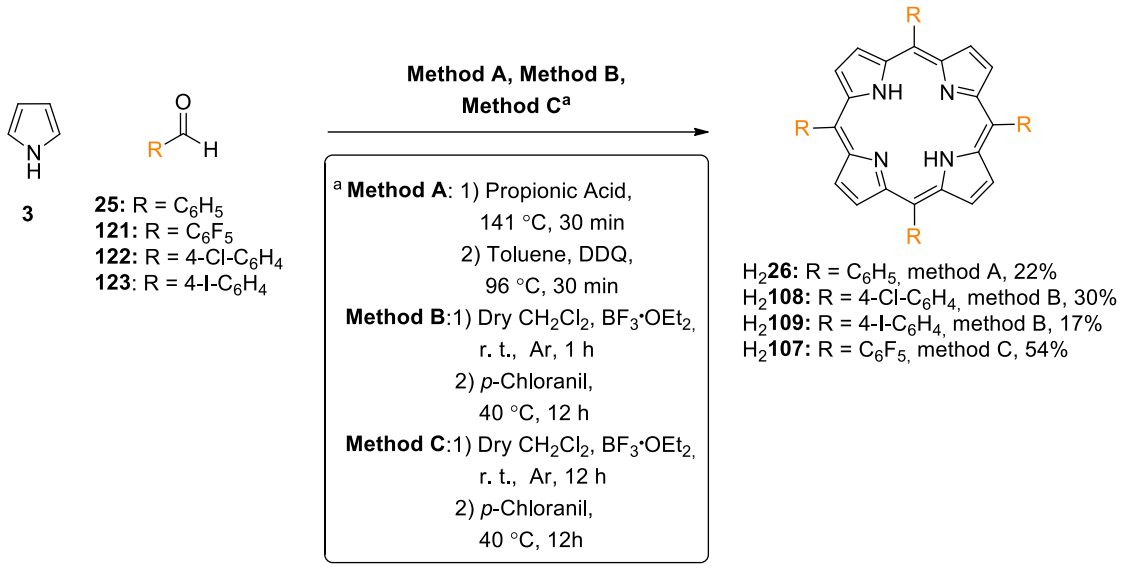

Scheme 21: Condensation reaction for the different precursors (H_2**26** and H_2**107**–H_2**109**).

Yields obtained from condensation reactions can be quite low due to polymerization of the pyrrole during the process. In total, 1.6 g of H_2**26** (22%, method A, Scheme 21), 670 mg of H_2**108** (30%, method B, Scheme 21), 72 mg of H_2**109** (17%, method B, Scheme 21), and 2 g of H_2**107** (54%, method C, Scheme 21) were prepared.

The Adler-Longo procedure is the easiest and fastest way to obtain H_2TPP H_2**26**, by precipitation of the porphyrin from propionic acid with methanol. Method B was used to obtain the other porphyrins in reasonable yields. However, this did not result in the formation of H_2**107** due to the high electron withdrawing effect of the fluorine atoms. Method C was a more efficient pathway for the preparation of compound H_2**107**.

4.4.3 *N*-Methylation of precursors

A library of *N*-methylated porphyrins was obtained from the panel of free base porphyrins. Fig. 35 compiles all of the structures of free base porphyrins tested with the various conditions of methylation to attempt mono-, di-, tri- or tetra-*N*-substitution.

4.4.3.1 *N*-Substituted TArP and OEP

First, we prepared the known *N*-substituted derivatives of 5,10,15,20-tetraphenylporphyrin (H_2**26**). The N^{21},N^{22},N^{23}-trimethylated porphyrin **[26t]$^+$** was obtained quantitatively following an optimized procedure by Senge *et al.* with a 10-fold excess of methyl trifluoromethanesulfonate in the presence of potassium carbonate (*condition a*, Scheme 22).[95] Treatment of porphyrin H_2**26** with a stoichiometric amount of the methylating agent in the absence of base (*condition b*) afforded the *N*-monomethylated species **26m** in 40% yield, similar to reports by Lavallee.[131,156] The use of *condition b* with 2 eq. of the methylating agent (*condition c*) at increased temperature led to both N^{21}-mono- and N^{21},N^{23}-dimethylated compounds **26m** and **26d** in 45% and 50% yields, respectively. All attempts to achieve $N^{21},N^{22},N^{23},N^{24}$-tetramethylation using various conditions and different methylating agents, from methyl iodide (weakest) to trimethyloxonium tetrafluoroborate (strongest), failed.

Similarly, methylation of H_2**120** was investigated. N^{21}-Mono- (**120m**) and N^{21},N^{22}-dimethylation (**[120d]$^+$**) have been previously reported,[15,21] thus porphyrin H_2**120** was treated under *condition b* to target the N^{21},N^{22},N^{23}-trimethylated species. However, only the N^{21},N^{22}-dimethylated salt **[120d]$^+$** was quantitatively obtained. As noted earlier, here dimethylation occurred on the adjacent pyrrole units (N21 and N22).[50a] This indicates the first fundamental difference in the reactivity of tetra-meso- and octa-*β*-substituted porphyrins.

Following the initial studies, the effect of electron withdrawing and donating groups of the meso-aryl substituents was investigated. For example, methylation of compound H_2**106** did not occur using *conditions a* or *b* on the bench. However, by employing a microwave apparatus, the N^{21}-monomethylated porphyrin **107m** was obtained in 2% yield. Attempts to optimize the reaction, including the use of a stronger methylating agent

([BF_4]·[OMe_3]) or an excess CF_3SO_3Me, were unsuccessful due to the strong deactivating effect of the EWG on the macrocycle. Thus, H_2**108** with fewer EWGs, using *condition b* afforded the N^{21}-monomethylated species **108m** in 69% yield. Similar to compound H_2**26**, doubling the equivalents of the methylating agent resulted in the formation of **[108d]**$^+$ in 40% yield.

However, due to the electron withdrawing chlorine atoms, *condition a* gave the N^{21},N^{22},N^{23}- trimethylated salt **[108t]**$^+$ in 60% yield, as opposed to compound **[26t]**$^+$ which was obtained quantitatively. Addition of a further 10 eq. (20 eq. in total) of the methylating agent (*condition d*, Scheme 22) gave the desired product **[108t]**$^+$ in a quantitative yield.

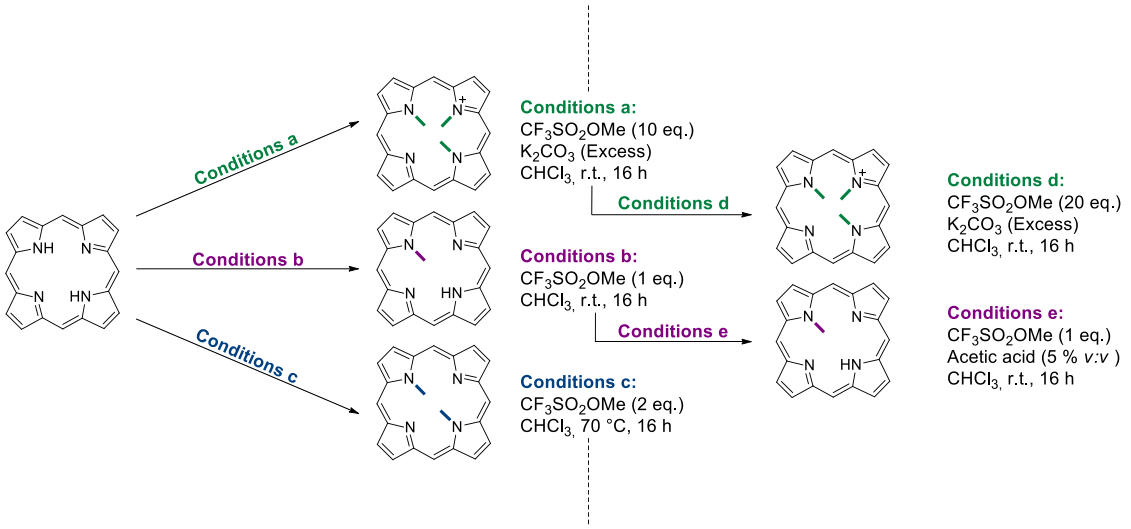

Scheme 22: Initial (a to c) approach and optimized conditions (d, e) for methylation of planar porphyrins.

A similar behavior was observed for N^{21}-monomethylation of porphyrins H_2**109** and H_2**110** giving 28% and 24% of **109m** and **110m**, respectively. In both cases, using two equivalents of methylating agent did not induce the formation of the N^{21},N^{23}-dimethylated species. The N^{21},N^{22},N^{23}-trimethylated forms were obtained for both compounds under *condition d* affording 77% of **[109t]**$^+$ and 60% of **[110t]**$^+$. Clearly, the strength of the EWG plays an important role in the efficiency of N^{21}-methylation. For the N^{21}-monomethylation of porphyrins H_2**108** to H_2**110**, the yield decreased from 69% to 19% going from chlorine to iodine. This diminishment of yield is also observed for the N^{21},N^{22},N^{23}-trimethylation and can be explained by the difference in Hammett values of iodine (σ = 0.27) and chlorine (σ = 0.22).[100] The exception to this is the N^{21},N^{22},N^{23}-trimethylation of compound H_2**109**. Compound **[109t]**$^+$ was obtained in a yield of 69% whereas **[109t]**$^+$ was afforded in 77% yield; however, this was likely the result of purification problems. Porphyrin H_2**111,** containing methoxy groups in the *m*-position of the aryl ring (σ = 0.12),

was treated under *condition a* affording 65% of the N^{21},N^{22},N^{23}-trimethylated salt **[111t]$^+$** and under *condition b* yielding 19% of N^{21}-monomethylated compound **111m**.

Next, porphyrins H_2**112**–H_2**114** containing electron donating groups (EDG) were investigated. Treatment of H_2**112** under *condition a* yielded a mixture of both N^{21},N^{23}-di- and N^{21},N^{22},N^{23}-trimethylated products **112d** and **[112t]$^+$** in yields of 7% and 73%, respectively, while *condition d* afforded **[112t]$^+$** in quantitative yield. Clearly, the presence of EDGs induces an electron-rich macrocycle enhancing the reactivity of the porphyrin core and causing multiple *N*-substitutions.

Table 7: Summary of yields for the various *N*-methylated porphyrins.

Entry	Hammett's values	Yields (%) N^{21}-CH_3 *Conditions (d)*	Yields (%) N^{21},$N^{22/23}$-$(CH_3)_2$ *Conditions (c)*	Yields (%) N^{21},N^{22},N^{23}-$(CH_3)_3$ *Conditions (e)*
1	0	75 (**26m**)	73 (**26d**)	>95 (**[26t]$^+$**)
2	0.23 (*p*-Cl)	15 (**108m**)	40 (**[108d]$^+$**)[a]	95 (**[108t]$^+$**)
3	0.18 (*p*-I)	28 (**109m**)	-	73 (**[109t]$^+$**)
4	0.23 (*p*-Br)	24 (**110m**)	-	71(**[110t]$^+$**)
5	-0.17 (*m*-OMe)	19 (**111m**)	-	65 (**[111t]$^+$**)
6	-0.27 (*p*-OMe)	50 (**112m**)	7 (**112d**)	73 (**[112t]$^+$**)
7	0.12 (*p*-Me)	45 (**113m**)	-	>95 (**[113t]$^+$**)
8	-0.10 (*m*-tBu)	8 (**114m**)[b]	-	60 (**[114t]$^+$**)[b]
9	-0.27 (*p*-OMe) /0.12 (*m*-OMe)	46 (**115m**)	86 (**[115d]$^+$**)[b]	-
10	-0.27 (*p*-OMe) /0.12 (*m*-OMe)	-	93 (**[116d]$^+$**)[b]	-
13	-0.17 (*p*-Me)	9 (**117m**)	5 (**[117d]$^+$**)[b]	-

[a] Structure of **[108d]$^+$** has N21/N22 instead of N21/N23 dimethylation pattern. [b] The noticeably lower yields for compounds **114m** and **[114t]$^+$** are a result of the low solubility of the starting material, which required a high dilution. [c] Structure of 5,15-diarylporphyrins involves N21-H, N23-Me/N24-Me instead of N21-Me/N23-Me as observed for the A_4 series.

A study by Cavaleiro *et al.* showed that the N^{21}-monomethylated products have increased basicity in comparison to their free base precursors due to the distortion induced by the *N*-substitution.[132] Consequently, the addition of a small amount of a weak acid can prevent further methylation. With this in mind, the addition of 5% (*v:v)* acetic acid (*condition e*, Scheme 22) allowed access to compound **112m** in a yield of 50%. *Condition e* was then applied to porphyrins H_2**113** and H_2**114** leading to 45% and 8% yields for the N^{21}-monomethylated products **113m** and **114m**, respectively. C*ondition d*

afforded the N^{21},N^{22},N^{23}-trimethylated salt **[113t]$^+$** in quantitative yield and **[114t]$^+$** in 60% yield. All yields obtained are summarized and presented in Table 7.

4.4.3.2 *N*-Substituted 5,15-Diarylporphyrins

In parallel, the *N*-methylation of 5,15-diarylporphyrins was studied. 5,15-Diarylporphyrins were chosen for their different macrocycle conformation. In line with the 5,10,15,20-tetraarylporphyrin, the distortion of their macrocycle is negligible, however, they show an elongation of the ring system along the 5,15-axis. This results in a rectangular shaped macrocycle, compared to the square shaped core usually seen for meso-tetrasubstituted analogs.[69a,157]

Initial attempts were made with compound H_2**115** and the *N*-monomethylated product **115m** was obtained in 46% using *condition e*. Following this, trimethylation was attempted using *condition a*; however, this gave the N^{21},N^{22}-dimethylated product **[115d]$^+$** in 86% yield. Forcing the N^{21},N^{22},N^{23}-trimethylation using *condition a* and microwave apparatus resulted in a mixture of N^{21},N^{22}-di- and N^{21},N^{22},N^{23}-trimethylated species. Similarly, compound H_2**115** gave **[116d]$^+$** in 93% yield under *condition a*, while **[116t]$^+$** could not be obtained under *conditions a* or *d* at higher temperature. Trials to monomethylate porphyrin H_2**116** using *condition e* were unsuccessful, too, giving less than 1% yield. Compound H_2**117** gave compound **117m** in 9% yield under *condition e* and compound **[117d]$^+$** in 5% yield under *condition a*. Using *condition a* at higher temperature or *condition d* failed to yield N^{21},N^{22},N^{23}-trimethylation. Finally, *N*-methylation attempts of compounds H_2**118** and H_2**119** using *condition e* or *condition a* were unsuccessful. With regards to the overall results of the NMR studies, *N*-methylation of the 5,15-porphyrins (A_2-system) proceeds differently to the meso-tetrasubstituted A_4-analogs. While the latter leads to a N^{21},N^{23}-dimethylation pattern, dimethylation of the former occurs on neighboring pyrrole rings under formation of monocationic salts, *i.e.*, yields N^{23},N^{24}-dimethylated macrocycles. We surmise that this might be a result of the core elongated macrocycle conformation in the precursor free bases, but this will ultimately require detailed theoretical calculations.

4.4.4 UV-vis and NMR observation

4.4.4.1 *N*-Substituted TArP and OEP

- *Study on the variation of the wavelength of the Soret Band*

Next, spectroscopic analyses such as UV-vis and ^{1}H NMR studies of the *N*-methylated porphyrins were utilized to investigate the degree of distortion in the porphyrin macrocycle. In UV-vis measurements, a bathochromic shift of the Soret band is usually

observed for distorted porphyrins compared to planar porphyrins.[49] Similarly, a chemical shift (upfield) is also noted for the inner protons (or the methyl units inserted) of the porphyrin core in the ^{1}H NMR spectrum upon the addition of methyl groups as discussed in part 1.[94a]

These trends were reflected in the compounds presented here. In an earlier study on the *N*-alkylation of highly nonplanar free base H_2**21** (Soret λ_{max} = 456 nm), a bathochromic shift of 20 nm was observed for the Soret band after insertion of one methyl unit (**21m**) and ultimately, the Soret band was shifted by 50 nm upon *N*-tetramethylation (**[21tt]$^{2+}$**).[95]

Table 8: UV-vis absorption data of Soret bands for free base porphyrins and their *N*-methylated derivatives in $CHCl_3$ and 1% NEt_3.

Entry	$\lambda_{\text{Soret band}}$ (nm) of free base	$\lambda_{\text{Soret band}}$ (nm) of N^{21}-CH_3	$\lambda_{\text{Soret band}}$ (nm) of N^{21},$N^{22/23}$-$(CH_3)_2$	$\lambda_{\text{Soret band}}$ (nm) of N^{21},N^{22},N^{23}-$(CH_3)_3$
1	419 (H_2**26**)	433 (**26m**)	459 (**26d**)	462 (**[26t]$^+$**)
2	420 (H_2**108**)	436 (**108m**)	463 (**[108d]$^+$**)[a]	466 (**[108t]$^+$**)
3	422 (H_2**109**)	439 (**109**m)	-	444 (**[109t]$^+$**)
4	439 (H_2**110**)	469 (**110**m)	-	471 (**[110t]$^+$**)
5	420(H_2**111**)	436 (**111**m)	-	469 (**[111t]$^+$**)
6	421 (H_2**112**)	439 (**112m**)	458 (**112[d]$^+$**)	475 (**[112t]$^+$**)
7	421 (H_2**113**)	444 (**113**m)	-	468 (**[113t]$^+$**)
8	421 (H_2**114**)	437 (**114**m)	-	473 (**[114t]$^+$**)

[a] Structure of **[105d]$^+$** has N21/N22 dimethylation pattern instead of N21/N23 as observed for the A4 precursors. [b] Structure of 5,15-diarylporphyrins involves N21-H, N23-Me/N24-Me instead of N21-Me/N23-Me as observed for the A_4 series.

The Soret band of compound H_2**26** appeared at 419 nm highlighting the difference in distortion in both parent free base compounds. N^{21}-Monomethylation (**26m**) resulted in a 14 nm shift, while the Soret band for **[26t]$^+$** was observed at 467 nm inducing a bathochromic shift of 48 nm for the insertion of three methyl units (Figure 36 and Table 8). The N^{21},N^{22},N^{23}-trimethylation **[108t]$^+$** and **[112t]$^+$** compared to porphyrins H_2**108** and H_2**112** gave similar trends (Δ_{abs} = 46 and Δ_{abs} = 54 nm, respectively). The larger shift in the tetraphenylporphyrin series compared to that in dodecasubstituted nonplanar porphyrins was a reflection that the latter become progressively more distorted. However, the former resulted in a larger relative increase of distortion.[48a,97a,128]

In all cases, introduction of a second *N*-methyl unit resulted in significantly more distinct spectral changes than introduction of the first, indicating significantly more distorted macrocycles (*vide infra*). Introducing a third methyl group was accompanied by a broadening of the absorption bands.

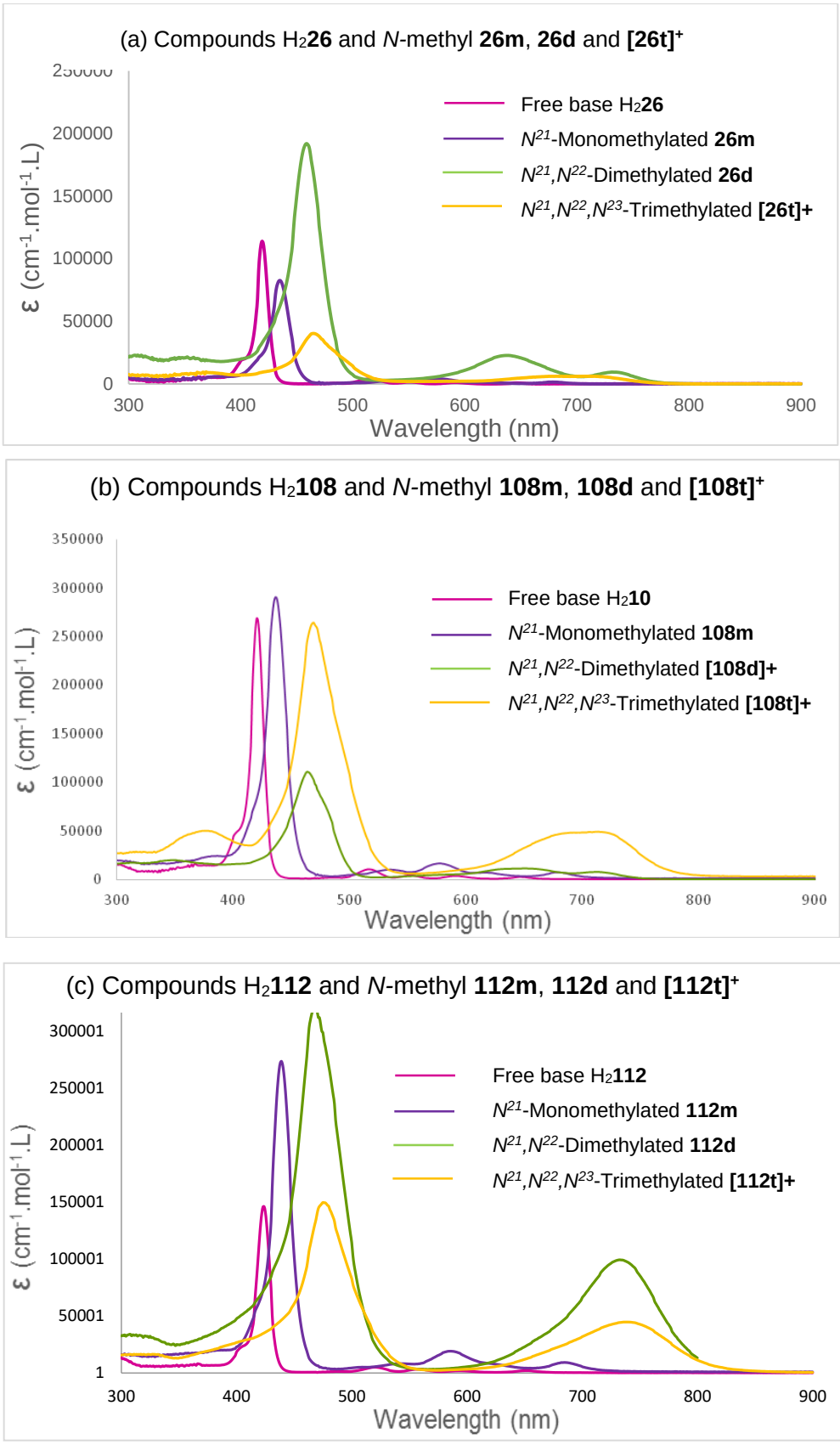

Figure 36: UV-vis spectra of compound H$_2$**26** (top), H$_2$**108** (middle) and H$_2$**112** (bottom) and their *N*-methylated derivatives in $CHCl_3$ (1% NEt_3).

Planar porphyrins typically have a well-resolved vibronic structure in the Q bands due to their single vibrational mode. In comparison, distorted porphyrins have multiple vibrational modes inducing a broadening of the vibronic structure in the Q bands.[42b, 158] Thus, core *N*-substituted nonplanar porphyrins show an overall behavior similar to peripherally substituted nonplanar porphyrins. Taking into consideration the overall bathochromic shift for the free base porphyrin to the N^{21},N^{22},N^{23}-trimethylated porphyrin, the shift observed for H_2**26** was smaller than the one for compounds H_2**108** and H_2**112** (Fig. 36). This trend showed that the electron density of the macrocycle had an impact on the distortion with EDGs giving a larger bathochromic shift following *N*-methylation.

Similar effects were observed in the ^{1}H NMR spectra of the *N*-substituted compounds. The *N*-H chemical shifts for the N^{21}-monomethyl product are found at −4.84 ppm (**26m**), −4.88 ppm (**108m**), and −4.77 ppm (**112m**) (Table 9).

Table 9: ^{1}H NMR chemical shifts for the *N*-R protons of free base porphyrins and their respective various degrees of *N*-methylation in $CDCl_3$

	Porph.	**δN21**	**δN22**	**δN23**	**δN24**
1	H_2**26**	−2.76 (H)	-	−2.76 (H)	-
2	**26m**	−4.06 (CH_3)	-	−4.84 (H)	-
3	**26d**	−2.90 (CH_3)	-	−2.90 (CH_3)	-
4	**[26t]$^+$**	−3.07 (CH_3)	−5.56 (CH_3)	−3.07 (CH_3)	-
5	H_2**108**	−2.85 (H)	-	−2.85 (H)	-
6	**108m**	−4.14 (CH_3)	-	−4.88 (H)	-
7	**[108d]$^+$**	−4.92 (CH_3)	−4.72 (CH_3)	−2.93 (H)	-
8	**[108t]$^+$**	−3.13 (CH_3)	−5.55 (CH_3)	−3.13 (CH_3)	-
9	H_2**109**	−2.89 (H)	-	−2.89(H)	*
10	**109m**	−4.81 (CH_3)	-	n/a	-
11	**[109t]$^+$**	−3.90 (CH_3)	-5.67 (CH_3)	-3.90 (CH_3)	-
12	H_2**110**	−2.89 (H)	-	−2.89 (H)	*
13	**110m**	−3.01 (CH_3)	-	n/a	-
14	**[110t]$^+$**	−3.16 (CH_3)	−5.62 (CH_3)	−3.16 (CH_3)	-
15	H_2**111**	−2.77 (H)	-	−2.77 (H)	*
16	**111m**	−4.07 (CH_3)	-	n/a	-
17	**[111t]$^+$**	−3.15 (CH_3)	−5.60 (CH_3)	−3.15 (CH_3)	-
18	H_2**112**	−2.79 (H)	-	−2.79 (H)	-
19	**112m**	−4.06 (CH_3)	-	−4.77 (H)	-
20	**112d**	−2.87 (CH_3)	-	−2.87 (CH_3)	-
21	**[112t]$^+$**	−3.02 (CH_3)	−5.32 (CH_3)	−3.02 (CH_3)	-
22	H_2**113**	−2.17 (H)	-	−2.17	*
23	**113m**	−4.69 (CH_3)	-	n/a	-
24	**[113t]$^+$**	−3.12 (CH_3)	−5.50 (CH_3)	−3.12 (CH_3)	-
25	H_2**114**	−2.67 (H)	-	−2.67 (H)	-
26	**114m**	−3.82 (CH_3)	-	n/a	-
27	**[114t]$^+$**	−2.98 (CH_3)	−5.47 (CH_3)	−2.98 (CH_3)	-

[a] Structure of **[1056d]$^+$** has N21/N22 dimethylation pattern.

The insertion of the first methyl group induced a significant change in the chemical shifts of the *N*-H groups, as the change observed between H_2**26** and **26m** is about 2.08 ppm. These differences were mainly due to the distortion resulting in a displacement of the *N*-H units outside of the aromatic ring current.[87c]

Looking further into the N^{21},N^{22}-dimethylation it was noticed that when symmetry was maintained, as in porphyrins **26d** and **112d**, the methyl groups on N21 and N23 had the same chemical shift. In contrast, with methylation of N21 and N22 (compound **[108d]**$^+$), the two methyl groups and the hydrogen protons displayed different chemical shifts at -4.92 ppm (N21), -4.72 ppm (N22) and -2.93 ppm (N23).

The addition of a third methyl group in compounds **26d** and **112d** caused the CH_3 signal of N21 and N23 to shift from -2.90 to -3.07 ppm (**[26t]**$^+$) and from -2.87 ppm to -3.02 ppm (**[112t]**$^+$). The signal for the additional methyl group in position N22 appeared at -5.56 ppm (**[26t]**$^+$) and -5.32 ppm (**[112t]**$^+$). Upon addition of a third methyl into the core of compound **[108d]**$^+$, a shift from -4.92 ppm to -3.13 ppm was observed for the methyl groups on N21 and N23 with the additional methyl unit (N22) being observed at -5.55 ppm (Table 9).

- *Study on the molar absorption coefficient*

The effect of the *N*-methylation is strongly evidenced by the modification of the molar extinction coefficients (Fig. 36). From results obtained, it appeared that the molar extinction coefficient was dependent on three factors: the electronic effect, the degree of *N*-substitution, and the conformation resulting from the *N*-substitution.

A series of A_4 porphyrins were studied *via* UV-vis spectroscopy (Fig. 36). From this, it was observed that the addition of electron withdrawing or donation groups on the periphery of the macrocycle (free base porphyrins, Fig. 36 pink spectrum) modified the absorption properties of the porphyrins with a better effect seen for the electron withdrawing units.

Upon the addition of methyl groups, an increase of the molar absorption coefficient ***ε*** value was seen for most of the compounds. Interestingly, the addition of two methyl units into the core of the porphyrins (Fig. 36, green spectrum) induced two different behaviors depending on the "*cis*"- (CH_3 in N23,N24) or "*trans*"- (CH_3 in N21, N23) methylation. Porphyrins **26d** and **112d** (neutral form) resulted in an increase of ***ε*** value compared to porphyrins H_2**26** and H_2**112,** respectively. In contrast **[108d]**$^+$ showed a decrease of the ***ε*** value. This decrease was explained by the cationic form of compound **[108d]**$^+$ and was

supported by the decrease observed upon the addition of a third methyl. The formation of a charge due to the third methyl resulted in a decrease of the ***ε*** value (Fig. 36, yellow spectrum) for each A_4 porphyrin series compared to the free base form (Fig. 36, pink spectrum).

4.4.4.2 *N*-Substituted 5,15-Diarylporphyrins

- *Study on the variation of the wavelength of the Soret Band*

The UV-vis properties of the 5,15-disubstituted series were quite similar to those of the 5,10,15,20-tetraarylsubstituted porphyrins. Introduction of one methyl unit to the core resulted in a bathochromic shift of the Soret band by 20 nm for each series of porphyrins indicating core distortion (Table 10).

Table 10: UV-vis absorption data of Soret bands for free base porphyrins and their *N*-methylated derivatives in $CHCl_3$ and 1% NEt_3.

Entry	$\lambda_{Soret\ band}$ (nm) of free base	$\lambda_{Soret\ band}$ (nm) of N^{21}-CH_3	$\lambda_{Soret\ band}$ (nm) of N^{21},$N^{22/23}$-$(CH_3)_2$
9	404 (H_2**115**)	424 (**115m**)	447 (**[115d]$^+$**)[b]
10	410 (H_2**116**)	-	452 (**[116d]$^+$**)[b]
11	406 (H_2**117**)	428 (**117m(a)**/*anti*) 442 (**117m(b)**/*syn*)	437 (**[117d]$^+$**)[b]

Due to the increased distortion upon introduction of a second methyl group, compounds **[115d]$^+$** and **[117d]$^+$** exhibited shifts of the Soret band larger than those seen for the free base planar analogs (Fig. 37). Intriguingly, the introduction of a methyl unit in compound H_2**117** gave porphyrin **117m** which exhibited a surprisingly widely-separated split Soret band, deviating from the common UV-vis pattern observed for the other porphyrins (Fig. 37, (b)). Studies on possible geometric isomers in solution by UV-vis have been reported by a few groups in the past,[159] and the present results were explained by the formation of two isomers, the *anti*-[**117m(a)**] and the *syn*-[**117m(b)**] isomers (Fig. 38, Fig. 39).

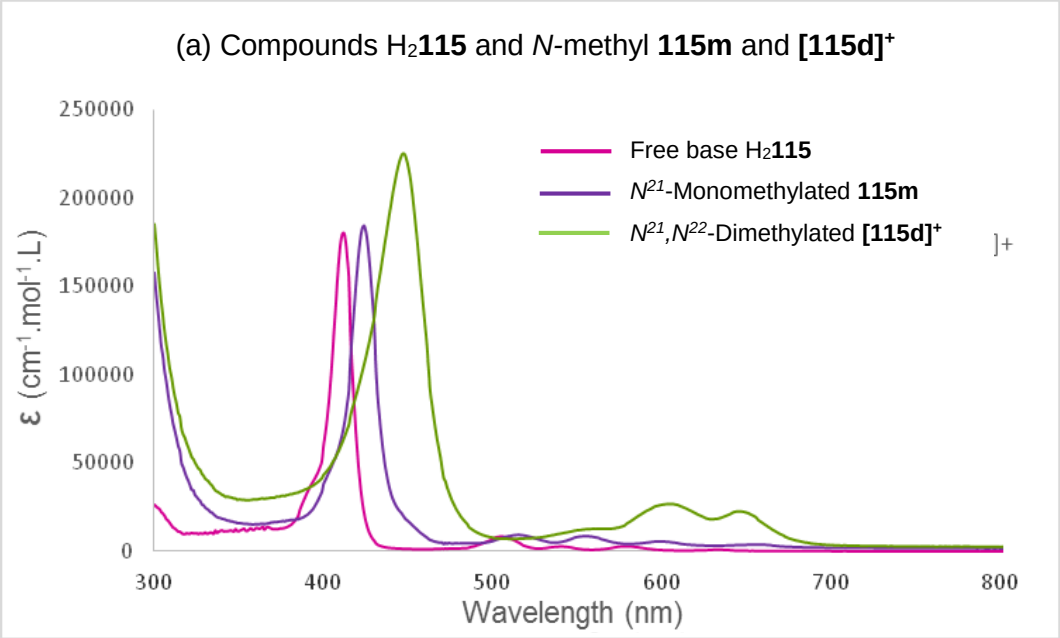

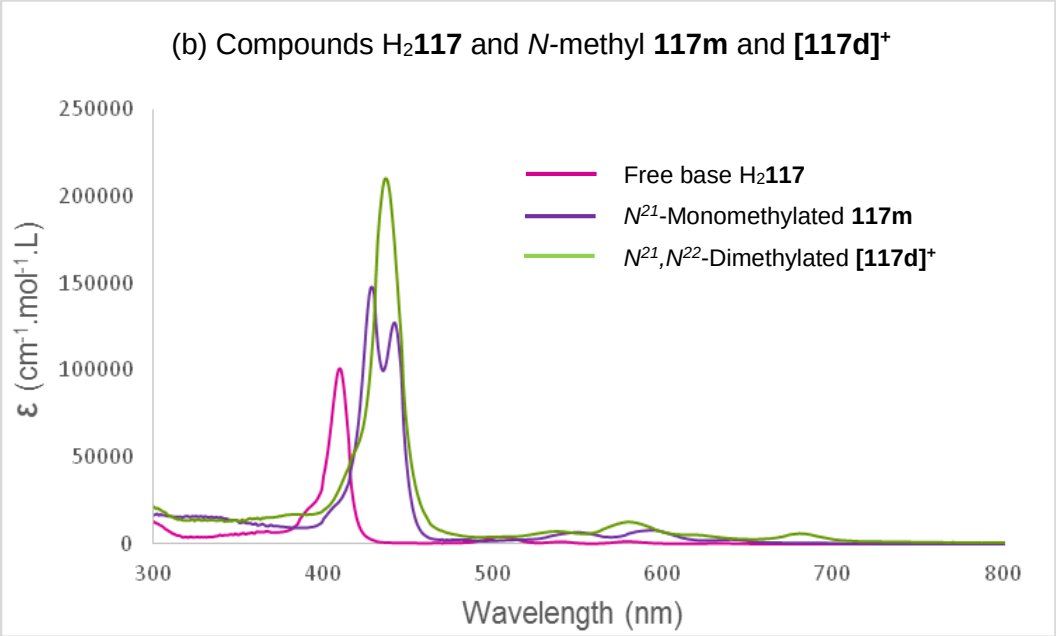

Figure 37: UV-vis spectra of compound H_2**115** (top) and H_2**117** (bottom) and their *N*-methylated derivatives in $CHCl_3$ (1% NEt_3).

This was confirmed through ^{13}C NMR spectroscopy which showed the presence of two close signals (Δ = 0.04 ppm) for the carbon atoms on N21 giving evidence for the hypothesis of a geometrical isomerization (Fig. 38).

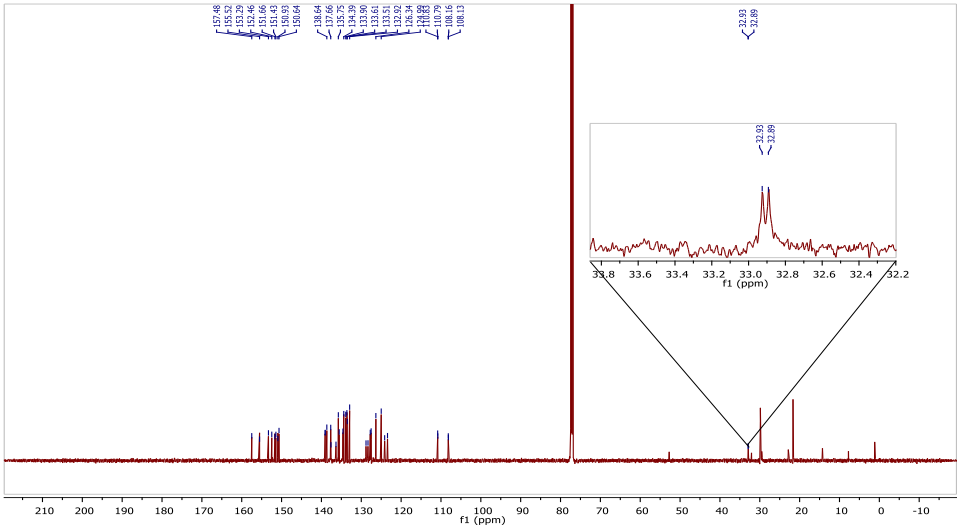

Figure 38: Doublet for the *N*-methyl units on N21 from the ^{13}C NMR of **117m** in $CDCl_3$.

The *anti*- and *syn*-conformations of compound **117m** (**117m(a)** and **117m(b)**) (Fig. 39) were also analyzed using the Soret band characteristics of each compound. For the macrocycle **[115d]+**, the addition of two methyl groups occurred in adjacent pyrroles (N23, N24), resulting in an *anti*-conformation (Fig. 39) compared to **26d** where the *N*-methylation occurred on the opposite pyrrole (N21, N23) displaying a *syn*-conformation.

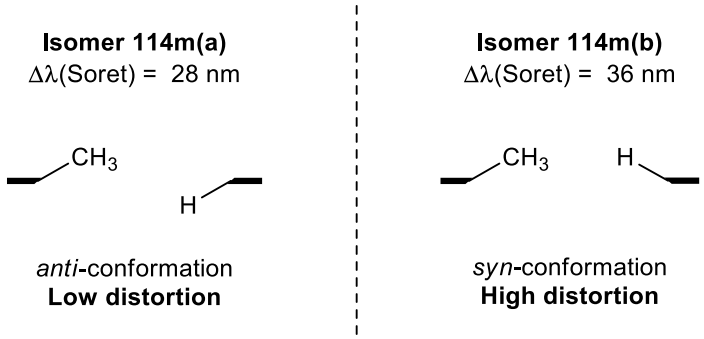

Figure 39: Geometry of the two isomers obtained for **117m**. *Δλ* corresponds to the difference of the Soret band absorption from H_2**117** to **117m** ((**a**) and (**b**)).

In line with the A_4 precursors, a chemical shift of the inner protons was observed for the A_2 precursors (around −3.10 ppm compared to approx. −2.80 ppm for the A_4 systems, Table 11). Note, after introduction of one methyl unit into the core of compound H_2**115**, leading to porphyrin **115m**, the respective signal appeared at −2.56 ppm compared to a chemical shift of −4.36 ppm for compound **117m** (similar to N^{21}-monomethyl-5,10,15,20-tetraarylporphyrin, Table 9). Incorporation of a second methyl unit into the macrocycle core of 5,15-diarylporphyrins gave results similar to the 5,10,15,20-tetraarylporphyrins. Signals in the range −3.10 ppm to −5.30 ppm were observed for all three porphyrins (**[115d]$^+$, [116d]$^+$** and **[117d]$^+$**, Table 11). Interestingly, the signal pattern (1 singlet signal

for 6 protons and 1 singlet signal for 1 proton) indicated that the methylation occurred on adjacent pyrroles (N23 and N24) with a pyrrole proton located on N21. The singlet observed for the two methyl groups in each case was attributed to the symmetry of the porphyrin. This symmetry was due to the well-known tautomerism of the *N*-H protons in the porphyrin core.[160]

Table 11: ^{1}H NMR chemical shifts for the *N*-R protons of free base porphyrins and their respective various degrees of *N*-methylation in $CDCl_3$.

Entry	Porph.	*δ*N21	*δ*N22	*δ*N23	*δ*N24
1	H_2**115**	−3.10 (H)	-	−3.10 (H)	-
2	**115m**	−4.51 (CH_3)	-	−2.56 (H)	-
3[a]	**[115d]$^+$**	n/a	-	−5.32 (CH_3)	−5.32 (CH_3)
4	H_2**115**	−3.07 (H)	-	−3.07 (H)	-
5[a]	**[115d]$^+$**	−2.23 (H)	-	−5.23 (CH_3)	−5.25 (CH_3)
6	H_2**117**	−3.13 (H)	-	−3.13 (H)	-
7	**117m**	−4.25 (CH_3)	-	−4.36 (H)	-
8[a]	**[117d]$^+$**	−2.44 (H)	-	−5.40 (CH_3)	−5.44 (CH_3)

[a] Structure of 5,15-diarylporphyrins involves N21-H, N23-Me/N24-Me instead of N21-Me/N23-Me as observed for the A_4 series.

Considering the symmetry of **[117d]$^+$**, the ^{1}H NMR spectrum displayed only one peak for six protons for the two *N*-methyl groups instead of two peaks integrating for three protons each. This symmetry involved an *N*-methylation pattern comparable to compound **[115d]$^+$** and consequently suggested an *anti*-conformation of compounds **[117d]$^+$**. This conformation resulted in a deviation (*Δ*abs) of the Soret band of **[117d]$^+$** of 31 nm from the Soret band of H_2**117.** The deviation of the Soret band observed for compound **117m(a)** was smaller (*Δ*abs = 22 nm) than the one observed for compound **[117d]$^+$** (*Δ*abs = 31 nm) indicating a smaller distortion of the core of compound **117m(a)**. However, the deviation of the Soret band observed for compound **117m(b)** was larger (*Δ*abs = 36 nm) indicating an increase in distortion of its macrocycle. This result also correlated with the color change observed from purple (planar, **117m(a)**) to green (nonplanar, **117m(b)**) and indicated that the isomer **117m(b)** had a distorted *syn*-conformation compared to the *anti*-conformation of **117m(a)**.

- *Study of the molar absorption coefficient*

A_2 porphyrins (Fig. 37) mostly showed the same pattern, as the molar extinction coefficient increased upon the addition of methyl groups. However, the formation of the cationic species, due to the N^{23},N^{24}-dimethylation (*cis* conformation), did not result in a diminution of the ε value. Compound **117m** with its two isomers showed that the *anti*-conformer **117m(a)** resulted in a higher absorption than the *syn*-conformer **117m(b)** (Fig. 37, (b), purple spectrum).

4.5 X-ray crystal structures

As previously stated in the introduction, conformational distortion of porphyrins is crucially related to their biological function.[1,44] However, most of the previous structural studies have focused on systems with peripheral steric strain (highly substituted porphyrins) while only a few crystallographic reports have addressed metal-free *N*-substituted porphyrins. During the course of this project, we were able to obtain structures for five new macrocycle types (**26m**, **26d**, **112m**, **[112t]$^+$**, and **[115d]$^+$**) and use these in conjunction with published structures[53,126,161,162,163,164,165] (Table 12) for the first comprehensive analysis of the structural properties of *N*-substituted porphyrins. The crystal structures and NSD analyses for this project were determined and solved by Dr. Keith J. Flanagan.

Two new structures of *N*-methyl substituted porphyrins [N^{21}-mono (**26m**) and N^{21},N^{23}-dimethylated (**26d**)] were determined and compared to the reference compound 5,10,15,20-tetraphenylporphyrin H_2**26** and N^{21},N^{22},N^{23}-trimethyl-5,10,15,20-tetraphenylporphyrin **[26t]$^+$** available in literature (Fig. 40).[53,161,162,163,166]

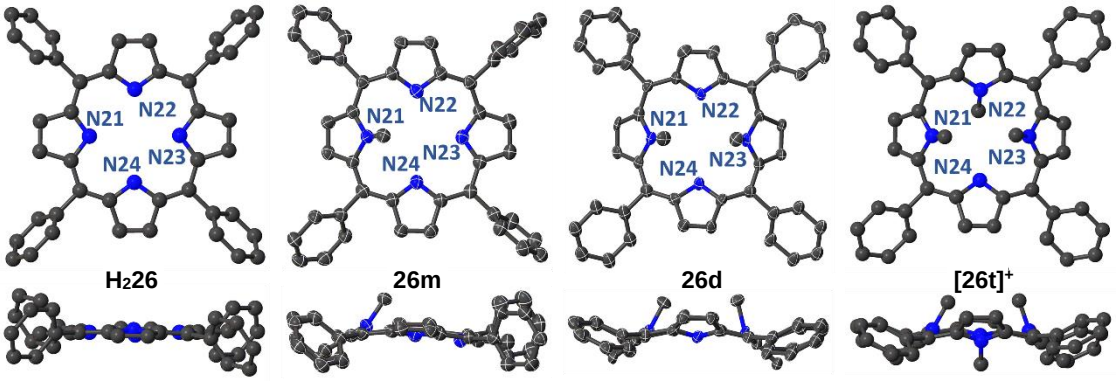

Figure 40: Views of molecular structures in the crystals: 5,10,15,20-tetraphenylporphyrin (H_2**26**),[161] N^{21}-monomethyl-5,10,15,20-tetraphenylporphyrin (**26m**), N^{21},N^{23}-dimethyl-5,10,15,20-tetraphenylporphyrin (**26d**), N^{21},N^{22},N^{23}-trimethyl-5,10,15,20-tetraphenylporphyrin (**[26t]$^+$**).[53] X-ray structure images (top and side-on) are shown with hydrogen atoms, minor disorder, and solvent molecules omitted for clarity. Structures of **26m** and **26d** have been drawn with thermal ellipsoids at 50% probability. The structures of H_2**26** and **[26t]$^+$** were drawn isotropically.

An interesting trend was observed while looking at the average deviation of the 24 macrocycle atoms from their least-squares-plane (Δ24): an increase in the overall macrocycle distortion is seen as result of the various *N*-methylation patterns. A large increase in the Δ24 from H_2**26** to **26m** is illustrated by the first insertion of a methyl unit.

Table 12: Selected structural parameters for *N*-substituted porphyrins.

	H_2**26**[160]	**26m_1**	**26m_2**	**26d_1**	**26d_2**	**[26t]$^+$**[53]
Pyrrole tilt (°)						
N21	6.545(7)	30.9(10)	28.4(10)	43.3(3)	43.1(3)	38.2(1)
N22	1.518(18)	7.5(10)	8.2(10)	28.9(3)	24.2(1)	30.4(11)
N23	6.545(7)	1.5(10)	6.1(10)	48.9(5)	38.4(3)	39.7(16)
N24	1.518(18)	11.8(9)	9.1(10)	30.6(14)	24.5(18)	18.2(12)
Structural parameters (Å)						
ΔN21[a]	-0.158	-0.427	0.422	0.247	-0.308	-0.307
ΔN22[b]	0.012	-0.083	0.020	0.035	0.002	0.183
ΔN23[c]	0.158	0.227	-0.063	0.300	-0.260	-0.328
ΔN24[d]	-0.012	0.024	-0.031	-0.013	-0.001	-0.066
ΔN[e]	0.085	0.190	0.134	0.149	0.143	0.221
Δ24[f]	0.068	0.299	0.256	0.711	0.608	0.570
ΔC_m[g]	0.023	0.062	0.075	0.037	0.048	0.076
ΔC_a[h]	0.034	0.134	0.095	0.333	0.273	0.232
ΔC_b[i]	0.063	0.431	0.368	1.171	0.999	0.933
Δ_{ip}[j]	0.199	0.161	0.232	0.588	0.315	0.152
Δ_{oop}[k]	0.261	1.388	1.161	3.372	2.857	2.644

Tables 12 (continued): Selected structural parameters for *N*-substituted porphyrins.

	H_2**110**[162,163]	**110m**	**[110t]$^+$**	**112m**[163]	H_2**112**[87c]	**[115d]$^+$**
Pyrrole tilt (°)						
N21	2.7(1)	35.7(2)	42.1(15)	27.2(5)	34.3(11)	30.4(1)
N22	2.8(1)	11.9(8)	30.2(16)	10.8(18)	27.0(11)	31.0(1)
N23	2.7(1)	10.0(4)	47.9(15)	7.7(13)	29.1(11)	6.7(1)
N24	2.8(1)	7.3(5)	22.3(9)	11.3(18)	31.7(10)	0.6(1)
Structural parameters (Å)						
ΔN21[a]	-0.023	0.418	-0.308	-0.399	-0.028	-0.390
ΔN22[b]	-0.030	0.070	0.109	0.073	0.111	0.381
ΔN23[c]	0.023	-0.130	-0.361	0.059	-0.107	0.212
ΔN24[d]	0.030	0.136	-0.060	0.001	0.038	-0.256
ΔN[e]	0.027	0.189	0.210	0.133	0.066	0.310
Δ24[f]	0.048	0.366	0.645	0.266	0.712	0.364
ΔC_m[g]	0.069	0.127	0.050	0.182	0.036	0.119
ΔC_a[h]	0.026	0.177	0.280	0.110	0.421	0.150
ΔC_b[i]	0.031	0.540	1.057	0.361	1.156	0.502
Δ_{ip}[j]	0.200	0.283	0.407	0.246	0.515	0.608
Δ_{oop}[k]	0.220	1.705	3.041	1.209	3.460	1.695

[a] Calculated deviation of N21 from the 24-atom mean plane. [b] Calculated deviation of N22 from the 24-atom mean plane. [c] Calculated deviation of N23 from the 24-atom mean plane. [d] Calculated deviation of N24 from the 24-atom mean plane. [e] Simulated displacement of the four internal nitrogen atoms from the 24-atom mean plane. [f] Average deviation from the least-squares plane of the 24-macrocycle atoms. [g] Average deviation of the meso-carbon atoms from the 24-atom mean plane. [h] Average deviation of the *α*-carbon atoms from the 24- atom mean plane. [i] Average deviation of the *β*-carbon atoms from the 24-atom mean plane. [j] Simulated total i*n*-plane distortion. [k] Simulated total out-of-plane distortion.

Upon addition of a second methyl group (**26m** to **26d**), a second increase in *Δ*24, larger than the first one observed for **26m**, is observed which results from crowding the cavity of the porphyrin core. It appears that the increase in distortion induced by the second *N*-

methyl unit allows us to reach a certain limit in the flexibility of the macrocycle as the incorporation of a third *N*-methyl groups (**[26t]**$^+$) induces a moderate decrease in *Δ*24 (**26d** to **[26t]**$^+$). The third methyl group is pointing towards the opposite direction in comparison to the two initial *N*-methyl units inserted. This counteracts the steric effect of the other two *N*-substituents thus decreasing the overall 24-atom ring strain applied by core substitutions.

The NSD analysis (Fig. 41)[167] supports the data obtained *via* X-ray structural analysis. The out-of-plane distortion of H_2**26** favors the $E_g(y)$ wave distortion mode with the second largest, albeit small, contribution to the $E_g(x)$ wave distortion mode. However, a large preference for the B_{2u} distortion mode with the second largest contribution to the $E_g(x)$ wave distortion mode is observed upon insertion of one methyl group (**26m**). A much larger contribution to the B_{2u} saddle distortion mode is then observed for **26d**, in comparison to **26m** with the second largest contribution now present in the A_{2u} propeller distortion mode. Macrocycle **[26t]**$^+$ shows a contribution to the B_{2u} saddle distortion mode similar to **26d**, however, a marginal decrease in values can be noted.

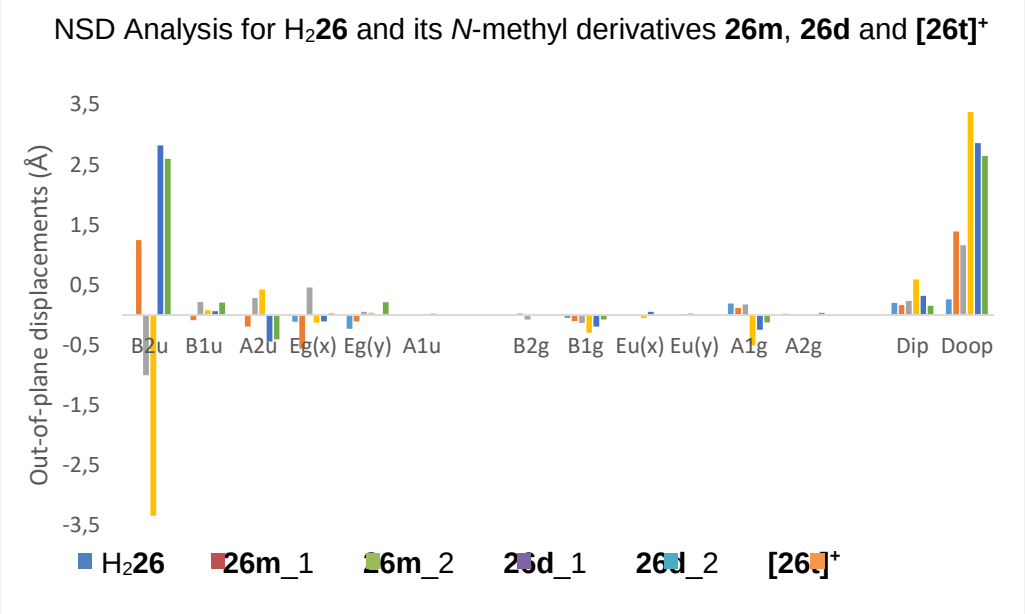

Figure 41: Normal structural decomposition (NSD) analysis of the X-ray crystallographic structures of H_2**26**, **26m**, **26d**, **[26t]**$^+$. **X**_# indicates that two or more macrocycles are present in the asymmetric unit and have been calculated separately.

A similar trend can be observed for the overall out-of-plane distortion (*Δ*oop) which is also representative of the *Δ*24 and can be summarized as follows: H_2**26**<**[26t]**$^+$<**26m**<**26d** (Table 12). Looking at the previous sets of data, it is clear to see

that the distortion of previously planar porphyrin macrocycles can be easily achieved through core substitution.[95,97a,128a]

Interestingly, in order to reach these high degrees of distortion using this method, the substitution of only two *N*-methyl units is necessary. This is the case given that only a moderate additional distortion is seen in the increase from two to three inner *N*-substituents and both the N^{21},N^{23}-di- and N^{21},N^{22},N^{23}-trimethylated structures can be considered to be almost equal in nonplanarity. Additionally, these systems feature a localized distortion on specific pyrrole units and can be illustrated by inspection of pyrrole tilt angles and the deviation from the 24-atom mean plane of internal nitrogen atoms (N21-N24) (Table 12).

Consequently, the pyrrole tilt angles from the 24-atom mean plane were investigated and showed a trend which can be summarized as follows: H_2**26**<**26m**<**[26t]**$^+$<**26d** for *N*-methyl substituted pyrroles. Individually, **26m** presents a much larger deviation of core nitrogen atoms from the 24-atom plane for the pyrrole bearing the nitrogen atom N21 than its counterparts, **26d** and **[26t]**$^+$. This suggests that the localized deviations of an N21 atom in the *N*-monomethylated porphyrin have a larger impact than that of higher substitutions due to the predominantly planar macrocycle. On the other hand, higher distortion results in lower *Δ*N (**26d),** suggesting a correlation between the number of internal core substituents and nitrogen atom deviation.

The above specification forced the consideration of a possible ‘counter-balancing’ effect created by the addition of a third *N*-Me unit into the cavity. The addition of only one methyl unit results in a larger local deviation of the core nitrogen atoms of the 24-atom mean-plane. The local effect is then overcome by the global distortion, upon *N*-substitution. The NMR analysis shown earlier (see 4.4.4) reveals that an upfield shift in the chemical shift of the inner protons is closely related to the number of substituents added into the cavity. However, in the case of porphyrin **26d**, the signals are very similar to those of the free base porphyrin (-2.90 ppm for **26d** and -2.76 ppm for H_2**26**) in comparison to those of porphyrin **26m** which present a shift in values from -2.76 to -4.06 and -4.73 for the *N*-Me units and the *N*-H units, respectively. These surprising results can be explained by the arrangement of the porphyrin. The crystal structure of **26d** (Fig. 42 showed both *N*-methyl units pointing away from the structure itself, decreasing the effect of the ring current on the *N*-Me protons and the electron density of the ring.

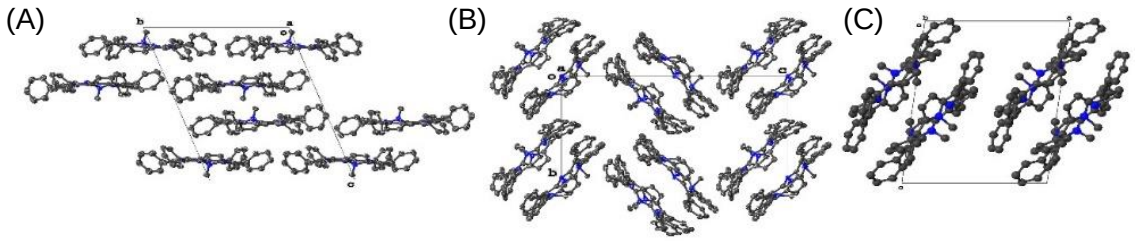

Figure 42: Moiety packing of compounds (A) **26m**, (B) **26d** and (C) **[26t]**$^{+}$, shown with hydrogen atoms, minor disorder, and solvent molecules omitted for clarity.

Moreover, the alternative packing of the molecule is evidence for the poor electronic environment of the *N*-methyl units. The alternate packing of **26d**, contrary to the packing diagrams of **26m** and **[26t]**$^{+}$ where there are fewer molecules interacting with the porphyrin ring, Fig. 42. This creates an electron deficient environment with effects the total ring current of the porphyrin ring resulting in the unexpected shift of signals seen in the ^{1}H NMR spectra as reported by Roucan *et al*.[96]

As previously stated, nonplanar porphyrins have been implicitly used for small molecule binding.[51a,97a,116c,168] The tilt of the pyrrole rings out of the porphyrin plane allows for the central imine and amine motifs of the porphyrin ring to interact with their environment and participate in hydrogen binding with small molecules such as solvents or anions.

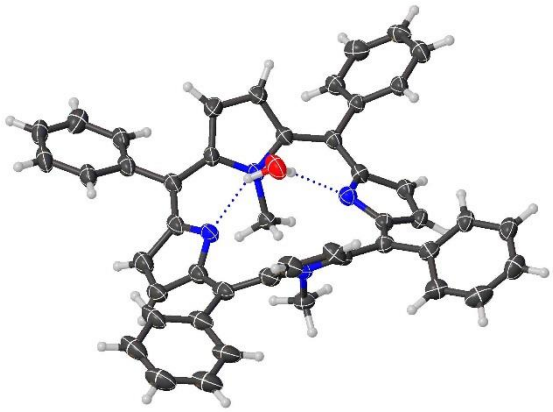

26d

Figure 43: View of the molecular structure of N21,N23-dimethyl-5,10,15,20-tetraphenylporphyrin (**26d**) showing a solvent water molecule interacting with the porphyrin core. Thermal ellipsoids indicate 50% probability.

This effect is also seen with *N*-substituted porphyrins, namely in the structure of **26d** (Fig. 43). The asymmetric unit of this structure contains a core bound water molecule which interacts with the imine pyrrole units *via* hydrogen bonding. This suggests that *N*-

substituted porphyrins have a sizable capacity to bind small molecules in the porphyrin core.

In the case of 5,10,15,20-tetrakis(*p*-methoxyphenyl)porphyrin (H_2**112**), two new N^{21}-mono- and N^{21},N^{22},N^{23}-trimethylated-5,10,15,20-tetrakis-*p*-methoxyphenyl)porphyrin **112m** and **[112t]$^+$** were determined (Fig. 44). The trend in the global distortion (Δ24) is closely similar to the one discussed previously for the 5,10,15,20-tetraphenylporphyrin series. The smallest deviation is seen for compound H_2**112** followed by **112m** and **[112t]$^+$**, the latter showing the largest deviation resulting in the following trend: H_2**112**<**112m**< **[112t]$^+$**.

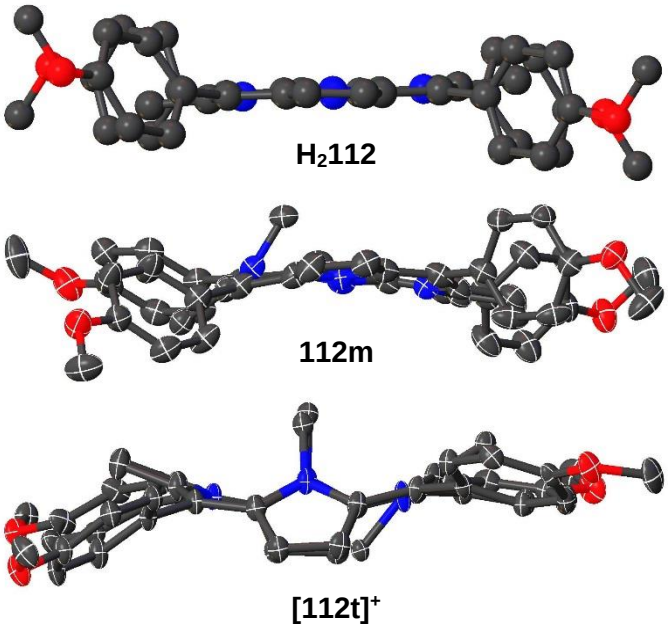

Figure 44: Side views of the molecular structures in the crystal of H_2**112**,[138] porphyrin **112m** and **[112t]$^+$**. Hydrogen atoms, minor disorder, and solvent molecules were omitted for clarity. Structures of **112** and **[112t]$^+$** are drawn with thermal ellipsoids indicating 50% probability. The structure of H_2**112** has been drawn isotropically.

Similarly to the previous series, NSD analysis on the structure of H_2**112** (Fig. 45) shows the largest contributions from the $E_g(x)$ wave distortion mode with a smaller contribution seen in the $E_g(y)$ wave distortion mode. A shift of the distortion mode to the B_{2u} sad type with the second largest presence in the $E_g(y)$ wave distortion mode was observed after insertion of one methyl group to the core nitrogen atom (**112m**). Similarly, a large increase is observed for the B_{2u} saddle distortion mode when three methyl groups occupy the core nitrogen atoms (**[112t]$^+$**) with the second largest contribution from the A_{2u} domed distortion mode. In this series also, there is a clear increase in the out-of-plane distortion: H_2**112**<**112m**<**[112t]$^+$**.

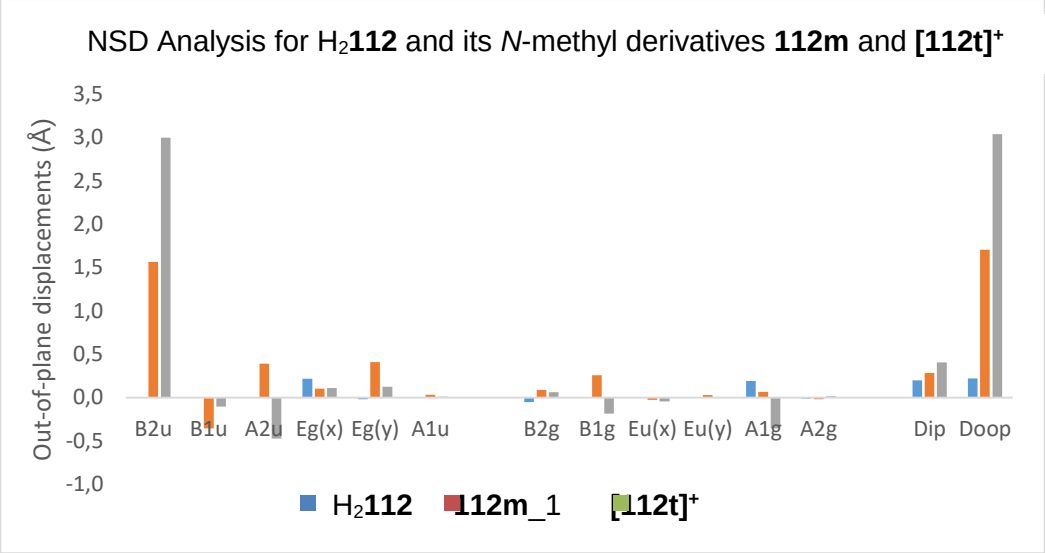

Figure 45: Normal structural decomposition (NSD) analysis of the X-ray crystallographic structures of H_2**112**, **112m** and **[112t]**$^+$. **X**_# indicates that two or more macrocycles are present in the asymmetric unit and have been calculated separately.

The addition of electron donating and withdrawing units to the porphyrin macrocycle is a well-established method to modulate the electronic properties of the porphyrin core. This also enhances the ability of the inner nitrogen atoms to undergo substitution as previously stated. However, how the inclusion of EWG's and EDG's affect the conformation of *N*-substituted porphyrins has been less established due to the relative scarcity of structural examples in the literature.[51a,97a] Here, the structure of **112m** (Fig. 44) was obtained and compared to the structure of **110m** which is available in the literature.[87c]

The overall distortion of the macrocycle (Fig. 46) shows that a strong electron-rich porphyrin such as **112m** results in a larger contribution to *Δ*N, *Δ*24, *Δ*Ca, *Δ*Cb, *Δ*ip and *Δ*oop. **110m** shows a larger contribution in only one area, *Δ*Cm. By varying the type of substituents, it is possible to influence the distortion present in *N*-substituted porphyrins and higher degrees of nonplanarity can be achieved using EDG's. Looking at the pyrrole tilt angles, **112m** shows the largest tilts for N21, N22, and N23 and the smallest tilt angle for N24 while the largest N24 tilt angle is present in porphyrin **26m**. Compound **110m** presents average values for the pyrrole tilt angles of N22, N23, and N24 lying in the middle of the one observed for **112m** and **26m**, however, it exhibits by far the smallest pyrrole tilt around N21.

In regards to the comparative NSD analysis of compounds **26m**, **110m** and **112m** (Fig. 46), it is clear that compound **112m** shows the largest contribution to the B2u distortion mode with its second largest contribution to the *Eg(y)* distortion mode. Compound **26m**

shows the second largest contribution to the B2u distortion mode, however, it appears to favor the *Eg(x)* distortion mode for its second largest contribution. The X-ray structure of **110m** shows the smallest contribution to the B2u distortion mode compared to the two other structures (**26m** and **112m**). Moreover, **110m** appears to favor the B1u distortion mode for the second largest contribution closely followed by the *Eg(x)* distortion mode.

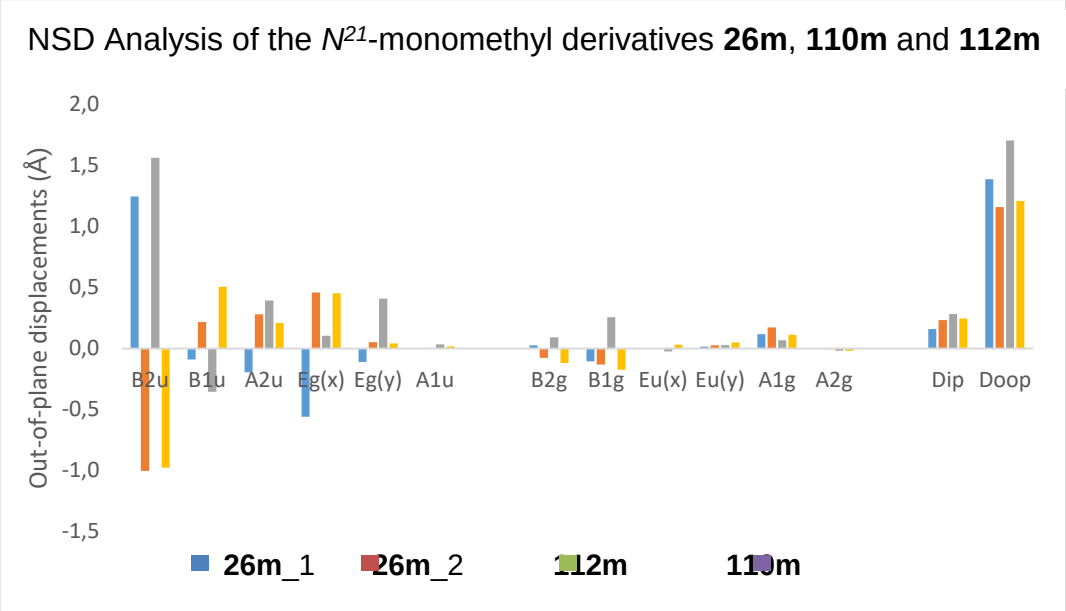

Figure 46: Normal structural decomposition (NSD) analysis of the X-ray crystallographic structures of **26m**, **110m**, and **112m**. **X**_# indicates that two or more macrocycles are present in the asymmetric unit and have been calculated separately.

N^{21},*N*^{23}-dimethylated TPP **26d** showed the highest distortion between the various possible *N*-substitution patterns, and thus its structure was compared to the well-known highly distorted porphyrin, H_2OETPP H_2**21** (Fig. 47). Looking back at the UV-vis results, it was noted that the shift of the Soret band is correlated to the distortion of the macrocycle. Here, compounds H_2**21** (456 nm) and **26d** (459 nm) present similar Soret bands (Table 13). This stands for a comparable distortion between the two porphyrin structures. This is also confirmed by the X-ray crystallographic studies as the overall distortions from the 24-atom mean plane are almost identical (Table 13).

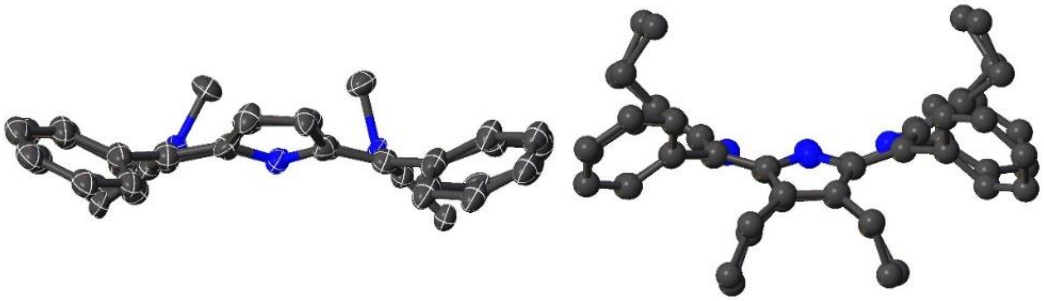

26d **$H_2$21**

Figure 47: N^{21},N^{23}-Dimethyl-5,10,15,20-tetraphenylporphyrin (**26d**), 2,3,7,8,12,13,17,18-octaethyl-5,10,15,20-tetraphenylporphyrin (H_2**21**)[87c] showing the edge-on view of both compounds. Views of the molecular structure in the crystal are shown with hydrogen atoms, minor disorder, and solvent molecules omitted for clarity.

Table 13: Comparison of the UV-vis data and the overall deviation of the macrocycle (*Δ*24) of **26d** and **21d**.

Entry	Porphyrin	*Δ*24 [Å]	*Δ*λ (nm)[a]
1	**26d**	0.712	37 (456)
2	H_2**21**	0.711	40 (459)

a *Δ*λ represents the shift of the Soret absorption band compared to free base TPP H_2**10** (419 nm)

The last structure is that of **[114d]$^+$** which represents the only other example of a porphyrin crystal structure showing an N^{21},N^{22}-substitution pattern (Fig. 48). The effects of this substitution cannot be ascertained as they were for the two previous series due to the fact that no crystal structure is available for compound H_2**114**.

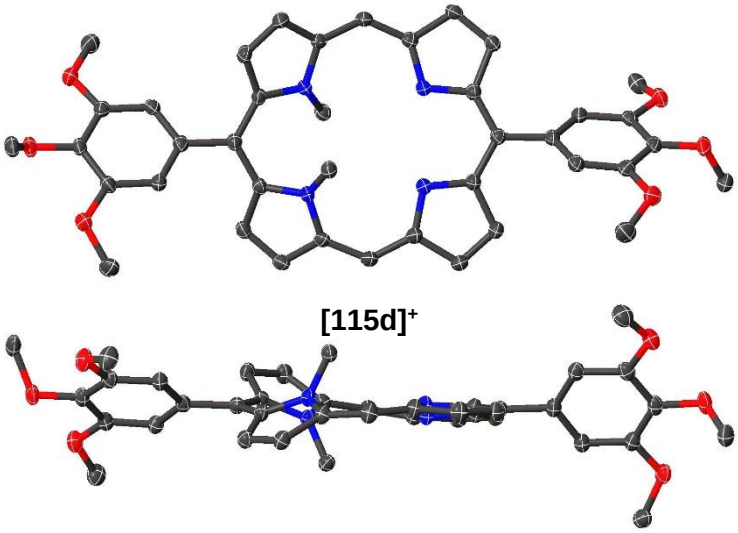

[115d]$^+$

Figure 48: Views of the molecular structure of N^{21}-hydro-N^{23},N^{24}-dimethyl-5,15-bis(3,4,5-trimethoxyphenyl)porphyrin trifluoromethanesulfonate salt (**[115d]+**) showing top- and side-views. Hydrogen atoms, minor disorder, and counter-ions were omitted for clarity. The structure has been drawn with thermal ellipsoids indicating 50% probability.

Therefore, a general increase in distortion can be observed for the pyrroles with the nitrogen N23 and N24, while the N21, N22 pyrroles stay relatively planar. This results in half of the porphyrin structure being distorted and clearly illustrates that the *N*-substitution induces a change in the pyrrole tilt angle of the pyrrole units bearing the *N*-substituent. The meso-substituent is much more in plane on the N21, N22 side (5-position) of the porphyrin macrocycle than the N23, N24 side (15-position), which is logical due to the aforementioned increase in distortion.

4.6 Conclusion and outlook

Methylation of the inner nitrogen atoms of free base porphyrins is an easy and facile method to induce considerable distortion of the macrocycle. A library of *N*-methylated porphyrins with various aryl substituents was successfully synthesized utilizing diverse and optimized alkylation conditions. This allows the tailored synthesis of *N*-methylated porphyrins bearing one to three methyl units in the porphyrin core. The efficiency and regioselectivity of the methylation are correlated to the peripheral substitution pattern. Additionally, the electron donating properties of substituents tend to enhance the reactivity, while electron withdrawing groups lower the efficiency of the methylation reaction.

N-Methylated porphyrins have very characteristic spectroscopic profiles in both NMR and UV-vis spectroscopy where the chemical and bathochromic shifts correlate with the structural conformation. These aspects have also been confirmed by single crystal X-ray analyses where the trends and changes observed in spectroscopic studies are reflected in associated structural changes. Comparison of the new and literature crystal structures of the planar free base and nonplanar *N*-substituted porphyrins revealed that, from a structural point of view, *N*-methylation of planar porphyrins results in significant structural changes and macrocycle distortion. The use of core substitution can also induce similar distortion than that observed in highly substituted porphyrins, such as compound **26d**, and in a rapid and simple manner. NSD was successfully applied to all structures and used to determine the distortion modes in porphyrin structures with an increasing number of *N*-substitution. In planar structures, there is a clear increase seen in the *Δ*oop distortion modes with the N^{21},$N^{22/23}$-disubstitutions showing the largest contributions. However, when working with nonplanar porphyrins, this trend is less evident. As seen in the *Δ*oop distortion modes, only a minor increase to nonplanarity is noted. To conclude, *N*-substitution of porphyrins provides a fast and reliable method to achieve nonplanarity with degrees of distortion analogous to that of highly peripheral substituted porphyrins.

Overall, *N*-substitution is a good method for systems combining core (*N*-substitution) and peripheral (*peri* interactions) steric strain to yield some of the most distorted porphyrins. The usual method to highly distort porphyrins (*e.g.*, OETPP) results in an inactivation of the periphery due to the large number of substituents. In contrast, *N*-substitution is of benefit as it allows for a similar distortion than highly distorted porphyrins, although does not diminish the possibility of functionalization of the periphery of the molecule. Moreover, these methods of *N*-substitution allows access to specific conformations and binding motifs *via* fine tuning of the properties and an easy control of the distortion depending on the type, number, regiochemistry, and steric bulk of substituents.

Additionally, the highly distorted structures obtained by *N*-substitution were used in the next chapter as potential organocatalysts.[96] These structures could also help in the design of new inhibitors akin to the mode of action of *N*-methylprotoporphyrin IX[117] or benefit the construction of supramolecular arrays without the use of charged species. The possibility of inserting definite units in the core, such as iodoalkyl groups in the porphyrins core as reported by Setsune *et al.*,[148] would be of interest given the ability to functionalize through the iodine (*e.g.*, Sonogashira reactions, nucleophilic substitutions, etc.), with a view to create porphyrins with useful properties (electron donor/acceptor complexes, photoactive systems, etc.). In addition to the particularity of these systems, the formation of charged species upon addition of *N*-units could widen their field of activity toward supramolecular systems. Diverse approaches would be then accessible to illustrate their use with regards to the design of ion-pair receptors towards the formation of potentially functional supramolecular complexes.

5 Free base and *N*-methylated porphyrins as organo-catalysts

5.1 Introduction

Organocatalysis is a recent field[169] which uses small metal-free molecules as catalysts. Over the last two decades it has attracted considerable attention from both academic researchers and the scientific industry.[170] Hajos-Parrish showed one of the first examples of an aldol reaction catalyzed by (*S*)-proline in 1974 (Scheme 23).[171]

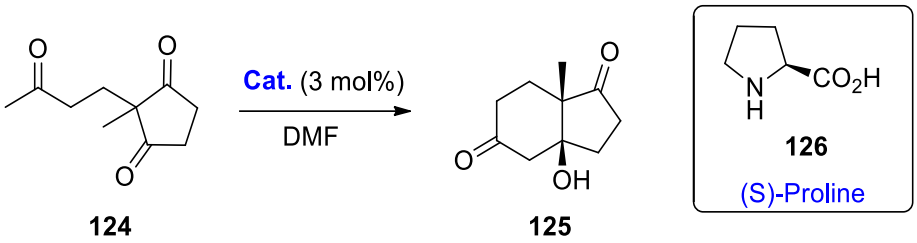

Scheme 23: (*S*)-proline **126** catalyzed aldol reaction.

Viewed as a unique example at that time, these reactions were in reality part of a larger interconnected field, resulting several years later in the emergence of the field called organocatalysis. The asset of this field is first the use of metal-free molecules, which represent an essential progress as part of the ongoing challenge of “green chemistry”, but also the use of a general mode of activation, which upon design can be applied to many useful reactions.

Before 1998, chiral transition metal catalysts dominated the enantioselective landscape.[172] A wide range of catalysts using metal complexes have been designed so far and the catalytic activity resides in the central metal which is capable of activating a panel of reactions such as Diels-Alder using Ti or Al (BINOL **127**),[173] hydrogenation, hydrosilylation or allylation using Rh or Ru (BINAP **128**),[174] epoxidation with Mn, Cr or Co (Salen **129**)[175] or cyclopropanation, aziridination or 1,4-addition reactions through the use of Cu, Mg or Sn catalysts (Bisoxaline **130**), to name but a few (Fig. 49).[169, 176]

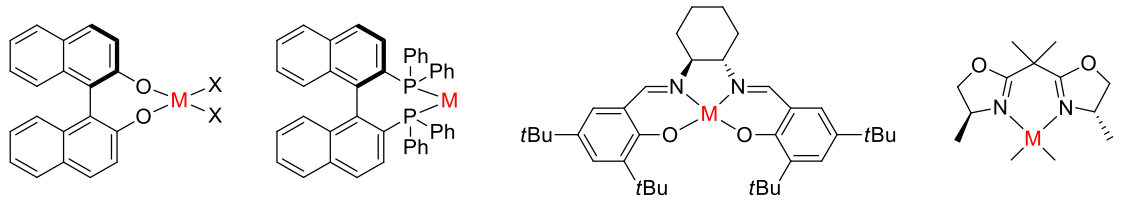

Figure 49: Various examples of chiral transition metal catalysts designed for enantioselective reactions.

From 1996, the development of metal-free catalysts was reported by a few research groups. Ketone motifs, for example, were used as catalysts to create dioxiranes *in situ* and thus activate enantioselective catalytic epoxidation.[170d,177] However, the design of a specific catalyst was required for each individual reactions. In 2000, MacMillan's research group showed the first highly enantioselective Diels–Alder reaction catalyzed by chiral amine bearing motifs derived from the field of Lewis acid catalysis.[178] The process developed uses the amine motif **132** which by attack of the nucleophile forms a reversible iminium intermediate **133** (Scheme 24). From this report, it was then possible to develop new generic modes of activation based on the formation of imidium molecules **133** and since then a broad range of amine-based catalysts have been designed and used to catalyze a variety of organic reactions such as 1,4-addition reactions,[179] cyclizations,[180] hydrogenations,[181] and other transformations.[182]

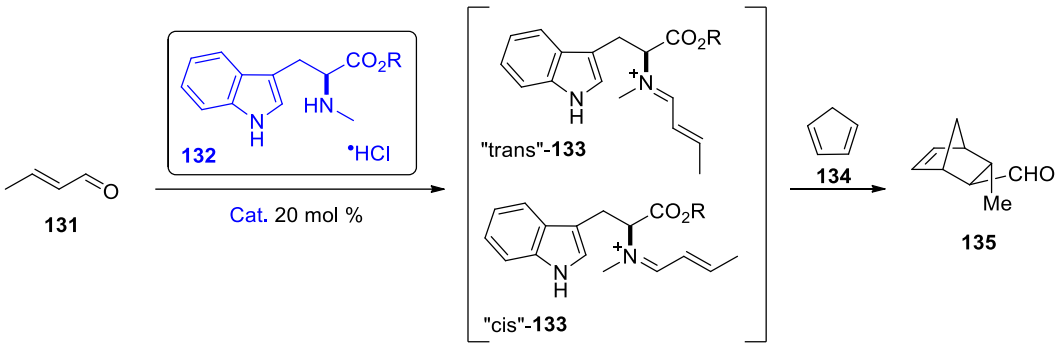

Scheme 24: Diels-Alder reaction catalyzed *via* formation of iminium intermediates.

Over the last 50 years, considerable attention has been directed towards the enantioselective catalysis of hydrogenation reaction technology.[183] So far, synthetic hydrogenation has been achieved using the well-known Noyori's catalyst **137** as a mediator to enhance that reaction; however, this catalyst is not a metal-free molecule (Fig. 50).

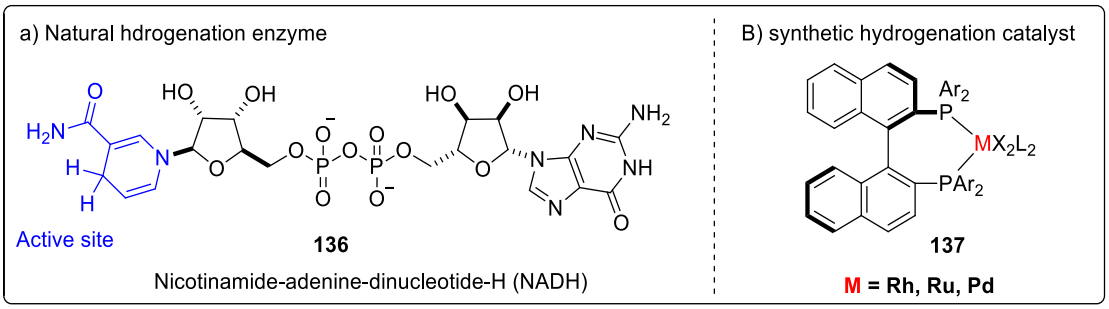

Figure 50: Natural (a) and synthetic Noyori's (b) catalysts.

In nature, enzymatic hydrogenation reactions are mediated by two different molecules working simultaneously, the reductive enzyme and a co-enzyme, for example NADH **136** (Fig. 50). Various catalysts have been designed based on the NADH active site motif, to be then used as a co-catalyst for the reduction reaction of *α*,*β*-unsaturated carbon bonds of aldehydes and ketones compounds in good *ee* (>90% *ee* and 88% *ee*, respectively).[176a] However, iminium catalysts showed some limits regarding their use as prochiral molecules and their reactivity towards nucleophiles to form chiral centers. They also display a non-reactivity toward zwitterion nucleophiles and the formation of a racemic mixture, due to the reversible nucleophilic addition. Consequently, the indole structure has been investigated for the formation of the iminium catalytic intermediates. The use of an indole molecule allowed for control towards the iminium geometry (only (Z)-geometry formed) and enhances the selectivity by introducing an alkyl chain to form the iminium molecule.[182b] Jørgensen also developed a very useful class of diarylprolinolether catalysts **138** (Fig. 51) in which the presence of the large aryl and silicium group restrict the iminium to only one geometry by shielding the top face of the catalysts.[184] These studies also showed that both iminium and zwitterions are required for a good enantioselective catalytic activity.

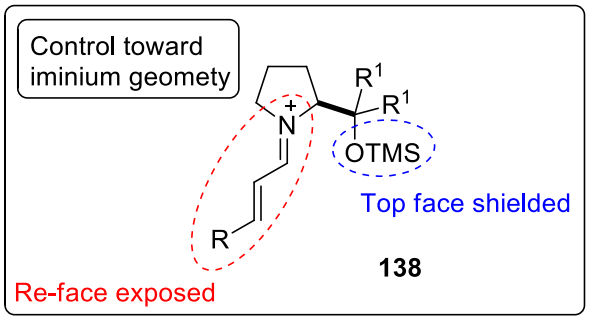

Figure 51: Jørgensen iminium intermediates.

The activity of this class of catalyst resides on both LUMO and HOMO activation, in comparison to the proline-based molecule (HOMO activation only) and the diamine-based molecules (LUMO activation only). The scope of this new category of catalysts is

very broad, as they can undergo activation of reactions such as hydrophosphination of enals[185] and cyclization[186] or hydroxylation of alkenes.[187] These catalysts also played a part in the development of a range of very useful and diverse organocatalysts.[188]

Alongside the development of amine, iminium and enamine catalysts, researchers developed phase transfer catalysts (PTC).[189] This method has been established in order to counteract the problems of reactivity in heterogeneous solutions. A catalyst, based on a cinchonine or cinchonidine motif **138** (Scheme 25), is added to the solution and transfers the reactant at the interface of the phases in order to activate the reaction (Scheme 25).[190] PTC can be used for a plethora of enantioselective reactions, such as asymmetric alkylation,[191] Michael, aldol and Mannich addition reactions,[192] nucleophilic aromatic substitution,[193] and epoxidation.[194]

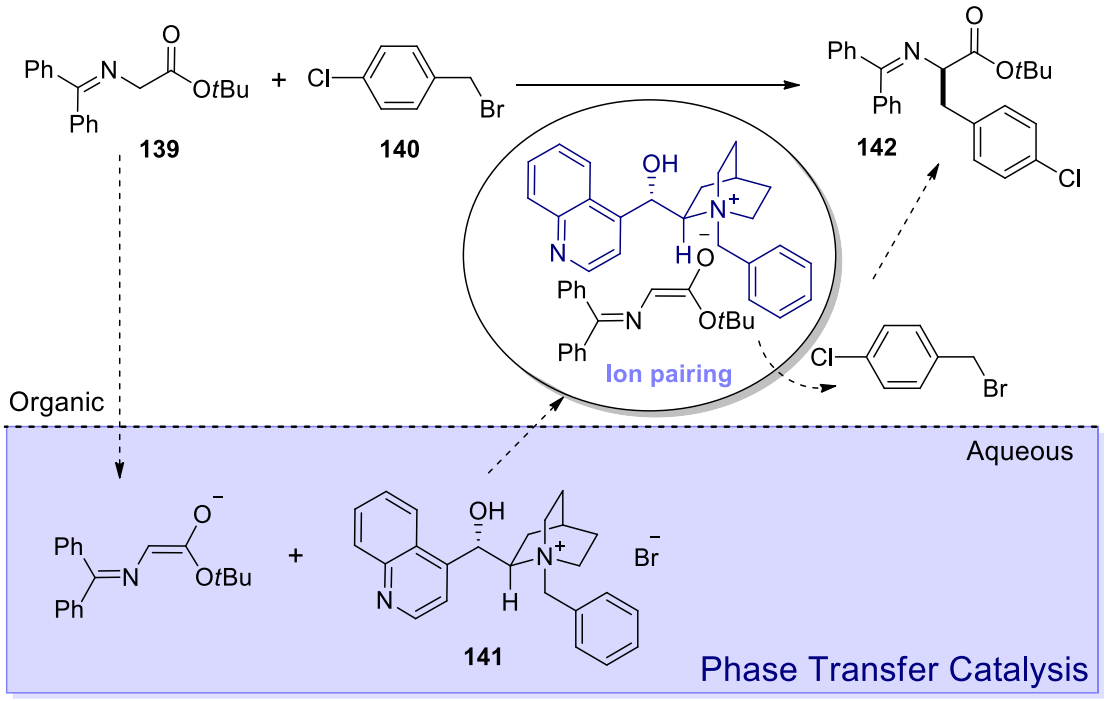

Scheme 25: Example of a phase transfer catalysis reaction.[190]

Following the PTC, catalysts based on H-bonding properties were investigated. Jacobsen reported a chiral Schiff base as a promising catalyst for Strecker reactions.[195] Further investigations showed that the urea motif is crucial to establish the H-bonding activation mode.[196] Modification using sulphur instead of oxygen atoms (*e. g.*, compounds **146**) to further activate the amine moieties enhanced the efficiency of the catalyst (Scheme 26). These urea type catalysts allow for the activation of a plethora of reactions with conversion from 81% with more than 90% *ee*.[197]

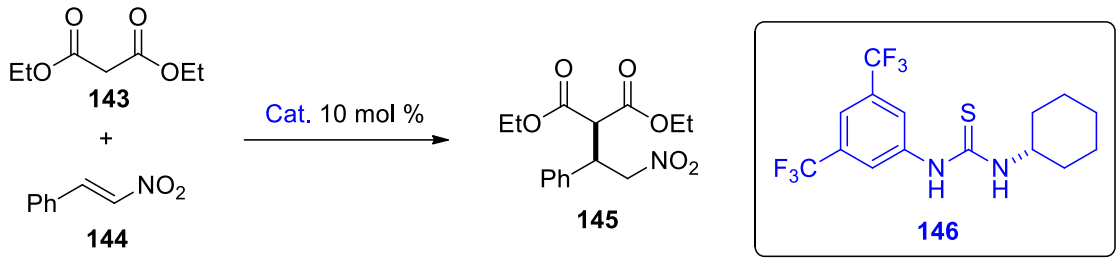

Scheme 26: Michael addition reaction catalyzed by bifunctional urea systems.

Nowadays, thiourea systems are well-established as organocatalysts, using hydrogen-bonding to activate various substrates and to target non-stereoselective and stereoselective reactions. The development of these systems, introducing various functional groups, leads to a broad variety of chiral systems. The incorporation of a second *active* motif such as in secondary and tertiary amine-thiourea catalysts can be often a necessity and resulted in more efficient catalytic activity, so-called bifunctionality.[198]

5.2 Bifunctional organocatalysis

Electrophilic activation of a substrate *via* hydrogen-bonding is a well-established strategy catalyzing organic transformation.[199] In 1985, Hine and co-workers reported the first example of catalysis mediated through hydrogen-bonding by showing that biphenylenediol could improve the reaction rate of epoxide aminolysis.[200]

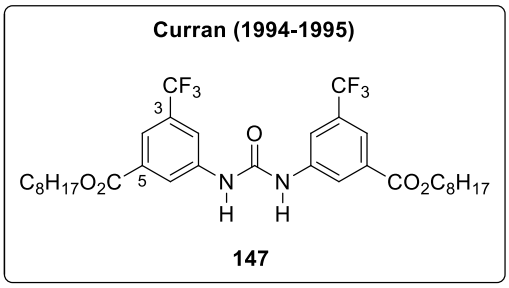

Figure 52: Diarylurea use as catalyst by Curran *et al*.[201]

In the 1990s, the first examples of achiral organocatalysts based on ureas were used. Their utilization in important organic reactions represented an unprecedented advancement in the field of organocatalysis. Then, Curran found that the use of sub-stoichiometric amounts of diarylurea **147** (Fig. 52) could not only improve the rate of some reactions,[201] but also the solubility of the catalyst in common organic solvents. Electron withdrawing groups at the C-3 and C-5 positions decreased the pK_a of the *N*-H bonds and therefore increased their hydrogen-bonding properties.[199,201]

Hydrogen-bonding catalysts may also contain a second catalytically active motif. The simultaneous action between two different catalytic modes is known as bifunctional catalysis.[202] Prominent examples of bifunctional organocatalysts in use are often derived from quinine **148** and quinidine **149**. The bifunctional properties of these compounds are highlighted below (Fig. 53).

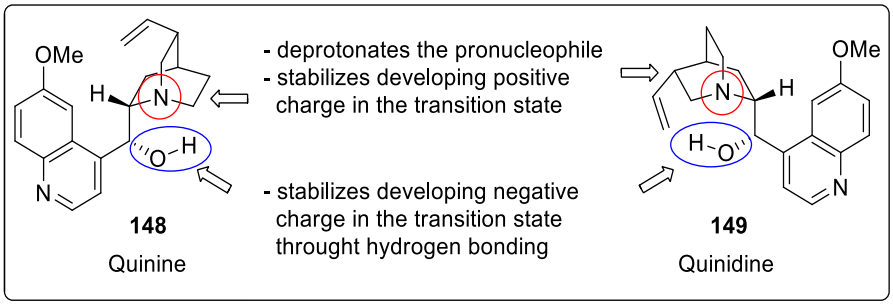

Figure 53: Active sites in quinine **148** and quinidine **149**.

The reactivity of **148** and **149** is based on their ability to deprotonate the pro-nucleophile through activation of the basic tertiary amine of the quinuclidine ring, while simultaneously activating the electrophilic component, by means of hydrogen-bonding.[203] Organic catalysts containing acid/base co-operation moieties[203] can be further improved by designing structures with different functionalities, such as hydrogen-bond donation.

Over the years, different classes of catalysts directly derived from **148** or **149** have been identified and explored, not only for their hydrogen-bonding properties but also for their specific ability to bind with a substrate in a well-defined geometry. The thiourea-substituted cinchona alkaloid derivatives designed by the research group of Professor Stephen Connon are a very good example of bifunctional systems.[98] The thiourea moiety activates one of the substrates through hydrogen-bonding, while the quinuclidine part acts as a base and activates the second substrate.

5.3 Tetrapyrroles as catalysts

Porphyrins, especially metalloporphyrins, have established themselves in the field of catalysis and show good activity (*e.g.*, catalase and peroxidase) for highly selective oxygenation and reduction reactions.[204] Examples are cytochromes P450 hemoproteins, previously discussed in chapter B, or coenzyme F430, found only in methanogenic Archaea.[205] The former contains heme as a cofactor and stands amongst the most important enzymes found in the body, as they play an active role in the metabolism of H_2O_2, xenobiotics, in hydroxylation and hydrolysis of proteins.[206,207]

Coenzyme F430 is a highly reduced tetrapyrrole (Fig. 54) bearing a nickel ion in its core. It is the active site of the enzyme methyl-coenzyme M reductase (MCR) which catalyzes the final step of methanogenesis. The MCR tightly binds to the F430 which activates the reaction between coenzyme B (CoB-SH) and methyl coenzyme M reductase (MeS-CoB) to form the heterodisulfide product (CoB-S-S-CoM) and methane.[208]

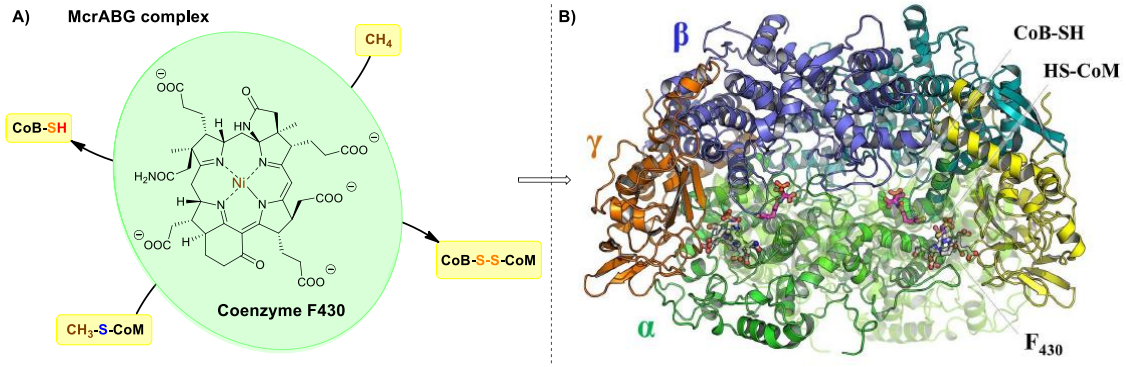

Figure 54: A) Microbiological formation of methane, B) Structure of methyl coenzyme M reductase.[209]

Another example of a natural tetrapyrrolic system is cobalamin or vitamin B_{12}. This cofactor is composed of a corrin ring chelating a cobalt ion. Corrins are reduced forms of tetrapyrroles. They are similar to porphyrins, except that the four pyrrole moieties are linked by only three methene bridges, forming an unsymmetrical macrocycle. Cobalamin is one of the eight B-vitamins and also the only one carrying a tetrapyrrolic macrocycle. It is responsible for the metabolism of human cells (cofactor of the DNA synthesis) and ensures the correct functioning of the nervous system (cofactor of the myelin synthesis).[210] The activity of all of these natural tetrapyrroles is based on the metal in the core of the porphyrin.

Over the past decades, metalloporphyrins were used to reproduce many natural processes.[211,212] Notably, they were utilized to catalyze a range of reactions such as C-H oxidation, which proceed *via* formation of high valence metal-oxygen complex intermediates.[213] The meso- and *β*-substitution of such systems results in less degradation of the macrocycle and prevents inactivation of catalytic activity.[214,215] The first oxidation systems with synthetic porphyrins were accomplished by Groves and coworkers in 1979.[216]

A classification system was proposed by Dolphin and Taylor in 1997, which categorized all the different metalloporphyrins used in oxidation catalysis based on their structure (Fig. 55).[217] The first generation contains all porphyrins with aryl groups at the meso-position but with no substituent at the aryl groups and at the *β*-position, such as

compound **150** in Fig. 55.[217] Changes in the aryl substituents led to the second generation **151**, and the third generation **152** was achieved by the addition of *β*-substituents.[218] Third generation catalysts showed the best catalytic activity.[219]

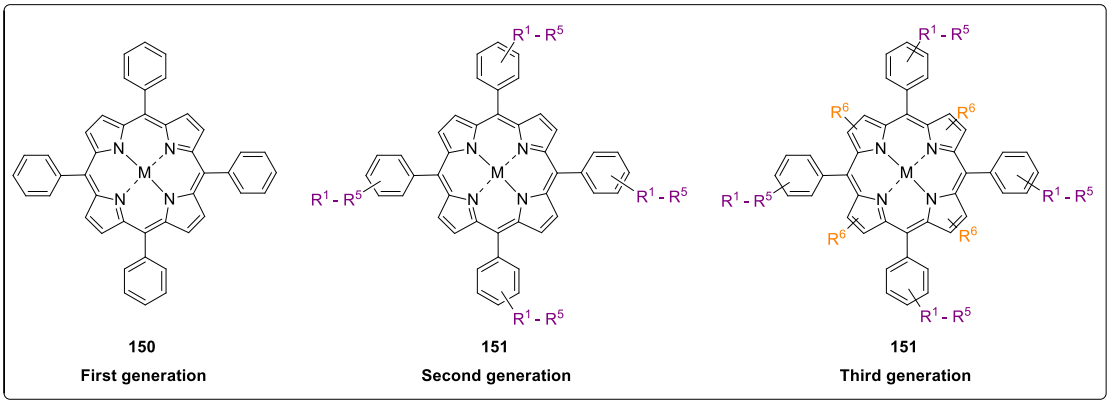

Figure 55: Different generations of catalytic metalloporphyrins.[214, 217, 220]

Other studies investigated the use of free base 5,10,15,20-tetraarylporphyrins as catalysts for photochemical reactions, which have shown high efficiency for singlet oxygen generation.[221] Interesting characteristics of porphyrins for such applications include their high absorption coefficients, photo-stability and excited state energy levels.[222]

However, no example in the literature used metal-free porphyrins as catalysts for organic reactions. Consequently, the question remains: are metal-free porphyrins able to activate organic reactions? In theory, yes! The structure of the core of the porphyrin contains very specific moieties which can be associated to the moieties observed on the bifunctional thiourea derivatives: the NH from the pyrrole units could undergo hydrogen-bonding (*e.g.*, thiourea part (Fig. 21), while the imine part could act as a basic functionality in the same way as the quinuclidine units. This was not mentioned until recently,[96] mainly due to the fact that the NH and *N*-lone pairs are buried in the macrocycle due to its planarity. Thus, the present work aims to investigate the idea of using distorted macrocycles in order to achieve accessibility of these functionalities. These systems are known to show an out-of-plane orientation of the amine and imine units, hence making them available to bind small organic molecules.

5.4 Concept

Bifunctionalized systems, such as (thio)ureas, have shown to be excellent compounds for the dual activation methodology in organocatalysis, as they allow one to activate the electrophile and deprotonate the pro-nucleophile. The chiral urea- and thiourea-

substituted cinchona alkaloid derivatives **148** and **149** described by Connon *et al.* have been found to be highly efficient for asymmetric Michael additions of malonates to nitroalkene compounds.[98,223] The quinuclidine ring activates the Michael donor while the thiourea moiety simultaneously activates the acceptor (Fig. 21).

Following this concept, highly distorted free base porphyrins (Fig. 56), more specifically the saddled shaped ones, have great potential as catalysts for base-catalyzed organic reactions such as Michael additions, Mannich reactions, and aldol reactions. The saddle shape causes the *N*-H protons to be pushed out-of-plane, making them more available for binding molecules.

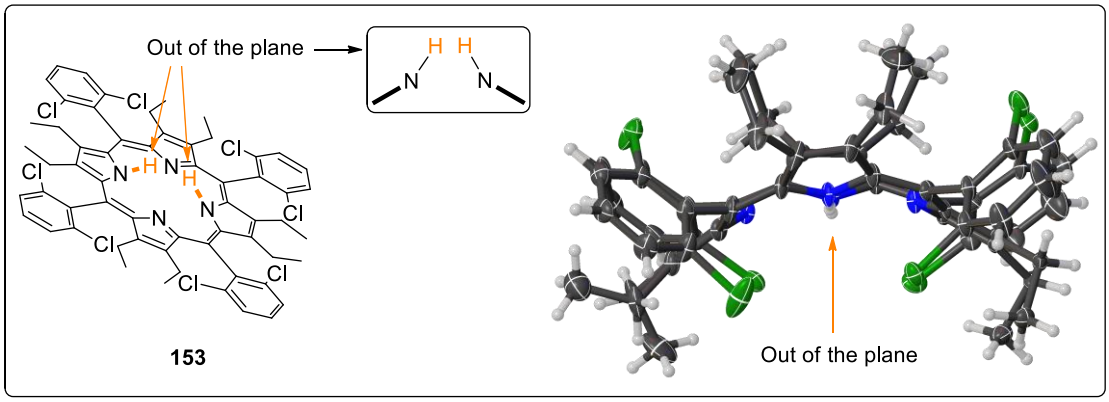

Figure 56: Highly distorted 5,10,15,20-tetrakis(2′,6′-dichlorophenyl)-2,3,7,8,12,13,17,18-octaethylporphyrin **153** and its crystal structure provided by Keith Flanagan.

With regards to *N*-methylated porphyrins, their characteristic feature is the distortion induced by the addition of a methyl group and their increased basicity, compared to their corresponding planar free base counterparts. Again, these two attributes allow the imine and amine groups to be both more accessible and more reactive in order to bind small molecules such as the reagents for Michael addition reactions. Consequently, the presence of both of these units and the enhancement of their properties should make these compounds highly suitable for bifunctional catalysis. The imine moiety could act as a base, deprotonating the pro-nucleophile, while the pyrrole units could act as hydrogen-bonding groups, activating the electrophile as illustrated below (Fig. 57).

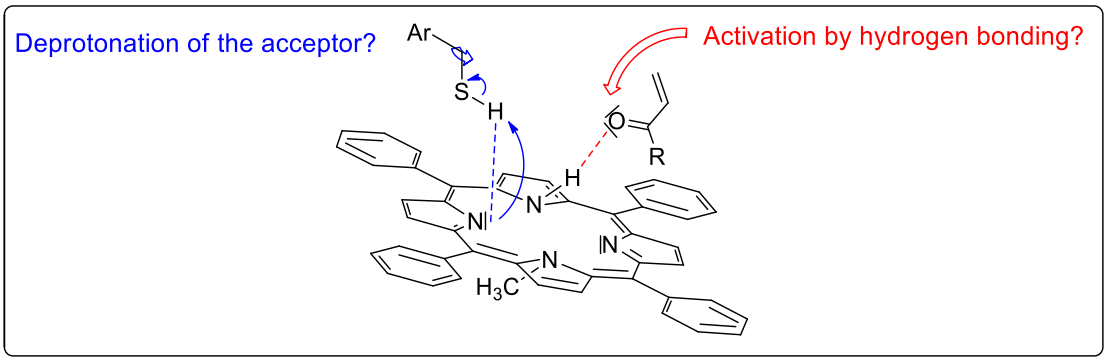

Figure 57: Hypothetic behavior of distorted porphyrins in bifunctional catalysis.

This last chapter will be divided into two parts. First, the establishment and optimization of a standard procedure was investigated, followed by the screening of a library of porphyrins with diverse properties, such as *N*-substituted porphyrins, cationic porphyrins, highly distorted porphyrins with variable electron density of the macrocycle, and planar porphyrins. The second part focused on the screening of a panel of designer porphyrins, synthesized in part 3, in response to the results obtained in the first part of this chapter.

5.5 Results and discussion

5.5.1 Initial tests and results

The Michael addition was chosen to test the viability of porphyrins, as this reaction type represents one of the main classical reactions used for bifunctional catalysis and involves nucleophilic attack at a Michael acceptor.[224,225,226] The investigation began with an examination of the potential catalytic activity of the highly distorted free base porphyrins 2,3,7,8,12,13,17,18-octaethyl-5,10,15,20-tetranitroporphyrin (OETNP **150**) and 2,3,7,8,12,13,17,18-octabromo-5,10,15,20-tetraphenylporphyrin (OBr_8TPP **151**) (Fig. 58). The peripheral substitution induces a high distortion, tilting the *N*-Hs out of the macrocycle and making them more available to bind small molecules.[222] The electron withdrawing substituents will result in an electron-poor macrocycle, increasing the acidity of the pyrrolic NH units and therefore enhancing the activation of the Michael acceptor. A range of Michael donors and acceptors were used to investigate the catalytic activity of these porphyrins.

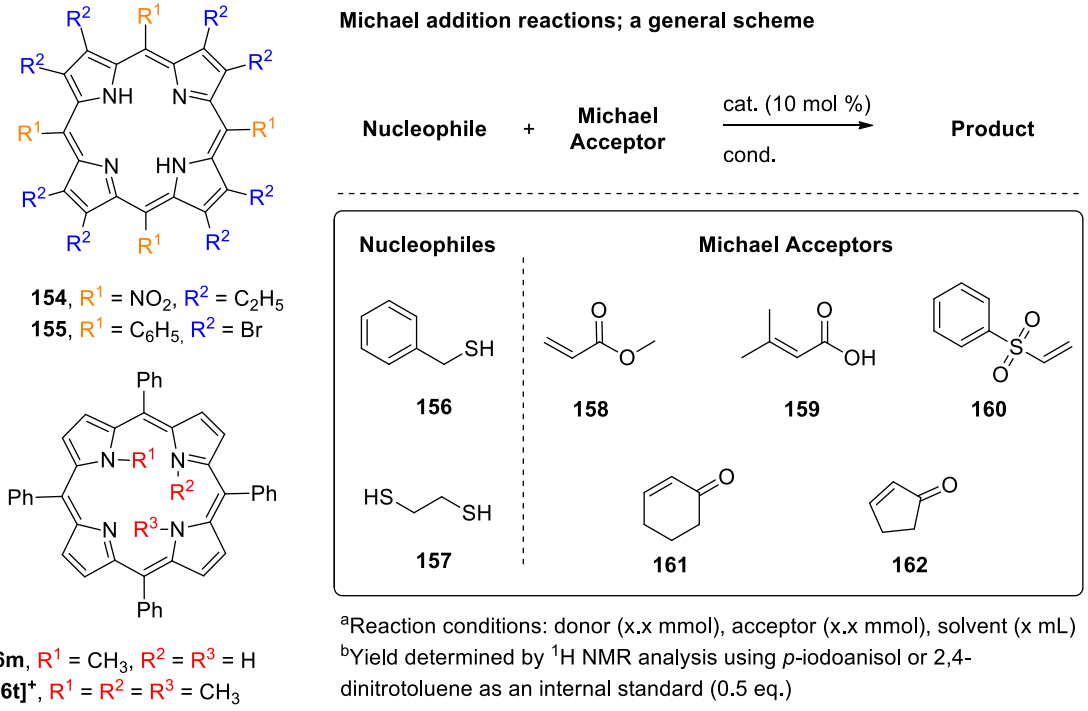

[a]Reaction conditions: donor (x.x mmol), acceptor (x.x mmol), solvent (x mL)
[b]Yield determined by ^1H NMR analysis using *p*-iodoanisol or 2,4-dinitrotoluene as an internal standard (0.5 eq.)

Figure 58: First porphyrins screened (left). Donors and acceptors employed for the screening (right).

A stoichiometric amount of each reagent and 10 mol % of the porphyrin were employed; unfortunately, they did not show any catalytic activity. The electron poor macrocycle induces a decrease in the basicity of the imine groups, resulting in less effective deprotonation of the nucleophile.

Thus, attention turned to *N*-substituted porphyrins with the use of N^{21}-monomethyl-tetraphenylporphyrin **26m** and N^{21},N^{22},N^{23}-trimethyl-tetraphenylporphyrin **[26t]$^+$** as a catalyst. As mentioned before in part 4, their intrinsic property is the distortion induced by the addition of a methyl group and their increased basicity, compared to their corresponding planar free base.

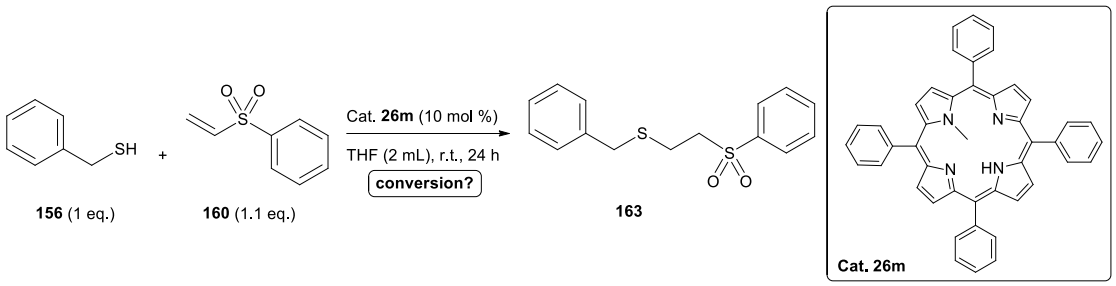

Scheme 27: Initial successful conditions reaction for the screening of Michael addition reaction using porphyrin **26m**.

The reaction chosen for the screening of these porphyrins was a thia-Michael addition, commonly catalyzed by bases[227], which used benzyl mercaptan **156** (1 eq.) and phenyl vinyl sulfone **160** (1.1 eq) with *N*-monomethylated tetraphenylporphyrin *N*-Me-TPP **26m** (10 mol %) to obtain product **163** (Scheme 27). Initial results were encouraging, as they showed 9% conversion and upon repetition, a consistent range of yields between 5–8% was obtained. The next logical step was to optimize the various conditions such as solvent, catalyst loading, the concentration of the reaction, etc., in order to achieve a better yield. Thus, it will allow establishment of standard conditions to then reliably screen a panel of porphyrins.

5.5.2 Optimization and establishment of a standard procedure

5.5.2.1 Influence of the solvent

The influence of solvents on the reaction was investigated by conducting a range of experiments shown in Table 14.

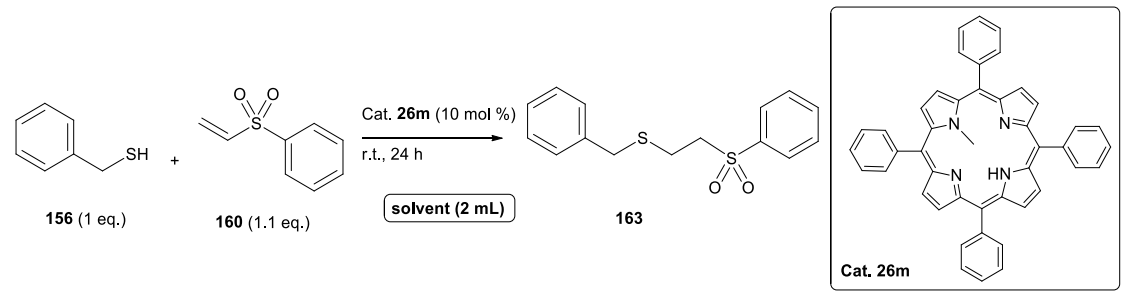

Table 14: Optimization of solvents for the screening conditions.

Entry	Solvent	Conv. (%)	Blank conv. (%)
1	THF	5–8	-
2	MeOH	90	90
3	CH_2Cl_2	9	-
4	DMF	-	-
5	$CHCl_3$	8	-

MeOH gave the best conversion; however, a reaction also took place in the reference sample showing that methanol itself enhanced the reaction. Only CH_2Cl_2 and $CHCl_3$ have led to conversions, where the conversion was only attributed to the catalyst and not the solvent. For this reason, CH_2Cl_2 was chosen as the solvent for all future experiments.

5.5.2.2 Optimization of the catalyst loading

Next, the effect of catalyst loading was investigated by varying the amount of porphyrin used from 1 to 10 mol %. The results obtained are presented in Table 15.

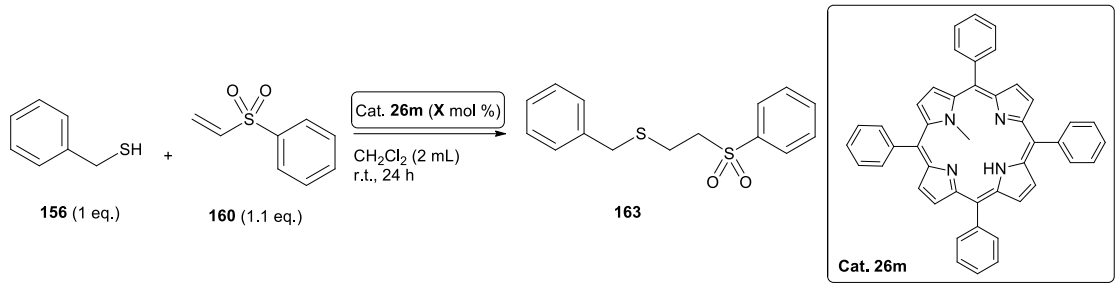

Table 15: Optimization of catalyst loading for the screening conditions.

Entry	Catalyst loading (X mol %)	Conv. (%)	Blank conv. (%)
1	1	Trace	-
2	2	2	-
3	3	8	-
4	4	6	-
5	5	6	-
6	10	7	-

From the results presented above, a catalyst loading of 3% gave a similar conversion to the experiment run with 10% catalyst loading (**entry 3** and **6**). Thus, in order to save valuable catalysts and to be able to repeat experiments, a catalyst loading of 3 mol % was chosen to continue with the optimizations.

5.5.2.3 Influence of the reagent concentration

The concentration of the reagents is also an important parameter to optimize as it determines the proximity of the molecules in solution. Diluted conditions can decrease the activity of the catalyst and consequently, the conversion; conversely a concentrated solution can improve and accelerate the reactivity of the catalyst. The different concentrations used are presented in Table 16.

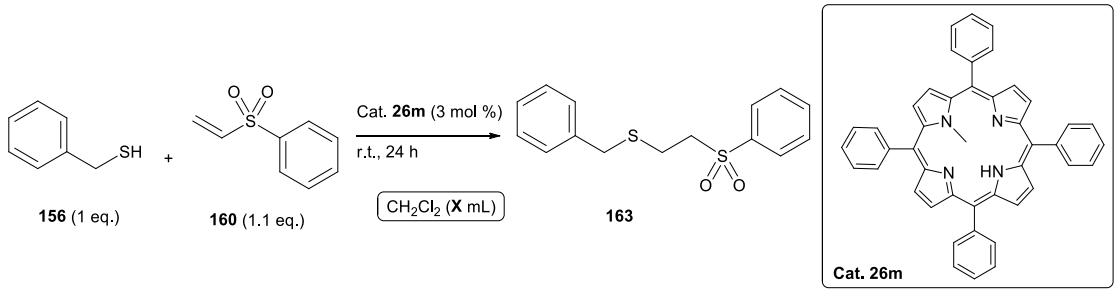

Table 16: Concentration optimizations for the screening conditions.

Entry	Volume of CH_2Cl_2 (mL)	Conv. (%)	Blank conv. (%)
1	0.1	66[a]	-
2	0.5	10[a]	-
3	1.0	-	-
4	1.5	-	-
5	2.0	5–8	-

[a] Conversion obtained by integration of the starting material **151** (consumed). Integration between reagent and product did not match.

As expected in **entry 1,** a more concentrated condition improved both reactivity and conversion. However, a side product appeared in **entries 1** and **2** giving higher conversion of starting material than expected. A possible explanation for the formation of side products is the oxidation of thiols by air or by oxygen contained in the solvent used for the reactions.[228]

5.5.2.4 Influence of air

In order to avoid the potential formation of dithiol species due to the reaction of the thiol with oxygen, the reaction was set up under argon and in dry and degassed CH_2Cl_2 (Table 17).

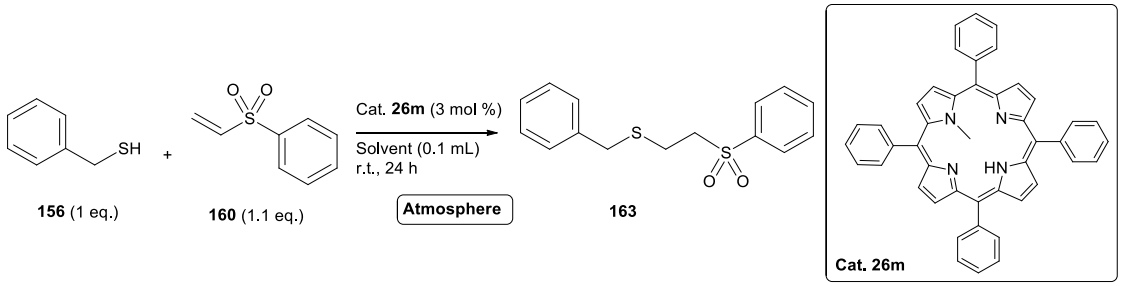

Table 17: Optimization of atmospheric parameters for the screening conditions.

Entry	Solvent	Atmosphere	Conv. (%)	Blank conv. (%)
1	**Dry CH_2Cl_2**	**Ar.**	65	-
2	**Dry CH_2Cl_2**	**Ar.**	97	-
3	**CH_2Cl_2**	**Air**	90	-

Initially, the results were promising with a depletion of the side product observed. Unfortunately, upon repetition the side product reappeared for each test. It was hypothesized from previous results that unreacted thiols can be oxidized when a sample of the solution is taken for ^{1}H NMR. The next idea was to force the reaction to completion to avoid possible oxidation of the unreacted thiols (Table 18). Moreover, due to the high reactivity of the benzyl mercaptan **156**, a different thiol was used: the 4-*tert*-butyl benzyl mercaptan **164**.

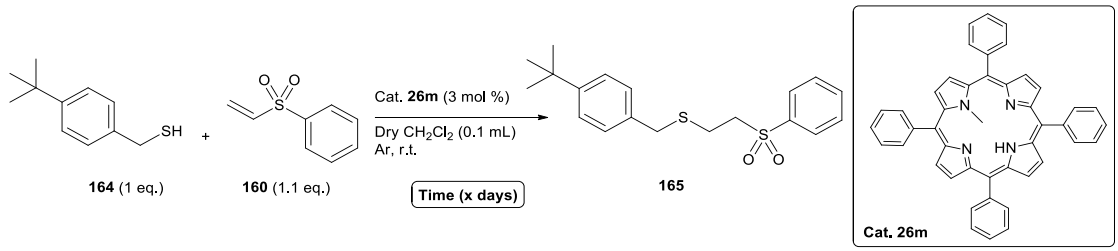

Table 18: Time to completion for the screening conditions.

Entry	Time (d.)	Conv. (%)	Blank conv. (%)
1	**1**	40	-
2	**2**	45	-
3	**3**	73[a]	-
4	**7**	86[a]	-
5	**9**	90[a]	-

[a] Conversion obtained by integration of the starting material **163** (consumed). Integration between reagent and product did not match.

Results show that above 50% conversion, side product formation occurred and even after nine days, the reaction did not reach completion.

With regards to the side products, a hypothesis was made about the internal standard used based on related research carried out by M. Kielmann *et al.*[229] 2,4-Dinitrotoluene contains nitro groups which are likely to react with thiols. Consequently, 2,4-dinitrotoluene (DNT) was replaced by dibromomethane as the internal standard. Results showed a lower conversion of 50% compared to the previous 70% conversion obtained. However, no side product was observed. These results were confirmed upon repetition, which gave a range of yields (50 to 60%).

In conclusion, the optimized conditions for the screening of different porphyrins are presented in the general Scheme 28. Moreover, a yield of 50% is suitable as a reference to test other porphyrins, as it allows comparison between more and less catalytically active porphyrins.

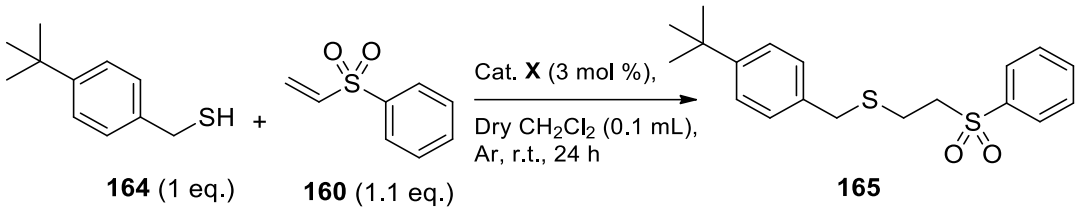

164 (1 eq.) **160** (1.1 eq.) **165**

Scheme 28: Optimized conditions used for the following screening catalytic activities of various porphyrins.

In addition, the formation of the compound was proven through a crystal structure of the product **165** (Fig. 59).

Figure 59: View of the molecular X-ray crystal structure of compound **165**. Atoms drawn in red are oxygen atoms and those in orange are sulfur atoms. Structure was determined by K. J. Flanagan.

The next step involved the screening of a large library of porphyrins with various electronic properties, structures and degrees of distortion. These differences will allow understanding of the mechanism of the porphyrin as a catalyst, but will also establish the requirements for the porphyrin to act as a catalyst.

5.5.3 Screening of various porphyrins

A range of porphyrins with diverse peripheral and core substitution patterns were prepared (see 3 and 4) and investigated to compare their catalytic activity (Fig. 60). These included the classic highly distorted free base porphyrin 2,3,7,8,12,13,17,18-octaethyl-5,10,15,20-tetraphenylporphyrin (H_2OETPP, **21**),[221] a chimera of the two archetypical, planar porphyrins H_2TPP **26** and **120** (H_2OEP = 2,3,7,8,12,13,17,18-octaethylporphyrin). H_2OETPP is structurally related to the more electron-deficient dodecasubstituted and catalytically inactive systems **77** and **154**.[230] Porphyrins with a varying degree of *N*-methylation were employed to compare core *versus* peripheral steric strain and to study the importance and involvement of both amine and imine moieties and to confirm a bifunctional mode of action.

The screening results are presented in Table 19. For porphyrins giving a conversion of 100% in concentrated solution (standard condition using 0.1 mL), the reaction was reproduced under diluted condition using 2 mL of solvents.

As predicted, free base planar porphyrins (**26**, **120**) did not give any conversion. Their structures have both “reactive” parts shielded inside the cavity, and thus, they were not available for binding with small molecules. The highly nonplanar porphyrin **21** gave a complete conversion under the established reaction conditions. H_2OETPP **21** has two unsubstituted imine units and two pyrrole *N*-H available for hydrogen bonding, which are both exposed due to the high degree of distortion present in the form of a *sad* structure. Under diluted conditions, a conversion of 80% to product **164** was still observed.

A comparison between compounds **26** and **26m** (no conversion *vs.* 50% conversion, respectively) potentially shows that the addition of a methyl unit into the cavity of the porphyrin promotes the efficiency of the catalyst. However, the opposite effect can be observed while investigating compounds **21** and **21m**. N^{21}-Monomethylation (**21m**) resulted in a decrease in conversion under dilute conditions, indicating that the best results are achieved when two pyrrole groups are available. Results obtained for compounds **26** and **26m** thus confirm that the distortion is a primary requirement to the catalytic activity of porphyrins. This is strongly supported by the screening of compounds **21d** and **[21tt]$^{2+}$** showing that as soon as two or more central nitrogen atoms were

substituted, a strong decline in conversion (**21d**) up to total inhibition (**[21tt]$^{2+}$**) of the catalytic process was noted. This supports the hypothesis that both amine and imine moieties are significantly involved in the catalytic process.

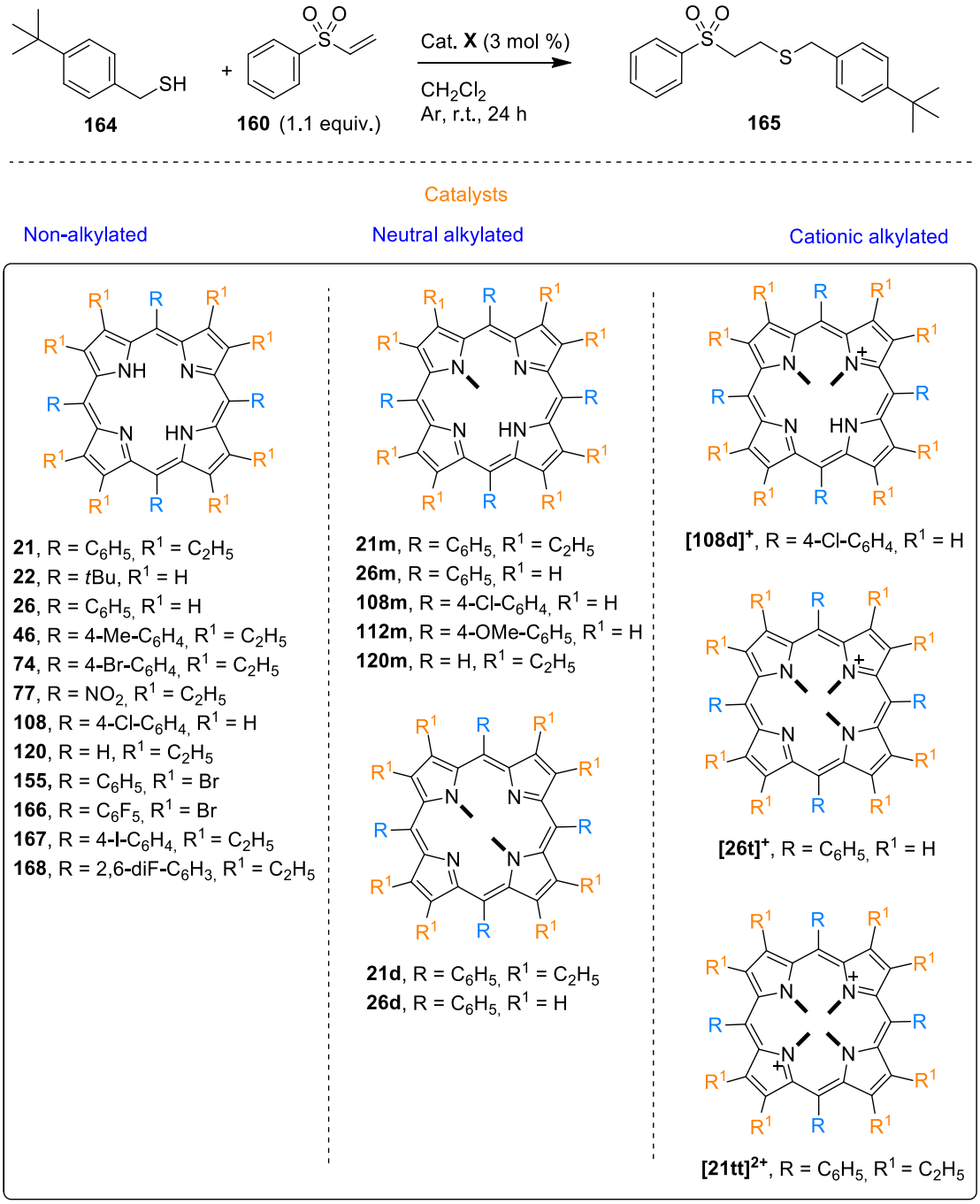

Figure 60: Various porphyrins screened as catalysts.

Table 19: Screening of a catalog of porphyrins.

entry	catalyst	*Δ*24 [Å][a]	λ_{max} [nm][b]	#NH	yield (%)[c]
1	-	n/a	n/a	n/a	0
2	**21**[55]	0.54[58b]	456, 555	2	>98 (80[e])
3	**21m**[95]	–	477, 735	1	>98 (<5[e])
4	**21d**[d]	–	488, 744	1	>98 (20[e])
5	**[21tt]$^{2+}$**[231]	0.61[231]	506, 756	0	0
6	**22**[127a]	–	446, 692	2	0
7	**26**[46b]	0.05/0.19[68]	417, 515	2	0
8	**26m**[58a]	0.26/0.3[232]	433, 677	1	50
9	**26d**[233]	0.61/0.71[69]	457, 630	0	5
10	**[26t]$^{+}$**[53]	0.44[75]	463, 715	0	0
11	**46**[234]	–	457, 710	2	>98 (75[e])
12	**74**	–	459, 515	2	0
13	**77**[235]	0.40[64c]	422, 663	2	0
14	**108**[d]	–	472, 683	2	0
15	**108m**[t.w.]	–	435, 678	1	3
16	**[108d]$^{+}$**[t.w.]	–	461, 710	1	86 (0[e])
17	**112m**[t.w.]	0.37[69]	437, 685	1	62
18	**120**[161]	0.02[69]	399, 498	2	0
19	**120m**[236]	–	410, 642	1	<5
20	**155**[80]	0.62[237]	468, 739	2	0
21	**166**[238]	0.56[239]	495, 711	2	0
22	**167**[d]	–	474, 685	2	0
23	**168**[d]	–	473, 674	2	0

[a] *Δ24* = Average deviation of the 24-macrocycle atoms from their least-squares plane as a measure of overall degree of nonplanarity in the solid state. [b] λ_{max} = Soret and long wavelength Q absorption bands in CH_2Cl_2 (+ 1% NEt_3) as a measure of macrocycle distortion in solution.[1,44,74] [c] Determined by ^{1}H NMR spectroscopy using an internal standard, [**cat**] = 7.1 x 10^{-2} M. [d] Porphyrin were given by Keith Flanagan. [e] Performed under dilute conditions, [**cat**] = 3.6 x 10^{-2} M

Intriguingly, porphyrin **[108d]$^{+}$** shows good catalytic activity (20% in concentrated conditions) despite the presence of the electron withdrawing aromatic groups. This was most likely due to the positive charge and the higher distortion displayed due to the '*cis*'-N^{21},N^{22}-dimethylation pattern.[232] This variant of N^{21},$N^{22/23}$-dimethylation leaves a pyrrole and an imine unit available for activation of both the Michael acceptor and donor, as opposed to the usual '*trans*'-N^{21},N^{23}-dimethylation (**21d**).

Next, variations of distortion modes were examined. As mentioned in part 3, highly substituted porphyrins often present a *sad* distortion mode. Other types of distortion can be encountered using porphyrins such as the 5,10,15,20-tetra(*tert*-butyl)porphyrin **22**,

which displays a *ruf* distortion mode. Macrocycles displaying this type of distortion are considered highly distorted macrocycles too, though no conversion was observed. The reason can be found in the fact that the *N*-H units, even though the porphyrin core is distorted, are still concealed in the porphyrin plane.[80]

In addition, variation of the electronic properties *via* peripheral substitution of various functional groups has a remarkable impact on the catalytic system. Theoretically, electron withdrawing groups should increase the acidity of the pyrrolic protons, and thus improve the binding affinity between the pyrrole units and the Michael acceptor. However, the tetrakis(*p*-bromophenyl)-OETArX porphyrin **74** is inactive. A possible explanation of the poor conversion is that the withdrawing effect decreases the pK_a of porphyrins, inducing lower reactivity of the imine groups. Usually, *p*-bromo substitutents are not considered as powerful electron withdrawing groups (σ_p = 0.26), though due to the structure of the porphyrin, four of these electron withdrawing units are present, resulting in the inactivation of the porphyrin towards the deprotonation of the nucleophiles. In comparison, the tetrakis(*p*-tolyl) derivative **46** displays a reactivity comparable to porphyrin **21**. This is due to the presence of the electron donating units (σ_p = -0.17), which enhances the affinity of the imine units toward the nucleophile. This indicates a potential bifunctional deprotonation of the nucleophile and activation of the Michael acceptor by the pyrrolic protons and the imine group of the porphyrin, respectively.

5.5.4 Comparative screening with common small organic bases

Clearly, distorted porphyrins are good candidates for catalysts. As organocatalytic free base porphyrins had not been reported so far, the necessity to provide a context regarding their efficiency was the next obvious step. Consequently, the most effective porphyrin, H_2OETPP **21**, was compared with a range of amine bases showing disparate basicities.

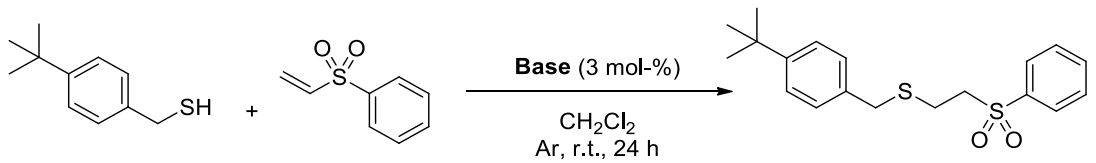

164 (1.0 eq.)[a] **160** (1.1 eq.)[a] **165**

Table 20: Screening of various bases under concentrated conditions.

Entry	Base	pK_{AH} [a]	Conv. [b](%)
Blank	-	-	0[a]
1	Aniline	4.6	Traces
2	Pyridine	5.2	Traces
3	Imidazole	6.8	85 (0)[c]
4	DMAP	9.7	> 98 (43)[c]
5	NEt_3	10.9	> 98 (76)[c]
6	H_2OETPP **19**	n/d	> 98 (80) [c]
7	DBU	13	> 98 (> 98)[c]

[a] Refers to the conjugated acid of the base listed. [b] Determined by ^{1}H NMR spectroscopy using an internal standard, [**cat**] = 7.1 x 10^{-2} M. [c] Performed under dilute conditions, [**cat**] = 3.6 x 10^{-2} M.

Amine molecules with weak basicity such as aniline or pyridine showed no catalytic activity in concentrated conditions (**entries 1** and **2**). Imidazole (**entry 3**), which has a moderate basicity, is a good catalyst in concentrated solutions, but did not show any catalytic behavior in diluted conditions. Upon an increase in the basicity, the use of diluted conditions was necessary to obtain a good comparison of the efficiency of the different bases. DMAP led to a 43% conversion (**entry 4**), NEt_3 showed a catalytic activity of 76% conversion (**entry 5**) and DBU (**entry 7**), the strongest base, promoted the conversion quantitatively. With regards to the porphyrin tested, its conversion reaches 80%, which is located between NEt_3 and DBU in terms of efficiency. Consequently, it appears that the basicity of porphyrins is capable of exceeding common bases such as NEt_3.

5.5.5 A comparative study on the basicity of nonplanar porphyrins

Additionally, NMR and UV-vis data of solutions of porphyrins with various weaker bases (Table 20) were obtained to confirm the high basicity of the porphyrin. The screening studies using various amine bases showed that OETPP is more basic than DMAP or even NEt_3. To confirm this high basicity, deprotonation studies of the conjugated acid of both NEt_3 and DMAP by porphyrins were performed. The conjugated acids were obtained by treatment of the base with HCl vapor to form the hydrochloric salt. Two porphyrins were chosen; H_2OETPP **21,** which is catalytically active and the tetrakis(*p*-bromo) analog **74,** which has no catalytic effect. Theoretically, deprotonation of the various bases should be observed using porphyrin **21**, and porphyrin **74** should not deprotonate the conjugated acids.

5.5.5.1 Deprotonation of amine bases by 21

First, spectroscopic studies using H_2OETPP **21** were carried out. In an NMR tube, both the porphyrin and the conjugated salts were mixed. The first salt used was DMAP·HCl and results are presented in Fig. 61.

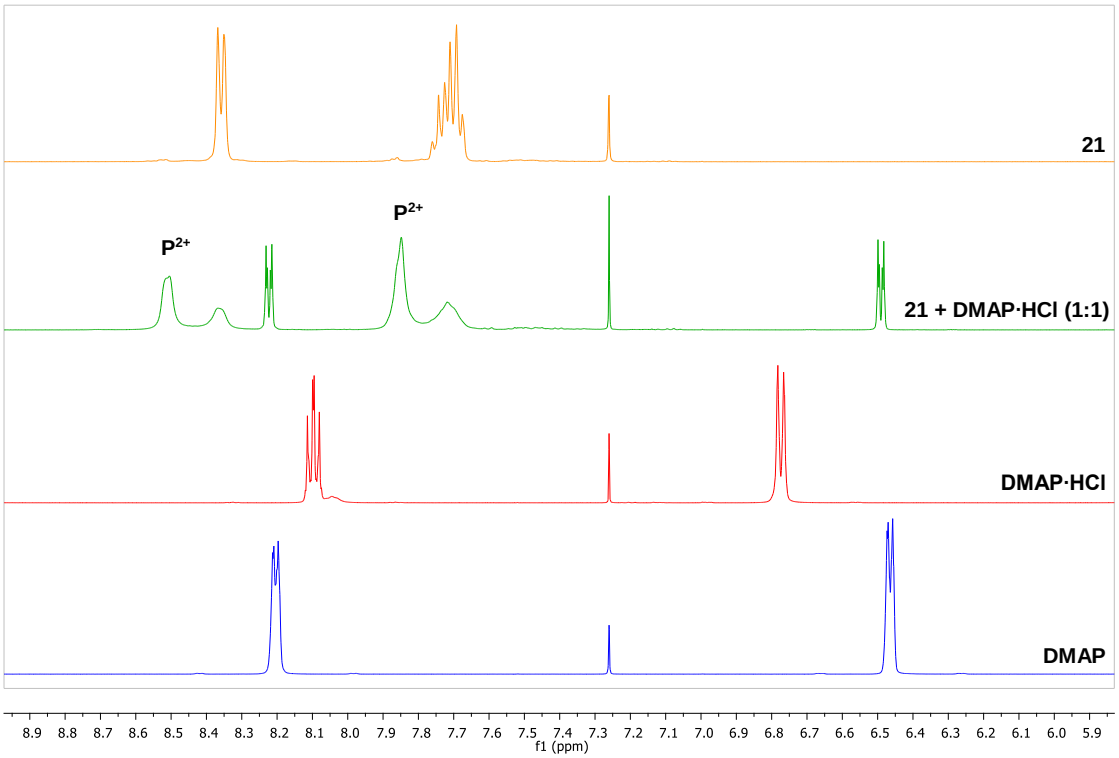

Figure 61: NMR studies of the deprotonation of DMAP·HCl by **21** in $CDCl_3$.

Looking at the NMR results, it is obvious that DMAP·HCl (middle line, red spectrum) is no longer present in the reaction mixture (green spectrum). It is then easy to assume that the DMAP·HCl has been deprotonated by the addition of the porphyrin forming the DMAP (bottom line, blue spectrum). The formation of the diprotonated form of the porphyrin (P^{2+}) is also visible in the NMR spectrum (green spectrum) along with some of the neutral form (orange spectrum).

In parallel, UV-vis studies were performed to further confirm the results obtained by NMR spectroscopy. Porphyrins have a very intense Soret band which is red-shifted by about 20 nm upon protonation. Results are presented below in Fig. 62.

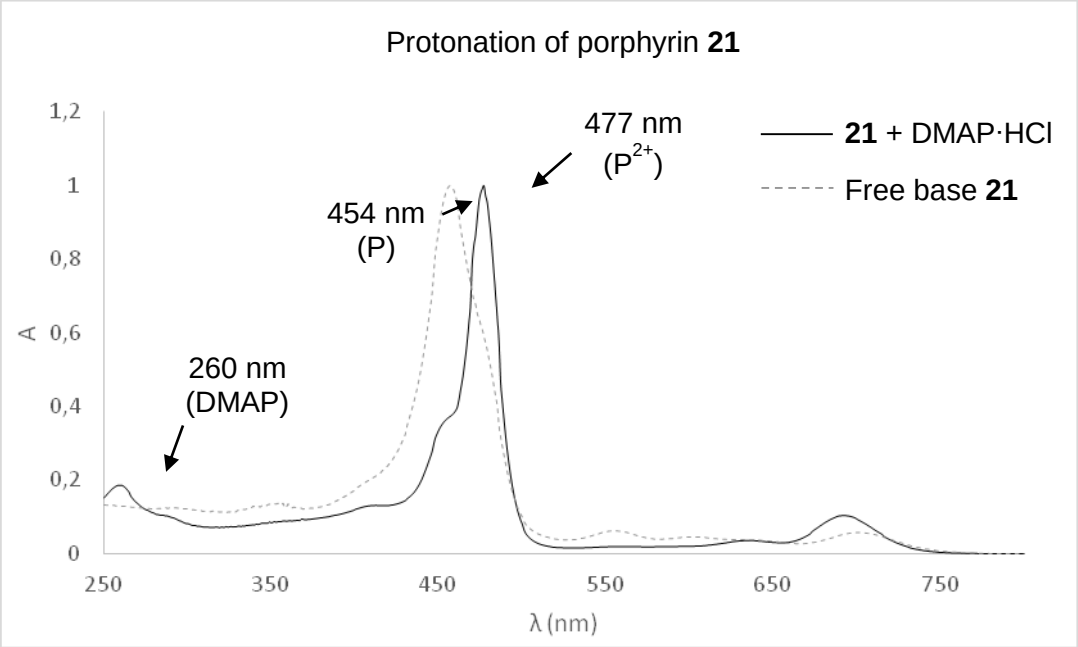

Figure 62: NMR studies on the protonation of **21** by DMAP·HCl in $CDCl_3$ (top), UV-vis studies on the protonation of **21** by DMAP·HCl in $CHCl_3$ (bottom).

The spectrum recorded (plain line) clearly shows a red-shift in comparison to the recorded spectrum of the neutral porphyrin (dashed line). The Soret band of the neutral porphyrin at 454 nm is shifted by 23 nm to the longer wavelengths (477 nm), which corresponds to its diprotonated species.

Next, the same studies were conducted using NEt_3·HCl and results are presented below in Fig. 63.

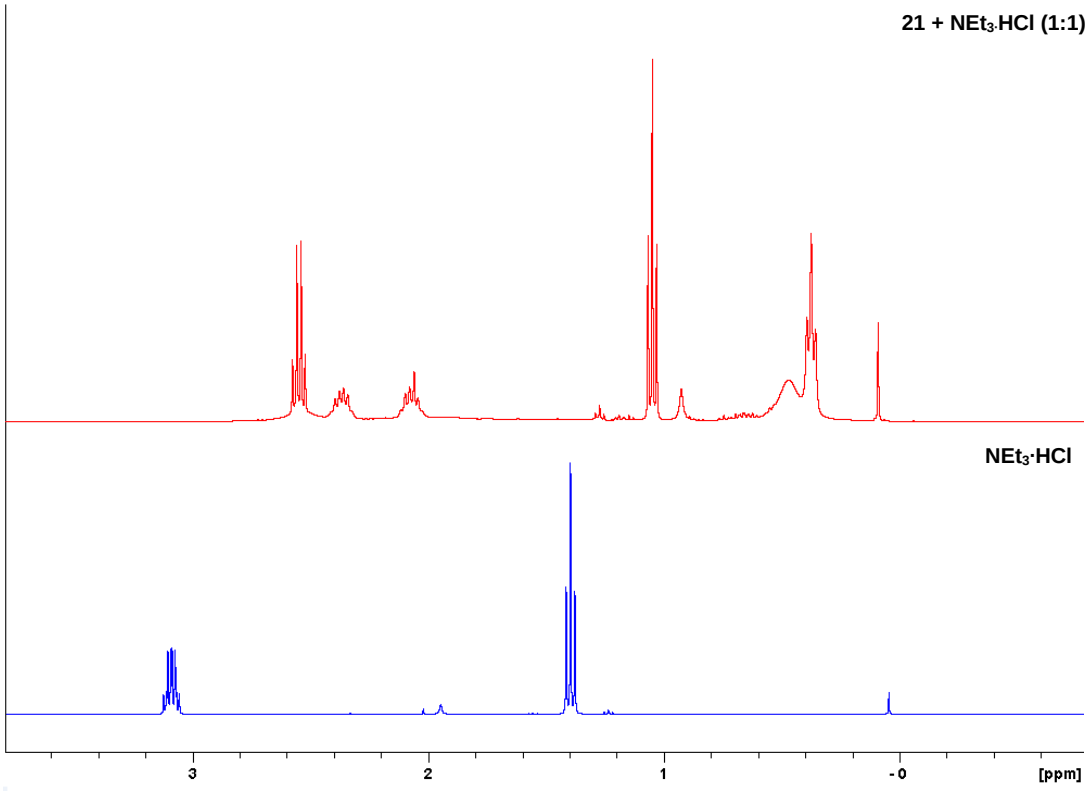

Figure 63: NMR studies of the deprotonation of NEt_3·HCl by **21** in $CDCl_3$.

Similar to DMAP·HCl, NEt_3·HCl (Fig. 63, blue spectrum) is deprotonated by the presence of the porphyrin and the base no longer appears in the reaction mixture (Fig. 63, red spectrum). These results clearly prove that the porphyrin is of higher basicity than strong amines such as NEt_3.

5.5.5.2 Deprotonation of amine bases by 74

To confirm that the deprotonation only happens with catalytically active porphyrins, similar studies using only DMAP were performed with porphyrin **74**. This porphyrin bears withdrawing electron substituents at its periphery and thus does not show any catalytic capabilities. Fig. 64 shows the results of the investigation by NMR and UV-vis spectroscopy of the deprotonation of DMAP·HCl by porphyrin **74**.

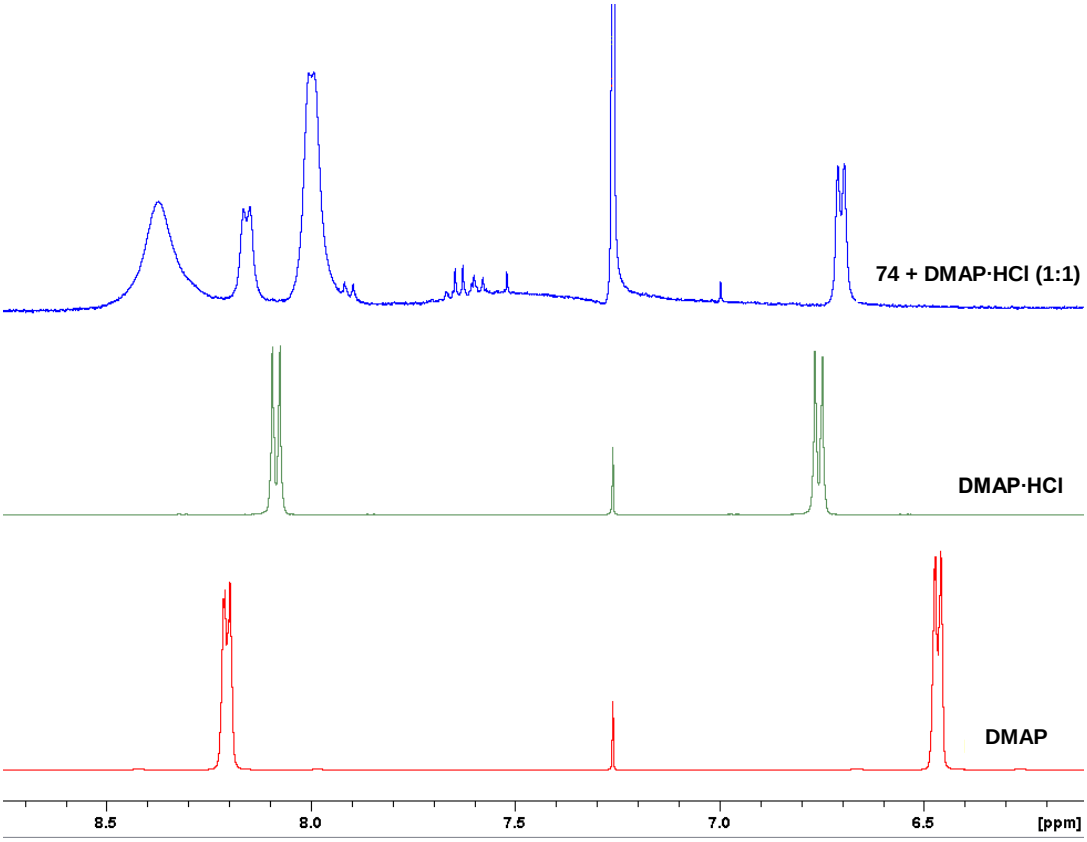

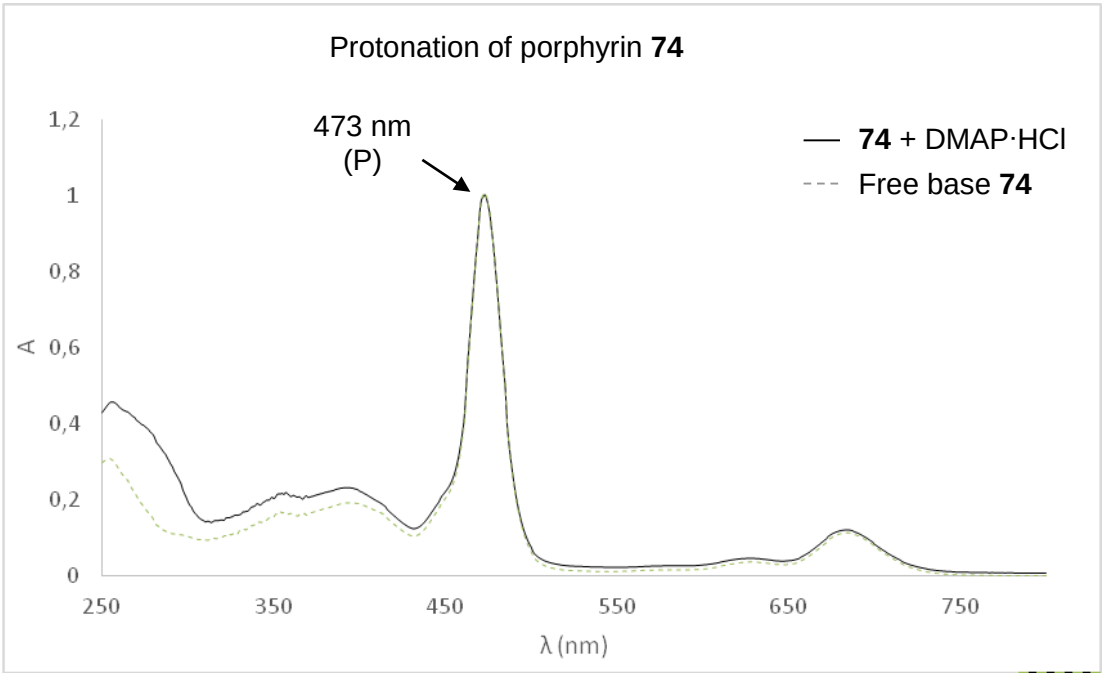

Figure 64: NMR studies on the protonation of **74** by DMAP·HCl in $CDCl_3$ (top), UV-vis studies on the protonation of **74** by DMAP·HCl in $CHCl_3$ (bottom).

As expected, no deprotonation of DMAP is observed in the NMR studies nor in the UV-vis spectrum. The mixture (Fig. 64, blue spectrum) shows no formation of the diprotonated porphyrin, and in comparison, signals corresponding to the DMAP·HCl (Fig.

64, green spectrum) are still observed. The offset observed in the NMR spectra is probably due to electrostatic interactions between the free base porphyrin **74** and DMAP·HCl. In the UV-vis spectra, it can be seen that the two spectra of the neutral porphyrin and the mix of DMAP and porphyrin **74** overlap perfectly. No bathochromic shift is observed, confirming no reaction of the porphyrin.

From these studies, it can be concluded that porphyrins with electron-rich macrocycles are basic enough to deprotonate strong bases, forming the dicationic species of the porphyrin. Consequently, it is logical to investigate the mechanism by which the catalytic screenings proceed using the porphyrin. Assuming the porphyrin is protonated by the pro-nucleophile, does this protonation also lead to the dicationic species?

5.5.5.3 Protonation of H_2OETPP 21 by thiol

In order to understand the mechanism behind the catalytic activity of the porphyrin, NMR studies similar to the one with the hydrochloric salts were conducted. Porphyrin **21** was mixed with the nucleophile in various ratios and the interactions were monitored by NMR spectroscopy. The results are presented in Fig. 65.

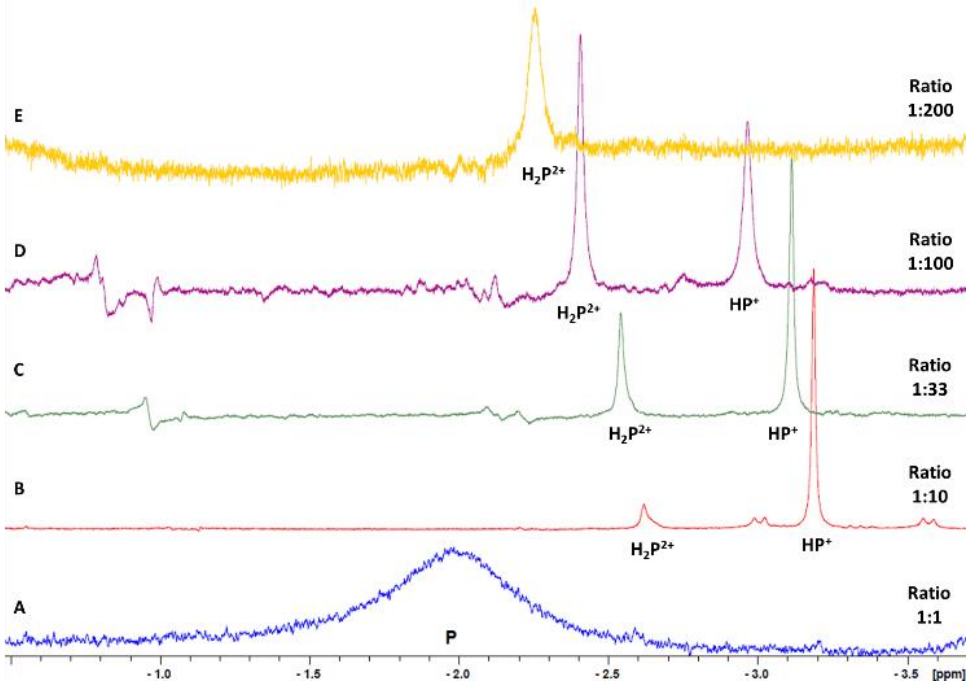

Figure 65: NMR spectra of the protonation of **21** by **164** at increasing substrate/catalyst ratios performed in $CDCl_3$. Only the area from 0 to -4 ppm is shown.

When an equimolar amount of material was added, no protonation of the porphyrin was observed (spectrum A, Fig. 65). Upon an increase in the amount of nucleophile present, the formation of two porphyrin species is observed (spectrum B-D, Fig. 65). Considering the NH proton signals observed at -2 ppm (spectrum A, Fig. 65), the two new signals

observed can only correspond to the mono- and the diprotonated form of porphyrin **21**. Ratios of porphyrin and nucleophile in a 1:10 (spectrum B, Fig. 65) and 1:33 (spectrum C, Fig. 65) indicate a major formation of the monoprotonated species. Upon increase of the thiol equivalence to 100 (spectrum D, Fig. 65), the diprotonated form became the main species in solution. The use 200 equivalents of thiol (spectrum E, Fig. 65) resulted in the disappearance of the monoprotonated species

Under standard conditions used for the catalytic reaction, the ratio considered for the reaction is of 1:33 between the porphyrin and the thiol, respectively (spectrum C, Fig. 65). As observed in Fig. 65, at that ratio the main species is the monoprotonated porphyrin. These results strongly support our hypothesis that the active species formed during the catalytic process is the monoprotonated porphyrin.

5.5.5.4 Study on the protonation of catalytically active and inactive porphyrins by thiol

The other idea was to investigate porphyrins such as N^{21}-methyl-tetrakis(*p*-chlorophenyl)porphyrin **108m** and N^{21}-methyl-5,10,15,20-tetraphenylporphyrin **26m** which led to a very low or moderate conversion, respectively. The same experiment, carried out on porphyrin **21** in part 5.5.5.3, was then examined using the aforementioned porphyrins. Each porphyrin was mixed with the nucleophile in different ratios to observe the potential protonation of the macrocycle. The results are presented in Table 21.

Table 21: Studies on the protonation of porphyrin **108m** and **26m** by thiol.

Entry	Exp. cond.	Conv. conc. / dil. (%)	Observation
1	**108m**+ Thiol (1:1)	3 / 0	No protonation
2	**108m** + Thiol (1:10)	3 / 0	No protonation
3	**108m** + Thiol (1:33)	3 /0	No protonation
4	**26m** + Thiol (1:1)	50 / 0	No protonation
5	**26m** + thiol (1:10)	50 / 0	No protonation
6	**26m** + Thiol (1:33)	50 / 0	No protonation

As expected, **108m** did not result in any protonation of the porphyrin, only a very low catalytic activity was observed. Similar results were obtained for porphyrin **26m,** which gave 50% conversion. These results can be explained by the fact that the spectra for this study were recorded in diluted conditions. The 50% conversion corresponded to results obtained in concentrated conditions. However, in diluted conditions no conversion was observed for compound **26m** also, explaining the absence of protonation observed during this study.

5.5.5.5 Activation of the electrophile *via* H-bonding

So far, it has been proven that porphyrins are able to activate pro-nucleophiles leading to protonation of the porphyrin. This step is only possible for highly distorted porphyrins with electron-rich macrocycles. Thus, the next step aimed to investigate the activation of the electrophile by the porphyrin. From the initial hypothesis, the electrophile might be activated through hydrogen-bonding with the pyrrole. Due to the weak interaction established between the electrophile **160** and the pyrrole units of the porphyrin, the environment of the electrophile will be different, influencing the proton signal of the nearby hydrogen atoms in the NMR spectrum. Four studies were set up to investigate this hypothesis (Fig. 66 and 67). The ^{1}H NMR spectrum of the electrophile used during the screening was recorded alone as a reference (Fig. 66, blue spectrum). Then the electrophile **160** was mixed with either: the active porphyrin H_2OETPP **21** (80% conversion, Fig. 66, red spectrum), an inactive nonplanar porphyrin **166** with an electron deficient macrocycle (0% conversion, Fig. 66, green spectrum), or the planar H_2TPP **26** or H_2OEP **120** (0% conversion, no spectrum recorded). The ^{1}H NMR spectrum for the planar porphyrins are not included here due to the perfect overlapping of each signal with the signals in the electrophile ^{1}H NMR spectrum.

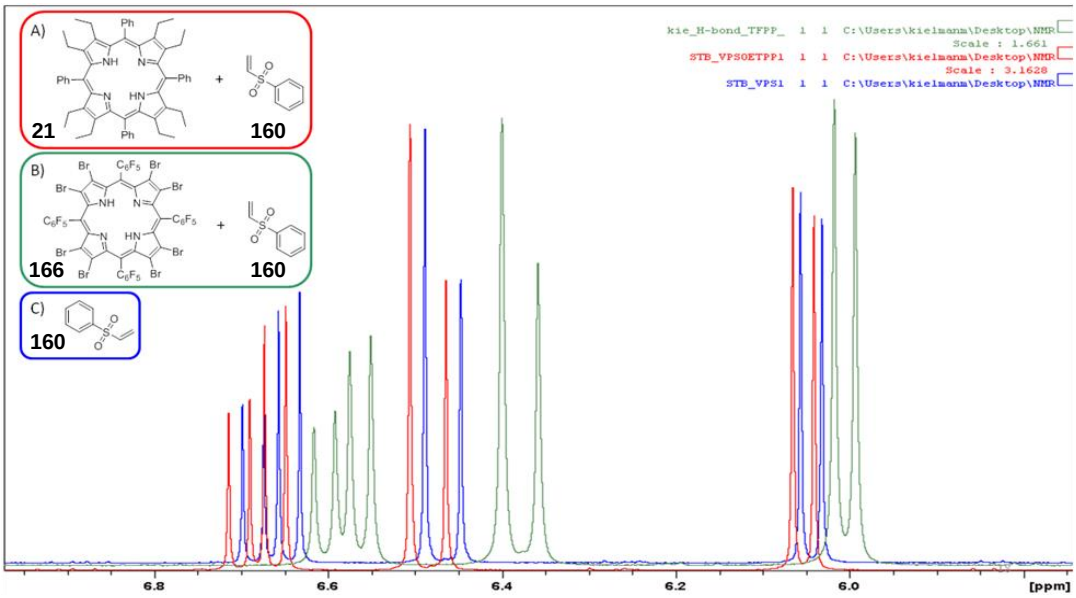

Figure 66: Overlay of ^{1}H NMR spectra of the electrophile **156** a) with **21**, b) with **166**, and c) alone in $CDCl_3$.

The ppm values for each spectrum in comparison to the reference are also presented in Fig. 67 and support the capability of the porphyrin towards hydrogen-bonding with the electrophile. In line with the initial hypothesis, the use of planar porphyrins did not induce any chemical shift of the NMR signals (Fig. 66, blue spectrum (c)). This indicates the

absence of any interaction between the porphyrin and the electrophile which can be easily rationalized by the fact that the active units of the porphyrin are shielded in the planar macrocycle.

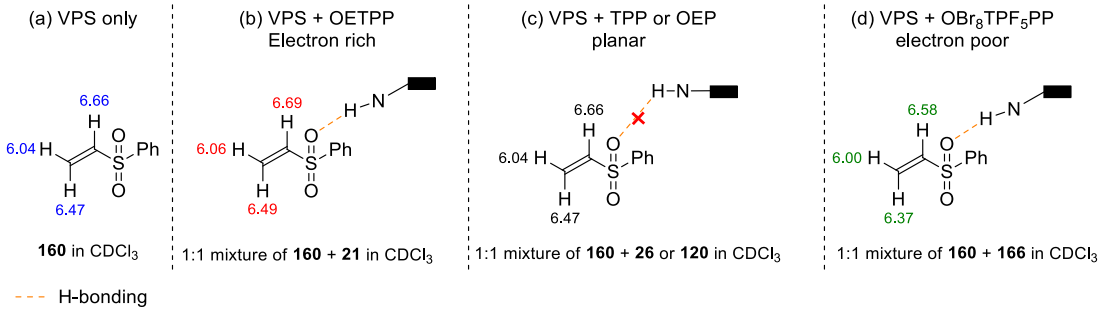

Figure 67: ^{1}H NMR shift observed for the VPS hydrogen atoms consequently to the binding between porphyrins **21**, **26**, **120** and **166** and VPS **160** in $CDCl_3$.

Results obtained with porphyrin **166** are more surprising (Fig. 65, green spectrum). An upfield shift is observed even though the porphyrin does not show any catalytic efficiency. These results can be explained by the strong electron deficiency of the macrocycle, enhancing the hydrogen-bonding between the pyrrole units and the electrophile. This indicates that the deprotonation of the nucleophile is the decisive step during the catalytic screening due to the loss of catalytic activity observed using porphyrin **166**, despite the good activation of the electrophile.

5.5.6 Scope of the catalyst

From the established procedure, it was then interesting to evaluate the scope of porphyrins as catalysts. For this reason, two studies were performed: the first study consisted of changing either the electrophile or the nucleophile. This examination was performed in collaboration with M. Kielmann, who varied the nucleophiles, while in the following part of this thesis, the objective was to explore a range of electrophiles. The second investigation was to explore the scope of the porphyrin as a catalyst.

5.5.6.1 Variation of the electrophiles

A range of electrophiles were screened in order to test the sensitivity of the catalysts toward the same reaction types. The results are presented below in Table 22.

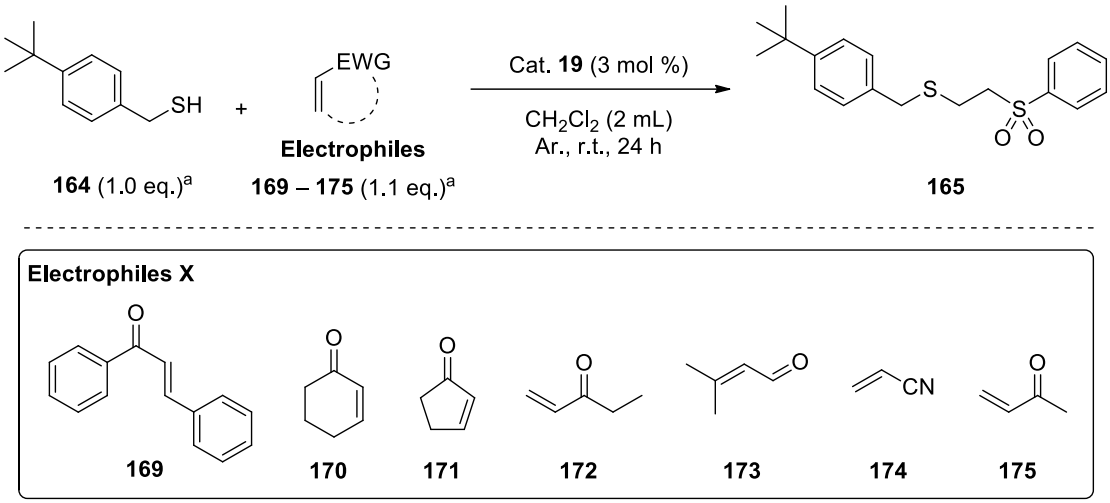

Table 22: Conversion obtained for the screening of various electrophiles.

Entry	Electrophiles	Conv. (%)
1	Blank	25
2	**169**	90
3	Blank	-
4	**170**	92
5	Blank	-
6	**171**	100
7	Blank	-
8	**172**	100
9	Blank	15
10	**173**	73
11	Blank	-
12	**174**	100
13	Blank	-
14	**175**	80

Overall, H_2OETPP **21** is capable of catalyzing Michael addition reaction with a broad range of electrophiles. The presence of the porphyrin as catalyst is required, however, **entry 1** and **9** showed a low conversion of 25 and 15%, respectively, without the presence of the porphyrin. Otherwise, very high conversion up to quantitative yields were noted for the various reactions screened.

5.5.7 Exploration toward potential new reactions

The use of porphyrins as catalysts for sulfa-Michael addition reactions, even with various electrophiles, proved to be successful. Consequently, other types of reactions were investigated in order to extend the scope of the porphyrin as a catalyst. To start, two reactions were chosen: Diels-Alder additions and aldol reactions.

5.5.7.1 Diels-Alder addition reactions

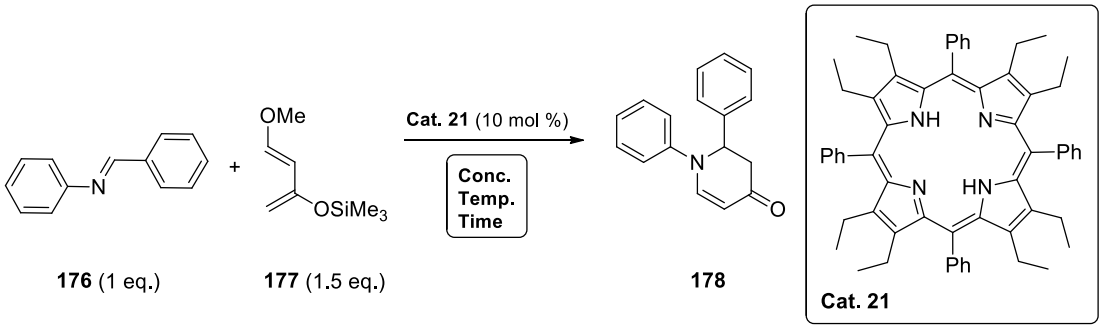

176 (1 eq.) **177** (1.5 eq.) **178**

Table 23: Investigation of various conditions for the Diels-Alder reactions using catalyst **21** as catalyst**.**

Entry	Solvents	C_{172} (mol.L^{-1})	Temp. (°C)	Time	Conv.(%)
Blank 1	CH_2Cl_2	0.05	0	3 h	-
1	CH_2Cl_2	0.05	0	3 h	-
Blank 2	CH_2Cl_2	0.05		3 h	-
2	CH_2Cl_2	0.05	rt	3 h	-
Blank 3	CH_2Cl_2	0.5	rt	3 h	-
3	CH_2Cl_2	0.5	rt	3 h	-
Blank 4	CH_2Cl_2	0.5	40	3 h	-
4	CH_2Cl_2	0.5	40	3 h	-
Blank 5	$CHCl_3$	0.5	rt	24 h	-
5	$CHCl_3$	0.5	rt	24 h	-
Blank 6	$CHCl_3$	0.5	70	24 h	-
6	$CHCl_3$	0.5	70	24 h	-
Blank 7	MeCN	0.5	rt	24 h	-
7	MeCN	0.5	rt	24 h	-
Blank 8	MeCN	0.5	82	24 h	-
8	MeCN	0.5	82	24 h	-
Blank 9	Isopropanol	0.5	rt	24 h	-
9	Isopropanol	0.5	rt	24 h	-
Blank 10	Isopropanol	0.5	82	24 h	-
10	Isopropanol	0.5	82	24 h	-

No positive results were obtained for the Diels-Alder addition reactions in standard conditions (**entry 1**). Changes of the reaction conditions showed that an increase in

temperature, longer reaction time or a more concentrated solution did not lead to conversion.

5.5.7.2 Aldol reactions

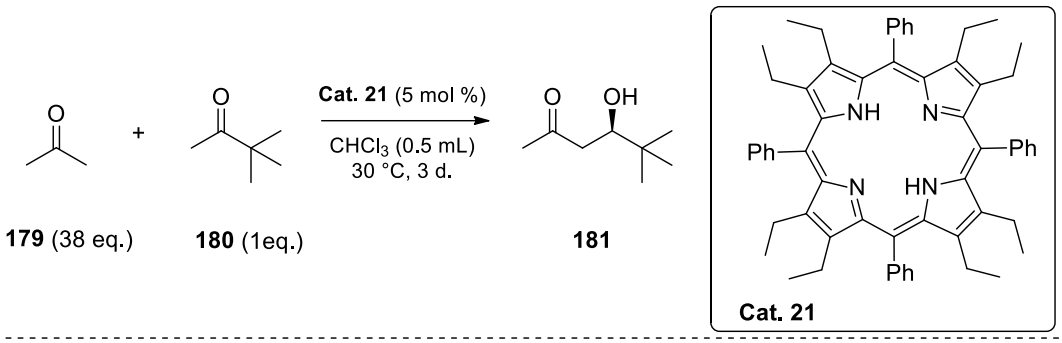

Table 24: Investigation of various conditions for the aldol reactions using porphyrin **19** as catalyst.

Entry	Solvent	Temp. (°C)	Reaction time	Conv. (%)
Blank	$CHCl_3$	30	3 d.	-
1	$CHCl_3$	30	3 d.	-

No conversion was observed using H_2OETPP **21** as a catalyst for an Aldol reaction.

5.5.8 Observation and conclusion part one

Porphyrin **26m** displays catalytic activity for reactions between thiols and Michael acceptors such as vinyl phenyl sulfone **160**. Optimization of the reaction conditions using **26m** resulted in a moderate conversion of 50% yield, which was a very suitable reference to compare a broad range of new porphyrin catalysts.

The screening of various porphyrins showed that distortion is the main requirement for the catalytic activity of porphyrins (*e.g.*, H_2TPP/H_2OEP *vs.* H_2OETPP). The planar conformation of compounds **26** and **120** does not allow for the availability of the inner functional units. In contrast, distorted porphyrins such as *N*-substituted compounds or highly substituted porphyrins showed moderate (**26m**, 50%) to excellent activity (**21**, quantitative) in concentrated conditions.

The H_2OETPP **21** and its various degrees of *N*-substitution **21m**, **21d** and **[21tt]$^{2+}$**, showed that the addition of one or more methyl groups into the core of porphyrins decreased the efficiency of the catalyst. Similar results were also noted upon using compounds **26m**, **26d** and **[26t]$^{+}$**, which show conversion of 50%, 20% and 0%, respectively. This suggests that the pyrrolic protons are greatly involved in the catalytic process. However, these results are slightly different for the H_2Cl_4TPP derivatives **108m** and **[108d]$^{+}$**; the conversion is higher after addition of two methyl groups (3% to 100%).

This is due to the substitution happening on N22 rather than N23, allowing one pyrrole unit (N23) to remain unsubstituted. This results in the highest distortion and better availability of the free pyrrole unit. Furthermore, the positive charge on N22 might help with the pre-assembly of the Michael acceptor and the nucleophile. This result led to the conclusion that the availability of both *N*-H and N units are a second requirement for the efficiency of a porphyrinic catalyst.

Moreover, the electronic properties of the porphyrins have an important impact on the conversion. The presence of electron withdrawing groups such as in **166** completely inactivates the activity of the porphyrin as catalyst in comparison to **21** despite their similar distortion. A possible explanation could be that electron withdrawing groups decrease the pK_a and inhibit the activity of imine groups, resulting in less activation of the nucleophile, while increasing the activity of the amine groups toward the electrophile. This hypothesis is reinforced by the NMR proton signals observed between the electrophile **160** and porphyrin **166**. Same results are observed between porphyrin **26m**, which gave a conversion of 50% and porphyrin **108m**, which gave only 3% conversion. In an opposite manner, the addition of electron donating groups on the peripheral aryl units, such as in porphyrin **112m**, results in a higher conversion than **108m** (3% *vs.* 62%, respectively) for which 11m also gave a better conversion than **26m** (50%). These results support the idea that a macrocycle with high electron density is a third major necessity for a good catalytic activity.

To finish, a mechanistical hypothesis was proposed in order to understand the catalytic process with porphyrins and is presented in Fig. 68.

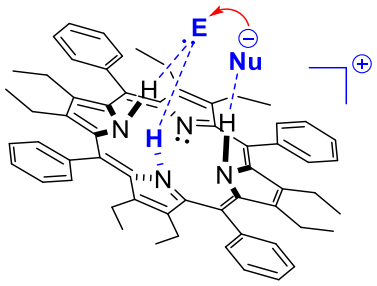

Figure 68: Schematic representation of the specific catalysis-like mechanism using porphyrins.

The results obtained so far strongly support a specific catalysis-like mechanism in which the porphyrin-thiolate ion-pair is catalytically relevant. In order for the thiol and porphyrin to react successfully, there must be one inner NH unit available. In the addition of the thiol to the porphyrin core, the thiol (RSH) protonates one of the imine nitrogens and the resulting thiolate anion (RS-) binds to one of the NH-units. The incoming electrophile is

then able to bind through two adjacent NH units, where one is from a pyrrolic nitrogen and the other from a protonated imine nitrogen. It is this specific binding motif that enables the catalysis to occur and thus it can be concluded that the catalytic system using porphyrins is bifunctional. Moreover, based on the NMR data (Fig. 65), it is most likely that the monoprotonated species is the dominant catalyst in solution.

In summary, free base highly distorted porphyrins bearing no electron withdrawing groups such as **21** present the best catalytic activity. Studies on the basicities showed that H_2OETPP **21** is capable of basicity exceeding standard amines such as DMAP and NEt_3. Consequently, it is clear that the distortion of the macrocycle increases the basic character of porphyrins. Taking into account the fact that porphyrins can be easily modified through substituent manipulation and variation, it is possible to fine-tune their electronic properties. This could eventually increase the basicity of the porphyrin to the extent that these are stronger than typical organic bases in use.

To prove and understand the concept of activation, further investigations are needed. It is clear from the first panel of porphyrins screened that the electron density and the distortion of the macrocycle are requirements for a good activity of the porphyrin. H_2OETPP **21** is a well-established highly distorted porphyrin; however, it is still possible to improve the potential of this structure by increasing the electron density (*e.g.*, the influence of electron donating aryl groups in the meso-positions). In addition, the distortion can also be modulated. One example would be the replacement of the ethyl groups present in H_2OETPP by longer or more bulkier chains (*e.g.*, butyl, isopropyl, etc.) which can enhance the distortion further.

5.5.9 Screening of nonplanar electron-rich porphyrins.

5.5.9.1 Synthetic strategy

So far, the most efficient porphyrin catalyst is H_2OETPP. The studies of various structures showed that the distortion and electron-rich character of the macrocycles are the main requirements for using free base porphyrins as organocatalysts. This part focused on the fine-tuning of the electronic properties of the macrocycle only. In addition, this project was a collaboration with M. Kielmann who examined the catalytic efficiency of a series of porphyrins with a graded degree of *β*-ethyl substituents (*e.g.*, EtxTPP series, part 1),[240] and also studied the impact on more hindered *β*-residues such as isopropyl, phenyl, isobutyl, etc. (Fig. 69, **183**).[241]

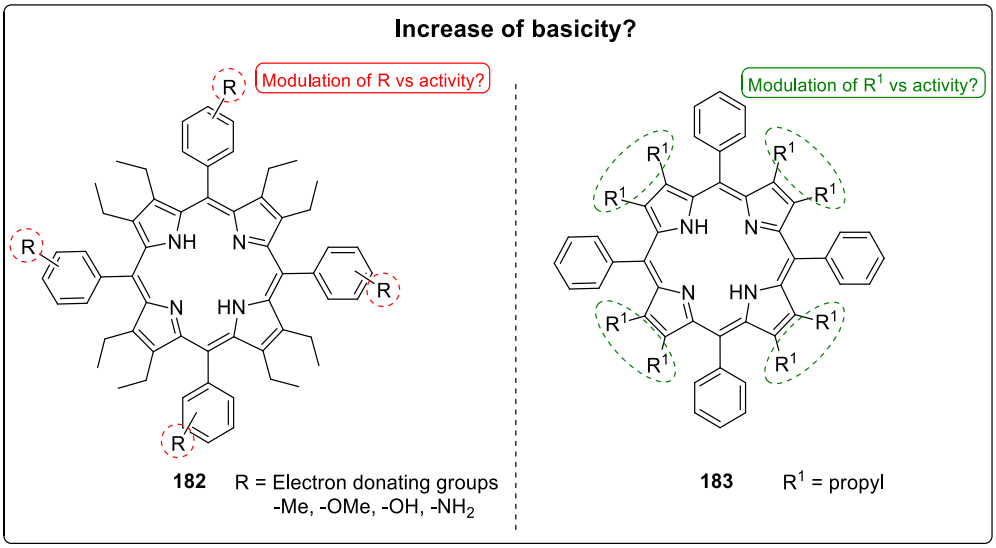

Figure 69: Effect of meso-substitution versus *β*-substitution on the catalytic process.

Herein, the effect of the fine-tuning of the electronic properties of the macrocycle (Fig. 68, **182**) will be investigated using porphyrins **46**–**49** and **51,** synthesized in part 3.

5.5.9.2 Screening of synthesized porphyrins

Similarly to the previous part, all porphyrins were screened using the optimized conditions of the Michael addition reaction in diluted conditions. This allows for a comparison with the results obtained for the conversion using H_2OETPP **21** (80%) which is so far the best conversion obtained. The results are presented in Table 25.

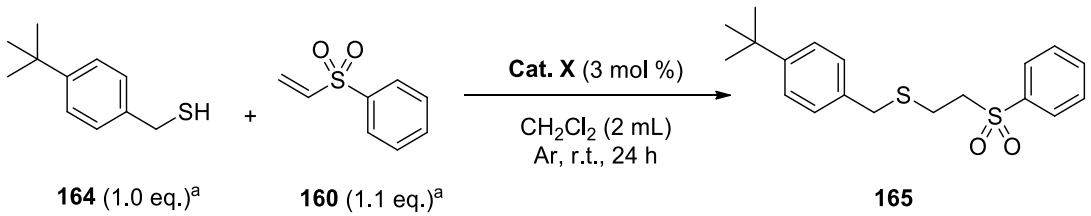

164 (1.0 eq.)[a] **160** (1.1 eq.)[a] **165**

Table 25: Yields obtained for electron-rich macrocycles.

Entry	Catalyst	*Δ24* [Å][a]	*λmax* [nm][b]	#NH	Yield (%)
1	-	n/a	n/a	n/a	0
2	**21**[20a]	0.54[20b]	456, 555	2	80
3	**47**	–	454, 703	2	92
4	**48**	0.78[c]	463, 689	2	0
5	**49**	–	472, 697	2	55
6	**51**	–	458, 706	2	0
7	**55**	0.82	458, 707	2	0

[a] *Δ24* = Average deviation of the 24-macrocycle atoms from their least-squares plane as a measure of overall degree of nonplanarity in the solid state. [b] λ_{max} = Soret and long wavelength Q absorption bands in CH_2Cl_2 (+ 1% NEt_3) as a measure of macrocycle distortion in solution.[1,44,74] [c] Values from poor data, only reported to speculate on the results obtained.

As expected, the addition of methoxy substituents to the *p*-position of the phenyl group (porphyrin **47**) increased the conversion obtained for the reaction (from 80% with **7** to 92% with **47** in diluted conditions). The results observed for porphyrin **48** are quite surprising at first. Indeed, it was expected that porphyrin **48** would give better results than porphyrin **21** or **47,** due to a higher electron density of the macrocycle, yet, no conversion was noted. Similar results were obtained for porphyrin **51** which should be even more electron-rich. The last compound was porphyrin **49**, once again the results were unexpected as this porphyrin had more electron donating groups than porphyrin **43** and still gave 55% conversion. Moreover, it technically had a similar structure to porphyrin **49** and should give similar conversions.

The results obtained for porphyrins **48** and **55** were rationalized by the high basicity of the macrocycles. While H_2OETPP **21** was capable of basicities exceeding NEt_3, here the electronic modulation of the peripheral substituents enhanced the basic character of the macrocycle even more. Consequently, some limitations were encountered such as the inactivation of the catalytic efficiency of the porphyrin. The optimization of the Michael addition conditions showed that the best conversion for the screening of the porphyrin was obtained in CH_2Cl_2 and the use of any other solvents led to a loss of catalytic activity. However, CH_2Cl_2 is well known to hydrolyze and generate a slightly acidic media. This loss in activity of the porphyrin catalyst can be correlated to the rapid protonation of the porphyrin given the acidity present in solution, thus forming the inactive dicationic species of porphyrins **48** and **55**. This argument is supported by Fig. 70 which shows the facile protonation of porphyrin **48** in CH_2Cl_2.

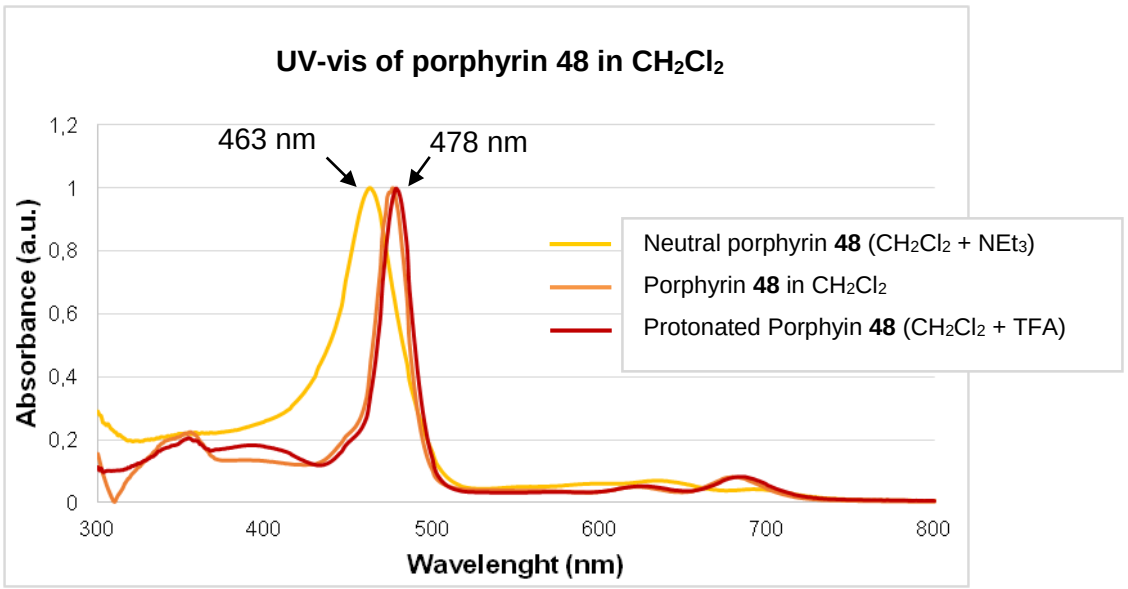

Figure 70: UV-vis of porphyrin **48** in CH_2Cl_2 with NEt_3 (yellow line, neutral form), in CH_2Cl_2 (orange line) and in CH_2Cl_2 with TFA (red line, protonated form).

In Fig 70, the neutral form of porphyrin **48** (Fig. 70, yellow spectrum) showed a Soret band at 463 nm. The spectrum associated with the porphyrin dissolved in CH_2Cl_2 (Fig. 70, orange spectrum) displayed an absorption value for the Soret band at 478 nm. Upon addition of TFA to CH_2Cl_2, the porphyrin is protonated forming the dicationic species (Fig. 70, red spectrum). This species showed comparable values of Soret band to the one observed for porphyrin **48** when dissolved in acidic CH_2Cl_2 (Fig. 70, orange spectrum). A comparative study of the three spectra clearly showed that the distorted porphyrin is highly basic, and thus was protonated by trace acidic impurities in CH_2Cl_2. Upon addition of TEA (Fig. 70, yellow spectrum), the porphyrin reverted back to its neutral form.

Similar examinations were carried out with porphyrin **49**. This porphyrin is more basic than **48,** due to the additional methoxy group on the *p*-position of each meso-aryl group, though it showed only moderate catalytic activity. Consequently, the behavior of **49** was studied by UV-vis in basic CH_2Cl_2, CH_2Cl_2 only, and acidic CH_2Cl_2.

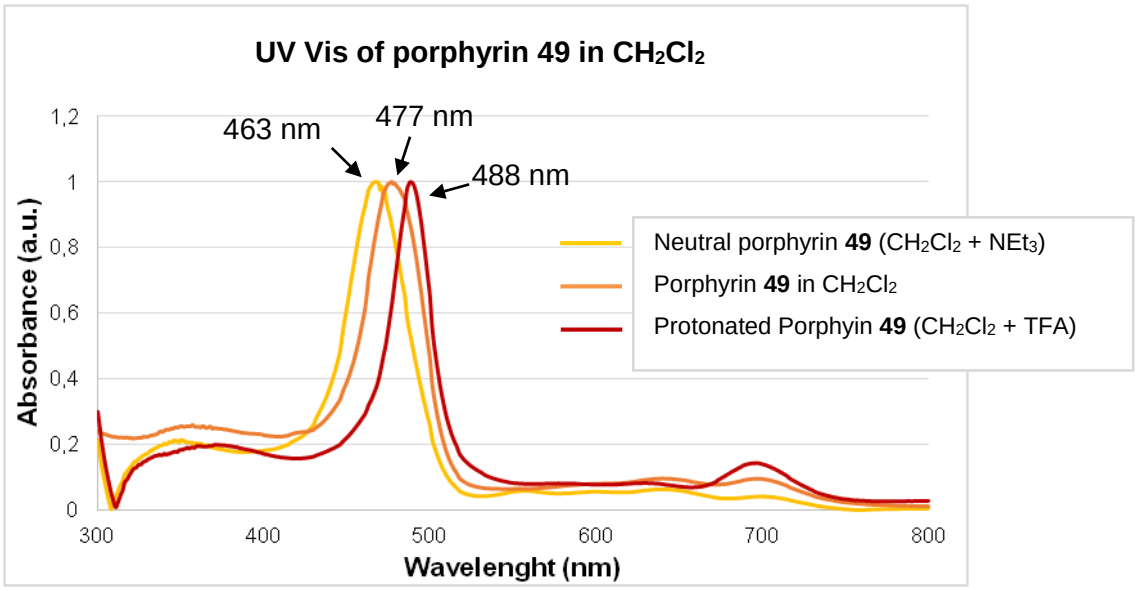

Figure 71: UV-vis of porphyrin **49** in CH_2Cl_2 with NEt_3 (yellow spectra, neutral form) and in CH_2Cl_2 (orange spectra, mono-protonated form) and in CH_2Cl_2 with TFA (red spectra, di-protonated form).

In the presence of base in CH_2Cl_2, the neutral form of the porphyrin is observed with a B band at 467 nm (Fig. 71, yellow spectra). In the presence of acid, the diprotonated form is present with a Soret band at 488 nm (Fig. 71, red spectra). When porphyrin **49** is then dissolved in CH_2Cl_2, a bathochromic shift of 14 nm of the Soret band is observed (Fig. 71, orange spectra). Consequently, it was assumed that upon dissolution of porphyrin **49** in CH_2Cl_2, the monoprotonated species is generated, as opposed to the diprotonated

species formed with porphyrin **48**. Porphyrin **49** contains one additional methoxy at the *p*-position of the meso-aryl residues compared to porphyrin **48** which results in a higher electron density, *i.e.*, higher basicity, of its macrocycle. Thus, porphyrin **49** was expected to form the dicationic species in CH_2Cl_2 similar to porphyrin **48**. This difference can be rationalized by the extra *p*-methoxy substituents on the meso-aryl groups of the porphyrin **49**. Due to the position of the methoxy in *o*-position generating a steric hindrance with the *β*-ethyl substituents. The orientation of the phenyl group changed with respect to the porphyrin plane. This potentially causes modifications in the electronic nature of the porphyrin **49** (*o*-substituted) *i.e.*, change in catalytic activity.

From these studies, it is clear that incorporation of electron donating units leads to an increase of the electron density, resulting in a higher basicity of the porphyrin. However, this high basicity imparts limitations on the catalytic activity. The porphyrins become too basic to be used in protic or slightly protic solvents such as CH_2Cl_2 due to the acid formed by the solvent. Optimizations of the solvents used were attempted, although were unsuccessful. Moreover, when CH_2Cl_2 was neutralized with K_2CO_3 before the catalytic screening of porphyrin **48**, no conversion was observed. Further investigations are required to understand the reason behind this loss of activity, however, initial results reveal that these results could be explained by the porphyrin conformation and the position in space of the *ortho*-methoxy residues.

The last porphyrin screened (**entry 7**, Table 25) was tested to study the effect of the *β*-substituents on the electronic properties of the porphyrin. A tetraphenylporphyrin with propyl groups at the *β*-positions (compound **55**), instead of ethyl groups, was subsequently synthesized (see 3.2.2.2). As mentioned in part 3.2.3.3, a similar distortion (Fig. 72) is observed between porphyrin **55**·$2CH_3CO_2H$ and porphyrin **21**·2TFA with *Δ*24 of 0.82 and 0.84, respectively.[58b] No conversion was obtained with porphyrin **55**. As shown in Fig 71, its distortion is similar to porphyrin **21** which gave one of the highest conversions recorded. The absence of conversion can be explained by the presence of the *β*-propyl groups given that they are more donating than the *β*-ethyl groups of porphyrin **21**.

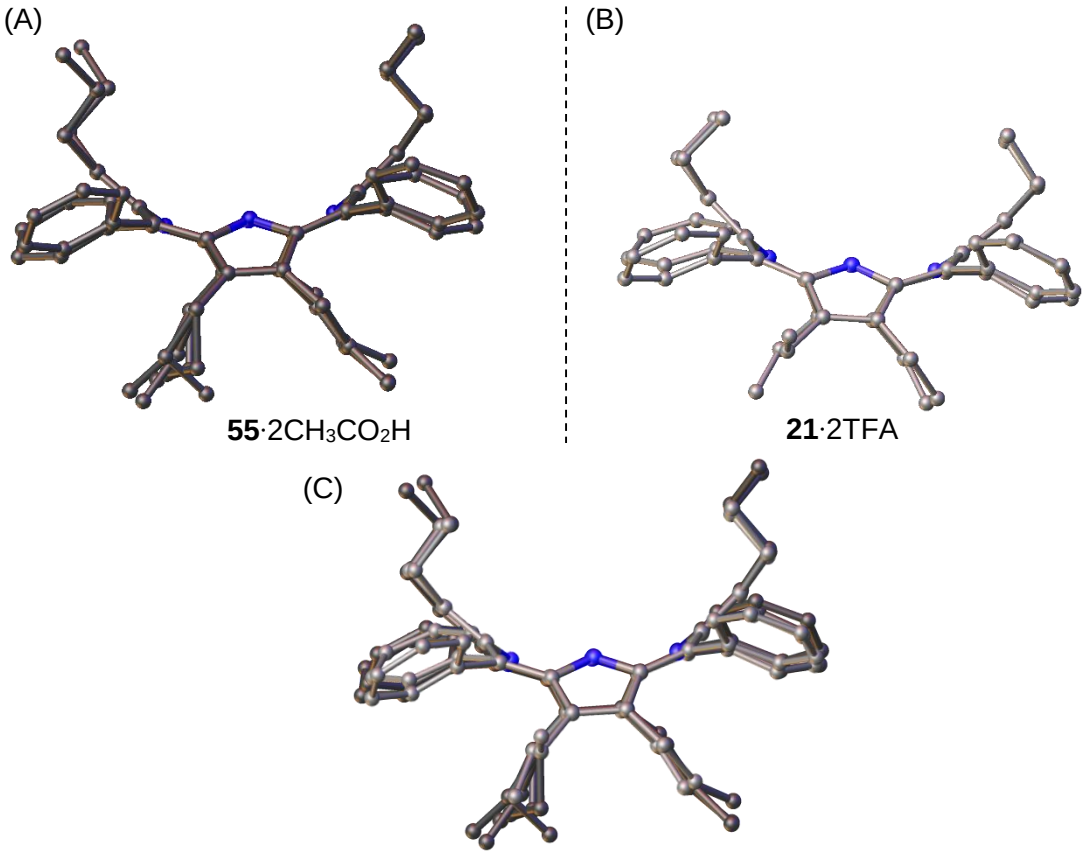

Figure 72: Comparison of the molecular view of the X-ray crystal structure of porphyrin **55**·2CH_3CO_2H (A) and **21**·2TFA (B). An overlay of both structure of the same size has been added for a better comparison (C). Hydrogen atoms and counter anions have been omitted for clarity.

Thus, the basicity of compounds **55** exceed the one observed in porphyrin **21** due to a higher electron density of the macrocycle. This high basicity results in the fast protonation of the inner imine units due to the acidic impurities of the CH_2Cl_2 (see Fig. 27) and thus a loss in the catalytic activity.

5.6 Observations and conclusion

It appeared that the initial hypothesis of the possible control of the basicity using either the tuning of the properties *via* addition of electron donating units or the modification of the distortion *via* the tuning of the *β*-position has been validated. It can be seen that upon insertion of a methoxy group, the conversion is increased from 80% (H_2OETPP **21**) to 92% (compound **47**). Upon addition of a second methoxy unit, the basicity became remarkably high and resulted in the loss of catalytic activity, due to instant diprotonation by the solvent. It can also be hypothesized that porphyrin **48**, did not lead to any conversion due to its distortion. The addition of the two methoxy groups in the *ortho*-positions results in a steric clash with the ethyl groups in the *β*-positions, leading to more enhanced distortion of the macrocycle (Δ24 = 0.78, Fig. 73).

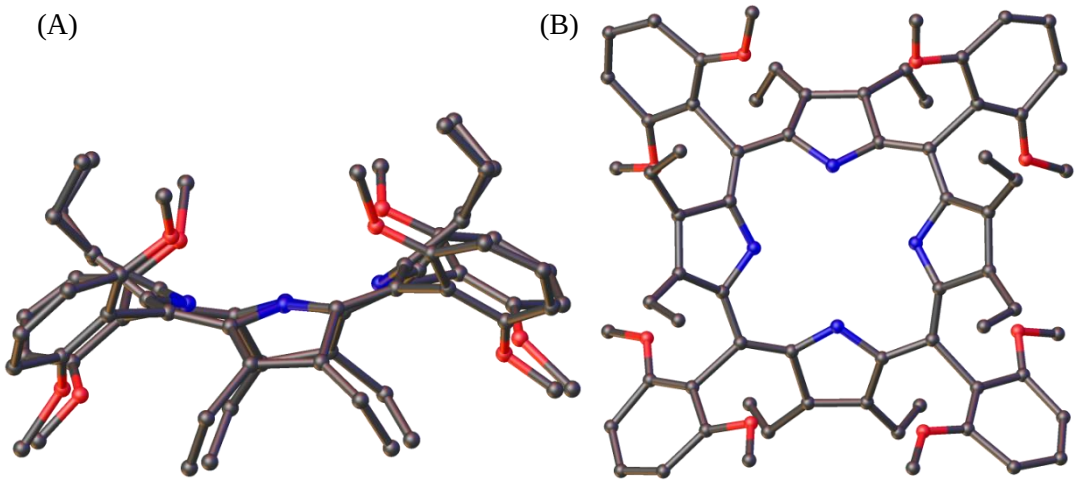

Figure 73: View of the molecular X-ray crystal structure of compound **48** (side view (A) and front view (b)). All the hydrogen atoms have been omitted for clarity.[2]

The results of this chapter opened a new and exciting avenue in both fields of porphyrin and organocatalysis. For the first time, free base and *N*-methylated porphyrins have been utilized as bifunctional organocatalysts in Michael additions. Distortion of the macrocycle has proven to be a vital prerequisite for the catalytic activity of porphyrins. Moreover, in a similar manner than that observed for natural tetrapyrrole-protein systems, conformational design was used to tailor the properties of the nonplanar porphyrins with regards to the availability of the NH units for hydrogen bonding and the basicity of the heterocyclic groups (*e.g.*, H_2OETPP **21** *vs.* catalyst **47**).

Consequently, it is clear to see that this project is only the foundation into the use of porphyrins as catalysts. The principles explained and outlined have already started to be implemented to other porphyrinoids such as porphyrinogens.[242] In addition, these tetrapyrrole molecules represent an ideal platform for catalysis due to the facile modulation of their structure, conformation and properties. A recent publication[59] from Norvaiša *et al.* showed the possibilities of using functional units as peripheral substituents in addition to distortion to achieve reversible anion-binding receptors. Using this principle, it is conceivable that similar platforms would be very useful for binding small molecules in specific arrangements and to reach enantioselective asymmetric catalysis.

[2] **This structure has not been properly solved as the crystal formed did not allow for a good diffraction, though the structure obtained is only here to support the comment stated in the main text.**

6 Experimental

General information: Sensitive: Reactions employing sensitive compounds were performed under 'Schlenk' conditions using argon as an inert gas to protect the corresponding compounds from air and moisture. A hot air gun under high vacuum followed by the purge of the flasks with argon were utilized to remove air and residual moisture from the instruments. This cycle was repeated up to three times as necessary. Air sensitive thiols were stored under argon at RT to prevent oxidation.[111] In some NMR spectra of the new 2,3,7,8,12,13,17,18-octaethyl-5,10,15,20-tetraarylporphyrins, the signals corresponding to the *β*-ethyl groups are broad. This is in accordance with conformational studies by Medforth *et al.* on decaalkylporphyrins.[243] Presumably, the highly substituted porphyrins exist as a mixture of atropisomers in the solution, causing signal broadening due to different interactions between *β*-ethyl groups and meso-substituents. Besides, broad range of melting points are observed for the same series of compounds and can be explained by the presence of residual solvent and the formation of supramolecular interactions between porphyrins and solvent molecules. Saddle shaped porphyrins are known to form cavities due to the distortion of their macrocycle. These cavities easily encapsulate solvent molecules stabilizing the whole complex *via* non-covalent interactions, resulting in the presence of solvents even in the solid state. Therefore, the broad range of melting points is a result of the breaking of these interactions, removal of the solvent molecules, and the melting of the porphyrin itself.

Materials: General chemicals were purchased from industrial suppliers and were used without further purification unless otherwise noted. Anhydrous DCM was obtained *via* distillation over phosphorus pentoxide and distillation. All starting materials and precursors such as porphyrins **26**,[13] **120**,[112] **154**[244],**21**,[54b] **77**,[245] **107**,[154] **165**,[238] **46**,[234] **22**,[127] **120m**,[125b,236] **[26t]+**,[58,131] **21m**,[95] **23**,[95] **[21tt]$^{2+}$**,[231] **74**,[232] **108m**,[96] **112m**,[96] **26d**,[232,233] [**108d]$^{+}$**,[96] **110**–**114**,[16] **115**–**117**,[155] as well as 3,4-diethylpyrrole **24**,[101–103] or 3,4-dipropylpyrrole **35**[104] and their respective starting materials **57**–**63**,[101–103] **64**,[104] **65**,[104] and **66**–**69**.[104] have been synthesized according to the literature and all known porphyrins had analytical data consistent with those reported in the corresponding literature.

Analytical Techniques: Analytical TLC was performed using sheets precoated with silica gel to a depth of 0.2 mm or aluminum oxide plates, both impregnated with fluorescence indicator F_{254}. Visualization was accomplished with a UV lamp. Flash

column chromatography was carried out using silica gel 60 (230–400 mesh) or aluminum oxide (neutral, activated with 6% H_2O, Brockman Grade III). Mass spectrometry analysis was performed with a Q-Tof Premier Waters MALDI quadrupole time-of-flight (Q-TOF) mass spectrometer equipped with Z-spray electrospray ionization (ESI) and matrix-assisted laser desorption ionization (MALDI) sources either in a positive or negative mode with DCTB (*trans*-2-[3-(4-*tert*-butylphenyl)-2-methyl-2-propenylidene]malononitrile) as the matrix. APCI experiments were performed on a Bruker microTOF-Q III spectrometer interfaced to a Dionex UltiMate 3000 LC. UV-vis absorption measurements were performed in DCM, DCM + 1% TEA, or toluene as solvent using a Shimadzu MultiSpec-1501. Melting points are uncorrected and were measured with a Stuart SMP-50 melting point apparatus. ^{1}H, ^{13}C NMR spectra were recorded at 400.13 MHz, 100.61 MHz and 376.59 MHz using Bruker DPX400, Bruker AV 600, and Bruker AV 400 devices, respectively. All NMR experiments were performed at 25 °C. Resonances δ are given in ppm units and referenced to the deuterium peak in the NMR solvent $CDCl_3$ (δ_H = 7.26 ppm, δ_C = 77.2 ppm). Signal multiplicities are abbreviated as follows: singlet = s, doublet = d, quartet = q, septet = sept, multiplet = m. Photophysical measurements were carried out in DCM or toluene as solvent. IR spectra were recorded on a PerkinElmer Spectrum 100 FTIR spectrometer utilizing the ATR sampling technique.

6.1 Synthesis of free base porphyrins

6.1.1 Highly substituted porphyrins

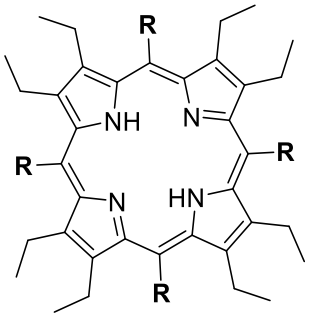

R = 2,6-di-OMe-C_6H_3

5,10,15,20-tetrakis(2,6-dimethoxyphenyl)-2,3,7,8,12,13,17,18-octaethylporphyrin 48:

3,4-Diethylpyrrole **24** (1 mL, 0.00812 moles, 1 eq.) and aldehyde **37** (1.21 g, 0.00731 moles, 0.9 eq.) were dissolved in dry CH_2Cl_2 (1 L). BF_3OEt_2 (0.1 mL, 0.000812 moles, 0.1 eq.) was added and the solution was stirred for 36 h at room temperature under argon. The reaction was monitored by TLC, then DDQ (1.84 g, 0.00812 moles, 1 eq.) was added and the reaction was stirred for 16 h. The reaction was stopped and filtered through a silica plug using CH_2Cl_2 to remove the unreacted aldehyde. The compound was then removed from the silica using CH_2Cl_2/MeOH (9:1) and gave a compound **48** as a green powder (1.352 g, 0.00128 moles, 70%) upon evaporation of the solvent under reduced pressure. M.p. < 149–175 °C; R_f = 0.60 (SiO_2, CH_2Cl_2:MeOH = 9:1, v/v); ^{1}H NMR (600 MHz, $CDCl_3$, 25 °C): δ = 0.28 (broad s, 24H, CH_2CH_3), 2.23 (broad s, 8H, CH_2CH_3), 2.46 (broad s, 8H, CH_2CH_3), 3.89 (s, 24H, *o*-OCH_3), 6.89-6.91 (d, J = 8.3 Hz 8H, H_{aryl}), 7.66-7.68 ppm (t, J = 8.2 Hz, 4H, H_{aryl}); ^{13}C NMR (100 MHz, $CDCl_3$, 25 °C): δ = 160.9, 143.5, 136.9, 132.6, 116.3, 107.2, 104.3, 56.0, 18.4, 14.3 ppm; UV-vis ($CHCl_3$ + 1% NEt_3): λ_{max} (log ε) = 389 (4.30), 464 (4.81), 599 (3.64), 632 (3.72), 689 nm (3.57); IR (ATR): $\tilde{\nu}$ = 3206, 2935, 2833, 2219, 1579, 1472, 1451, 1252, 1107, 1018, 888, 775, 743, 715 cm^{-1}; HRMS (MALDI) *m/z* calcd. for $C_{68}H_{78}N_4O_8$ $[M^+H]^+$: 1079.5892, found 1079.5898.

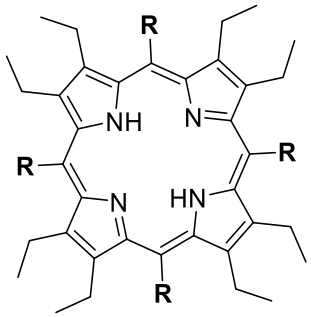

R = 2,4,6-tri-OMe-C_6H_3

5,10,15,20-tetrakis(2,4,6-trimethoxyphenyl)-2,3,7,8,12,13,17,18-octaethylporphyrin 49:

3,4-Diethylpyrrole **24** (1 mL, 0.00812 moles, 1 eq.) and aldehyde **40** (1.43 g, 0.00731 moles, 0.9 eq.) were dissolved in dry CH_2Cl_2 (1 L). BF_3OEt_2 (0.1 mL, 0.000812 moles, 0.1 eq.) was added and the solution was stirred for 36 h at room temperature under argon. The reaction was monitored by TLC, then *p*-chloranil (1.84 g, 0.00812 moles, 1 eq.) was added and the reaction was stirred for 3 d. The reaction was stopped and filtered through a silica plug using CH_2Cl_2 to remove the unreacted aldehyde. The compound was then removed from the silica using CH_2Cl_2/MeOH (9:1) and gave a green powder, compound **49** (0.217 g, 0.000181 moles, 10 %), upon evaporation of the solvent under reduced pressure. M.p. = 186–199 °C; R_f = 0.58 (SiO_2, CH_2Cl_2:MeOH = 9:1, v/v); ^{1}H NMR (600 MHz, $CDCl_3$, 25 °C): δ = 0.44 (broad s, 24H, CH_2CH_3), 2.32 (broad s, 8H, CH_2CH_3), 2.48 (broad s, 8H, CH_2CH_3), 3.79 (s, 24H, *o*-OCH_3), 4.06 (s, 12H, *o*-OCH_3), 6.47 ppm (s, 8H, H_{aryl}), ^{13}C NMR (100 MHz, $CDCl_3$, 25 °C): δ = 163.7, 161.6, 144.8, 11.1, 106.3, 91.0, 56.1, 55.8, 18.5, 15.3, 14.3 ppm; UV-vis ($CHCl_3$ + 1% NEt_3): λ_{max} (log ε) = 353 (4.11), 472 (4.84), 598 (3.62), 640 (3.73), 697 nm (3.64); IR (ATR): $\tilde{\nu}$ = 2933, 2830, 2202, 1599, 1578, 1453, 1412, 1331, 1224, 1204, 1154, 1123, 1123, 1056, 1033, 951, 812 cm^{-1}; HRMS (MALDI) *m/z* calcd. for $C_{72}H_{86}N_4O_{12}$ $[M^+H]^+$: 1199.6315, found 1199.6305.

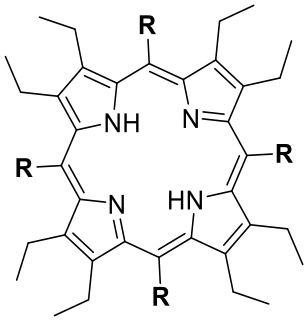

R = 3,5-di-Me-4-OMe-C_6H_2

5,10,15,20-tetrakis(3,5-dimethyl-6-methoxyphenyl)-2,3,7,8,12,13,17,18-octaethylporphyrin 51:

3,4-Diethylpyrrole **24** (0.833 mL, 0.00677 moles, 1 eq.) and aldehyde **42** (1.00 g, 0.00609 moles, 0.9 eq.) were dissolved in dry CH_2Cl_2 (1 L). BF_3OEt_2 (0.83 mL, 0.000677 moles, 0.1 eq.) was added and the solution was stirred for 36 h at room temperature under argon. The reaction was monitored by TLC, then DDQ (1.54 g, 0.00677 moles, 1 eq.) was added and the reaction was stirred for 3 d. The reaction was stopped and filtered through a silica plug using CH_2Cl_2 to remove first the unreacted aldehyde. The compound was purified by two successive silica columns using CH_2Cl_2 to remove the aldehyde and CH_2Cl_2/MeOH (9:1). After evaporation of the solvent under reduced pressure compound **51** was obtained as a green powder (0.9431 g, 0.0008802 moles, 52%). M.p. = 259–269 °C; R_f = 0.64 (SiO_2, CH_2Cl_2:MeOH:NEt_3 = 9:1:1, v/v); ^{1}H NMR (600 MHz, $CDCl_3$, 25 °C): δ = -1.22 (s, 2H, N*H*$_2$), 0.08 (m, 12H, CH_2*CH*$_3$), 0.45 (m, 12H, CH_2*CH*$_3$), 2.24 (m, 16H, *CH*$_2$$CH_3$), 2.64-2.66 (d, *J* = 6.7 Hz, 24H, *m*-CH_3), 4.01 (s, 12H, *p*-OCH_3), 8.15 (s, 4H, H_{aryl}) 8.18 ppm (s, 4H, H_{aryl}); ^{13}C NMR (100 MHz, $CDCl_3$, 25 °C): δ = 159.3, 144.2, 143.4, 143.1, 137.6, 137.3, 133.6, 131.1, 130.8, 129.5, 60.6, 16.7, 16.6, 15.3, 14.9 ppm; UV-vis (CH_2Cl_2 + 1% NEt_3): λ_{max} (log ε) = 348 (4.48), 458 (5.37), 556 (4.13), 604 (4.04), 706 nm (3.85); IR (ATR): $\tilde{\nu}$ = 3263, 2970, 2932, 2873, 2208, 1648, 1595, 1515, 1443, 1409, 1375, 1310, 1289, 1230, 1184, 1158, 1107, 1052, 1003, 951, 887, 825, 786, 762, 691, 624, 584 cm^{-1}; HRMS (MALDI) *m/z* calcd. for $C_{72}H_{86}N_4O_4$ $[M^+H]^+$: 1071.6722, found 1071.6715.

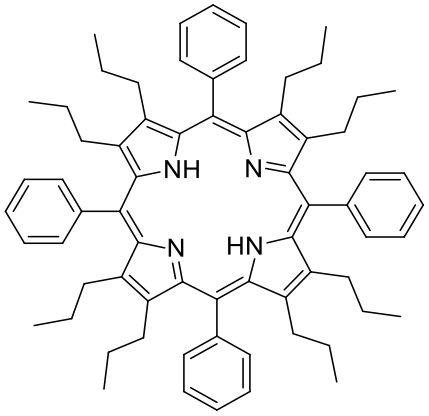

2,3,7,8,12,13,17,18-octapropyl-5,10,15,20-tetraphenylporphyrin 55 and 22,24-dihydro-2,3,7,8,12,13,17,18-octapropyl-5,10,15,20-tetraphenylporphyrin acetate salt 55·2Cl:

3,4-Dipropylpyrrole **36** (0.675 mL, 0.00446 moles, 1 eq.) and aldehyde **25** (0.476 mL, 0.00469 moles, 1.05 eq.) were dissolved in dry CH_2Cl_2 (1 L). BF_3OEt_2 (0.55 mL, 0.000446 moles, 0.1 eq.) was added and the solution was stirred for 24 h at room temperature under argon. The reaction was monitored by TLC, then DDQ (1.01 g, 0.00446 moles, 1 eq.) was added and the reaction was stirred for 16 h. The reaction was stopped and filtered through a silica plug using CH_2Cl_2 to remove first the unreacted aldehyde. A TLC was done showing two green compounds. A column was attempted with CH_2Cl_2/Hexane, however a part of the compound crashed out leading to 137 mg (0.000144 moles, 13%) of a bright green salt of the protonated form of **55, 55**·2Cl. M.p. = 248–260 °C; R_f = 0.43 (SiO_2, $CHCl_3$:EtOAc = 9:1, v/v); ^{1}H NMR (600 MHz, $CDCl_3$, 25 °C): δ = -0.13 (Brd s, 12H, $CH_2CH_2\mathit{CH_3}$), 0.26 (Brd m, 12H, $CH_2CH_2\mathit{CH_3}$), 0.72-0.84 (Brd m, 8H, $CH_2\mathit{CH_2}CH_3$), 1.20-1.31 (Brd m, 12H, $\mathit{CH_2CH_2}CH_3$), 1.94 (Brd s, 8H, $\mathit{CH_2}CH_2CH_3$) 2.23 (Brd s, 4H, $\mathit{CH_2}CH_2CH_3$), 7.77 (Brd s, 8H, *m*-H_{aryl}), 7.83 (Brd s, 8H, *o*-H_{aryl}), 8.39 (Brd s, 2H, *p*-H_{aryl}), 8.45 ppm (Brd s, 2H, *p*-H_{aryl}); UV-vis (CH_2Cl_2 + 1% TFA): λ_{max} (log ε) = 404 (4.54), 470 (5.54), 629 (4.01), 686 nm (4.52); IR (ATR): $\tilde{\nu}$ = 3057, 2960, 2930, 2870, 2208, 1552, 1508, 1432, 1377, 1348, 1223, 1177, 1157, 1137, 1074, 1023, 999, 927, 888, 827, 801, 735, 724, 698 cm^{-1}; HRMS (MALDI) *m/z* calcd. for $C_{68}H_{78}N_4$ $[M^+H]^+$: 951.6299, found 951.6308. The rest was evaporated leading to 114.2 mg (0.00012 moles, 11%) of **55**. M.p. = 203–223 °C; R_f = 0.81 (SiO_2, $CHCl_3$:EtOAc = 9:1, v/v); ^{1}H NMR (600 MHz, $CDCl_3$, 25 °C): δ = 0.24 (Brd s, 24H, $CH_2CH_2\mathit{CH_3}$), 0.84 (Brd s, 16H, $CH_2\mathit{CH_2}CH_3$), 2.28 (Brd s, 8H, $\mathit{CH_2}CH_2CH_3$), 2.51 (Brd s, 8H, $\mathit{CH_2}CH_2CH_3$), 7.89 (Brd s, 12H, *p,o*-H_{aryl}), 8.65 ppm (Brd s, 8H, *m*-H_{aryl}), ^{13}C NMR (100 MHz, $CDCl_3$, 25 °C): δ = 150.4, 144, 3, 138.9, 138.3, 137.8, 136.1, 131.1, 129.6, 124.1, 28.7, 26.3, 15.8, 15.1 ppm; UV-vis ($CHCl_3$ + 1% NEt_3): λ_{max} (log ε) = 347 (4.21), 458 (5.01), 557 (3.84), 602

(3.67), 707 nm (3.34); IR (ATR): $\tilde{\nu}$ = 3055, 2956, 2927, 2867, 2210, 1980, 1694, 1596, 1549, 1465, 1463, 1443, 1376, 1346, 1260, 1176, 1136, 1087 1072, 1020, 1001, 971, 924, 890, 837, 801, 735, 697, 611 cm^{-1}; HRMS (MALDI) *m/z* calcd. for $C_{68}H_{78}N_4$ $[M^+H]^+$: 951.6299, found 951.6308.

6.2 *N*-Methylated porphyrins

6.2.1 *N*-Methylation of 5,10,15,20-tetraarylporphyrins

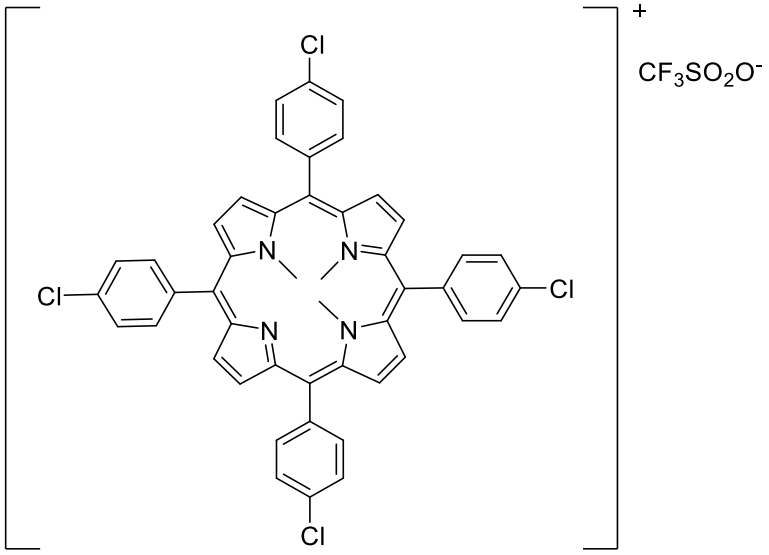

***N*^{21},*N*^{22},*N*^{23}-Trimethyl-5,10,15,20-tetrakis(*p*-chlorophenyl)porphyrin trifluoromethanesulfonate salt [106t]$^{+}$[CF_3SO_3]:**

In a 250 mL three-necked round-bottomed flask, 5,10,15,20-tetrakis(*p*-chlorophenyl)porphyrin H_2**106** (100 mg, 0.1333 mmol) and K_2CO_3 (1.4 g excess) were dissolved in 50 mL of CH_2Cl_2. The solution was heated to reflux, and CF_3SO_2OMe (0.291 mL, 2.66 mmol, 20 eq.) was added. After being heated to reflux for 16 h, the mixture was cooled to room temperature and K_2CO_3 was removed by filtration. The solvent was evaporated under reduced pressure and the product was subjected to column chromatography (SiO_2; CH_2Cl_2:EtOAc = 10:0–9:1, *v:v*) with the first fraction (purple) giving starting material and the second fraction (green) affording the desired compound. After the evaporation of solvent *in vacuo*, a green powder of the title compound was obtained (100 mg, 0.0321 mmol, 95%). M.p. = 280–285 °C; R_f = 0.21 (SiO_2, CH_2Cl_2:EtOAc = 1:1, *v:v*); ^{1}H NMR (400 MHz, $CDCl_3$, 25 °C): δ = -3.13 (s, 6H, *N*-CH_3), -5.55 (s, 3H, *N*-CH_3), 7.24 (m, 2H, $H_{\beta\text{-}}$), 7.46 (d, J = 4.6 Hz, 2H, $H_{\beta\text{-}}$), 7.95 (d, J = 7.6 Hz, 4H, H_{aryl}), 8.02 (d, J = 7.6 Hz, 4H, H_{aryl}), 8.21 (s, 2H, $H_{\beta\text{-}}$), 8.43 (s, 2H, $H_{\beta\text{-}}$), 8.52 (broad s, 4H, H_{aryl}), 8.71 ppm (broad s, 4H, H_{aryl}); ^{13}C NMR (100 MHz, $CDCl_3$, 25 °C): δ = 139.9, 138.9, 138.3, 137.9, 137.4, 134.2, 130.8, 130.8, 129.9, 129.8, 128.8, 123.9, 121.1, 121.1, 120.1, 120.1, 119.5, 31.3, 29.8 ppm; UV-vis ($CHCl_3$): λ_{max} (log ε) = 376 (4.70), 469 (5.42), 714 nm (4.69); IR (ATR): $\tilde{\nu}$ = 2955, 1583, 1449, 1395, 1259, 1220, 1148, 1089, 1027, 1009, 955, 894, 821, 797, 719, 702, 658, 635, 569 cm^{-1}; HRMS (MALDI) *m/z* calcd. for $C_{47}H_{33}N_4Cl_4^+$ [M$^+$]: 793.1454, found 793.1459.

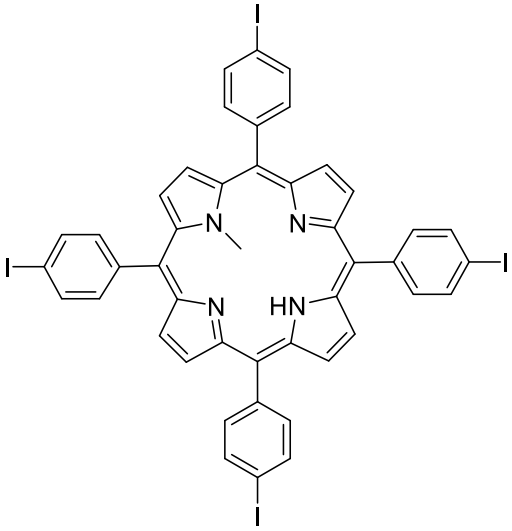

***N*^{21}-Methyl-5,10,15,20-tetrakis(*p*-iodophenyl)porphyrin** (**106m**):

5,10,15,20-Tetrakis(*p*-iodophenyl)porphyrin H_2**107** (25 mg, 0.0235 mmol) was dissolved in 25 mL of CH_2Cl_2 with 5% acetic acid (*v/v*), then CF_3SO_2OMe (0.0026 mL, 0.0235 mmol, 1 eq.) was added. After the solution was heated to reflux for 16 h, the mixture was cooled to room temperature and washed with a 1M ammonia solution. The unreacted starting material (first fraction) was removed *via* column chromatography eluting with a solution of CH_2Cl_2/EtOAc (7:3). The second fraction was obtained using EtOAc. After evaporation of the solvent *in vacuo* a purple solid of **107m** was obtained (7 mg, 0.0065 mmol, 28%). M.p. >350 °C; R_f = 0.83 (SiO_2, CH_2Cl_2:MeOH = 9:1, *v:v*); ^{1}H NMR (400 MHz, $CDCl_3$, 25 °C): δ = -4.81 (s, 3H, *N*-CH_3), 7.84 (s, 2H, $H_{\beta\text{-}}$), 8.00 (d, J = 6.1 Hz, 2H, H_{aryl}), 8.19–8.22 (m, 6H, H_{aryl}) 8.24 (d, J = 7.7 Hz, 2H, H_{aryl}), 8.31 (d, J = 6.3 Hz, 4H, H_{aryl}), 8.48 (s, 2H, $H_{\beta\text{-}}$), 8.51 (d, J = 4.6 Hz, 2H, $H_{\beta\text{-}}$), 8.62(s, 2H, H_{aryl}), 8.63 ppm (d, J = 4.7 Hz, 2H, $H_{\beta\text{-}}$); ^{13}C NMR (100 MHz, $CDCl_3$, 25 °C): δ = 154.2, 149.8, 140.5, 140.0, 138.9, 138.3, 136.6, 136.5, 136.1, 135.9, 135.2, 127.5, 123.5, 121.8, 97.2, 95.9, 29.2 ppm; UV-vis ($CHCl_3$): λ_{max} (log ε) = 439 (5.43), 537 (3.98), 579 (4.20), 615 (3.79), 679 nm (3.74); HRMS (MALDI) *m/z* calcd. for $C_{45}H_{28}N_4I_4$ $[M^+H]^+$: 1132.8544, found 1132.8571.

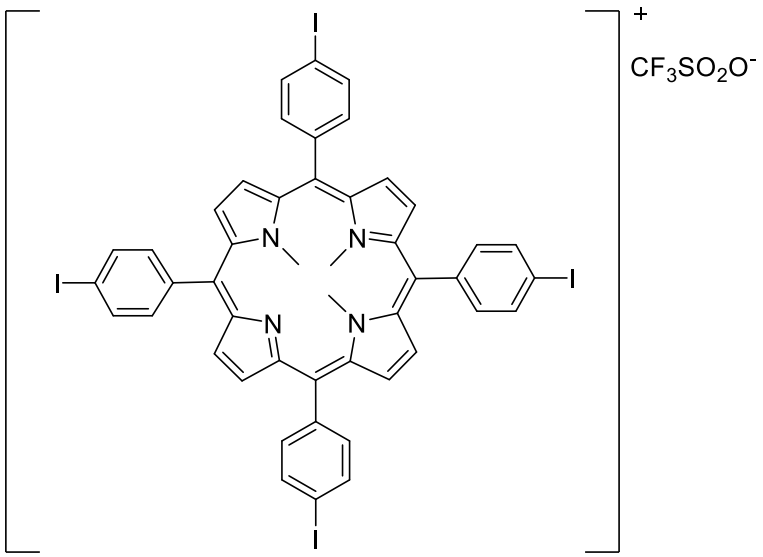

***N*^{21},*N*^{22},*N*^{23}-Trimethyl-5,10,15,20-tetrakis(*p*-iodophenyl)porphyrin trifluoromethanesulfonate salt [107t]$^{+}$[CF_3SO_3]:**

5,10,15,20-Tetrakis(*p*-iodophenyl)porphyrin H_2**107** (25 mg, 0.0235 mmol) was dissolved in 15 mL of CH_2Cl_2. Then K_2CO_3 (1.4 g excess) was added and the mixture was stirred for 5 min, followed by addition of CF_3SO_2OMe (0.051 mL, 0.47 mmol, 20 eq.). After the solution was heated to reflux for 16 h, the mixture was cooled to room temperature and K_2CO_3 was removed by filtration. The solvent was evaporated under reduced pressure and the product was purified by column chromatography (SiO_2; CH_2Cl_2:EtOAc = 10:0–9:1, *v:v*) yielding, after evaporation of the solvent gave a green solid of the title compound (20 mg, 0.0172 mmol, 73%). M.p. >300 °C; R_f = 0.70 (SiO2, CH_2Cl_2:MeOH = 9:1, *v:v*); ^{1}H NMR (400 MHz, $CDCl_3$, 25 °C): δ = -5.67 (s, 3H, *N*-CH_3), -3.19 (s, 6H, *N*-CH_3), 7.24 (d, *J* = 4.5 Hz, 2H, $H_{\beta\text{-}}$), 7.47 (d, *J* = 4.6 Hz, 2H, $H_{\beta\text{-}}$), 8.12 (broad s, 2H, H_{aryl}), 8.21 (s, 2H, $H_{\beta\text{-}}$), 8.21–8.27 (broad s overlaping with singlet at 8.21, 2H, H_{aryl}), 8.32 (d, *J* = 8.1 Hz, 4H, H_{aryl}), 8.40 (d, *J* = 7.4 Hz, 4H, H_{aryl}), 8.43 ppm (s, 2H, H_{aryl}); ^{13}C NMR (100 MHz, $CDCl_3$, 25 °C): δ = 160.0, 157.4, 155.4, 151.2, 139.8, 139.4, 138.8, 138.7, 137.6, 134.4, 131.4, 123.5, 121.0, 120.1, 119.6, 99.1, 98.0, 30.8, 29.8 ppm; UV-vis ($CHCl_3$/1% NEt_3): λ_{max} (log ε) = 342 (4.20), 444 (4.98), 629 nm (4.20); IR (ATR): $\tilde{\nu}$ = 2922, 1575, 1450, 1388, 1257, 1159, 1028, 1002, 893, 813, 717, 636, 571 cm^{-1}; HRMS (MALDI) *m/z* calcd. for $C_{47}H_{33}N_4I_4$ [M]$^+$: 1160.8854, found 1160.8884.

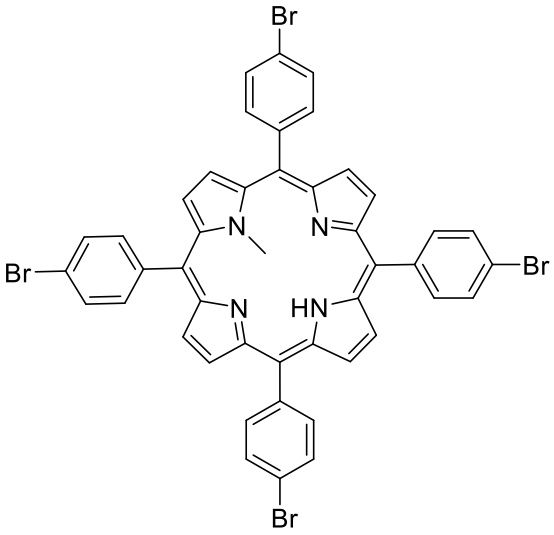

***N*^{21}-Methyl-5,10,15,20-tetrakis(*p*-bromophenyl)porphyrin 108m**:

Free base porphyrin H_2**108** (100 mg, 0.108 mmol) was dissolved in 100 mL of CH_2Cl_2. The mixture was stirred for 5 min then CF_3SO_2OMe (0.0118 mL, 0.108 mmol, 1 eq.) was added. After the solution was heated to reflux for 16 h, the mixture was cooled to room temperature and washed with 1M ammonia solution. The unreacted starting material (first fraction) was removed using a column chromatography eluting with a solution of CH_2Cl_2/EtOAc (7:3). The second fraction, containing the desired compound was obtained using EtOAc. After evaporation of the solvent *in vacuo* a purple solid of **108m** was obtained (25 mg, 0.02647 mmol, 24%). .M.p. >300 °C; R_f = 0.57 (SiO_2, CH_2Cl_2:MeOH = 9:1, *v:v*); ^{1}H NMR (600 MHz, $CDCl_3$, 25 °C): δ = -3.01 (s, 3H, *N*-CH_3), 7.72 (s, 2H, $H_{\beta\text{-}}$), 7.80–7.82 (m, 3H H_{aryl}), 7.84 (d, J = 7.3 Hz, 2H, $H_{\beta\text{-}}$), 7.88-7.90 (m, 5H, H_{aryl}), 8.05 (d, J = 4.5 Hz, 2H, $H_{\beta\text{-}}$), 8.10 (s, 2H, $H_{\beta\text{-}}$), 8.30 (d, J = 4.6 Hz, 2H, H_{aryl}), 8.33 (s, 2H, H_{aryl}), 8.38 ppm (d, J = 7.1 Hz, 4H, H_{aryl}); ^{13}C NMR (150 MHz, $CDCl_3$, 25 °C): δ = 145.8, 140.6, 140.2, 137.6, 136.9, 135.9, 132.0, 131.4, 129.1, 128.7, 128.4, 127.9, 127.4, 101.1, 29.9 ppm; UV-vis ($CHCl_3$): λ_{max} (log ε) = 363 (4.34), 469 (5.04), 605 (3.94), 645 (4.01), 746 nm (4.11); IR (ATR): $\tilde{\nu}$ = 1440, 1141, 1076, 1015, 967, 792, 757, 721, 698 cm^{-1}; HRMS (MALDI) *m/z* calcd. for $C_{45}H_{28}N_4Br_4$ $[M^+H]^+$: 940,9092, found 940.9120.

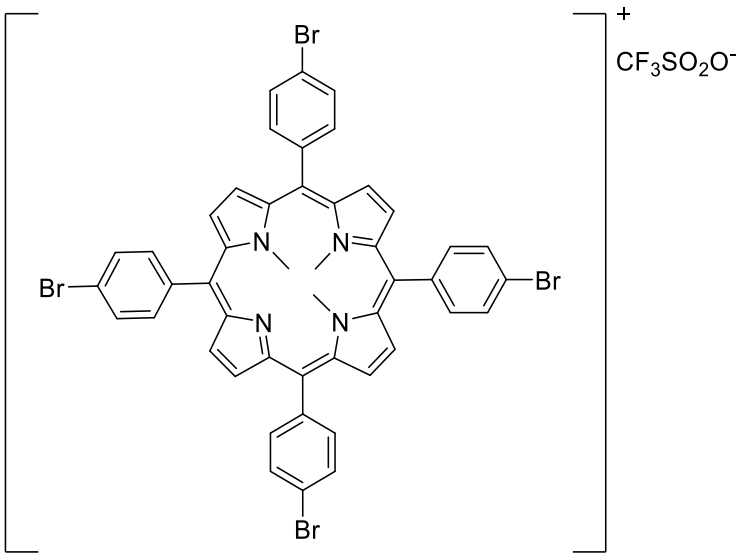

***N*^{21},*N*^{22},*N*^{23}-Trimethyl-5,10,15,20-tetrakis(*p*-bromophenyl)porphyrin trifluoromethanesulfonate salt [108t]$^+$[CF_3SO_3]**:

Porphyrin H_2**108** (150 mg, 0.160 mmol) were dissolved in 50 mL of CH_2Cl_2. Then K_2CO_3 (1.4 g excess) was added and the mixture was stirred for 5 min, followed by addition of CF_3SO_3Me (0.350 mL, 3.2 mmol, 20 eq.). After the solution was heated to reflux for 16 h, the mixture was cooled to room temperature and K_2CO_3 was removed by filtration. The solvent was evaporated under reduced pressure and the product was purified by column chromatography (SiO_2; CH_2Cl_2:EtOAc = 10:0–9:1, *v:v*) yielding, after evaporation of the solvent, a green solid of the title compound (110.7 mg, 0.114 mmol, 71%). M.p. >300 °C; R_f = 0.65 (SiO_2, CH_2Cl_2:MeOH = 9:1, *v:v)*; ^{1}H NMR (600 MHz, $CDCl_3$, 25 °C): δ = -5.62 (s, 3H, *N*-CH_3), -3.16 (s, 6H, *N*-CH_3), 7.21 (d, *J* = 4.7 Hz, 2H, $H_{\beta\text{-}}$), 7.25 (s, 2H, $H_{\beta\text{-}}$), 7.42 (d, *J* = 4.6 Hz, 2H, $H_{\beta\text{-}}$), 7.64 (s, 1H, pyridine peak), 8.07 (d, *J* = 7.8 Hz, 4H, H_{aryl}), 8.14 (d, *J* = 8.1 Hz, 4H, H_{aryl}), 8.18 (s, 2H, $H_{\beta\text{-}}$), 8.39 (s, 2H, H_{aryl}), 8.44 (broad s, 2H, H_{aryl}), 8.59 (s, 2H, H_{aryl}) 8.62 ppm (broad s, 2H, H_{aryl}), ^{13}C NMR (150 MHz, $CDCl_3$, 25 °C): δ = 159.8, 157.2, 155.5, 151.5, 149.8, 140.0, 139.5, 139.1, 138.2, 135.7, 134.1, 132.6, 131.5, 130.8, 126.7, 125.8, 123.7, 123.4, 120.9, 120.0, 119.3, 31.1, 29.7. ppm; UV-vis ($CHCl_3$/1% NEt_3): λ_{max} (log ε) = 378 (4.12), 471 (4.91), 690 (4.13), 715 nm (4.15); IR (ATR): $\tilde{\nu}$ = 1577, 1432, 1258, 1149, 1067, 1059, 1004, 816, 717, 702, 636, 569 cm^{-1}; HRMS (MALDI) *m/z* calcd. for $C_{47}H_{33}N_4Br_4$ $[M]^+$: 972.9398, found 972.9391.

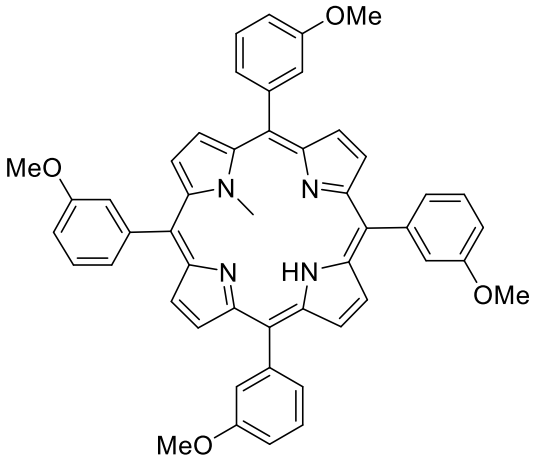

***N*^{21}-Methyl-5,10,15,20-tetrakis(*m*-methoxyphenyl)porphyrin 108m**:

Porphyrin H_2**109** (100 mg, 0.136 mmol) was dissolved in 100 mL of CH_2Cl_2. The mixture was stirred for 5 min then CF_3SO_3Me (0.0095 mL, 0.136 mmol, 1 eq.) was added. After the solution was heated to reflux for 16 h, the mixture was cooled to room temperature and washed with 1M ammonia solution. The unreacted starting material was removed on a column with a solution of CH_2Cl_2/EtOAc (7:3) and the desired compound was extracted from a column with EtOAc. The solvent was evaporated under reduced pressure and the product was purified by column chromatography (SiO_2; CH_2Cl_2:EtOAc = 10:0–9:1, *v:v*) yielding, after evaporation of the solvent, a purple solid of compound **109m** (20.6 mg, 0.02758 mmol, 19%). M.p. = 177-183 °C; R_f = 0.72 (SiO_2, CH_2Cl_2:MeOH = 9:1, *v:v*); ^{1}H NMR (400 MHz, $CDCl_3$, 25 °C): δ = -4.07 (s, 3H, *N*-CH_3), 4.03 (d, *J* = 5.4 Hz, 6H, OCH_3), 4.09 (s, 6H, OCH_3), 7.28 (s overlapping $CHCl_3$, 2H, $H_{\beta\text{-}}$), 7.34 (d, 2H, *J* = 8.6 Hz, H_{aryl}), 7.36 (d, 2H, *J* = 8.6 Hz, H_{aryl}), 7.54 (s, 2H, $H_{\beta\text{-}}$), 7.67 (dd, *J* = 16.7, 8.5 Hz, 2H, H_{aryl}), 7.74 (s, 2H, H_{aryl}), 7.77 (s, 1H, H_{aryl}), 7.80 (d, *J* = 7.0 Hz, 1H, H_{aryl}), 7.88–7.83 (m, 2H, H_{aryl}), 7.93 (s, 1H, H_{aryl}), 8.08 (s, 1H, H_{aryl}), 8.52 (d, *J* = 4.2 Hz, 2H, H_{aryl}), 8.52 (d, *J* = 4.2 Hz, 2H, $H_{\beta\text{-}}$), 8.69 (d, *J* = 2.5 Hz, 2H, H_{aryl}), 8.88 ppm (d, *J* = 4.1 Hz, 2H, $H_{\beta\text{-}}$); ^{13}C NMR (150 MHz, CDCl3) δ = 158.4, 158.1, 156.8, 153.5, 152.3, 143.9, 143.6, 139.2, 133.8, 132.5, 130.6, 128.6, 128.2, 127.8, 127.6, 127.2, 125.48, 123.26, 121.27, 120.07, 119.37, 118.27, 113.66, 113.44, 113.31, 55.71, 55.54, 29.7 ppm; UV-vis ($CHCl_3$): λ_{max} (log ε) = 436 (5.35), 533 (4.11), 575 (4.21), 619 (4.05), 676 nm (4.04); IR (ATR): $\tilde{\nu}$ = 1572, 1421, 1283, 1163, 1041, 905, 73, 697 cm^{-1}; HRMS (MALDI) *m/z* calcd. for $C_{49}H_{40}N_4O_4$ $[M^+H]^+$: 749.3128, found 749.3145.

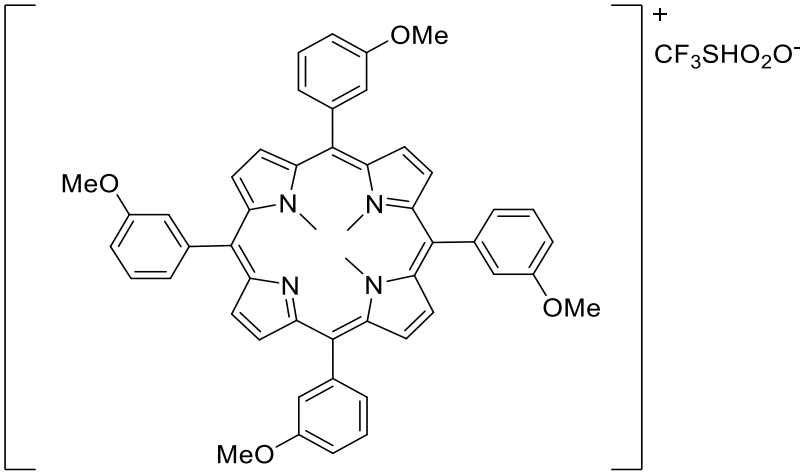

N^{21},N^{22},N^{23}-Trimethyl-5,10,15,20-tetrakis(*m*-methoxyphenyl)porphyrin trifluoromethanesulfonate salt [109t]$^+$[CF_3SO_3]:

Free base H_2**109** (100 mg, 0.136 mmol) was dissolved in 50 mL of CH_2Cl_2. Then K_2CO_3 (1.4 g excess) was added and the mixture was stirred for 5 min, followed by addition of CF_3SO_3Me (0.298 mL, 2.72 mmol, 20 eq.). After the solution was heated to reflux for 16 h, the mixture was cooled to room temperature and K_2CO_3 was removed by filtration. The solvent was evaporated *in vacuo* and the product was purified by column chromatography (SiO_2; CH_2Cl_2:EtOAc = 10:0–9:1, *v:v*) yielding, after evaporation of the solvent under reduced pressure, the title compound as a green solid (69.2 mg, 0.089 mmol, 65%). M.p. = 190-196°C; R_f = 0.64 (SiO_2, CH_2Cl_2:MeOH = 9:1, *v:v*); ^{1}H NMR (400 MHz, $CDCl_3$, 25 °C): δ = -5.60 (s, 3H, *N*-CH_3), -3.15 (s, 6H, *N*-CH_3), 4.14 (s, 6H, OCH_3), 4.17 (s, 6H, OCH_3), 7.30 (d, *J* = 4.7 Hz, 2H, $H_{\beta\text{-}}$), 7.45 (d, *J* = 2.3 Hz, 1H, H_{aryl}), 7.47 (t, *J* = 1.9 Hz, 2H, H_{aryl}), 7.49 (d, *J* = 2.4 Hz, 1H, H_{aryl}), 7.51 (d, *J* = 4.1 Hz, 2H, $H_{\beta\text{-}}$), 7.85 (t, *J* = 7.8 Hz, 3H, H_{aryl} + 1$H_{\beta\text{-}}$), 7.93 (t, *J* = 7.8 Hz, 3H, H_{aryl} + 1$H_{\beta\text{-}}$), 8.07 (s, 4H, H_{aryl}), 8.25 (s, 4H, H_{aryl}), 8.48 (s, 2H, $H_{\beta\text{-}}$); ^{13}C NMR (100 MHz, $CDCl_3$, 25 °C): δ = 160.2, 159.1, 157.6, 155.8, 151.6, 141.8, 140.9, 134.3, 132.0, 131.8, 131.5, 130.2, 129.0, 124.0, 121.0, 120.7, 119.3, 115.3, 56.2, 56.0, 31.0 ppm; UV-vis ($CHCl_3$): λ_{max} (log ε) = 360 (4.44), 469 (5.20), 683 (4.39), 710 nm (4.39); IR (ATR): $\tilde{\nu}$ = 2934, 1592, 1573, 1413, 1317, 1262, 1140, 1029, 993, 861, 785, 710, 695, 635, 571 cm^{-1}; HRMS (MALDI) *m/z* calcd. for $C_{51}H_{45}N_4O_4$ [M]$^+$: 777.3441, found 777.3476.

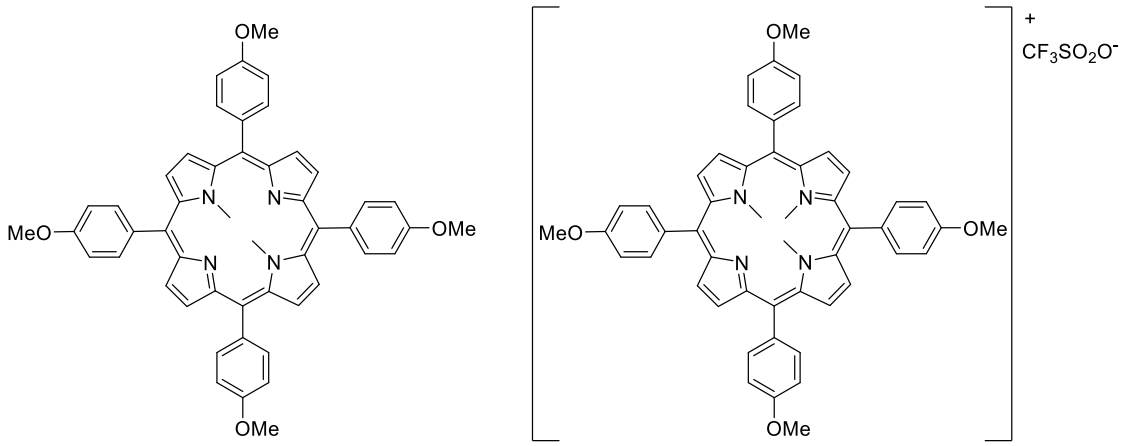

N^{21},N^{23}-Dimethyl-5,10,15,20-tetrakis(*p*-methoxyphenyl)porphyrin 110d and N^{21},N^{22},N^{23}-Trimethyl-5,10,15,20-tetrakis(*p*-methoxyphenyl)porphyrin trifluoromethanesulfonate salt [110t]$^{+}$[CF_3SO_3]:

In a 250 mL three-necked round-bottomed flask, 5,10,15,20-tetrakis(*p*-methoxyphenyl)porphyrin H_2**110** (200 mg, 0.2724 mmol) and K_2CO_3 (1.4 g excess) were dissolved in 50 mL of CH_2Cl_2. The solution was heated to reflux and CF_3SO_3Me (0.298 mL, 2.724 mmol, 10 eq.) was added. After the solution was heated to reflux for 16 h, the mixture was cooled to room temperature and K_2CO_3 was removed by filtration. The solvent was evaporated under reduced pressure and the product was purified by column chromatography (SiO_2; CH_2Cl_2:MeOH = 10:0–9:1, *v:v*) yielding a first green product, compound **110d** (14.6 mg, 0.0191 mmol, 7%). M.p. >300 °C; R_f = 0.83 (SiO_2, CH_2Cl_2:MeOH = 9:1, *v:v*); ^{1}H NMR (400 MHz, $CDCl_3$, 25 °C): δ = -2.87 (s, 6H, *N*-CH_3), 4.10 (s, 12H, O-CH_3), 7.12 (s, 4H, $H_{\beta\text{-}}$), 7.49 (d, J = 8.7 Hz, 8H, H_{aryl}), 8.41 (d, J = 8.7 Hz, 8H, H_{aryl}), 8.50 ppm (s, 4H, H_{aryl}), ^{13}C NMR (100 MHz, $CDCl_3$, 25 °C): δ = 139.7, 133.8, 130.4, 125.4, 118.9, 114.0, 113.9, 55.8, 31.0 ppm; UV-vis ($CHCl_3$): λ_{max} (log ε) = 468 (5.49), 733 nm (4.98); IR (ATR): $\tilde{\nu}$ = 2922, 1596, 1508, 1458, 1414, 1254, 1174, 1149, 1027, 830, 730, 713, 666, 635, 608, 596, 568 cm^{-1}; HRMS (MALDI) *m/z* calcd. for $C_{50}H_{42}N_4O_4$ $[M^+H]^+$: 763.3284, found 763.3287. Further elution yielded a second green fraction which gave a solid of the title salt **[110t]$^+$** (154.3 mg, 0.0321 mmol, 73%). M.p. = 285–290 °C; R_f = 0.54 (SiO_2, EtOAc); ^{1}H NMR (400 MHz, $CDCl_3$, 25 °C): δ = -5.32 (s, 3H, *N*-CH_3), -3.02 (s, 6H, *N*-CH_3), 4.13 (d, J = 4.5 Hz, 12H, O-C*H*3), 7.17 (d, J = 4.7 Hz, 2H, $H_{\beta\text{-}}$), 7.37 (d, J = 4.7 Hz, 2H, $H_{\beta\text{-}}$), 7.49 (d, J = 8.9 Hz, 4H, H_{aryl}), 7.55 (d, J = 8.9 Hz, 4H, H_{aryl}), 8.12 (s, 2H, $H_{\beta\text{-}}$), 8.35 (s, 2H, $H_{\beta\text{-}}$), 8.42 (broad s, 4H, H_{aryl}), 8.59 ppm (broad s, 4H, H_{aryl}); ^{13}C NMR (100 MHz, $CDCl_3$, 25 °C): δ = 162.3, 161.6, 159.9, 157.6, 156.1, 151.6, 140.3, 139.4, 133.7, 133.3, 133.0, 131.3, 122.8, 120.6, 119.7, 119.0, 114.9, 113.9, 55.9, 55.8, 30.3, 29.6 ppm; UV-vis ($CHCl_3$): λ_{max} (log ε) = 475 (5.18), 738 nm (4.65); IR (ATR): $\tilde{\nu}$ = 3468, 2930, 2559, 2039, 1596, 1567, 1507, 1442, 1411, 1296,

1248, 1174, 1146, 1115, 1028, 968, 894, 829, 792, 729, 705, 663, 634, 606, 566 cm^{-1}; HRMS (MALDI) *m/z* calcd. for $C_{51}H_{45}N_4O_4$ $[M]^+$: 777.3441, found 777.3455.

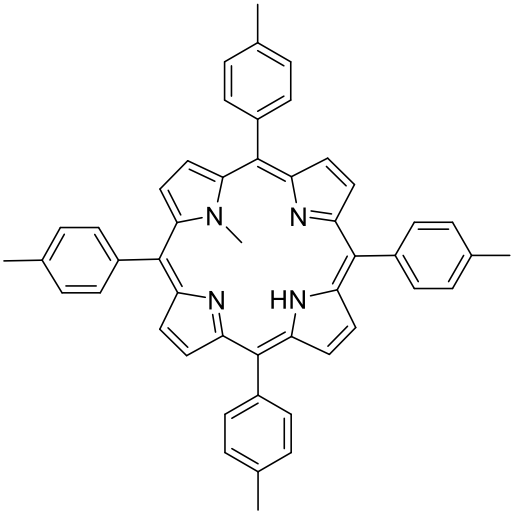

***N*^{21}-Methyl-5,10,15,20-tetrakis(*p*-tolyl)porphyrin 111m**:

5,10,15,20-Tetrakis(*p*-tolyl)porphyrin H_2**111** (100 mg, 0.149 mmol) was dissolved in 100 mL of CH_2Cl_2 with 5% of acetic acid. The mixture was stirred for 5 min, then CF_3SO_2OMe (0.0163 mL, 0.149 mmol, 1 eq.) was added. After the solution was heated under reflux for 16 h, the mixture was cooled to room temperature and washed with a 1M ammonia solution. Unreacted starting material was removed on a silica column eluting with a solution of CH_2Cl_2/EtOAc (7:3) and the desired compound was extracted from the column with EtOAc. The solvent was evaporated under reduced pressure and the product was purified by column chromatography (SiO_2; CH_2Cl_2:EtOAc = 10:0–9:1, *v:v*), yielding, after evaporation of the solvent, compound **111m** as a purple solid (45.6 mg, 0.0665 mmol, 45%). M.p. >350 °C; R_f = 0.72 (SiO_2, CH_2Cl_2:MeOH = 9:1, *v:v*); ^{1}H NMR (400 MHz, $CDCl_3$, 25 °C): δ = -4.69 (s, 3H, *N*-C*H*$_3$), 2.74 (d, *J* = 4.2 Hz, 12H, C*H*$_{3\text{-aryl}}$), 7.65 (d, *J* = 7.7 Hz, 2H, *H*$_{aryl}$), 7.70 (d, *J* = 7.5 Hz, 2H, *H*$_{aryl}$), 7.76 (d, *J* = 7.7 Hz, 4H, *H*$_{aryl}$), 7.82 (s, 2H, *H*$_{\beta\text{-}}$), 8.18 (d, *J* = 7.3 Hz, 2H, *H*$_{aryl}$), 8.37 (d, *J* = 7.4 Hz, 2H, *H*$_{aryl}$), 8.45 (broad s, 4H), 8.54 (s, 2H, H$_{\beta\text{-}}$), 8.63 (d, *J* = 4.7 Hz, 2H, *H*$_{\beta\text{-}}$), 8.76 ppm (d, *J* = 4.7 Hz, 2H, *H*$_{\beta\text{-}}$); ^{13}C NMR (410 MHz, $CDCl_3$, 25 °C): δ =159.1, 155.1, 142.2, 140.7, 139.8, 138.5, 138.2, 138.0, 137.1, 136.8, 135.1, 127.9, 127.5, 126.8, 126.1, 122.2, 122.1, 119.3, 110.0, 49.6, 21.5 ppm; UV-vis ($CHCl_3$): λ_{max} (log ε) = 342 (4.66), 444 (5.61), 629 (4.56), 677 nm (4.55); IR (ATR): $\tilde{\nu}$ = 3024, 1605, 1452, 1299, 1241, 1221, 1183, 1151, 1029, 964, 809, 721, 705, 632, 567 cm^{-1}; HRMS (MALDI) *m/z* calcd. for $C_{49}H_{40}N_4$ $[M^+H]^+$: 685.3353, found 685.3331.

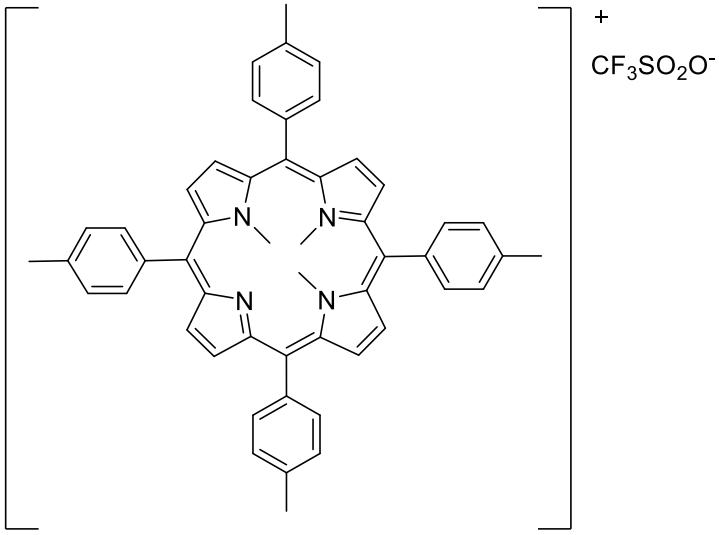

***N*^{21},*N*^{22},*N*^{23}-Trimethyl-5,10,15,20-tetrakis(*p*-tolyl)porphyrin trifluoromethanesulfonate salt [111t]$^+$[CF_3SO_3]:**

Porphyrin H_2**111** (100 mg, 0.149 mmol) was dissolved in 50 mL of CH_2Cl_2. Then K_2CO_3 (1.4 g excess) was added and the mixture was stirred for 5 min, followed by addition of CF_3SO_3Me (0.163 mL, 0.149 mmol, 10 eq.). After the solution was heated to reflux for 16 h, the mixture was cooled to room temperature and K_2CO_3 was removed by filtration. The solvent was evaporated under reduced pressure and the product was purified by column chromatography (SiO_2; CH_2Cl_2:EtOAc = 10:0–9:1, *v:v*) yielding, after evaporation of the solvent, the title compound as a green powder (105.7 mg, 0.148 mmol, 99%). M.p. >350 °C; R_f = 0.82 (SiO_2, CH_2Cl_2:MeOH = 9:1, *v:v*); ^{1}H NMR (400 MHz, $CDCl_3$, 25 °C): δ = -5.50 (s, 3H, *N*-CH_3),-3.12 (s, 6H, *N*-CH_3), 2.74 (s, 12H, C$H_{3\text{-aryl}}$), 7.22 (d, *J* = 4.6 Hz, 2H, $H_{\beta\text{-}}$), 7.43 (d, *J* = 4.6 Hz, 2H, $H_{\beta\text{-}}$), 7.77 (d, *J* = 7.8 Hz, 4H, H_{aryl}), 7.83 (d, *J* = 7.9 Hz, 4H, H_{aryl}), 8.18 (s, 2H, $H_{\beta\text{-}}$), 8.34 (broad s, 4H, H_{aryl}), 8.42 (s, 2H, $H_{\beta\text{-}}$), 8.53 ppm (broad s, 4H, H_{aryl});^{13}C NMR (100 MHz, $CDCl_3$, 25 °C): δ = 160.1, 157.6, 156.0, 151.7, 141.7, 140.6, 139.1, 138.3, 138.0, 137.2, 133.9, 132.0, 130.2, 129.2, 123.5, 121.0, 120.6, 119.1, 30.8, 21.8 ppm; UV-vis ($CHCl_3$): λ_{max} (log ε) = 384 (5.08), 468 (5.80), 718 nm (5.13); IR (ATR): $\tilde{\nu}$ = 2918, 1604, 1431, 1261, 1221, 1185, 1146, 1029, 967, 855, 813, 788, 720, 706, 664, 634, 565 cm^{-1}; HRMS (MALDI) *m/z* calcd. for $C_{51}H_{45}N_4$ [M]$^+$: 713.3648, found 713.3644.

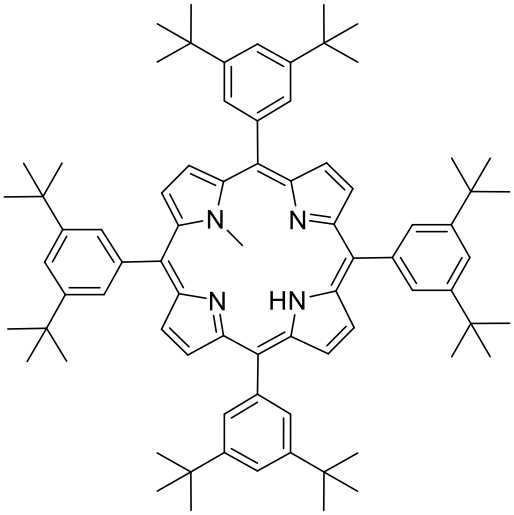

N^{21}-Methyl-5,10,15,20-tetrakis(*m*-(3,5-di-*tert*-butylphenyl))porphyrin 112m:

5,10,15,20-Tetrakis(*m*-(3,5-di-*tert*-butylphenyl))porphyrin H_2**112** (50 mg, 0.078 mmol) was dissolved in 100 mL of CH_2Cl_2 with 5% (*v:v)* of acetic acid. The mixture was stirred for 5 min then CF_3SO_2OMe (0.0050 mL, 0.078 mmol, 1 eq.) was added. After the solution was heated to reflux for 16 h, the mixture was cooled to room temperature and washed with a 1M ammonia solution. Unreacted starting material was removed on a silica column eluting with a solution of CH_2Cl_2/EtOAc (7:3) and the desired compound was extracted from the column with EtOAc. The solvent was evaporated under reduced pressure and the residue was purified by column chromatography (SiO_2; CH_2Cl_2:EtOAc = 10:0–9:1, *v:v*) yielding, after evaporation of the solvent, a purple solid of **112m** (7 mg, 0.00649 mmol, 8%). M.p. >350 °C; R_f = 0.60 (SiO_2, CH_2Cl_2:MeOH = 9:1, *v:v*); ^{1}H NMR (400 MHz, $CDCl_3$, 25 °C): δ = -3.80 (s, 3H, *N*-CH_3), 1.47 (m, 36H, *tert*-butyl), 1.62 (m, 18H, *tert*-butyl), 1.83 (m, 18H, *tert*-butyl), 7.79 (m, 2H, H_{aryl}), 7.85 (broad s, 2H, H_{aryl}), 7.95 (broad s, 2H, H_{aryl}), 8.01 (broad s, 2H, H_{aryl}), 8.26 (broad s, 2H, H_{aryl}), 8.38 (broad s, 2H, H_{aryl}), 8.44 (s, 2H, $H_{\beta\text{-}}$), 8.88 (s, 2H, $H_{\beta\text{-}}$), 8.93 ppm (m, 4H, $H_{\beta\text{-}}$); ^{13}C NMR (100 MHz, $CDCl_3$, 25 °C): δ = 156.8, 152.4, 151.4, 151.1, 141.0, 134.0, 133.1, 132.4, 129.1, 126.0, 123.2, 122.0, 121.1, 34.9, 31.8, 31.3, 31.2, 29.5 ppm; UV-vis ($CHCl_3$): λ_{max} (log ε) = 437 (5.44), 473 (4.00), 579 (4.19), 679 nm (3.78); IR (ATR): $\tilde{\nu}$ = 2955, 1589, 1460, 1412, 1394, 1363, 1251, 1222, 1149, 1067, 1030, 899, 865, 826, 796, 732, 711, 636, 571 cm^{-1}; HRMS (MALDI) *m/z* calcd. for $C_{77}H_{96}N_4$ $[M^+H]^+$: 1177,7707, found 1077.7716.

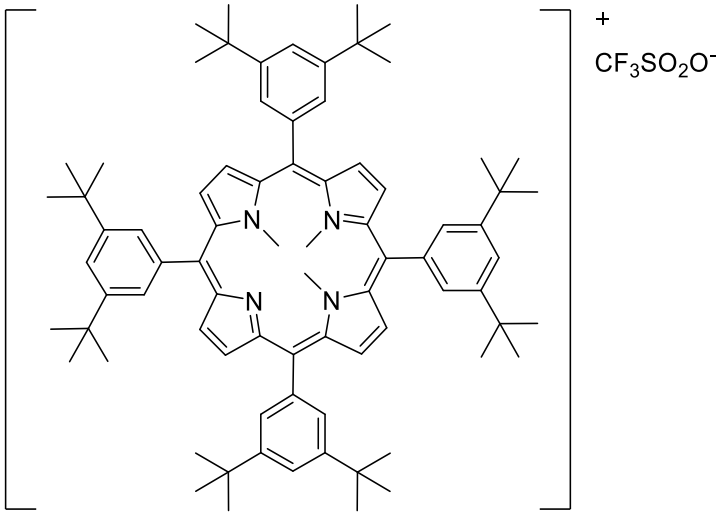

N^{21},N^{22},N^{23}-Trimethyl-5,10,15,29-tetrakis(*m*-(3.5-di-*tert*-butylphenyl)porphyrin trifluoromethanesulfonate salt [112t]$^+$[CF_3SO_3]:

5,10,15,20-Tetrakis(*m*-(3,5-di-*tert*-butylphenyl))porphyrin H_2**112** (100 mg, 0.094 mmol) was dissolved in 150 mL of CH_2Cl_2. Then K_2CO_3 (1.4 g excess) was added and the mixture was stirred for 5 min, followed by addition of CF_3SO_3Me (0.102 mL, 1.54 mmol, 10 eq.). After the solution was heated to reflux for 16 h, the mixture was cooled to room temperature and K_2CO_3 was removed by filtration. The solvent was evaporated under reduce pressure and the product was purified by column chromatography (SiO_2; CH_2Cl_2:EtOAc = 10:0–9:1, *v:v*) yielding, after evaporation of the solvent, a green solid of the title salt (62.2 mg, 0.05624 mmol, 60%). M.p. = 287-290 °C; R_f = 0.74 (SiO_2, CH_2Cl_2:MeOH = 9:1, *v:v*); ^{1}H NMR (600 MHz, $CDCl_3$, 25 °C): δ = -5.47 (s, 3H, *N*-CH_3), -2.98 (s, 6H, *N*-CH_3), 1.67 (d, *J* = 10.9 Hz, 72H, *tert*-butyl), 7.29 (d, *J* = 4.7 Hz, 2H, $H_{\beta\text{-}}$), 7.48 (d, *J* = 4.7 Hz, 2H, $H_{\beta\text{-}}$), 7.96 (s, 2H, H_{aryl}), 8.01 (s, 2H, H_{aryl}), 8.21 (s, 2H, $H_{\beta\text{-}}$), 8.25 (broad s, 4H, H_{aryl}) 8.39 (s, 2H, $H_{\beta\text{-}}$), 8.46 (broad s, 2H, H_{aryl}), 8.59 (broad s, 2H, H_{aryl}); ^{13}C NMR (100 MHz, $CDCl_3$, 25 °C): δ = 160.8, 157.7, 155.8, 152.0, 150.6, 140.0, 139.1, 133.9, 133.5, 133.0, 125.2, 123.9, 122.8, 121.7, 121.4, 119.3, 118.7, 35.5, 35.4, 31.3, 31.8, 29.8 ppm; UV-vis ($CHCl_3$): λ_{max} (log ε) = 383 (4.32), 473 (5.08), 695 (4.30), 725 nm (4.31); HRMS (MALDI) *m/z* calcd. for $C_{79}H_{101}N_4$ [M]$^+$: 1105.8021, found 1105.8050.

6.2.2 *N*-methylation of 5,15-diarylporphyrins

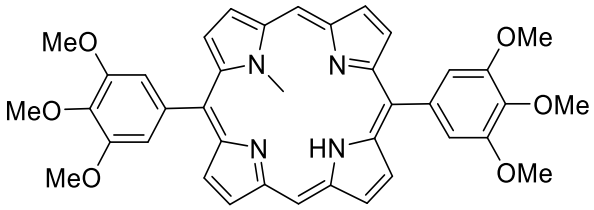

***N*^{21}-Methyl-5,15-bis(3,4,5-trimethoxyphenyl)porphyrin 113m:**

5,15-Bis(3,4,5-trimethoxy)phenylporphyrin H_2**113** (100 mg, 0.156 mmol) was dissolved in 50 mL of CH_2Cl_2 with 5% of acetic acid. The mixture was stirred for 5 min, then CF_3SO_2OMe (0.0095 mL, 0.156 mmol, 1 eq.) was added. After the solution was heated to reflux for 16 h, the mixture was cooled to room temperature and washed with a 1M ammonia solution. Unreacted starting material was removed on a silica column with a solution of CH_2Cl_2/EtOAc (7:3) and the desired compound was extracted with EtOAc. The solvent was evaporated under reduced pressure and the product was purified by column chromatography (SIO_2; CH_2Cl_2:EtOAc = 10:0–9:1, *v:v*) yielding, after evaporation of the solvent, a purple solid of compound **113m** (47.2 mg, 0.0718 mmol, 46%). M.p. >300 °C; R_f = 0.66 (SiO_2, CH_2Cl_2:MeOH = 9:1, *v:v*); ^{1}H NMR (600 MHz, $CDCl_3$, 25 °C): δ = -4.51 (s, 3H, *N*-CH_3), -2.56 (s, 1H, *N*-*H*), 3.99 (s, 3H, *p*-OCH_3), 4.03 (s, 6H, *m*-OCH_3), 4.19 (s, 6H, *m*-OCH_3), 4.20 (s, 3H, *p*-OCH_3),7.39 (s, 2H, H_{aryl}), 7.55 (s, 1H, $H_{\beta\text{-}}$), 7.91 (d, *J* = 4.3 Hz, 1H, $H_{\beta\text{-}}$), 8.37 (d, *J* = 4.5 Hz, 1H, $H_{\beta\text{-}}$), 8.85 (d, *J* = 4.0 Hz, 1H, $H_{\beta\text{-}}$), 8.95 (d, *J* = 4.3 Hz, 1H, $H_{\beta\text{-}}$), 9.07 (d, *J* = 4.2 Hz, 1H, $H_{\beta\text{-}}$), 9.14 (d, *J* = 4.1 Hz, 2H, H_{aryl}), 9.35 (d, *J* = 4.7 Hz, 1H, $H_{\beta\text{-}}$), 10.09 ppm (d, *J* = 3.1 Hz, 2H, H_{aryl}); ^{13}C NMR (100 MHz, $CDCl_3$, 25 °C): δ = 156.8, 153.1, 152.0, 151.7, 139.8, 137.9, 137.0, 135.6, 134.0, 133.6, 133.5, 128.7, 127.9, 119.1, 118.0, 113.0, 112.7, 110.2, 105.8, 61.3, 61.3, 56.4, 56.4, 29.7 ppm; UV-vis ($CHCl_3$): λ_{max} (log ε) = 424 (5.27), 515 (3.97), 555 (3.94), 597 (3.76), 659 nm (3.60); IR (ATR): $\tilde{\nu}$ = 2981, 1577, 1498, 1458, 1406, 1333, 1231, 1124, 1058, 1001, 964, 923, 851, 793, 714, 687 cm^{-1}; HRMS (MALDI) *m/z* calcd. for $C_{39}H_{36}N_4O_6$ $[M^+H]^+$: 657.2713, found 657.2740.

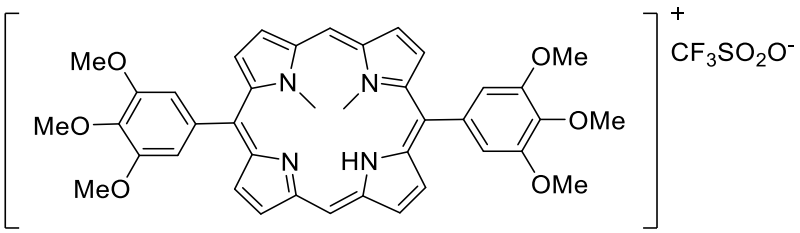

N^{21}-Hydro-N^{23},N^{24}-dimethyl-5,15-bis(3,4,5-trimethoxyphenyl)porphyrin trifluoromethanesulfonate salt [113d]$^+$[CF_3SO_3]:

Free base H_2**113** (100 mg, 0.156 mmol) was dissolved in 50 mL of CH_2Cl_2. Then K_2CO_3 (1.4 g excess) was added and the mixture stirred for 5 min, followed by addition of CF_3SO_3Me (0.171 mL, 1.56 mmol, 10 eq.). After the solution was heated to reflux for 16 h, the mixture was cooled to room temperature and K_2CO_3 was removed by filtration. The solvent was evaporated under reduced pressure and the product was purified by column chromatography (SiO_2; CH_2Cl_2:EtOAc = 10:0–9:1, *v:v*) yielding, after evaporation of the solvent, the title compound as a green solid (88.1 mg, 0.131 mmol, 86%). M.p. >300 °C; R_f = 0.51 (SiO_2, CH_2Cl_2:MeOH = 9:1, *v:v*); ^{1}H NMR (600 MHz, $CDCl_3$, 25 °C): δ = -5.32 (s, 6H, *N*-CH_3), 4.02 (s, 6H, o-OCH_3), 4.19 (s, 3H, p-OCH_3), 4.22 (s, 3H, p-OCH_3), 4.25 (s, 6H, o-OCH_3), 7.40 (s, 2H, H_{meso}), 7.92 (s, 2H, H_{aryl}), 8.41 (d, J = 4.7 Hz, 2H, $H_{\beta\text{-}}$), 8.82 (d, J = 4.8 Hz, 2H, $H_{\beta\text{-}}$), 9.14 (d, J = 4.7 Hz, 2H, $H_{\beta\text{-}}$), 8.55 (d, J = 4.8 Hz, 2H, $H_{\beta\text{-}}$), 10.68 ppm (s, 2H, H_{aryl}); ^{13}C NMR (100 MHz, $CDCl_3$, 25 °C): δ = 154.0, 153.7, 152.5, 152.4, 152.1, 147.3, 141.4, 138.8, 136.2, 135.3, 134.1, 133.3, 122.4, 122.3, 121.8, 121.5, 116.7, 113.2, 109.1, 109.6, 61.6, 61.5, 57.2, 56.7, 28.7 ppm; UV-vis ($CHCl_3$): λ_{max} (log ε) = 447 (5.35), 604 (4.43), 646 nm (4.35); IR (ATR): $\tilde{\nu}$ = 2981, 1577, 1491, 1411, 1328, 1326, 1155, 1121, 1028, 995, 927, 838, 799, 720, 692, 635, 568 cm^{-1}; HRMS (MALDI) *m/z* calcd. for $C_{40}H_{39}N_4O_6$ $[M]^+$: 671.2870, found 671.2897.

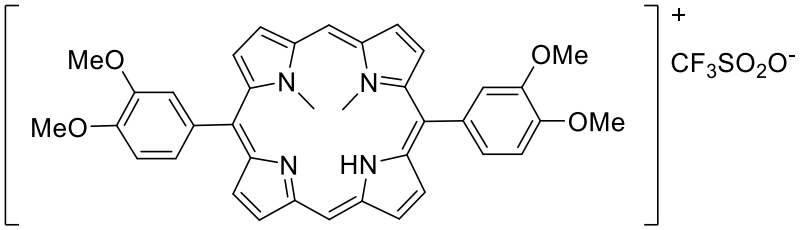

N^{21}-Hydro-N^{23},N^{24}-dimethyl-5,15-bis(3,4-dimethoxyphenyl)porphyrin trifluoromethanesulfonate salt [114d]$^+$[CF_3SO_3]:

Porphyrin H_2**114** (50 mg, 0.0858 mmol) was dissolved in 50 mL of CH_2Cl_2. Then K_2CO_3 (1.4 g excess) was added and the mixture was stirred for 5 min, followed by addition of CF_3SO_3Me (0.094 mL, 0.858 mmol, 10 eq.). After the solution was heated to reflux for 16 h, the mixture was cooled to room temperature and K_2CO_3 was removed by filtration. The solvent was evaporated under reduced pressure and the product was purified by column chromatography (SiO_2; CH_2Cl_2:EtOAc = 10:0–9:1, *v:v*) yielding, after evaporation of the solvent, the title compound as a green solid (49 mg, 0.0802 mmol, 93%). M.p. >350 °C; R_f = 0.68 (SiO_2, CH_2Cl_2:MeOH = 9:1, *v:v*); ^{1}H NMR (600 MHz, $CDCl_3$, 25 °C): δ = -5.24 (d, *J* = 13.6 Hz, 6H, *N*-CH_3), -2.23 (s, 1H, *N*-*H*), 4.05 (s, 3H, O-CH_3), 4.20 (s, 3H, O-CH_3), 4.25 (s, 3H, O-CH_3), 4.30 (s, 3H, O-CH_3), 7.35 (d, *J* = 7.7 Hz, 1H, H_{aryl}), 7.58 (d, *J* = 8.1 Hz, 1H, H_{aryl}), 7.71 (s, 2H, $H_{\beta\text{-}}$), 8.18 (d, *J* = 7.7 Hz, 1H, H_{aryl}), 8.30 (s, 2H, $H_{\beta\text{-}}$), 8.36 (s, 1H, H_{meso}), 8.80 (d, *J* = 8.7 Hz, 2H,$H_{\beta\text{-}}$), 9.08 (s, 2H, $H_{\beta\text{-}}$), 9.50 (d, *J* = 3.2 Hz, 2H, H_{aryl}), 9.53 (d, *J* = 3.2 Hz, 2H, H_{aryl}) 10.61 (s, 1H, H_{meso}), 10.66 ppm (d, *J* = 6.1 Hz, 1H, H_{aryl}); ^{13}C NMR (150 MHz, $CDCl_3$) δ = 152.5, 150.2, 150.0, 148.4, 147.5, 146.8, 136.2, 133.4, 133.2, 131.3, 122.4, 122.3, 121.3, 118.6, 112.1, 110.7, 109.3, 57.0, 56.7, 56.5, 29.8 ppm; UV-vis ($CHCl_3$): λ_{max} (log ε) = 452 (5.97), 615 (4.18), 650 nm (4.18); IR (ATR): $\tilde{\nu}$ = 3484, 2981, 1596, 1514, 1491, 1463, 1412, 1328, 1253, 1232, 1169, 1139, 1030, 968, 922, 849, 802, 763, 716, 690, 635, 575 cm^{-1}; HRMS (MALDI) *m/z* calcd. for $C_{38}H_{35}N_4O_4$ $[M]^+$: 611.2658, found 611.2653.

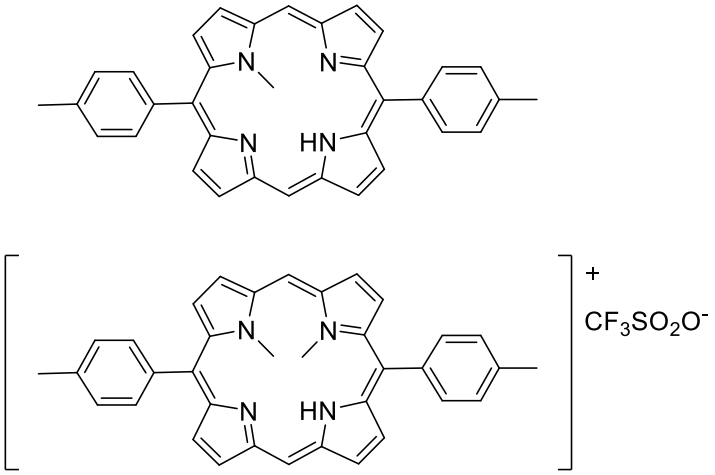

N^{21}-Methyl-5,15-bis(*p*-tolyl)porphyrin 114m and N^{21}-*hydro*-N^{23},N^{24}-dimethyl-5,15-bis(*p*-tolyl)porphyrin trifluoromethanesulfonate salt $[115d]^+[CF_3SO_3]$:

Porphyrin H_2**115** (50 mg, 0.102 mmol) was dissolved in 50 mL of CH_2Cl_2 (5%, *v:v,* acetic acid). The mixture was stirred for 5 min then CF_3SO_3Me (0.012 mL, 0.102 mmol, 1 eq.) was added. The reaction was monitored by TLC after 16 h showing initial formation of the product. Another equivalent of CF_3SO_2OMe was added and the reaction was stirred for an additional 16 h. This step was repeated (for a total of 3 eq. methylating agent). TLC control after 48 h showed the formation of a second compound. The reaction was stopped, cooled and washed with 1M ammonia solution. Unreacted starting material was removed on a column with a solution of CH_2Cl_2/EtOAc (7:3) and the mixture, containing the two formed products, was extracted from the column with EtOAc. The solvent was evaporated under reduced pressure and products were purified by column chromatography (SiO_2; CH_2Cl_2:EtOAc = 10:0–9:1, *v:v*) yielding a first fraction, which, after evaporation of the solvent, gave compound **115m** as a purple powder (4.6 mg, 0.0091 mmol, 9%). M.p. >300 °C; R_f = 0.96 (SiO_2, CH_2Cl_2:MeOH = 9:1, *v:v*); ^{1}H NMR (600 MHz, $CDCl_3$, 25 °C): δ = -4.30 (d, J = 54.5 Hz, 3H, *N*-CH_3), 2.74 (s, 3H, C$H_{3\text{-aryl}}$), 7.58 (d, J = 7.2 Hz, 1H, H_{aryl}), 7.62 (d, J = 7.3 Hz, 1H, H_{aryl}), 7.65 (d, J = 6.3 Hz, 1H, H_{aryl}), 7.73 (d, J = 6.0 Hz, 1H, H_{aryl}), 8.06 (d, J = 6.0 Hz, 2H, H_{aryl}), 8.21 (d, J = 7.0 Hz, 1H, H_{aryl}), 8.48 (d, J = 5.9 Hz, 1H, H_{aryl}), 8.62 (d, J = 4.2 Hz, 1H, $H_{\beta\text{-}}$), 9.03 (d, J = 4.3 Hz, 1H, $H_{\beta\text{-}}$), 9.12 (d, J = 4.2 Hz, 1H, $H_{\beta\text{-}}$), 9.15 (d, J = 4.4 Hz, 1H, $H_{\beta\text{-}}$), 9.15 (d, J = 4.4 Hz, 1H, $H_{\beta\text{-}}$), 9.16 (d, J = 4.4 Hz, 1H, $H_{\beta\text{-}}$), 9.16 (d, J = 4.4 Hz, 1H, $H_{\beta\text{-}}$), 9.34 (d, J = 4.3 Hz, 1H, $H_{\beta\text{-}}$), 9.36 (d, J = 4.4 Hz, 1H, $H_{\beta\text{-}}$), 9.39 (d, J = 4.4 Hz, 1H, $H_{\beta\text{-}}$), 10.36 (s, 1H, H_{meso}), 10.43 (s, 1H, H_{meso}); ^{13}C NMR (150 MHz, $CDCl_3$): δ = 157.5, 155.5, 153.3, 152.5, 151.7, 151.4, 150.9, 150.6, 139.1, 139.0, 138.6, 137.7, 137.6, 136.3, 135.7, 135.5, 134.6, 134.4, 133.9, 133.6, 133.5, 132.9, 128.8, 128.3, 127.7, 127.5, 126.3, 125.0, 124.1, 123.4, 110.8, 110.8, 108.1, 108.1, 32.9, 32.9, 21.7, 21.7 ppm; UV-vis ($CHCl_3$): λ_{max} (log ε) = 428

(5.17),442 (5.11), 549 (3.84), 594 (3.91), 641 (3.48); HRMS (MALDI) *m/z* calcd. for $C_{35}H_{28}N_4$ $[M^+H]^+$: 505.2392, found 505.2415. A second fraction yielded a green solid of the title salt (2.4 mg, 0.0046 mmol, 5%). M.p. >350 °C; R_f = 0.72 (SiO_2, CH_2Cl_2:MeOH = 9:1, *v:v*); ^{1}H NMR (600 MHz, $CDCl_3$, 25 °C): δ = -5.42 (s, 6H, *N*-CH_3), -2.44 (s, 1H, *N*-*H*), 2.74 (s, 3H, C$H_{3\text{-aryl}}$), 2.79 (s, 3H, C$H_{3\text{-aryl}}$), 7.67 (d, *J* = 7.5 Hz, 2H, H_{aryl}), 7.89 (d, *J* = 7.5 Hz, 2H, H_{aryl}), 8.07 (d, *J* = 7.7 Hz, 2H, H_{aryl}), 8.35 (d, *J* = 4.5 Hz, 2H, $H_{\beta\text{-}}$), 8.55 (d, *J* = 7.8 Hz, 2H, H_{aryl}), 8.88 (d, *J* = 4.6 Hz, 2H, $H_{\beta\text{-}}$), 9.09 (d, *J* = 4.6 Hz, 2H, $H_{\beta\text{-}}$), 9.58 (d, *J* = 4.6 Hz, 2H, $H_{\beta\text{-}}$), 10.78 ppm (s, 2H, H_{meso}); ^{13}C NMR (150 MHz, $CDCl_3$): δ = 153.4, 152.5, 152.0, 147.2, 142.0, 139.0, 138.9, 136.7, 136.3, 135.8, 135.1, 133.5, 130.6, 128.8, 123.2, 122.0, 121.8, 109.7, 38.3, 21.8, 21.8, 21.6 ppm; UV-vis ($CHCl_3$): λmax (log ε) = 437 (5.32), 538 (3.85), 579 (4.10), 681 nm (3.76); IR (ATR): $\tilde{\nu}$ = 3656, 2981, 2918, 1605, 1493, 1457, 1381, 1299, 1240, 1222, 1183, 1149, 1078, 1028, 963, 809, 721, 705, 633, 571 cm^{-1}; HRMS (MALDI) *m/z* calcd. for $C_{36}H_{31}N_4$ $[M]^+$: 519.2549, found 519.2557.

6.3 Catalytic screening

All reactions were carried out in screw-cap 1 mL vials under a protective argon atmosphere. All solvents used were degassed and dried over Al_2O_3. Screening in diluted conditions was set up in 5 mL round-bottomed flasks. The nucleophile (1.1 eq.), catalyst (3 mol %) and Michael acceptor (1 eq.) were dissolved in the appropriate solvent and the mixture was stirred in the dark at rt for 24 h. For each reaction a blank sample without catalyst was set up, too. At the end of each reaction, the internal standard (CH_2Br_2, 0.5 eq.) was added to the reaction mixture and a ^{1}H NMR spectrum was recorded. The conversion was determined *via* quantitative ^{1}H NMR using an internal standard by comparison of the product integrals with the integrals of the internal standard.

Kinetic measurements: Porphyrin **21** and compound **165** were mixed in the corresponding ratio and dissolved in CD_2Cl_2. The NMR spectra were recorded at a frequency of 600.13 MHz.

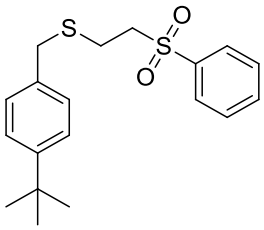

4-(tert-butyl)benzyl)(2-(phenylsulfonyl)ethyl)sulfane 165:
Vinyl phenyl sulfone **160** (370 mg, 1.61 mmol) and 4-*tert*-butylbenzyl mercaptan **164** (300 µL, 1.61 mmol) were dissolved in dry and degassed CH_2Cl_2. DBU (24.5 µL, 0.161 mmol, 10 mol %) was then added and the reaction was stirred at rt for 24 h. The solvent was evaporated and the product was purified with a 2M sodium hydroxide solution followed by recrystallization from hot hexane, yielding a white solid of compound **165** (200 mg, 0.539 mmol, 34%). M.p. = 63.9–66.5°C; R_f = 0.4 (SiO_2, CH_2Cl_2:EtOAc = 8:2, v/v); ^{1}H NMR (400 MHz, $CDCl_3$, 25 °C): δ = 1.33 (s, 9H, *tert*-butyl), 2.73 (m, 2H, S-*CH*$_2$CH$_2$), 3.23-3.13 (m, 2H, S-CH$_2$*CH*$_2$), 3.66 (s, 2H, Ar-CH$_2$-S), 7.12 (d, J = 8.3 Hz, 2H, CH_{aryl}), 7.29–7.26 (m, 2H, CH_{aryl}), 7.59 (t, J = 7.7 Hz, 2H, CH_{aryl}), 7.70 (t, J = 7.5 Hz, 1H, CH_{aryl}), 7.87 ppm (dd, J = 8.4Hz, 2H, CH_{aryl}); ^{13}C NMR (100 MHz, $CDCl_3$, 25 °C): δ = 150.4, 138.8, 134.8, 134.3, 133.9, 129.4, 128.5, 128.2, 125.7, 55.9, 36.1, 34.5, 31.3, 23.8 ppm; IR: ν_{max} (neat): 2958, 1447, 1316, 1304, 1286, 1206, 1148, 1120, 1083, 848, 834, 793, 751, 741, 720, 686, 657, 552 cm^{-1}; HRMS (ESI) *m/z* calcd. for $C_{19}H_{25}O_2S_2$ $[M+H]^+$: 349.1290, found 349.1286.

6.4 X-ray Crystallography

Crystal Structure Determinations: Crystals were grown following the protocol developed by Hope, by dissolving the compounds in CH_2Cl_2, layering with methanol or hexane and allowing for slow diffusion over time. In some cases, this was aided by slow evaporation once the layers had mixed completely.[246] Diffraction data for all compounds were collected on a Bruker APEX 2 DUO CCD diffractometer by using graphite-monochromated MoK_α radiation (λ = 0.71073 Å) and Incoatec IμS CuK_α radiation (λ = 1.54178 Å). Crystals were mounted on a MiTeGen MicroMount and collected at 100(2) K by using an Oxford Cryosystems Cobra low-temperature device. Data were collected by using omega and phi scans and were corrected for Lorentz and polarization effects by using the APEX software suite.[247] The structures were solved with Direct Methods and refined against $|F_2|$ with XL using least squares minimization.[248] Non-hydrogen atoms were refined with anisotopical thermal parameters. Hydrogen atoms were generally placed into geometrically calculated positions and refined using a riding model. The *N*-H hydrogen atoms were located using different maps and refined using the standard riding model. All images were prepared by using Mercury CSD 2.0[249] or Olex2.[248a]

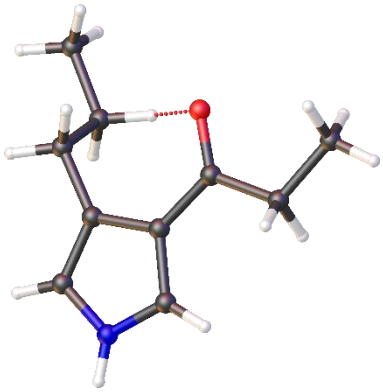

Crystal data for 2,3,7,8,12,13,17,18-octapropyl-5,10,15,20-tetraphenylporphyrin 69: $C_{10}H_{15}NO$, M = 125.23 g/mol, triclinic, space group $P\bar{1}$, a = 7.2447(8) Å, b = 7.3296(7) Å, c = 10.1604(10) Å, α = 83.556(3) °, β = 77.452(4) °, γ = 69.537(4) °, V = 493.02(9) Å^3, Z = 2, T = 200(2) K, μ(MoKα) = 0.072 mm^{-1}, *Dcalc* = 1.113 g/cm^3, 5679 reflections measured (2.969° ≤ 2Θ ≤ 27.624°), 2294 unique (R_{int} = 0.0314, R_{sigma} = 0.0405) which were used in all calculations. The final R_1 was 0.0448 (I > 2σ(I)) and wR_2 was 0.1106 (all data). Donor hydrogen H1 located on the difference map and refined with restraints (DFIX).

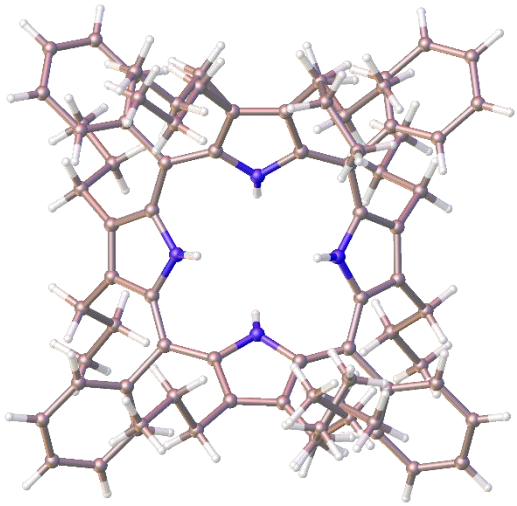

Crystal data for 2,3,7,8,12,13,17,18-octapropyl-5,10,15,20-tetraphenylporphyrin 55·CH_3CO_2H: $C_{79}H_{100}N_4O_{11}$, M = 1281.62 g/mol, triclinic, space group $P\bar{1}$, a = 13.1824(6) Å, b = 13.6365 Å, c = 21.9808(10) Å, α = 77.8193(19)°, β = 78.461(2)°, γ = 71.6571(18)°, V = 3627.9(3) $Å^3$, Z = 2, T = 100(2) K, μ(MoKα) = 0.078 mm^{-1}, *Dcalc* = 1.173 g/cm^3, 60629 reflections measured (2.338° ≤ 2Θ ≤ 26.498°), 14991 unique (R_{int} = 0.1070, R_{sigma} = 0.0993) which were used in all calculations. The final R_1 was 0.0733 (I > 2σ(I)) and wR_2 was 0.1661 (all data). Three ethyl groups are disordered and are modelled in two positions (C71C72C73; C82C83) with 56:44; 69:31 occupancies. One ethyl was modelled in three positions (C172C173) with 49:30:21% occupancies. Restraints used in modelling this disorder: DFIX, SADI, SIMU and SUMP for the three part disorder. One acetic acid molecule was modelled in two positions with 72:28% occupancy using restraints (DFIX, SIMU). Hydrogen atoms on acid moieties were located on the difference map and refined using restraints (DFIX). One acetic acid is disordered over the inversion and was modelled at 50% occupancy using a rigid group with restraints (SIMU).

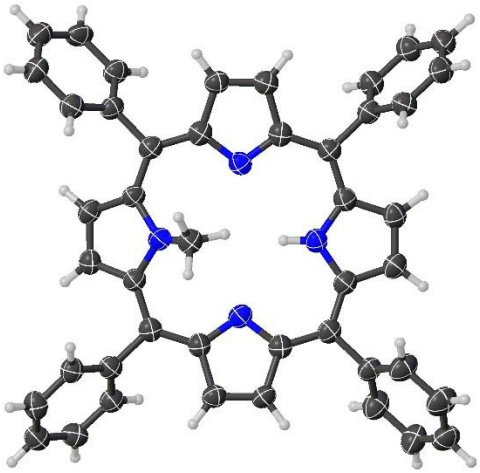

Crystal data for *N*^{21}-monomethyl-5,10,15,20-tetraphenylporphyrin 26m: $C_{45}H_{32}N_4$, M = 628.74 g/mol, triclinic, space group $P\bar{1}$, a = 13.7893(7) Å, b = 14.9069(8) Å, c = 19.3164(10)Å, α = 108.234(2)°, β = 108.234(2)°, γ = 101.614(3)°, V = 3620.5(3) Å^3, Z = 4, T = 100(2) K, μ(MoKα) = 0.526 mm^{-1}, *Dcalc* = 1.154 g/cm^3, 36917 reflections measured (7.464° ≤ 2Θ ≤ 136.972°), 12845 unique (R_{int} = 0.0676, R_{sigma} = 0.0760) which were used in all calculations. The final R_1 was 0.0779 (I > 2σ(I)) and wR_2 was 0.2187 (all data). Solvent molecules (H_2O) in the structure was squeezed using platon squeeze as no reliable solution could be modelled. Large K value in the Analysis of Variance is associated to the very weak reflections in the high angle data. Low bond precision on c-c bonds is associated to the very weak reflections in the high angle data. Missing reflection are associated with only 97.3% of collected data.

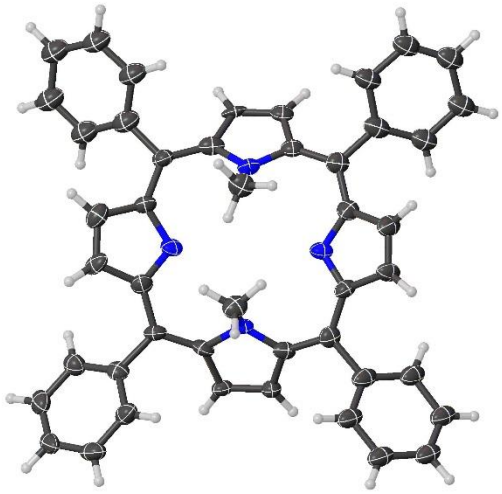

Crystal data for N^{21},N^{23}-dimethyl-5,10,15,20-tetraphenylporphyrin 26d: $C_{92}H_{68}N_8$, *M* =1285.54 g/mol, monoclinic, space group P 1 n 1, *a* = 14.7319(11) Å, *b* = 12.3812(9) Å, *c* = 24.5671(18) Å, *α* = 90°, *β* = 107.071(2) °, *γ* = 90°, *V* = 4283.6(5) Å^3, *Z* = 4, *T* = 100.0 K, μ(MoKα) = 0.059 mm^{-1}, *Dcalc* = 0.997 g/cm^3, 87949 reflections measured (1.451° ≤ 2Θ ≤ 25.380°), 15670 unique (R_{int} = 0.0412, R_{sigma} = 0.0327) which were used in all calculations. The final R_1 was 0.0717 (I > 2σ(I)) and wR_2 was 0.1960 (all data). The structure was refined as a 2-component inversion twin. Phenyl rings (C151_1>C156_1, C101_2 > C106_2, C101_1>C106_1, C51_1>C56_1, C151_2> C156_2, C51_2>C56_2) were fixed using the restraint (SIMU). The alpha and beta carbons (C18 C17 C16) were fixed using the restraint (SIMU). Solvent molecules (H_2O) in the structure was squeezed using platon squeeze as no reliable solution could be modelled. Large K value in the Analysis of Variance is associated to the very weak reflections in the high angle data.

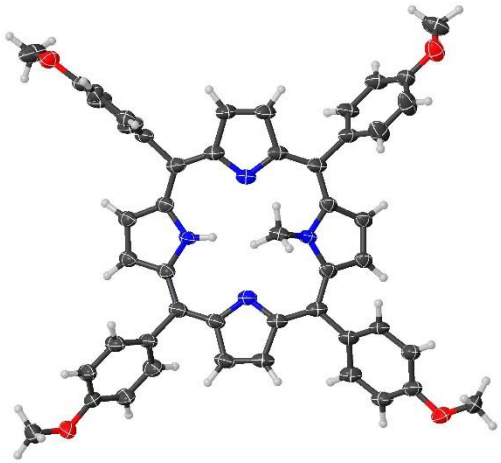

Crystal data for *N*^{21}-monomethyl-5,10,15,20-tetrakis(4-methoxyphenyl)porphyrin 112m: $C_{49}H_{40}N_4O_4$, *M* = 748.85 g/mol, monoclinic, space group P 1 21/c 1, *a* = 13.818(7) Å, *b* = 15.957(9) Å, *c* = 20.117(11) Å, *α* = 90°, *β* = 92.552(14)°, *γ* = 90°, *V* = 4431(4) Å^3, *Z* = 4, *T* = 100(2) K, μ(MoKα) = 0.072 mm^{-1}, *Dcalc* = 1.122 g/cm^3, 119390 reflections measured (1.951° ≤ 2Θ ≤ 26.453°), 9059 unique (R_{int} = 0.0400, R_{sigma} = 0.0168) which were used in all calculations. The final R_1 was 0.0615 (I > 2σ(I)) and wR_2 was 0.1384 (all data). The pyrrole units at N21 and N23 were modelled over two positions in an 80:20 % occupancy using restraints (SADI, DFIX, and SIMU). The methoxy group O1−C57 was modelled over two positions in an 80:20 % occupancy using restraints (SADI and SIMU). Solvent molecules (H_2O, $CDCl_3$) in the structure were squeezed using platon squeeze as no reliable solution could be modelled. Large K value in the analysis of variance is associated to the very weak reflections in the high angle data.

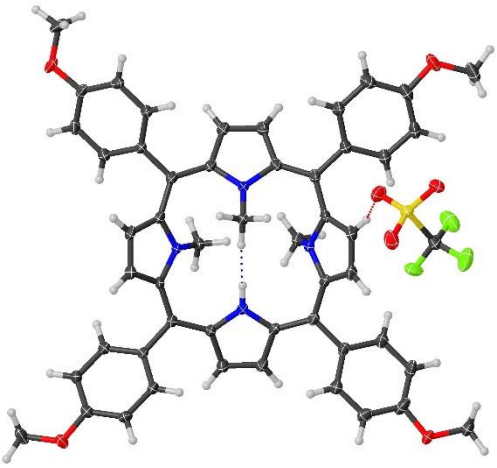

Crystal data for N^{21},N^{22},N^{23}-trimethyl-5,10,15,20-tetrakis(4-methoxyphenyl)porphyrin [112t]$^+$[CF_3SO_3]: $C_{52}H_{46}F_3N_4O_7S$, *M* = 927.99 g/mol, monoclinic, space group P 1 21/c 1, *a* = 16.1055(6) Å, *b* = 8.0297(3) Å, *c* = 34.4166(14) Å, *α* = 34.4166(14) °, *β* = 90°, *γ* = 102.3050(10)°, *V* = 4348.6(3) Å^3, *Z* = 4, *T* = 100(2) K, μ(MoKα) = 0.149 mm^{-1}, *Dcalc* = 1.417 g/cm^3, 66623 reflections measured (2.608° ≤ 2Θ ≤ 25.498°), 8092 unique (R_{int} = 0.1140, R_{sigma} = 0.0496) which were used in all calculations. The final R_1 was 0.0521 (I > 2σ(I)) and wR_2 was 0.1289 (all data). The structure was solved containing one unit in the asymmetric cell one trifluoromethanesulfonate solvate. The structure was modelled over two positions at C26 (C26A) in an 80:20% occupancy. No restraints or constraints were necessary. The trifluoromethanesulfonate solvate was modelled over two positions in an 80:20% occupancy using similarity restraint (SIMU) and similar distances restraint. The C and N bound H atoms were placed in their expected calculated positions and refined as riding model: N—H = 0.88 Å, C—H = 0.95–0.98 Å, with U_{iso}(H) = 1.5U_{eq}(C) for methyl H atoms and 1.2U_{eq} (C, N) for all other atoms other H atoms.

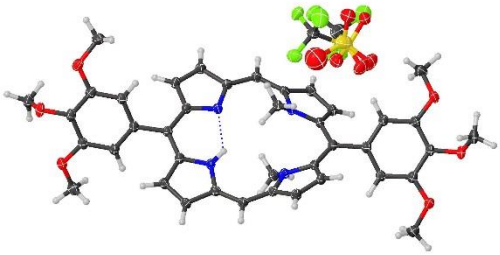

Crystal data for N^{23},N^{24}-dimethyl-5,15-di(3,4,5-trimethoxyphenyl)porphyrin [115d]$^{+}$ [CF_3SO_3]: $C_{41}H_{39}F_3N_4O_9S$, M = 820.82 g/mol, monoclinic, space group P 1 21/c 1, a = 7.6298(3) Å, b = 29.1766(9) Å, c = 19.2119(6) Å, α = 90°, β = 95.085(2)°, γ = 90°, V = 4260.0(3) Å^3, Z = 4, T = 100(2) K, μ(MoKα) = 1.277 mm^{-1}, *Dcalc* = 1.280 g/cm^3, 50790 reflections measured (2.761° ≤ 2Θ ≤ 66.741°), 7526 unique (R_{int} = 0.0628, R_{sigma} = 0.0357) which were used in all calculations. The final R_1 was 0.0490 (I > 2σ(I)) and wR_2 was 0.1351 (all data). The structure was solved containing one unit in the asymmetric cell one trifluoromethanesulfonate solvate. The trifluoromethanesulfonate solvate was modeled over two positions (75:25% occupancy) using restraints (SIMU and ISOR). Solvent molecules (DCM) in the structure was squeezed using platon squeeze as no reliable solution could be modeled. The C and N bound H atoms were placed in their expected calculated positions and refined as riding model: N–H = 0.88 Å, C–H = 0.95–0.98 Å, with U_{iso}(H) = 1.5U_{eq}(C) for methyl H atoms and 1.2U_{eq} (C, N) for all other atoms other H atoms. Large K value in the analysis of variance is associated with the very weak reflections in the high angle data. Missing reflection is associated with only 99.9% of collected data.

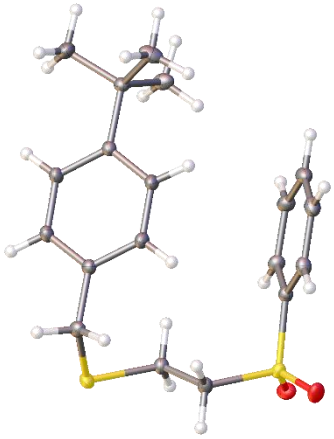

Crystal Data for 4-(tert-butyl)benzyl)(2-(phenylsulfonyl)ethyl)sulfane 164: $C_{19}H_{24}O_2S_2$, *M* =348.50 g/mol, triclinic, space group P-1 (no. 2), *a* = 9.1874(2) Å, *b* = 10.2925(2) Å, *c* = 19.9859(4) Å, *α* = 79.1780(10)°, *β* = 86.4240(10)°, *γ* = 76.4260(10)°, *V* = 1804.10(6) Å^3, *Z* = 4, *T* = 100.01 K, μ(MoKα) = 0.302 mm^{-1}, *Dcalc* = 1.283 g/cm^3, 235120 reflections measured (4.138° ≤ 2Θ ≤ 71.696°), 16812 unique (R_{int} = 0.0253, R_{sigma} = 0.0100) which were used in all calculations. The final R_1 was 0.0311 (I > 2σ(I)) and wR_2 was 0.0892 (all data). The structure was solved with two molecules in the asymmetric unit. The second of these molecules contained a disordered tert-butyl group C1 (a-c) to C3 (a-c). This disordered moiety was modelled over three positions in a 40:40:20% occupancy using the restraint (ISOR).

6.5 NSD Analysis

NSD calculations were performed by Dr. K. J. Flanagan.

The theoretical background and development of this method have been described by Shelnutt *et al*.[1,27b,40d,67a] NSD is a conceptually simple method that employs the decomposition of the conformation of the macrocycle by a basis set composed of its various normal modes of vibration, affording clear separation of the contributing distortions to the macrocycle conformation in a quantitative fashion. For calculations, the NSD engine program established by Shelnutt was used.[250]

REFERENCES

[1] M. O. Senge, S. A. MacGowan, J. M. O'Brien, *Chem. Commun.*, **2015**, *51*, 17031–17063.

[2] J. L. W. Thudichun, *Rep. Med. Privy Counc*. **1867**, *10*, 152–152.

[3] W. S. Caughey, J. A. Ibers, *J. Am. Chem. Soc*., **1977**, *99*, 6639–6645; b) J. A. Ballantine, A. F. Psaila, A. Pelter, P. Murray-Rust, V. Ferrito, P. Schembri, V. Jaccarini*, J. Chem. Soc., Perkin Trans. 1*, **1980**, 1080–1089; c) P. R. Ortiz de Montellano, K. L. Kunze, B. A. Mico, *Molec. Pharmacol*., **1980**, *18*, 602–605; d) K. L. Kunze, P. R. Ortiz de Montellano, *J. Am. Chem. Soc*., **1981**, *103*, 4225–4230.

[4] a) M. F. Perutz, *Proc. R. Soc. Lond. B., Biol.*, **1980**, *208*, 135–162; b) P. R. Ortiz de Montellano, *Ann. Rep. Med. Chem.*, **1984**, *19*, 201–211; c) A. Forman, M. W. Renner, E. Fujita, K. M. Barkigia, M. C. W. Evans, K. M. Smith, J. Fajer, *Isr. J. Chem.*, **1989**, *29*, 57–64; d) R. Huber, *Eur. J. Biochem.*, **1990**, *187*, 283–305; e) M. Bixon, J. Fajer, G. Feher, J. H. Freed, D. Gamliel, A. J. Hoff, H. Levanon, K. Möbius, R. Nechushtai, J. R. Norris, A. Scherz, J. L. Sessler, D. Stehlik, *Isr. J. Chem.,* **1992**, *32*, 369–371; f) M. O. Senge, *J. Photochem. Photobiol. B: Biol*., **1992**, *16*, 3–36.

[5] H.A. Dailey, T.A. Dailey in *The Porphyrin Handbook, Vol 12* (Eds: K.M. Kadish, K.M. Smith, R. Guilard), Academic Press, New York, **2003**, pp 93–121.

[6] P. Karlson, *J. Clin. Chem. Clin. Bio.*, **1981**, *19*, 43–47.

[7] G. P. Moss, *Pure Appl. Chem.*, **1987**, *59*, 779–832.

[8] W. Küster, *Ber. Dtsch. Chem. Ges.*, **1912**, *45*, 1935-1946.

[9] D. Wöhrle, *Adv. Mater.*, **1997**, *9*, 1191–1192.

[10] M. O. Senge, *Chem. Commun.*, **2011**, *47*, 1943–1960.

[11] P. Rothemund, *J. Am. Chem. Soc*., **1935**, *57*, 2010–2011.

[12] A. D. Adler, F. R. Longo, W. Shergalis, *J. Am. Chem. Soc*., **1964**, *86*, 3145–3149.

[13] A. D. Adler, F. R. Longo, J. D. Finarelli, J. Goldmacher, J. Assour, L. Korsakoff, *J. Org. Chem.*, **1967**, *32*, 476–476.

[14] K. Rousseau, D. Dolphin, *Tetrahedron Lett.*, **1974**, *48*, 4251–4254.

[15] a) R. G. Little, J. A. Anton, P. A. Loach, J. A. Ibers, *J. Heterocycl. Chem.*, **1975**, *12*, 343–349; b) R.G. Little, *J. Heterocyclic Chem.,* **1981**, *18*, 129–133.

[16] a) J. S. Lindsey, in *The Synthesis of Meso-Substituted Porphyrins, Vol 17,* (Eds: F. Montanari, L. Casella) , Springer, Dordrecht, **1994**, pp 49–86.

[17] a) S. W. Staley, B. Eliasson, P.C. Kearney, I. C. Schreiman, J.S. Lindsey, in *Molecular Electronic Devices* (Eds. F.L. Carter, R.E. Siatkowski, H. Wohltjen), Elsevier Science Publishers B.V., Amsterdam, **1988**, pp. 543–554.

[18] a) J. S. Lindsey, in *The Porphyrin Handbook, Vol. 1* (Eds.: K. M. Kadish, K. M. Smith, R. Guilard), Academic Press, New York, **2000**, pp. 45–118; b) J. S. Lindsey, *Acc. Chem. Res*., **2010**, *43*, 300–311.

[19] a) B. J. Littler, Y. Ciringh, J. S. Lindsey, *J. Org. Chem.,* **1999**, *64*, 2864–2872; b) P. D. Rao, S. Dhanalekshmi, B. J. Littler, J. S. Lindsey, *J. Org. Chem.*, **2000**, *65*, 7323–7344; c) J. K. Laha, S. Dhanalekshmi, M. Taniguchi, A. Ambroise, J. S. Lindsey, *Org. Proc. Res. Dev*., **2003**, *7*, 799–812.

[20] a) S. Plunkett, M. O. Senge, *ECS Trans.,* **2011**, *35*, 147–157; b) A. Wiehe, Y. M. Shaker, J. C. Brandt, S. Mebs, M. O. Senge, *Tetrahedron,* **2005**, *61*, 5535–5564, c) A. Treibs, N. Häberle, *Liebigs Ann*. *Chem.*, **1968**, 183–207.

[21] a) A. Wiehe, C. Ryppa, M. O. Senge, *Org. Lett.,* **2002**, *4*, 3807–3809; b) S. Hatscher, M. O. Senge, *Tetrahedron Lett.*, **2003**, *44*, 157–160.

[22] H. Ogoshi, H. Sugimoto, T. Nishiguchi, T. Watanabe, Y. Matsuda, Z.Yoshida, *Chem. Lett.,* **1978**, *7*, 29–32.

[23] J. S. Manka, D. S. Lawrence, *Tetrahedron Lett.,* **1989**, *30*, 6989–6992.

[24] R. P. Briñas, C. Brückner, *Tetrahedron*, **2002**, *58*, 4375–4381.

[25] M. Paoli, J. Marles-Wright, A. Smith, *DNA Cell Biol*., **2002**, *21*, 271– 280.

[26] S. R. Yeh, S. Han, D. L. Rousseau, *Acc. Chem. Res*., **1998**, *31*, 727–736.

[27] a) A. M. Berghuis, G. D. Brayer, *J. Mol. Biol*. **1992**, *223*, 959–976; b) W. Jentzen, X. Z. Song, J. A. Shelnutt, *J. Phys. Chem. B,* **1997**, *101*, 1684–1699.

[28] S. E. J. Bowman, K. L. Bren, *Nat. Prod. Rep*., **2008**, *25*, 1118–1130.

[29] J. A. Hodge, M. G. Hill, H. B. Gray, *Inorg. Chem*., **1995**, *34*, 809–812.

[30] a) P. A. Arnold, D. R. Benson, D. J. Brink, M. P. Hendrich, G. S. Jas, M. L. Kennedy, D. T. Petasis, M. Wang, *Inorg. Chem*., **1997**, *36*, 5306–5315; b) A. B. Cowley, M. L. Kennedy, S. Silchenko, G. S. Lukat-Rodgers, K. R. Rodgers, D. R. Benson, *Inorg. Chem*., **2006**, *45*, 9985–10001.

[31] a) M. F. Perutz, *Nature,* **1979**, *228*, 726–734; b) R. van Grondelle, J. P. Dekker, T. Gillbro, V. Sundstrom, *Biochim. Biophys. Acta,* **1994**, *1187*, 1–65.

[32) A. Freer, S. Prince, K. Sauer, M. Papiz, A. Hawthornthwaite-Lawless, G. McDermott, R. Cogdell, N. W. Isaacs, *Structure*, **1996**, *4*, 449–462.

[33] a) J. P. Collman, R. R. Gag, C. A. Reed, *J. Am. Chem. Soc.*, **1974**, *96*, 2629–2631;b) J. P. Collman, R. R. Gagne, C. A. Reed, T. R. Halbert, G. Lang, W. T. Robinson, *J. Am. Chem. Soc.*, **1975**, *97*, 1427–1439; c) J. P. Collman, J. I. Brauman, E. Rose, K. S. Suslick, *Proc. Nati. Acad. Scf. USA*, **1978**, *75*, 1052–1055; d) J. M. Burke, J. R. Kincaid, S. Peters, R. R. Gagne, J. P. Collman, T. G. Spiro; *J. Am. Chem. Soc.*, **1978**, *100*, 6083–6088; e) J. P. Colmann, L. Fu, *Acc. Chem. Res.*, **1999**, *32*, 455–463.

[34] a) B. Morgan, D. Dolphin, in *Synthesis and Structure of Biomimetic Porphyrins*, *Vol. 64* (Eds: J. W. Buchler), Springer, Berlin, Heidelberg; **1987**, pp 115–203 b) J. A. Lukin, C. Ho, *Chem. Rev.*, **2004**, *104*, 1219–1230.

[35] a) Y. Yuan, M. F. Tam, V. Simplaceanu, C. Ho, *Chem. Rev*., **2015**, *115*, 1702–1724; b) M. Bringas, A. A. Petruk, D. A. Estrin, L. Capece, M. A. Marti, *Nature*, *Scientific reports*, **2017,** *Article 10926*.

[36] a) W. A. Eaton, E. R. Henry, J. Hofrichter, A. Mozzarelli, *Nat. Struct. Mol. Biol.,* **1999**, *6*, 351–358; b) W. A. Eaton, E.R. Henry , J. Hofrichter, S. Bettati , C. Viappiani , A. Mozzarelli, *IUBMB Life*, **2007**, *59*, 586–599.

[37] a) O. H. W. Kao, J. H. Wang, *Biochemistry*, **1965**, *4,* 342–347; b) G. S. Hammond, C H. S. Wu, *Adv. Chem. Ser*., **1968**, *77*, 186–207; c) I. A. Cohen, W. S. Caughey, *Biochemistry*, **1968**, *7,* 636–641; d) D. Brault, M. Rougee, *Biochemistry.*, **1974**, *13,* 4598–4602; e) D. Brault, M. Rougee, *Biochemistry*, **1974**, *13,* 4591–4597; f) G. C. Wagner, R. J. Kassner, *J. Am. Chem. Soc.*, **1974**, *96,* 5593–5595 ; g) W. S. Brinigar, C K. Chang, *J. Am. Chem. Soc.*, **1974**, *96,* 5595–5597; h) D. L. Anderson, C J. Weschler, F. Basolo,: *J. Am. Chem. Soc.*, **1974**, *96,* 5599–5600; i) J. Almog, J. E. Baldwin, R. L. Dyer, J. Huff, C J. Wilkerson, *J. Am. Chem. Soc.*, **1974**, *96,* 5600–5601; j) W. R. Scheidt, C A. Reed, *Chem. Rev.,* **1981**, *81,* 543–555; k) L. Latos-Grazynski, R. J. Cheng, G. N. La Mar, A. L. Balch, *J. Am. Chem. Soc.*, **1982**, *104,* 5992–6000.

[38] a) E. B. Fleischer, T. S. Srivastava, *J. Am. Chem. Soc*., **1969**, *91*, 2403–2405; b) C. Maricondi, W. Swift, D. K. Straub, *J. Am. Chem. Soc.*,**1969** *91*, 5205–5210; c) A. B. Hoffman, D. M. Collins, V. W. Day, E. B. Fleischer, T. S. Srivastava, J. L. Hoard, *J. Am. Chem. Soc.*, **1972**, *94*, 3620–3626.

[39] a) J. Almog, J. E.Baldwin, R. L. Dyer, M. Peters, *J. Am. Chem. Soc.,* **1975***, 97,* 226–227; b) H. Ogoshi, H. Sugimoto, Z. Yoshida, *Tetrahedron Lett*., **1976**, 4481–4484; c) H. Ogoshi, H. Sugimoto, Z. Yoshida, *Tetrahedron Lett.*, **1977**, *18*, 1515–1518; d) J. P. Collman, J. I., Brauman, K. M. Doxsee, *Proc. Natl. Acad. Sci.*,**1979**, *76,* 6035–6039; e) M. Momenteau. B. Loock, J. Mispelter, E. Bisagni, *Nouv. J. Chem.,* **1979***, 3,* 77–79; f) W. B. Cruse, O. Kennard. G. M. Sheldrick, A. D. Hamilton. S. G. Hartley, A. R. Battersby, *J. Chem. Soc, Chem. Commun.*, **1980**, 700–701; g) J. S. Lindsey, D. C. Mauzerall. H. Linschitz, *J. Am. Chem. Soc.*, **1983**, *105,* 6528–6529; h) M. Momenteau. J. Mispclter. B. Loock. E. Bisagni. *J. Chem. Soc. Perkin Trans. 1*, **1983**, 189–196.

[40] a) M. O. Senge, in *The Porphyrin Handook*, *Vol. 1*, (Eds: K. M. Smith, K. M. Kadish, R. Guilard) Academic Press, New York, **2000**, pp. 239–347; b) R. E. Haddad, S. Gazeau, J. Pecaut, J.-C. Marchon, C. J. Medforth, J. A. Shelnutt, *J. Am. Chem.Soc.*, **2003**, *125*, 1253–1268; c) J. A. Shelnutt, X. Z. Song, J. G. Ma, S. L. Jia, W. Jentzen, C. J. Medforth, *Chem. Soc. Rev.*, **1998**, *27*, 31–42; d) W. Jentzen, J. Ma, J. A. Shelnutt, *Biophys. J.*, ***1998***, *74*, 753–763.

[41] S. A. MacGowan, M. O. Senge, *Chem. Commun.*, **2011**, *47*, 11621–11623.

[42] a) M. O. Senge, V. Gerstung, K. Ruhlandt-Senge, S. Runge, I. Lehmann, *J. Chem. Soc. Dalton Trans.* **1998**, 4187–4200; b) M. O. Senge, W. W. Kalisch, *Inorg. Chem.* **1997**, *36*, 6103–6116; c) M. O. Senge, J. Richter, I. Bischoff, A. Ryan, *Tetrahedron,* **2010**, *66*, 3508–3524.

[43] a) R. G. Alden, M. R. Ondrias, J. A. Shelnutt, *J. Am. Chem. Soc.*, **1990**, *112*, 691–697; b) J. A. Shelnutt, *J. Phys. Chem.*, **1989**, *93*, 6283–6290; c) J. A. Shelnutt, C. J. Medforth, M. D. Berber, K. M. Barkigia, K. M. Smith, *J. Am. Chem. Soc.*, **1991**, *113*, 4077–4087; d) L. D. Sparks, C. J. Medforth, M. S. Park, J. R. Chamberlain, M. R. Ondrias, M. O. Senge, K. M. Smith, J. A. Shelnutt, *J. Am. Chem. Soc.*, **1993**, *115*, 581–592; e) K. K. Anderson, J. D. Hobbs, L. A. Luo, K. D. Stanley, J. M. E. Quirke, J. A. Shelnutt, *J. Am. Chem. Soc.*, **1993**, *115*, 12346–12352; f) X. Z. Song, W. Jentzen, S. L. Jia, L. Jaquinod, D. J. Nurco, C. J. Medforth, K. M. Smith, J. A. Shelnutt, *J. Am. Chem. Soc.*, **1996**, *118*, 12975–12988.

[44] M. O. Senge, *Chem. Commun.* **2006**, 243–256.

[45] A. M. Santoro, M. C. Lo Giudice, A. D'Urso, R. Lauceri, R. Purrello, D. Milardi, *J. Am. Chem. Soc.,* **2012**, *134*, 10451–10457; b) Z. Valicsek, O. Horváth, *Microchem. J.,* **2013**, *107*, 47–62.

[46] a) E. B. Fleischer, *J. Am. Chem. Soc.*,**1963**, *85*, 1353–1354; b) M. J. Hamor, T. A. Hamor, J. L. Hoard, *J. Am. Chem. Soc.*, **1964**, *86*, 1938–1942; c) E. B. Fleischer, C. K. Miller, L. E. Webb, *J. Am. Chem. Soc.*, **1964**, *86*, 2342–2347.

[47] O. A. Golubchikov, S .G. Pukhovskaya, E. M. Kuv-Shinova, *Russ. Chem. Rev*., **2005**, *74*, 249–264.

[48] a) A. Stone, E. B. Fleischer, *J. Am. Chem. Soc*. **1968**, *90*, 2735–2748; b) M. O. Senge, *Z. Naturforsch. B*, **2000**, *55b*, 336–344.

[49] D. K. Lavallee, *The Chemistry and Biochemistry of N-Substituted Porphyrins*, VCH Publishers, Inc., New York, **1987**.

[50] a) A. Neuberger, J. J. Scott, *Proc*. *R*. *Soc*. *Lond. A: Math*. *Phys*. *Sc*i., **1952**, *213*, 307–326; b) S. Pukhoskaya, Y. Ivanova, D. The Nam, A. Vashurin, O. Golubchikov, *J. Porphyr. Phthalocya.*, **2015**, *19*, 858–864.

[51] a) M. O. Senge, *Z. Naturforsch. B* **1999**, *54*, 821–824; b) J. Takjeda, M. Sato, *Chem. Lett.*, **1995**, *11*, 971–972.

[52] a) R. E. Oakes, S. J. Spence, S. E. J. Bell, *J. Phys. Chem. A*, **2003**, *107*, 2964–2973; b) M. O. Senge, T. Ema, K. M. Smith, *J. Chem. Soc*., *Chem. Commun*., **1995**, 733–734.

[53] M. O. Senge, *J. Porphyr. Phthalocya*, **1999**, 3, 216–223.

[54] J. S. Lindsey, H. C. Hsu, I. C. Schreiman, *Tetrahedron Lett.*, **1986**, *27*, 4969–4970.

[55] B. Evans, K. M. Smith, J. H. Fuhrhop, *Tetrahedron Lett.*, **1977**, *18*, 443–446.

[56] W. W. Kalisch, M. O. Senge, *Tetrahedron Lett.*, **1996**, *37*, 1183–1186.

[57] a) W. R. Scheidt, Y. J. Lee, in *Structure and Bonding Metal Complexes with Tetrapyrrole Ligands I* (Eds: J. W. Buchler), Springer Berlin Heidelberg, Berlin, Heidelberg, **1987**, pp. 1–70; b) K. M. Barkigia, M. D. Berber, J. Fajer, C. J. Medforth, M. W. Renner, K. M. Smith, *J. Am. Chem. Soc.*, **1990**, *112*, 8851–8857; c) A. Regev, T. Galili, C. J. Medforth, K. M. Smith, K. M. Barkigia, J. Fajer, H. Levanon, *J. Phys. Chem*, **1994**, *98*, 2520–2526.

[58] a) H. M. G. Al-Hazimi, A. H. Jackson, A. W. Johnson, M. Winter, *J. Chem. Soc., Perkin Trans. 1*, **1977**, 98–103.

[59] K. Norvaiša, K. J. Flanagan, D.Gibbons, M. O. Senge, *Angew. Chem. Int. Ed.*, **2019**, *58*, 1–6.

[60] M. O. Senge, M. W. Renner, W. W. Kalisch, J. Fajer, *J. Chem. Soc.*, *Dalton Trans.*, **2000**, 381–385.

[61] a) A. Forman, M. W. Renner, E. Fujita, K. M. Barkigia, M. C. W. Evans, K. M. Smith, J. Fajer, *Isr. J. Chem.,* **1989**, *29*, 57–64; b) H. E. Toma, K. Araki, *Coord. Chem. Rev.,* **2000**, *196*, 307–329; c) H. S. Cho, D. H. Jeong, M. C. Yoon, Y. H. Kim, Y. R. Kim, D. Kim, S. C. Jeoung, S. K. Kim, N. Aratani, H. Shinmori, A. Osuka, *J. Phys. Chem. A,* **2001**, *105*, 4200–4204; d) D. Kim, A. Osuka, *Acc. Chem. Res.,* **2004**, *37*, 735–745.

[62] a) R. J. Abraham, B. Evans, K. M. Smith, *Tetrahedron*, **1978**, *34*, 1213–1220; b) W. R. Scheidt, Y. J. Lee, *Struct. Bond. (Berlin)*, **1987**, *64*, 1–73; c) M. O. Senge, C. W. Eigenbrot, T. D. Brennan, J. Shusta, W. R. Scheidt, *Inorg. Chem.* **1993**, *32*, 3134–3142.

[63] a) S. Gentemann, C. J. Medforth, T. P. Forsyth, D. J. Nurco, K. M. Smith, J. Fajer, D. Holten, *J. Am. Chem. Soc.* **1994**, *116*, 7363–7368; b) M. W. Renner, K. M. Barkigia, Y. Zhang, C. J. Medforth, K. M. Smith, J. Fajer., *J. Am. Chem. Soc.*, **1994**, *116*, 8582–8592; c) P. Tagliatesta, J. Li, M. Autret, E. V. Caemelbecke, A. Villard, F. D'Souza, K. M. Kadish, *Inure. Chem.*, **1996**, *35*, 5570–5576; d) D. J. Norco, C. J. Medforth, T. P. Forsyth, M. M. Homestead, K. M. Smith, *J. Am. Chem. Soc.*, **1996**, *118*, 10918–10919; e) J. Faker, *J. Pep. Res.*, **2000**, *4*, 382–385.

[64] a) D. Dolphin, *J. Heterocyclic. Chem.*, **1970**, *7*, 275–283; b) J. Takeda, T. Ohio, M. Sato, *Inure. Chem.*, **1992**, *31*, 2877–2880; c) P. Harappa, M. Net haji, V. Krishnan, *Chem. Let.*, **1993**, *22*, 869–872; d) P. Ochsenbein, K. Ayougou, D. Mandon, J. Fissher, R. Weiss, R. N. Austin, K. Jayaraj, A. Gold, J. Terner, J. Fajer, *Angew. Chem. Int. Ed.*, **1994**, *33*, 348–350; e) K. M. Kadish, E. V. Caemelbecke, F. D'Souza, C. J. Medforth, K. M. Smith, A. Tabard, R. Guilard, *Inorg. Chem.*, **1995**, *34*, 2984–2989; f) A. B. J. Parusel, T. Wondimagegn, A. Ghosh, *J. Am. Chem. Soc.*, **2000**, *122*, 6371–6374.

[65] a) S. Gentemann, C. J. Medforth, T. Ema, N. Y. Nelson, K. M. Smith, J. Fajer, D. Holten, *Chem. Phys. Lett.*, **1995**, *245*, 441–447; b) C. M. Drain, C. Kirmaier, C. J. Medforth, D. J. Nurco, K. M. Smith, D. Holten, *J. Phys. Chem.*, **1996**, *100*, 11984–11993; c) S. Gentemann, N. Y. Nelson, L. Jaquinod, D. J. Nurco, S. H. Leung, C. J. Medforth, K. M. Smith, J. Fajer, D. Holten, *J. Phys. Chem. B*, **1997**, *101*, 1247–1254.

[66] a) W. L. Bragg, *Camb. Phil. Soc. Proc.*, **1912**, *17*, 43–57; b) W. L. Bragg, *Proc. R. Soc. Lond.*, **1913**, *A89*, 248–277; c) W. Friedrich, P. Snipping, M. Laue, **1912**, reprinted; d) P. Forman, *Arch. Hist. Exact Sci.*, **1969**, *6*, 38–71, e) M. Eckert, *Ann. Phys.*, **2012**, *524*, A83–A85.

[67] W. Jentzen, M. C. Simpson, J. D. Hobbs, X. Song, T. Ema, N. Y. Nelson, C. J. Medforth, K. M. Smith, M. Veyrat, *J. Am. Chem. Soc.*, **1995**, *117*, 11085–11097.

[68] *a)* M.O. Senge, W. W. Kalisch, *Z. Naturforsch, B: Chem. Sci*, **1999**, *54*, 943–959.

[69] a) M. O. Senge, C. J. Medforth, T. P. Forsyth, D. A. Lee, M. M. Olmstead, W. Jentzen, R. K. Pandey, J. A. Shelnutt, K. M. Smith, *Inorg. Chem.* **1997**, *36*, 1149–1163; b) M. O. Senge, K. Dahms, *Acta Cryst.,* **2014**, *E70*, m251; c) K. J. Flanagan, E. M. Mothi, L. Kötzner, M. O. Senge, *Acta Cryst.,* **2015**, *E71*, 1397–1400; d) M. O. Senge, K. J. Flanagan, A. A. Ryan, C. Ryppa, M. Donath, B. Twamley, *Tetrahedron,* **2016**, *72*, 105–115, e) J. Schindler, S. Kupfer, A. A. Ryan, K. J. Flanagan, M. O.Senge, B. Dietzek, *Coord. Chem. Rev.*, **2018**, *360*, 1–16.

[70] D. L. Cullen, E. F. Meyer, Jr., K. M. Smith, *Inorg. Chem.,* **1977**, *16*, 1179–1186.

[71] A. Meindl, S. Plunkett, A. A. Ryan, K. J. Flanagan, S. Callaghan, M. O. Senge, *Eur. J. Org. Chem.*, **2017**, 3565–3583; b) A. Meindl, A. A. Ryan, K. J. Flanagan, M. O. Senge, *Heterocycles,* **2017**, *94*, 1518–1541.

[72] N. N. Sergeeva, M. O. Senge, *Tetrahedron Lett.,* **2006**, *47*, 6169–6172.

[73] B. Röder, M. Büchner, I. Rückmann, M. O. Senge, *Photochem. Photobiol. Sci.*, **2010**, *9*, 1152–1158.

[74] C. J. Medforth, M. O. Senge, K. M. Smith, L. D. Sparks, J. A. Shelnutt, *J. Am. Chem. Soc.*, **1992**, *114*, 9859–9869.

[75] M. Gouterman, *J. Chem. Phys.*, **1959**, *30*, 1139–1161.

[76] M. Gouterman, *J. Mol. Spectrosc*. **1961**, *6*, 138–163; b) M. Gouterman, G. H. Wagnière, L. C. Snyder, *J. Mol. Spectrosc*., **1963**, *11*, 108–127.

[77] a) D. G. Whitten, I. G. Lopp, P. D. Wildes, *J. Am. Chem. Soc.*, **1968**, *90*, 7196–7200; b) M. Gouterman, In *The Porphyrins*, *Vol III,* (Eds: D. Dolphin), Academic, New York, Part A, **1978**, pp 1–165; c) M. Nappa, J. S. Valentine, *J. Am. Chem. Soc*., **1978**, *100*, 5075–5080; d) M. Y. R. Wang, B. M. Hoffman, *J. Am. Chem. Soc.*, **1984**, *106*, 4235–4240; e) M. Rubio, B. O. Rios, L. Serrano-Andres, M. Merchan, *J. Chem. Phys.*, **1999**, *110*, 7202–7209.

[78] a) L. R. Milgrom, in *The Colours of Life*, Oxford University Press, Oxford; **1997**; b) O. Horváth, Z. Valicsek, A. Vogler, *Inorg. Chem. Commun.,* **2004***, 7*, 854–857; c) R. Huszánk, G. Lendvay, O. Horváth, *J. Biol. Inorg. Chem*., **2007**, *12*, 681–690; d) Z. Valicsek, G. Lendvay, O. Horváth, *J. Porph. Phthalocyan*., **2009**, *13*, 910–926; e) Z. Valicsek, O. Horváth, G. Lendvay, I. Kikas, I. Skoric, *J. Photoch. Photobio. A.,* **2011***, 218*, 143–155.

[79] R. Giovannetti, The Use of Spectrophotometry UV-Vis for the Study of Porphyrins, Macro To Nano Spectroscopy, Jamal Uddin, IntechOpen, **2012**, pp 87–108, DOI: 10.5772/38797. Available from: https://www.intechopen.com/books/macro-to-nano-spectroscopy/the-use-of-spectrophotometry-uv-vis-for-the-study-of-porphyrins.

[80] M. Biesaga, K. Pyrzynska, M. Trojanowicz, *Talanta,* **2000**, *51*, 209–224.

[81] R. Giovannetti, L. Alibabaei, F. Pucciarelli, *Inorg. Chim. Acta*, **2010**, *363*, 1561–1567.

[82] E. D. Becker, R. B. Bradley, *J. Chem. Phys.*, **1959**, *31*, 1413–1414.

[83] J. Ellis, A. H. Jackson, G.W. Kenner, J. Lee, *Tetrahedron Lett.*, **1960**, 23–27.

[84] R. J. Abraham, *Mol. Phys*., **1961**, *4*, 145–152.

[85] C. W. Haigh, R. B. Mallion, *Prog. NMR Spectrosc*., **1980**, *13*, 303–344; b) P. Lazzeretti, *Prog. NMR. Spectrosc*., **2000**, *36*, 1–88.

[86] H. Günther, in *Chemistry*, 2nd Edition, (Eds: J. Wiley & Sons), Chichester, **1995**.

[87] a) S. J. Perkins, *J. Mag. Reson*., **1980**, *38*, 297–312; b) S. J. Perkins, *Biol. Mag. Reson.,* **1982**, *4*, 193–336; c) C. J. Medforth, C. M. Muzzi, K. M. Shea, K. M. Smith, R. J. Abraham, S. Jia, J. A. Shelnutt, *J. Chem. Soc., Perkin Trans. 2*, **1997**, 839–844.

[88] a) J. A. Pople, W. G. Schneider, H. J. Bernstein, in *'High Resolution NMR'*, (eds :McGraw-Hill Book Co.), New York, **1959**; b) J. W. Emsley, J. Feeney, L. H. Sutcliffe, *'High Resolution NMR Spectroscopy'*, Pergamon, New York, **1966**; c) L. M. Jackmann, S. Sternhell, in *Organic Chemistry*,*Vol 5* 2nd Edition, Pergamon Press, New York, **1969**; d) E.D. Becker, *'High Resolution NMR*, *Theory and Chemical Applications'*, Academic Press, New York, **1969**; e) F. A. Bovey, *'NMR Spectroscopy*', Academic Press, New York, **1969**;

[89] H. H. Inhoffen, H. Brockmann Jr., K. M. Bliesener, *Liebigs. Ann. Chem*., **1969**, *730*, 173–185.

[90] R. J. Abraham, A. H. Jackson, G.W. Kenner, *J. Chem. Soc*., **1961**, 3468–3474.

[91] W. S. Caughey, W. S. Koski, Biochemistry, **1962**, *1*, 923–931.

[92] a) R. J. Abraham, A. H. Jackson, G. W. Kenner, D. Warburton, *J. Chem. Soc.*, **1963**, 853–862; b) P. Burbidge, G. L. Collier, A. H. Jackson, G. W. Kenner, *J. Chem. Soc*., **1967**, 930–931.

[93] a) R. C. Haddon, V. R. Haddon, L. M. Jackman, *Fortschr. Chem. Forsch*., **1971**, *16*, 103–220; b) H. Ogoshi, E. Watanabe, Z. Yoshida, *Tetrahedron*, **1973**, *29*, 3241–3245.

[94] a) W. S. Caughey, P. K. Ibers, *J. Org. Chem*., **1963**, *28*, 269–270; b) G. M. McLaughlin, *J. Chem. Soc., Perkin Trans. 2*, **1974**, 136–140.

95 M. O. Senge, W. W. Kalisch, S. Runge, *Liebigs Ann. Recl.* **1997**, *7*, 1345–1352.

[96] a) M. Roucan, M. Kielmann, S. J. Connon, S. S. R. Bernhard, M. O. Senge, *Chem. Commun.* **2017**, *54*, 26–29.

[97] a) M. O. Senge, *ECS Trans*., **2015**, *66*, 1–10; b) T. P. G. Sutter, R. Rahimi, P. Hambright, J. C. Bommer, M. Kumar, P. Neta, *J. Chem. Soc. Faraday Trans.*, **1993**, *89*, 495–502.

[98] S. H. McCooey, S. J. Connon, *Angew. Chem. Int. Ed.,* **2005**, *117*, 6525–6528.

[99] The Porphyrin Handbook, Eds: K. M. Kadish, K. M. Smith, R. Guilard, Academic Press, San Diego, **2000**.

[100] D. H. McDaniel, H. C. Brown, *J. Org. Chem.*, **1958**, 23, 420–427.

[101] a) J. B. Tindall, *Ind. Eng. Chem.* **1941**, *33*, 65–66; b) I. Ugi, U. Fetzer, U. Eholzer, H. Knupfer, K. Offerman, *Angew. Chem. Int. Ed.* **1965**, *4,* 472–484; c) S. Kambe, H. Yasuda, *Bull. Chem. Soc. Jpn.,* **1968**, *41*, 1444–1446.

[102] D. H. R. Barton, S. Z. Zard, *J. Chem. Soc. Chem. Commun.* **1985**, 1098–1100.

[103] S. D. Roth, T. Shkindel, D. A. Lightner, *Tetrahedron* **2007**, *63*, 11030–11039.

[104] E. Kang, G. H. Teo, H. Barnett, J. Anderson, C. E. Loader, *Can. J. Chem.*, **1978**, *56*, 221–225.

[105] a) F. Paul, J. Patt, J. F. Hartwig, *J. Am. Chem. Soc.,* **1994**, *116*, 5969–5970; b) A. S. Guram, R. A. Rennels, S. L. Buchwald, *Angew. Chem. Int. Ed.,* **1995**, *34*, 1348–1350; c) J. Louie, J. F. Hartwig, *Tetrahedron Lett*., **1995**, *36*, 3609–3612; d) M. S. Driver, J. F. Hartwig, *J. Am. Chem. Soc.,* **1996**, *118*, 7217–7218; e) J. F. Hartwig, S. Richards, D. Barañano, F. Paul, *J. Am. Chem. Soc.,* **1996**, *118*, 3626–3633; f) J. P. Wolfe, S. Wagaw, S. L. Buchwald, *J. Am. Chem. Soc.,* **1996**, *118*, 7215–7216; g) S. Wagaw, R. A. Rennels, S. L. Buchwald, *J. Am. Chem. Soc.,* **1997**, *119*, 8451–8458.

[106] Y. Chen, X. P. Zhang, *J. Org. Chem.,* **2003**, *68*, 4432–4438.

[107] a) T. Takanami, M. Hayashi, F. Hino, K. Suda, *Tetrahedron Lett.,* **2003**, *44*, 7353–7357; b) K. B. Fields, J. V. Ruppek, N. L. Snyder, X. P. Zhang, in *Handbook of Porphyrin Science, Vol. 3* (Eds.: K. M. Kadish, K. M. Smith, R. Guilard), World Scientific Publishing, Singapore, **2010**, pp. 367–427.

[108] F. F. Blicke*, Org. Reactions,* **2011***, 1,* 303–341*.*

[109] a) L. Spialter, J. A. Pappalardo, In *The Acyclic Aliphatic, Tertiary Amines*; The Macmillan Co.: New York, **1965**; p 14–29; b) K. Suga, S. Watanabe, T. Fujita, T. P. Pan, *Bull. Chem. Soc. Jpn.* **1969**, *42*, 3606–3608; c) K. Koh, R. N. Ben, T. Durst, *Tetrahedron Lett.,* **1993**, *34*, 4473–4476; d) J. A. O'Meara, N. Gardee, M. Jung, R. N. Ben, T. Durst, *J. Org. Chem.,* **1998**, *63*, 3117–3119; e) F. Valot, F. Fache, R. Jacquot, M. Spagnol, M. Lemaire, *Tetrahedron Lett.,* **1999**, *40*, 3689–3692; f) J. McMurry, Organic Chemistry with Biological Applications, 2nd ed., Brooks/cole, **2011**.

[110] I. D. Entwistle, A. E. Jackson, R. A. W. Johnstone, R. P. Telford, *J. Chem. Soc*., *Perkin Trans. 1,* **1977**, 443–444.

[111] a) J. R. Sampey, *J. Am. Chem. Soc.,* **1930**, *52*, 88–92; b) C. F. Winans, H. Adkins, *J. Am. Chem. Soc.,* **1932**, *54*, 306–312**;** c) D. Balcom, A. Furst, *J. Am. Chem. Soc.,* **1953**, *75*, 4334–4334; d) M. Lauwiner, R. Roth, P. Rys, *Applied Catalysis A: General*, **1999**, *177*, 9–14; e) D. Channe Gowda, B. Mahesh, S. Gowda, *Indian J. Chem. Sec. B.*, **2001**, *40B*, 75–77; f) T. Tsukinoki, H. Tsuzuki, *Green Chem.*, **2001**, *3*, 37–38; g) D. Sawant, R. Kumar, P. R. Maulik, B. Kundu, *Org. Lett.,* **2006**, *8*, 1525–1528; h) K. Zhu , M. P. Shaver, S. P. Thomas, *Chem. Sci.*, **2016**, *7*, 3031–3035.

[112] a) U. Eisner, A. Lichtarowicz, R. P. Linstead, *J. Chem. Soc.*, **1957**, 733–739; b) G. D. Hartman, L. M. Weinstock, *Org. Synth.*, **1979**, *59*, 183–188; c) J. L. Sessler, A. Mozzafari, M. R. Johnson, *Org. Synth*.; **1992**, *70*, 68–74.

[113] K. M. Smith, in Porphyrin and Metalloporphyrin, (Eds : K. M. Smith), Elsevier Scientific Publishng Company, Amsterdam, **1975**, pp 3–27.

[114] W. K. McEwen, *J. Am. Chem. Soc.*, **1936**, *58*, 1124–1129.

[115] F. De Matteis, A. H. Gibbs, A. H. Jackson, S. Weerasinghe, *FEBS Letters*, **1980**, *119*, 109–112.

[116] G. S. Marks, D. T. Allen, C. T. Johnson, E. P. Sutherland, K. Nakatsu R. A. Whitney, *Mol. Pharmacol.*, **1985**, *27*, 459–465.

[117] a) I. V. Sazanovich, A. Van Hoek, A. Yu. Panarin, V. L. Bolotin, A. S. Semeykin, D. B. Berezin, V. S. Chirvony, *J. Porph. Phthalocyan.*, **2005**, *9*, 59–67; b) B. Berezin, Doctoral Dissertation in Chemistry (IGKhTU, Ivanovo, **2007**); c) M. Kielmann, M. O. Senge, *Angew. Chem.*, *Int. Ed.*, **2019**, *58*, 418–441.

[118] a) M. O. Senge, *J. Porph. Phthalocyan.*, **1998**, *2*, 107–121; b) D. L. Cullen, L. V. Desai, J. A. Shelnutt, M. Zimmer, *Struct. Chem*., **2001**, *12*, 127–136; c) Z. Song , A. O. Adeyemo, J. Baker, S. M. Traylor, M. L. Lightfoot, *Ga. J. Sci.*, **2011**, *69*, 89–101.

[119] D. Lecerof, M. Fodje, A. Hansson, M. Hansson, S. Al-Karadaghi, *J. Mol. Biol.*, **2000**, *297*, 221–232.

[120] a) F. De Matteis, J. Jarvisalo, A. H. Gibbs, *Mol. Pharmacol.*, **1978**, *14*, 1099–1106; b) P. R. Ortiz de Montellano, M. A. Correia, *Ann. Rev. Pharmacol. Toxicol.*, **1983**, *23*, 481–503.

[121] a) B. Goldberg, A. Stern, Arch. Biochem. Biophys., **1977**, *178*, 218–225; b) J. K. French, C. C. Winterbourn, R. W. Carrell, *Biochem. J.*, **1978**, *173*, 19–26; c) S. Saito, H. A. Itano, *Proc. Natl. Acad. Sci.*, U.S.A., **1981**, *78*, 5508–5512; d) P.R. Ortiz de Montellano, K. L. Kunze, *J. Am. Chem. Soc.*, **1981**, *103*, 6534–6536.

[122] a) D. K. Lavallee, A. White, A. Diaz, J. P. Battioni, D. Mansuy, *Tetrahedron Lett.*, **1986**, *27*, 3521–3524; b) J. Mercer-Smith, S. Figard, D. K. Lavallee, S. Svitra, *J. Nucl. Med.*, **1985**, *26*, 437–437.

[123] W. K. McEwen, *J. Am. Chem. Soc.*, **1946**, *68*, 711–713.

[124] M. G. Ahmed, R. W. Alder, G. H. James, M. L. Sinnott, M. C. Whiting, *Chem. Commun.*, **1968**, *23*, 1533–1354.

[125] a) G. R. Dearden, A. H. Jackson, *Chem. Commun.*, **1970**, 205–206; b) M. J. Broadhurst, R. Grigg, G. Shelton, A. V. Johnson, *Chem. Commun.*, **1970**, 231–233.

[126] A. M. Abeysekera, R. Grigg, J. Trocha-Grimshaw, K. Henrick, *Tetrahedron*, **1979**, *36*, 1857–1868.

[127] a) T. Ema, M. O. Senge, N. Y. Nelson, H. Ogoshi, K. M. Smith, *Angew. Chem., Int. Ed.*, **1994**, *33*, 1879–1881; b) M. O. Senge, I. Bischoff, N. Y. Nelson, K. M. Smith, *J. Porph. Phthalocyan.*, **1999**, *3*, 99–116.

[128] a) M. O. Senge, T. P. Forsyth, L. T. Nguyen, K. M. Smith, *Angew. Chem., Int. Ed.*, **1994**, *33*, 2485–2487; b) B. Cheng, O. Q. Munro, H. M. Marques, W. R. Scheidt, *J. Am. Chem. Soc.*, **1997**, *119*, 10732–10742.

[129] a) O. S. Finikova, A. V. Cheprakov, P. J. Carroll, S. Dalosto, S. A. Vinogradov, *Inorg. Chem.*, **2002**, *41*, 6944–6946; b) S. Al-Karadaghi, R. Franco, M. Hansson, J. A.

Shelnutt, G. Isaya, G. C. Ferreira, *Trends Biochem. Sci.*, **2006**, *31*, 135–142; c) A. Medlock L. Swartz, T. A. Dailey, H. A. Dailey, W. N. Lanzilotta, *Proc. Natl. Acad. Sci. U.S.A.*, **2007**, *104*, 1789–1793;

[130] H. J. Callot, J. Fisher, R. Weiss, *J. Am. Chem. Soc.*, **1982**, *104*, 1272–1276.

[131] D. K. Lavallee, A. E. Gebala, *Inorg. Chem.*, **1974**, *13*, 2004–2008.

[132] J. A. S. Cavaleiro, M. F. P. N. Condesso, A. H. Jackson, M. G. P. M. S. Neves, K. R. N. Rao, B. K. Sadashiva, *Tetrahedron Lett.*, **1984**, *25*, 6047–6048.

[133] G. P. Arsenault, E. Bullock, S. F. MacDonald, *J. Am. Chem. Soc.*, **1960**, *82*, 4384–4389.

[134] a) K. M. Smith, R. K. Pandey, *Tetrahedron Lett.*, **1986**, *24*, 2717–2720; b) R. K. Pandey, A. H. Jackson, K. M. Smith, *J. Chem. Soc., Perkin I*, **1991**, *0*, 1211–1220; c) R. K. Pandey, X. Zhenga, M. P. Dobhala, K. M. Smith, *J. Porph. Phthalocyan.*, **2008**, *12*, 131–141; d) W. Naito, N. Yasuda, T. Morimoto, Y. Shigeta, H. Takaya, I. Hisaki, H. Maeda, *Org. Lett.*, **2016**, *18*, 3006−3009.

[135] K. M. Smith, G. W. Craig, *J. Org. Chem.*, **1983**, *48*, 4302−4306; b) K. M. Smith, 0. M. Minnetian, *J. Chem. Soc., Perkin I*, **1986**, *0*, 277–280.

[136] R. C. Ellingson, A. H. Corwin, *J. Am. Chem. Soc.*, **1946**, *68*, 1112–1115.

[137] a) H. J. Callot, B. Chevrier, R. Weiss, *J. Am. Chem. Soc.*, **1978**, *100*, 4733–4741; b) K. Ichimura, *Bull. Chem. Soc. Jpn.*, **1978**, *51*, 1444–1449.

[138] Y. Harel, J. Manassen, *J. Am. Chem. Soc.*, **1978**, *100*, 6228–6234.

[139] H. J. Callot, T. Tschamber, B. Chevrier, R. Weiss, *Angew. Chem.*, *Int. Ed.*, **1975**, *14*, 567–568.

[140] a) R. Bonnett, R. J. Ridge, E. H. Appelman, *Chem. Commun*., **1978**, 310–311; b) Y. Tamura, J. Miramikawa, M. Ikeda, *Synthesis*, **1977**, 1–17.

[141] H. J. Callot, *Tetrahedron Lett.*, **1979**, *33*, 3093–3096.

[142] H. J. callot, E. Schaeffer, *Tetrahedron Lett.*, **1977**, *3*, 239–242.

[143] a) H. J. Callot, F. Metz, R. Cromer, *Nouv. J. Chim.*, **1984**, *8*, 759–763; b) H. J. Callot, R. Cromer, *Nouv. J. Chim.*, **1984**, *8*, 765–770.

[144] a) H. Ogoshi, E. I. Watanabe, N. Koketsu, Z. I. Yoshida, *J. Chem. Soc.*, *Chem. Commun*., **1974**, 943–944; b) H. J. Callot, E. Schaeffer, *Tetrahedron Lett.*, **1980**, *21*, 1335–1338; c) H. J. Callot, E. Schaeffer, *J. Organomet. Chem.*, **1980**, *193*, 111–115; d) D. Dolphin, D. J. Halko, E. Johnson, *Inorg. Chem.*, **1981**, *20*, 4348–4351.

[145] H. Ogoshi, E. I. Watanabe, N. Koketsu, Z. I. Yoshida, *Bull. Chem. Soc. Jpn.*, **1976**, 49, 2529–2436.

[146] S. I. Aizawa, Y. Tsuda, Y. Ito, K. Batano, S. Funahashi, *Inorg. Chem.*, **1993**, *32*, 1119–1123.

[147] B. Badet, These, Univ. Pierre et Marie Curie, **1980**.

[148] J. I. Setsune, H. Takeda, *Tetrahedron Lett.*, **1995**, *36*, 5903–5904.

[149] Y. Watanabee, T. Aida, S. Inoue, *Macromolecules*, **1990**, *23*, 2612–2617.

[150] a) J. T. Crivello, J. H. W. Lam, *Macromolecules*, **1977**, *10*, 1307–1315 ; b) J. T. Crivello, *Adv. Polym. Sci.*, **1984**, *62*, 1–48; c) S. Hayase, Y. Onishi, S. Suzuki, M. Wada, *Macromolecules*, **1986**, *19*, 968–973; d) Y. Fukuchi, T. Takahashi, H. Nogushi, M. Saburi, Y. Uchida; *Macromolecules*, **1987**, *20*, 2316–2317.

[151] T. Aida, K. Kawaguchi, S. Inoue, *Macromolecules*, **1990**, *23*, 3887–3892.

[152] Y. Watanabee, T. Aida, S. Inoue, *Macromolecules*, **1991**, *24*, 3970–3972.

[153] W. Suzuki, H. Kotani, T. Ishizuka, T. Kojima, *J. Chem. Am. Soc.,* **2019**, *141*, 5987–5994.

[154] a) J. S. Lindsey, H. C. Hsu, P. C. Kearney, A. M. Marguerettaz, J. S. Lindsey, *J. Org. Chem.,* **1987**, *52*, 827–836.

[155] M. O. Senge, M. Fazekas, M. Pintea, M. Zawadzka, W. J. Blau, *Eur. J. Org. Chem.,* **2011**, *2011*, 5797–5816.

[156] O. P. Anderson, D. K. Lavallee, *J. Am. Chem. Soc.* **1977**, *99*, 1404–1409.

[157] A. D. Bond, N. Feeder, J. E. Redman, S. J. Teat, J. K. M. Sanders, *Cryst. Growth Des.* **2002**, *2*, 27–39.

[158] a) K. M. Barkigia, L. Chantranupong, K. M. Smith, J. Fajer, *J. Am. Chem. Soc.* **1988**, *110*, 7566–7567; b) A. Y. Lebedev, M. A. Filatov, A. V. Cheprakov, S. A. Vinogradov, *J. Phys. Chem. A* **2008**, *112***,** 7723–7733.

[159] a) P. R. Olivato, M. G. Mondino, M. H. Yreijo, B. Wladislaw, M. B. Bjorklund, L. Marzorati, G. Distefano, M. Dal Colle, G. Bombieri, A. Del Pra, *J. Chem. Soc.*, *Perkin Trans. 2,* **1998**, 109–114; b) M. Khattab, S. Chatterjee, A. H. A. Clayton, F. Wang, *New J. Chem.* **2016**, *40*, 8296–8304.

[160] a) J. Braun, M. Koecher, M. Schlabach, B. Wehrle, H. H. Limbach, E. Vogel, *J. Am. Chem. Soc.*, **1994**, *116*, 6593–6604. B) Jr. K. M. Merz, C. H. Reynolds, *J. Chem. Soc., Chem. Commun.,* **1988**, *0*, 90–92.

[161] S. J. Silvers, A. Tulinsky, *J. Am. Chem. Soc.,* **1967**, *89*, 3331–3337.

[162] W. Chen, M. E. El-Khouly, S. Fukuzumi, *Inorg. Chem,.* **2011**, *50*, 671–678.

[163] D. K. Lavallee, O. P. Anderson, *J. Am. Chem. Soc.,* **1982**, *104*, 4707–4708.

[164] Y. Yamamoto, A. Yamamoto, S. Y. Furuta, M. Horie, M. Kodama, W. Sato, K. Y. Akiba, S. Tsuzuki, T. Uchimaru, D. Hashizume, F. Iwasaki, *J. Am. Chem. Soc.,* **2005**, *127*, 14540–14541.

[165] J. W. Lauher, J. A. Ibers, *J. Am. Chem. Soc.,* **1973**, *95*, 5148–5152.

[166] T. E. Clement, L. T. Nguyen, R. G. Khoury, D. J. Nurco, K. M. Smith, *Heterocycles,* **1970**, *45*, 651–658.

[167] J. Schindler, S. Kupfer, A. A. Ryan, K. J. Flanagan, M. O. Senge, B. Dietzek, *Coord. Chem. Rev.* **2018**, *360*, 1–16.

[168] M. Kuroki, T. Aida, S. Inoue, *J. Am. Chem. Soc*., **1987**, *109*, 4737–4738.

[169]) D. A. Evans, D. W. C. MacMillan, K. R. Campos, *J. Am. Chem. Soc*., **1997**, *119*, 10859–10860.

[170] a) U. Eder, G. Sauer, R. Wiechert, *Angew. Chem.*, *Int. Ed. Engl.,* **1971**, *10*, 496–497; b) C. Agami, F. Meyneir, C. Puchot, *Tetrahedron,* **1984**, *40*, 1031–1038; c) M. J. O'Donnell, W. D. Bennett, S. Wu, *J. Am. Chem. Soc.,* **1989**, *111*, 2353–2355; d) D. Yang, Y. C. Yip, M. W. Tang, M. K. Wong, J. H. Zheng, K. K. Cheung, *J. Am. Chem. Soc.,* **1996**, *118*, 491–492; e) E. J. Corey, F. Xu, M. C. Noe, *J. Am. Chem. Soc.,* **1997**, *119*, 12414–12415; f) D. Yang, M. K. Wong, Y. C. Yip, X. C. Wang, M. W. Tang, J. H. Zheng, K. K. Cheung, *J. Am. Chem. Soc.,* **1998**, *120*, 5943–5952; g) E. J. Corey, Y. Bo, J. Busch-Petersen, *J. Am. Chem. Soc.,* **1999**, *120*, 13000–13001; h) Y. Iwabuchi, M. Nakatani, N. Yokoyama, S. Hatakeyama, *J. Am. Chem. Soc.* **1999**, *120*, 10219–10220.

[171] Z. G. Hajos, D. R. Parrish, *J. Org. Chem*., **1974**, *39*, 1615–1621.

[172] W. S. Knowles, M. J. Sabacky, *Chem. Comm.*, **1968**, 1445–1446; b) L. Horner, S. Siegel, H. Butle, *Angew. Chem. Int. Ed. Engl.*, **1968**, *7*, 942–942; c) B. Bogdanović, B. Henc, A. Lősler, B. Mester, H. Pauling, G. Wilke, *Angew. Chem. Int. Ed. Engl.*, **1973**, *12*, 953–984; d) A. Nakamura, A. Konishi, R. Tsujitani, M. A. Kudo, S. Otsuka, *J. Am. Chem. Soc.*, **1978**, *100*, 3449–3461; e) K. Berghus, A. Hamsen, A. Rensing, A. Wolhermann. T. Kauffmann., *Angew. Chem. Int. Ed. Engl.*, **1981**, *20*, 117–118; f) T. Hayashi, A. Yamamoto, Y. Ito, H. Miura, K. Yanagi, *J. Am. Chem. Soc.*, **1989**, *111*, 6301–6311; f) J. Okuda, *Angew. Chem. Int. Ed. Engl.*, **1992**, *31*, 47–48; g) M. B. Carter, B. Schiott, A. Gutiérrez, S. L. Buchwald, *J. Am. Chem. Soc.*, **1994**, *116*, 11667–11670; h) M. Kablaoui, S. L. Buchwald, *J. Am. Chem. Soc.*, **1996**, 3182–3191; i) K. Severin, R. Bergs, W. Beck, *Angew. Chem. Int. Ed. Engl.*, **1998**, *37*, 1934–1654.

[173] a) Y. Huang, X. Feng, B. Wang, G. Zhang, Y. Jiang, *Synlett.*, **2002**, *12*, 2122–2124; b) D. E. Ward, M. Santos Souweha, *Org. Lett.,* **2005**, *7*, 3533–3536.

[174] a) R. Noyori, T. Okhuma, M. Kitamura, H. Takaya, N. Sayo, H. Kumobayashi, S. Akuragawa, *J. Am. Chem. Soc.,* **1987**, *109*, 5856–5858, b) S Akutagawa, *App. Cat. A: Gen.*, **1995**, *128*, 171–307.

[175] a) E. M. McGarrigle, D. G. Gilheany, *Chem Rev.*, **2005**, *105*, 1563–1602; b) Q. P. Shi, Z. H. Shi, N. G. Li, Y. P Tang, W. Li, H. Tang, W. Zhang, M. Z. Shen, J. A. Duan, *Curr. Org. Chem.*, **2013**, *17*, 2936–2970.

[176] a) D. A. Evans, D. M. Barnes, J. S. Johnson, T. Lectka, P. von Matt, S. J. Miller, J. A, Murry, R.D. Norcross, E.A. Shaughness, K. R. Campos, *J. Am. Chem. Soc*., **1999**, *121*, 7582–7594; b) P. Goodrich, C. Hardacre, C. Paun, A. Ribeiro, S. Kennedy, M. J. V. Lourenço, H. Manyar, C. A. Nieto de Castro, M. Besnea, V. I. Pârvulescu, *Adv. Synth. Catal*., **2011**, *353*, 995–1004.

[177] a) Y. Tu, Z. X. Wang, Y. Shi, *J. Am. Chem. Soc.*, **1996**, *118*, 9806–9807; b) S. E. Denmark, Z. Wu, C. M. Crudden, H. Matsuhashi, *J. Org. Chem.*, **1997**, *62*, 8288–8289.

[178] K. A. Ahrendt, C. J. Borths, D. W. C. MacMillan, *J. Am. Chem. Soc.*, **2000**, *122*, 17, 4243–4244.

[179] a) N. A. Paras, D. W. C MacMillan, *J. Am. Chem. Soc.*, **2001**, *123*, 4370–4371; b) N. A. Paras, D. W. C MacMillan, *J. Am. Chem. Soc.*, **2002**, *124*, 7894–7895; c) J. F. Austin, D. W. C. MacMillan, *J. Am. Chem. Soc.*, **2002**, *124*, 1172–1173; d) A. B. Northrup, D. W. C. MacMillan, *J. Am. Chem. Soc.*, **2002**, *124*, 2458–2460; e) S. P. Brown, N. C. Goodwin, D. W. C. MacMillan, *J. Am. Chem. Soc.*, **2003**, *125*, 1192–1194.

[180] W. S. Jen, J. M. Wiener, D. W. C. MacMillan, *J. Am. Chem. Soc.*, **2000**, *122*, 9874–9875.

[181] a) S. G. Ouellet, J. B. Tuttle, D. W. C. MacMillan, *J. Am. Chem. Soc.*, **2005**, 127, 32–33; b) J. B. Tuttle, S. G. Ouellet, D. W. C. MacMillan, *J. Am. Chem. Soc.*, **2006**, 128, 12662–12663.

[182] a) J. F. Austin, S. G. Kim, C. J. Sinz, W. J. Xiao, D. W. C. MacMillan, *PNAS,* **2004**, *101*, 5482–5487; b) R. K. Kunz, D. W. C. MacMillan, *J. Am. Chem. Soc.*, **2005**, *127*, 3240–3241; c) Y. K. Chen, M. Yoshida, D. W. C. MacMillan, *J. Am. Chem. Soc.*, **2006**, *12*8, 9328–9329; d) S. Lee, D. W. C. MacMillan, *J. Am. Chem. Soc.*, **2007**, *127*, 15438–15439.

[183] (a) S. Akabori, S. Sakurai, Y. Izumi, Y. Fujii, *Nature*, **1956**, *178*, 323–324; b) R. Noyori, *Angew. Chem., Int. Ed. Engl.*, **2002**, *41*, 2008–2022.

[184] M. Marigo, T. C. Wabnitz, D. Fielenbach, K. A. Jorgensen, *Angew. Chem. Int. Ed.,* **2005**, *44*, 794–797; b) J. Franzen, M. Marigo, D. Fielenbach, T. C. Wabnitz, A. Kjarsgaard, K. A. Jorgensen, *J. Am. Chem. Soc.,* **2005**, *127*, 18296–18304.

[185] A. Carlone, G. Bartoli, M. Bosco, L. Sambri, P. Melchiorre, *Angew. Chem. Int. Ed.*, **2007**, 46, 4504–4506.

[186] D. Enders, M. R. M. Hüttl, C. Grondal, G. Raabe, *Nature, **2006***, 441, 861–863.

[187] L. Albrecht, H. Jiang, G. Dickmeiss, B. Gschwend, S. G. Hansen, K. A. Jørgensen, *J. Am. Chem. Soc.*, **2010**, 132, 9188–9196.

[188] a) N. Halland, P. S. Aburel, K. A. Jørgensen, *Angew. Chem. Int. Ed., **2003***, *42*, 661–665; b) K. Frisch, A. Landa, S. Saaby, K. A. Jørgensen, *Angew. Chem. Int. Ed., **2005***, *44,* 6058–6063.

[189] C. M. Starks, *J. Am. Chem. Soc.*, **1971**, *93*, 195–199.

[190] B. Lygo, B. Andrews, *Acc. Chem. Res.*, **2004**, *37*, 518–525.

[191] a) U. H. Dolling, P. Davis, E. J. J. Grabowski, *J. Am. Chem. Soc.*, **1984**, *106*, 446–447; b) S. Shirakawa, K. Yamamoto, M. Kitamura, K. Maruoka, *Angew. Chem. Int. Ed.*, **2005**, *44*, 625–628; c) T. Ooi, M. Takeuchi, M. Kameda, K. Maruoka, *J. Am. Chem. Soc.*, **2000**, *122*, 5228–5229.

[192] a) F. Y. Zhang, E. J. Corey, *Org. Lett*, **2000**, *2*, 1097–1100; b) T. Ooi, M. Kameda, M. Taniguchi, K. Maruoka, *J. Am. Chem. Soc.*, **2004**, *126*, 9685–9694; c) A. Okada, T. Shibuquchi, T, Ohshima, H. Masu, K. Yamaquchi, M. Shibasaki, *Angew. Chem. Int. Ed.*, **2005**, *44*, 4564–4567.

[193] S. Kobbelgaard, M. Bella, K. A. Jørgensen, *J. Org. Chem.*, **2006**, *71*, 4980–4987.

[194] a) N. Shibata, T. Ishimaru, E. Suzuki, K. L. Kirk, *J. Org. Chem.,* **2003**, *68*, 2494–2497; b) T. Ooi, D. Ohara, M. Tamura, K. Maruoka; *J. Am. Chem. Soc.*, **2004**, *126*, 6844–6845; c) E. Murugan, A. Siva, *Synthesis*, **2005**, 2022–2028; d) R. He, X. Wang, T. Hashimoto, K. Maruoka, *Angew. Chem. Int. Ed.*, **2008**, *47*, 9466–9468.

[195] M. S. Sigman, E. N. Jacobsen, *J. Am. Chem. Soc.*, **1998**, *120*, 4901–4902.

[196] P. Vachal, E. N. Jacobsen, *J. Am. Chem. Soc.*, **2002**, *120*, 10012–10014.

[197] a) A. G. Wenzel, E. N. Jacobsen, *J. Am. Chem. Soc.*, **2002**, *124*, 12964–12965; b) M. S. Taylor, E. N. Jacobsen, *J. Am. Chem. Soc.*, **2004**, *126*, 10558–10559; c) T. Yoon, E. N. Jacobsen, *Angew. Chem. Int. Ed.*, **2005**, *124*, 466–468; d) G. D. Joly, E. N. Jacobsen, *J. Am. Chem. Soc.*, **2004**, *126*, 4102–4103.

[198] a) T. Okino, Y. Hoashi, Y. Takemoto, *J. Am. Chem. Soc.*, **2003**, *128*, 12672–12673; b) Y. Hoashi, T. Yabuta, Y. Takemoto, *Tetrahedron Lett.*, **2003**, *45*, 9185–9188.

[199] E. N. Jacobsen, M. S. Taylor, *Angew. Chem. Int. Ed.*, **2006**, *45*, 1520–1543.

[200] J. Hine, S. M. Linden, V. M. Kanagasabapathy, *J. Org. Chem.*, **1985**, *50*, 5096–5099.

[201] D. P. Curran, L. H. Kuo, *J. Org. Chem.*, **1994**, *59*, 3259–3261.

[202] a) S. J. Connon, *Chem. Commun.*, **2008**, 2499–2510; b) B. Vakulya, S. Varga, A. Csámpai, T. Soós, *Org. Lett.*, **2005**, *7*, 1967–1969; c) M. Shibasaki, N. Yoshikawa, *Chem. Rev.*, **2002**, *102*, 2187–2210.

[203] H. Hiemstra, H. Wynberg, *J. Am. Chem. Soc.*, **1981**, *103*, 417–430.

[204] X. Gao, X. Wen, L. Esser, B. Quinn, L. Yu, C. Yu, D. Xia, *Biochemistry*, **2003**, *42*, 9067–9080.

[205] R. K. Thauer, *Microbiology*, **1998**, *144*, 2377–2406.

[206] I. Hanukoglu, B. S. Suh, S. Himmelhoch, A. Amsterdam, *J. Cell. Biol.*, **1990**, *111*, 1373–1381.

[207] F. Lederer, *Bioch.,* **1994**, *76*, 674–692.

[208] E. C. Duin, *Tetrapyrroles,* **2009**, 352–374; b) K. Zheng, P. D. Ngo, V. L. Owens, X-P. Yang, S. O. Mansoorabadi, *Sciences*, **2016**, *354*, 339–342.

[209] T. Wagner, C. E. Wegner, J. Kahnt, U. Ermler, S. Shima, *J. Bacteriol.*, **2017**, *199*, 1–15.

[210] a) A. Miller, M. Korem, R. Almog, Y. Galboiz, *J. Neurol. Sci.*, **2005**, *233*, 93–97; b) K. Yamada*, Met*. *Ions Life Sci*., **2013**, *13*, 295–320.

[211] a) L. B. Josefsen, R. W. Boyle,, *Theranostics*, **2012**, *2*, 916–966; b) J. F. C. Mario, V. C. S. Ana, A. H. Cesar, M. A. P. Sara, M. P. Mariette, *Curr. Org. Synth*, **2014**, *11*, 127–140; c) J. M. Dabrowski, B. Pucelik, A. Regiel-Futyra, M. Brindell, O. Mazuryk, A. Kyzioł, L.G. Arnaut, *Coord. Chem. Rev*. **2016**, *325*, 67–101; d) O. Horváth, Z. Valicsek, M.A.

Fodor, M.M. Major, M. Imran, G. Grampp, A. Wankmüller, *Coord. Chem. Rev.,* **2016**, *325*, 59–66; e) I. N. Meshkov, V. Bulach, Y.G. Gorbunova, F. E. Gostev, V.A. Nadtochenko, A.Y. Tsivadze, M.W. Hosseini, *Chem. Commun*. **2017**, *53*, 9918–9921; f) M. J. Calvete, S.M. Pinto, M.M. Pereira, C.F. Geraldes, *Coord. Chem. Rev.* **2017**, *333*, 82–107.

[212] J. Collman, V. Zhang, X. Lee, E. Uffelman, J. Brauman, *Science,* **1993**, *261*, 1404–1411.

[213] M. Costas, *Coord. Chem. Rev*, **2011**, *255*, 2912–2932.

[214] B. Meunier, *Chem. Rev.*, **1992**, *92*, 1411–1456.

[215] C. Chang, M. Kuo, *J. Am. Chem. Soc.*, **1979**, *101*, 3413–3415.

[216] J. T. Groves, T. E. Nemo, R. S. Myers, *J. Am. Chem. Soc.*, **1979**, *101*, 1032–1033.

[217] D. Dolphin, T. G. Traylor, L. Y. Xie, *Acc. Chem. Res*., **1997**, *30*, 251–259.

[218] T. G. Traylor, S. Tsuchiya, *Inorg. Chem.*, **1987**, *26*, 1338–1339.

[219] J. Haber, L. Matachowski, K. Pamin, J. Poltowicz, *J. Mol. Catal. A Chem.,* **2003**, *198*, 215–221.

[220] M. Komori, K. Nishio, M. Kitada, K. Shiramatsu, K. Muroya, M. Soma, K. Nagashima, T. Kamataki, *Biochemistry*, **1990**, *29*, 4430–4433.

[221] P. R. Ogilby, *Chem. Soc. Rev.*, **2010**, *39*, 3181–3209.

[222] M. A. Faustino, M. G. Neves, J. A. Cavaleiro, M. Neumann, H. D. Brauer, G. Jori, *Photochem. Photobiol.*, **2000**, *72*, 217–225.

[223] S. H. McCooey, S. J. Connon, *Angew. Chem. Int. Ed.,* **2005**, *44*, 6367–6370.

[224] B. Kótai, G. Kardos, A. Hamza, V. Farkas, I. Pápai, T. Soós, *Chem. Eur. J.,* **2014**, *20*, 5631–5639.

[225] T. Okino, Y. Hoashi, T. Furukawa, X. Xu, Y. Takemoto, *J. Am. Chem. Soc*., **2005**, *127*, 119–125.

[226] O. V. Serdyuk, C. M. Heckel, S. B. Tsogoeva, *Org. Biomol. Chem.*, **2013**, *11*, 7051–7071.

[227] a) R. Connor, W. M. R. McClellan, *J. Org. Chem.*, **1939**, *3*, 570–577; b) R. Alleti, W. S. Oh, M. Perambuduru, C. V. Ramana, V. Prakash Reddy, *Tetrahedron Lett.*, **2008**, *49*, 3466–3470.

[228] a) N. Iranpoor, B. Zeynizadeh, *Synthesis*, **1999**, 49–50; b) M. A. Walters, J. Chaparro, T. Siddiqui, F. Williams, Ulku, C.; Rheingold, A. L. *Inorg. Chim. Acta,* **2006**, *359*, 3996–4000, c) H.Golchoubian, F. Hosseinpoor, *Catal. Commun.*, **2007**, *8*, 697–700.

[229] M. Kielmann, K. J. Flanagan, K. Norvaiša, D. Intrieri, M. O. Senge, *J. Org. Chem*., **2017**, *82*, 5122–5134.

[230] M. O. Senge, C. J. Medforth, L. D. Sparks, J. A. Shelnutt, K. M. Smith, *Inorg. Chem.,* **1993**, *32*, 1716–1723.

[231] T. E. Clement, L. T. Nguyen, R. G. Khoury, D. J. Nurco, K. M. Smith, *Heterocycles*, **1997**, *45*, 651–658.

[232] M. Roucan, K. J. Flanagan, J. O'Brien, M. O. Senge, *Eur. J. Org. Chem*. **2018**, *46*, 6432–6446.

[233] S. M. S. Chauhan, B. Vijayaraghavan, K. V. Rao, *Indian J. Chem., Sect. Org. Chem. Incl. Med. Chem.*, **1987**, *26*, 122–124.

[234] R. J. Cheng, Y. H. Chen, C. C. Chen, G. H. Lee, S. M. Peng, P. P. Y. Chen, *Inorg. Chem.*, **2014**, *53*, 8848–8850.

[235] a) M. O. Senge, *J. Chem. Soc., Dalton Trans.*, **1993**, 3539–3549. Such porphyrins can also undergo SNAr reactions with thiols.[68]

[236] R. Grigg, A. Sweeney, G. R. Dearden, A. H. Jackson, A. W. Johnson, *J. Chem. Soc. D*, **1970**, 1273–1274.

[237] K. M. Kadish, M. Lin, E. Van Caemelbecke, G. De Stefano, C. J. Medforth, D. J. Nurco, N. Y. Nelson, B. Krattinger, C. M. Muzzi, L. Jaquinod, Y. Xu, D. C. Shyr, K. M. Smith, J. A. Shelnutt, *Inorg. Chem.*, **2002**, *41*, 6673–6687.

[238] D. Mandon, P. Ochsenbein, J. Fischer, R. Weiss, K. Jayaraj, R. N. Austin, A. Gold, P. S. White, O. Brigaud, P. Battioni, D. Mansuy, *Inorg. Chem.*, **1992**, *31*, 2044–2049.

[239] E. R. Birnbaum, J. A. Hodge, M. W. Grinstaff, W. P. Schaefer, L. Henling, J. A. Labinger, J. E. Bercaw, H. B. Gray, *Inorg. Chem*. **1995**, *34*, 3625–3632.

[240] M. Kielmann, N. Grover, W. W. Kalisch, M. O. Senge, *Eur. J. Org. Chem*., 2019, *14*, 2448–2452.

[241] M. Kielmann, "Molecular Engineering of Porphyrins as Organocatalysts and Methods Development for New Highly Substituted Porphyrins", (Ph.D. Diss., Trinity College Dublin, University of Dublin, **2019**).

[242] M. K. Chahal, D. Payne, Y. Matsushita, J. Labuta, K. Ariga, J. P. Hill, ChemRivX., **2019,** Preprint.

[243] C. J. Medforth, M O. Senge, T. P. Forsyth, J. D. Hobbs, J. A. Shelnutt, K. M. Smith, *Inorg. Chem*., **1994**, *33*, 3865–3872.

[244] S. Rayati, S. Zakavi, E. Bohloulbandi, M. Jafarian, M. R. Avei, *Polyhedron* **2012**, *34*, 102–107.

[245] E. Watanabe, S. Nishimura, H. Ogoshi, Z. Yoshida, *Tetrahedron,* **1975**, *31*, 1385–1390.

[246] H. Hope, *Prog. Inorg. Chem.* **2007**, 1–19.

[247] a) in *Saint*, Version 8.37a ed., Bruker AXS, Inc., Madison, WI, **2013**; b) in *SADABS*, version 2016/2 ed., Bruker AXS, Inc, Madison, WI,, **2014**; c) in *APEX3*, Version 2016.9-0 ed., Bruker AXS, Inc., Madison, WI,, **2016**.

[248] a) O. V. Dolomanov, L. J. Bourhis, R. J. Gildea, J. A. K. Howard, H. Puschmann, *J. Appl. Crystallogr.,* **2009**, *42*, 339–341; b) G. Sheldrick, *Acta Cryst. Sect. A* **2015**, *71*, 3–8.

[249] C. F. Macrae, I. J. Bruno, J. A. Chisholm, P. R. Edgington, P. McCabe, E. Pidcock, L. Rodriguez-Monge, R. Taylor, J. van de Streek, P. A. Wood, *J. Appl. Cryst*. **2008**, *41*, 466–470.

[250] in *NSDGUI*, Version 1.3 alpha ed., Sandia National Laboratory: New Mexico, **2001**.